MULTI-OMICS STUDY ON GUT MICROBIOTA RELATED TO FAECAL MICROBIOTA TRANSPLANTATION

EDITED BY: Zhangran Chen, Yanling Wei, Jialiang Yang, Leyi Wang and Zeyou Chen

PUBLISHED IN: Frontiers in Microbiology

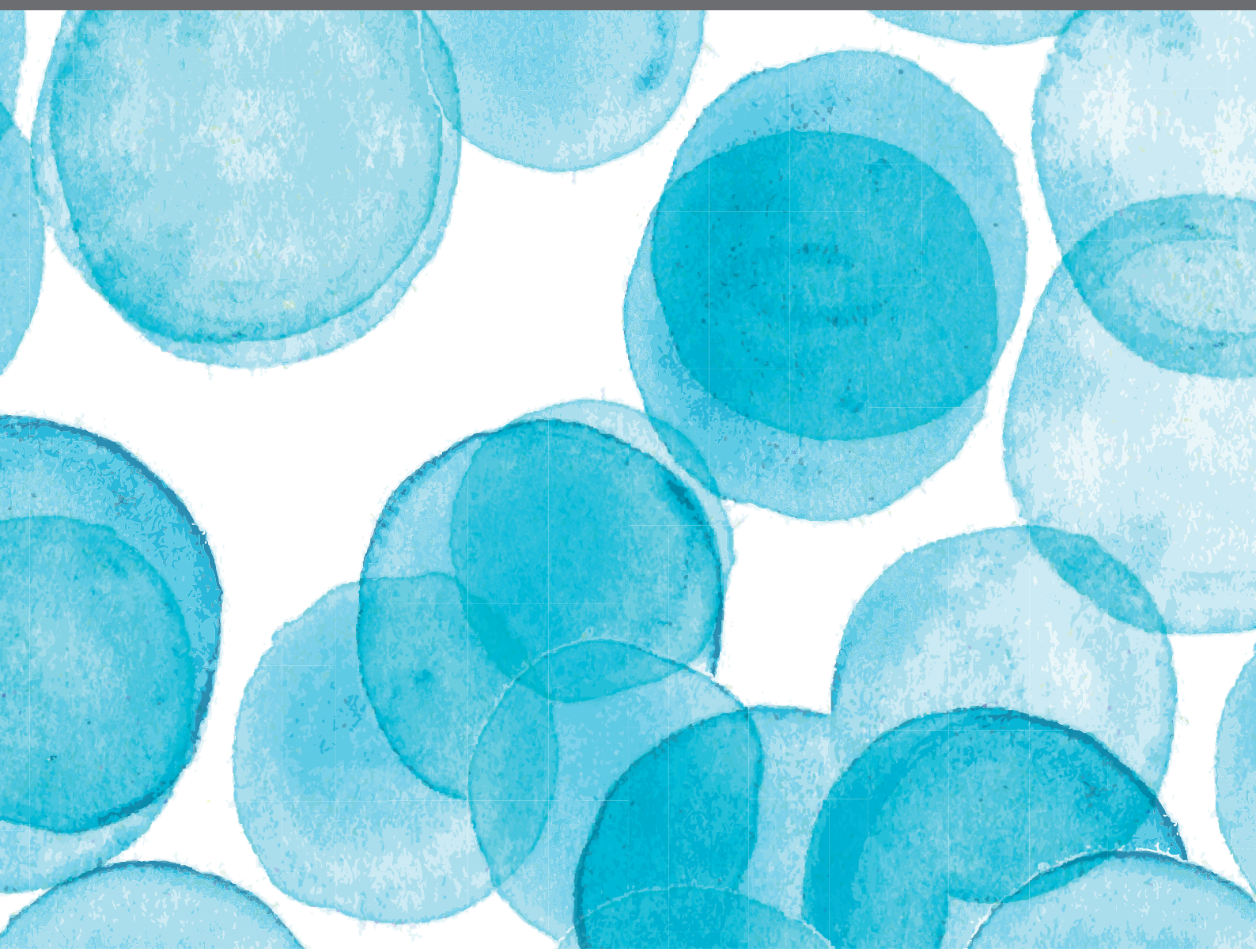

frontiers Research Topics

ISSN 1664-8714
ISBN 978-2-88976-580-5
DOI 10.3389/978-2-88976-580-5

About Frontiers

Frontiers is more than just an open-access publisher of scholarly articles: it is a pioneering approach to the world of academia, radically improving the way scholarly research is managed. The grand vision of Frontiers is a world where all people have an equal opportunity to seek, share and generate knowledge. Frontiers provides immediate and permanent online open access to all its publications, but this alone is not enough to realize our grand goals.

Frontiers Journal Series

The Frontiers Journal Series is a multi-tier and interdisciplinary set of open-access, online journals, promising a paradigm shift from the current review, selection and dissemination processes in academic publishing. All Frontiers journals are driven by researchers for researchers; therefore, they constitute a service to the scholarly community. At the same time, the Frontiers Journal Series operates on a revolutionary invention, the tiered publishing system, initially addressing specific communities of scholars, and gradually climbing up to broader public understanding, thus serving the interests of the lay society, too.

Dedication to Quality

Each Frontiers article is a landmark of the highest quality, thanks to genuinely collaborative interactions between authors and review editors, who include some of the world's best academicians. Research must be certified by peers before entering a stream of knowledge that may eventually reach the public - and shape society; therefore, Frontiers only applies the most rigorous and unbiased reviews.
Frontiers revolutionizes research publishing by freely delivering the most outstanding research, evaluated with no bias from both the academic and social point of view. By applying the most advanced information technologies, Frontiers is catapulting scholarly publishing into a new generation.

What are Frontiers Research Topics?

Frontiers Research Topics are very popular trademarks of the Frontiers Journals Series: they are collections of at least ten articles, all centered on a particular subject. With their unique mix of varied contributions from Original Research to Review Articles, Frontiers Research Topics unify the most influential researchers, the latest key findings and historical advances in a hot research area! Find out more on how to host your own Frontiers Research Topic or contribute to one as an author by contacting the Frontiers Editorial Office: frontiersin.org/about/contact

MULTI-OMICS STUDY ON GUT MICROBIOTA RELATED TO FAECAL MICROBIOTA TRANSPLANTATION

Topic Editors:
Zhangran Chen, Xiamen University, China
Yanling Wei, Army Medical University, China
Jialiang Yang, Geneis (Beijing) Co. Ltd, China
Leyi Wang, University of Illinois at Urbana-Champaign, United States
Zeyou Chen, Nankai University, China

Citation: Chen, Z., Wei, Y., Yang, J., Wang, L., Chen, Z., eds. (2022). Multi-omics Study on Gut Microbiota Related to Faecal Microbiota Transplantation. Lausanne: Frontiers Media SA. doi: 10.3389/978-2-88976-580-5

Table of Contents

frontiers | Frontiers in Microbiology

EDITORIAL
published: 22 June 2022
doi: 10.3389/fmicb.2022.944879

Editorial: Multi-Omics Study on Gut Microbiota Related to Faecal Microbiota Transplantation

*Jingtong Wu[1], Leyi Wang[2], Yanling Wei[3], Jialiang Yang[4], Zeyou Chen[5], Pei Hao[1], Yinyin Lv[1], Min Wang[6], Feng Liao[7], Longgang Chang[7], Yanmin Liu[6] and Zhangran Chen[1,6,7]**

[1] Department of Gastroenterology, Zhongshan Hospital Affiliated to Xiamen University, Xiamen, China, [2] Veterinary Diagnostic Laboratory, College of Veterinary Medicine, University of Illinois, Urbana, IL, United States, [3] Department of Teaching Support, Army Medical University, Chongqing, China, [4] Geneis (Beijing) Co., Ltd., Beijing, China, [5] College of Environmental Science and Engineering, Nankai University, Tianjin, China, [6] Inner Mongolia Shuangqi Pharmaceutical Co., Ltd., Huhhot, China, [7] Shenzhen Wedge Microbiology Research Co., Ltd., Shenzhen, China

Keywords: gut microbiota, faecal microbiota transplantation, probiotics, disease pathogenesis, COVID-19, metabolic disorders

Editorial on the Research Topic

Multi-Omics Study on Gut Microbiota Related to Faecal Microbiota Transplantation

OPEN ACCESS

Edited by:
George Tsiamis, University of Patras, Greece

Reviewed by:
Vassiliki Karapapa, Municipality of Agrinio, Greece

***Correspondence:**
Zhangran Chen
zhangran22105@163.com

Specialty section:
This article was submitted to Systems Microbiology, a section of the journal Frontiers in Microbiology

Received: *16 May 2022*
Accepted: *30 May 2022*
Published: *22 June 2022*

Citation:
Wu J, Wang L, Wei Y, Yang J, Chen Z, Hao P, Lv Y, Wang M, Liao F, Chang L, Liu Y and Chen Z (2022) Editorial: Multi-Omics Study on Gut Microbiota Related to Faecal Microbiota Transplantation. Front. Microbiol. 13:944879. doi: 10.3389/fmicb.2022.944879

With the advancement of multi-omics technology and experimental animal models, researchers have gained extensive information regarding the varied disease types associated with gut microbiota dysbiosis, and the causal role of gut microbiota in disease progression. As an emerging disease intervention way, faecal microbiota transplantation (FMT) has consistently demonstrated its potential in other diseases such as inflammatory bowel disease (IBD), irritable bowel syndrome (IBS), slow transit constipation, hepatic encephalopathy, autism, and metabolic syndrome more than recurrent *Clostridium difficile* infection (rCDI). However, many points remained to be further revealed in the FMT procedures. For example, it is necessary to screen and determine the healthy microbiome of stool donors to monitor the safety and efficacy of FMT. It is also important to reveal the mechanism for the efficacy of adopting FMT, which may supply a better footprint for the precise application of FMT. It is also worthy to note that other forms of microbiota transplantation besides FMT, are also promising.

This current Research Topic brings 11 references together summarizing the recent developments covering, the potential relevance of gut dysbiosis in the progression of diseases, technology and practical application of FMT.

Regarding the potential relevance of gut dysbiosis in the progression of diseases, six articles in this Research Topic individually mentioned the association of gut microbiota with drug resistances, appendectomy, age-related macular degeneration (AMD), encephalopathy caused by microbial infection, neonatal health, and obesity. Previous research showed that resistant bacteria displayed metabolic slowdown, while the molecular mechanism remains poorly understood. Through comparative proteomics analysis, Shen et al. identified nine genes involved in metabolism pathways significantly associated with MICs of amikacin/cotrimoxazole, which suggests that alteration of the metabolic network was directly correlated with antibiotic resistance. Increasing evidence has revealed that the human appendix plays important biological roles in regulating the intestinal immune system and microbiome. Cai et al. explored the alterations of gut bacterial and fungal communities associated with appendectomy in 60 subjects and found that the effects of appendectomy on the fecal fungal community are more marked and durable than on bacteria.

Sepsis-associated encephalopathy (SAE) is defined as diffuse brain dysfunction without the central nervous system (CNS) infection in sepsis patients. Zhao et al. investigated the predictors associated with hospital mortality in patients with SAE and established a comprehensive visual predictive nomogram of hospital mortality, which performed better than the SAPS II with a higher net benefit. Li et al. characterized fecal microbiome and metabolomics profiles in a mouse model of laser-induced Choroidal neovascularization (CNV) and identified that Lachnospiraceae_UCG-001 and Candidatus_*Saccharimonas*, were strongly correlated with altered fecal metabolites, which might help develop novel therapeutic strategies of nAMD. Modulating the gut microbiota may be an effective strategy for alleviating obesity and related metabolic disorders. Xin et al. developed a feasible freeze-thaw pretreatment protocol to improve the extraction of microbial DNA from meconium, which would help researchers that aim to investigate the gut microbiota characteristics associated with neonatal diseases. Zou et al. evaluated the anti-obesity effects of ginsenoside Rb1 in HFD-fed mice and found the multiscale mechanisms that might account for the therapeutic effect of Rb1 against obesity. Due to the accumulating data, it is necessary to conduct computational methods for potential microbe–disease association prediction, Yang et al. constructed a comprehensive microbe–disease network by integrating known microbe–disease associations from three novel large-scale databases and extended the random walk with restart (RWR) to the network for prioritizing candidate disease-related microbes. The results suggested that it is an effective method for prioritizing novel disease-related microbes, thereby aiding our understanding of disease pathogenesis.

The selection of reliable healthy donors is a critical success factor of FMT while screening and determining the health status are involved with assessments, including health questionnaires, clinical evaluation, stool testing, blood testing, and gut microbiota test. Yu et al. developed an artificial intelligence (AI) model to identify patients who were positive for COVID-19 according to the results of the first CT examination after admission and predict the progression combined with laboratory findings, which might help efficiently exclude those subjects with COVID-19 for donor check. Although FMT is applied in constipated patients, yet the underlying mechanism remains unclear. Zhang et al. evaluated the clinical efficacy and gut microbiota remodeling ability of FMT and found the efficacy of FMT for treating constipation might be correlated with the abundance of key bacteria such as *Fusicatenibacter* and *Paraprevotella*, and butyrate production. Intestinal dysbiosis, which refers to loss of microbiome diversity and structure homeostasis in the intestine, has been proven to be associated with premature infant necrotizing enterocolitis (NEC). Lin et al. found that NEC is characterized by metabolism dysregulation, FMT and sulperazone combination treatment showed the highest benefits for the NEC. Inspired by the similarity of the intestinal and vaginal microbiota, the success of FMT inspired vaginal microbiota transplantation (VMT) proposed for the treatment of vaginal dysbacteriosis. Safe, standard, and efficient VMT will bring new hope to patients with gynecological diseases and have a good prospect of application (Han et al.).

Overall, this Research Topic provides readers with the potential relevance of gut dysbiosis in the progression of diseases, technology and practical application of FMT. However, the current Research Topic has a few limitations. Half of the accepted papers are still involved in investigating the relationship between host disease and gut microbiota, which somewhat deviate from the original intention to include more FMT-related Research Topics. And there seems to be few deep discussion concerning the mechanism of how FMT play the roles. More clinical research should be carried out to support the new therapeutic strategies targeting gut microbiota through FMT. Metagenomics, metabolomics, cultivating omics, and other omics, combined with high-throughput analysis are needed to identify the exact cross-links between host disease and gut microbiota associated with FMT.

AUTHOR CONTRIBUTIONS

JW, PH, YLv, MW, FL, LC, YLi, and ZC wrote and revised this article. LW, YW, JY, and ZC help co-edit the Research Topic. All authors made a substantial, direct, and intellectual contribution to this work and approved it for publication.

FUNDING

This work was supported by grants from the National Natural Science Foundation of China (Grant No. 81900541).

ACKNOWLEDGMENTS

We greatly appreciate the contributions to this Research Topic by all authors and reviewers. We also thank all the guest associated editors of the Research Topic, and the Editorial board of the journal of Frontiers, for their support.

Conflict of Interest: JY was employed by Geneis (Beijing) Co., Ltd. MW, YLi, and ZC were employed by Inner Mongolia Shuangqi Pharmaceutical Co., Ltd. FL, LC, and ZC were employed by Shenzhen Wedge Microbiology Research Co., Ltd.

The remaining authors declare that the research was conducted in the absence of any commercial or financial relationships that could be construed as a potential conflict of interest.

Publisher's Note: All claims expressed in this article are solely those of the authors and do not necessarily represent those of their affiliated organizations, or those of the publisher, the editors and the reviewers. Any product that may be evaluated in this article, or claim that may be made by its manufacturer, is not guaranteed or endorsed by the publisher.

frontiers in Microbiology

REVIEW
published: 18 June 2021
doi: 10.3389/fmicb.2021.643422

Role of Vaginal Microbiota Dysbiosis in Gynecological Diseases and the Potential Interventions

Yiwen Han[1,2], *Zhaoxia Liu*[1]* *and Tingtao Chen*[1,3]*

[1] Department of Obstetrics and Gynecology, The Second Affiliated Hospital of Nanchang University, Nanchang, China, [2] Queen Mary School, Nanchang University, Nanchang, China, [3] National Engineering Research Center for Bioengineering Drugs and the Technologies, Institute of Translational Medicine, Nanchang University, Nanchang, China

Vaginal microbiota dysbiosis, characterized by the loss of *Lactobacillus* dominance and increase of microbial diversity, is closely related to gynecological diseases; thus, intervention on microbiota composition is significant and promising in the treatment of gynecological diseases. Currently, antibiotics and/or probiotics are the mainstay of treatment, which show favorable therapeutic effects but also bring problems such as drug resistance and high recurrence. In this review, we discuss the role of vaginal microbiota dysbiosis in various gynecological infectious and non-infectious diseases, as well as the current and potential interventions.

OPEN ACCESS

Edited by:
Yanling Wei,
Army Medical University, China

Reviewed by:
Valentina Taverniti,
University of Milan, Italy
Wenkai Ren,
South China Agricultural University, China

***Correspondence:**
Tingtao Chen
chentingtao1984@163.com
Zhaoxia Liu
lzxia77@163.com

Specialty section:
This article was submitted to Systems Microbiology, a section of the journal Frontiers in Microbiology

Received: *24 February 2021*
Accepted: *19 May 2021*
Published: *18 June 2021*

Citation:
Han Y, Liu Z and Chen T (2021) Role of Vaginal Microbiota Dysbiosis in Gynecological Diseases and the Potential Interventions. Front. Microbiol. 12:643422. doi: 10.3389/fmicb.2021.643422

Keywords: vaginal microbiota transplantation, bacterial vaginitis, antibiotics, *Lactobacillus*, gynecological diseases

INTRODUCTION

The vagina is an important and complex ecosystem, dominated by *Lactobacillus*, but also containing a small number of fungi and parasites, and the balanced microbial communities are vital for female health (Bradford and Ravel, 2017; Gupta et al., 2019). However, the microbial balance can be disrupted and leads to various infectious diseases, characterized by overgrowth of anaerobic bacteria (agent of bacterial vaginitis and atrophic vaginitis, BV and AV) and *Candida albicans* (agent of vulvovaginal candidiasis, VVC), and infections of *Trichomonas vaginalis* (agent of trichomonal vaginitis), *Neisseria gonorrhoeae* (agent of gonorrhea), *Mycoplasma genitalium* (agent of cervicitis), *Chlamydia trachomatis* (agent of pelvic inflammatory disease, PID), and various viruses including human papillomavirus (HPV, agent of cervical cancer), herpes simplex virus-2 (HSV-2, agent of genital ulcers), and human immunodeficiency virus (HIV, agent of acquired immunodeficiency syndrome, AIDS) (Gupta et al., 2019). In addition, some non-infectious diseases, e.g., induced abortions (with BV microbiome, etc.), intrauterine adhesions (IUA, with reduced *Lactobacillus* and increased *Gardnerella*, *Prevotella*, etc.), miscarriage (with BV microbiome), preterm (with BV microbiome), infertility (with BV microbiome), polycystic ovarian syndrome (PCOS, with reduced *Lactobacillus crispatus*, and increased *mycoplasma* and *Prevotella*), uterine fibroid (with increased *Lactobacillus iners*), and menstrual disorders (with increased uterine *Gardnerella*, *Prevotella*, *Sneathia*, and *Veillonella*), also show associations with microbial dysbiosis (Hay, 2004; Chen et al., 2017; Pelzer et al., 2018; Liu et al., 2019; Hong et al., 2020a,b), posing a serious threat to women's reproductive health.

At present, the most conventional treatment strategy for microbial disorders is antibiotics (metronidazole, clotrimazole, azithromycin, etc.), which has a good therapy effect while accompanied with various adverse effects and recurrence (Cudmore et al., 2004; Bradshaw et al., 2006; Xie et al., 2017; Khosropour et al., 2018; Paez-Canro et al., 2019). Recently, probiotics based on *Lactobacillus* have shown promise in treating not only infectious diseases (e.g., BV, fungal infection,

and urinary tract infections) but also non-infectious diseases (e.g., preterm, infertility, and PCOS) (Hanson et al., 2016; Lopez-Moreno and Aguilera, 2020). However, the treatment outcome of probiotics is usually mixed, which may be due to the fact that these diseases are usually caused by multiple microbes rather than one. Excitingly in 2019, Ahinoam et al. conducted a clinical study of vaginal microbiota transplantation (VMT) in five patients with recurrent BV, finding that four of them achieved long-term remission and established a long-term vaginal microbiota dominated by *Lactobacillus* (Lev-Sagie et al., 2019). Therefore, intervention on vaginal microbiota is significant and promising in treating gynecological diseases. Thus, in this review, we elaborated the role of microbiota dysbiosis in various gynecological infectious and non-infectious diseases, and the current and potential interventions.

VAGINA AND VAGINAL MICROBIOTA

The vagina is a stretchable, muscular duct connecting the uterus and external genitalia, and is responsible for the physiological functions of female sexual intercourse, menstrual discharge, and delivery of the fetus (Farage and Maibach, 2006). Its mucosal system, consisted of a stratified squamous epithelium and cervicovaginal fluid (CVF), is vital in maintaining vaginal health by immune response, antimicrobial products (e.g., B-defensin), finely balanced microbial communities, etc. (Torcia, 2019). Among these, the vaginal microbiota is the most changeable and vulnerable one in response to internal and external stimulus (Gajer et al., 2012).

Recently, the detailed composition and relative abundance of vaginal microbiota has been determined by high-throughput 16s rRNA sequencing, characterizing five microbial community state types (CST) in asymptomatic women (Ravel et al., 2011). Four of them (CST-I, II, III, V) were dominated by *Lactobacillus* species, while CST-IV was heterogenous and polymicrobial, characterized by lower level of *Lactobacillus* and higher level of anaerobic bacteria including *Gardnerella*, *Atopobium*, *Mobiluncus*, *Prevotella*, *Streptococcus*, *Mycoplasma*, and *Ureaplasma* (Ravel et al., 2011). At present, over 140 *Lactobacillus* species have been identified, but the only species that normally dominate the vaginal microbiota are *L. crispatus*, *Lactobacillus gasseri*, *Lactobacillus jensenii*, and *L. iners* (Smith and Ravel, 2017). They are considered as keystones of vaginal health, as they can produce lactic acid, hydrogen peroxide, and bacteriocins, maintaining acidic environment and preventing pathogen growth (Gupta et al., 2019); adhere to epithelium, repelling other bacteria adhesion (Torcia, 2019); and regulate immune and inflammatory response, enhancing the resistance of vagina to diseases (Aldunate et al., 2015). Thus, *Lactobacillus* dominance is generally considered as a hallmark of healthy vagina (Ma et al., 2012).

It is generally known that vaginal microbiota disturbance is highly related to various gynecological diseases, especially BV, which is characterized by the alteration of vaginal microbiome from *Lactobacillus* dominance to anaerobic and facultative bacteria (*Gardnerella*, *Atopobium*, *Prevotella*, *Megasphaera*, *Leptotrichia*, *Sneathia*, etc.) dominance (Ling et al., 2010; Srinivasan et al., 2012; Nasioudis et al., 2017). BV has been shown to be associated with various other reproductive tract disorders, including infertility, preterm, cervical cancer, and HIV acquisition (Leitich and Kiss, 2007; van Oostrum et al., 2013; Torcia, 2019). It is also reported that many sextually transmitted infections (STI), such as infections of *N. gonorrhoeae* and *C. trachomatis*, are facilitated by vaginal microbiota dysbiosis and more prevalent in BV-positive women (Lewis et al., 2017). In addition, as the microbiota research progresses intensively, a growing number of studies have linked vaginal microbiota dysbiosis to various gynecological non-infectious diseases, among which Liu et al. found that compared with healthy people, IUA patients had lower percentage of *Lactobacillus*, and higher percentage of *Gardnerella* and *Prevotella* (Liu et al., 2019); Hong et al. found that patients with PCOS had lower *Lactobacillus* and higher *Mycoplasma* and *Prevotella* than controls (Hong et al., 2020b); and Chen et al. found that *Lactobacillus* were less abundant, while *L. iners* were more abundant in patients with uterine fibroid than individuals without (Chen et al., 2017).

Therefore, as the balanced vaginal microbiota plays a significant role in female health, interventions aimed at restoring the healthy microbiota composition can be a good and reasonable therapy for gynecological diseases.

ROLE OF MICROBIOTA DYSBIOSIS IN INFECTIOUS DISEASES AND INTERVENTIONS

Until now, infection is one of the leading causes of gynecological disease, which is usually characterized by vaginal dysbiosis (van de Wijgert and Jespers, 2017). Below, we introduce the common infectious diseases, including common vaginitis, viral infections, and other infections, and discuss the therapy effects of restoring *Lactobacillus*-dominated vaginal microbiota by antibiotic and probiotic interventions (**Figure 1**).

Microbiota Dysbiosis and Interventions in Common Vaginitis

Microbiota Dysbiosis in BV and Interventions

Bacterial vaginitis is the most common lower genital tract disease among fertile women and can predispose women to various STI and adverse birth outcome (Lewis et al., 2017). It mainly manifests as mucosal inflammation including abnormal vaginal discharge (increased, yellowish, and fishy odor) and sensation of itching and burning (Onderdonk et al., 2016). Currently, the routine treatment is oral and intravaginal antibiotics, usually clindamycin and metronidazole (Faught and Reyes, 2019). However, long-term use of antibiotics is likely to develop antimicrobial resistance and cause recurrent infections (Lev-Sagie et al., 2019).

Studies showed that BV is caused by replacement of *Lactobacillus* dominance by multiplication of over 10 anaerobic bacteria, such as *Gardnerella*, *Atopobium*, *Prevotella*, *Megasphaera*, *Leptotrichia*, and *Sneathia*, and probiotics based on

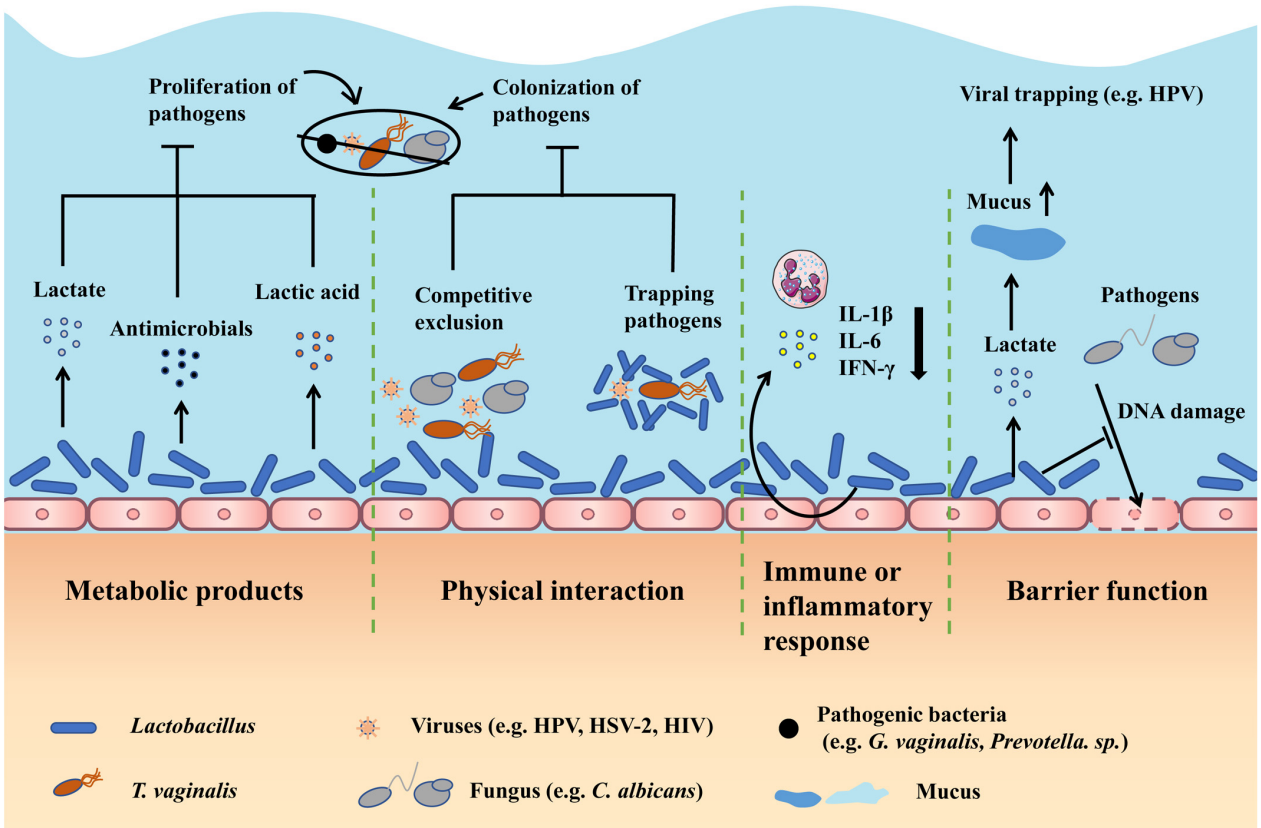

FIGURE 1 | Therapy effects of restoring *Lactobacillus*-dominated vaginal microbiota in infectious diseases. First, *Lactobacillus* can produce metabolites including lactate, antimicrobials, and lactic acid to inhibit the proliferation of pathogens. Second, *Lactobacillus* can competitively exclude pathogens from adhering to epithelium and trap pathogens by direct physical contact to prevent the colonization of pathogens. Third, *Lactobacillus* can regulate the immune or inflammatory response, particularly relieving the inflammation by decreasing cytokines like IL-1β. Fourth, *Lactobacillus* can improve the barrier function by producing lactate, which can increase the mucus viscosity to facilitate viral trapping, and inhibiting pathogens from damaging the DNA of epithelial cells. DNA, deoxyribonucleic acid.

Lactobacillus that used to regulate microbiota have been revealed beneficial in treating BV (Nasioudis et al., 2017; Wang et al., 2019). *In vitro* and clinical studies showed that *Lactobacillus* could reduce the pathogen colonization by preventing the pathogen adhering to epithelium (Ma et al., 2019), inhibit the pathogen growth by producing bacteriocins (Ma et al., 2019), maintain the acidic environment by generating lactic acid (Kim and Park, 2017), and relieve inflammatory response, in particular significantly reduce IL-1β and IL-6 cytokines (Hemalatha et al., 2012). Thus, antibiotics with probiotics can effectively cure BV by correcting the vaginal microbiota and improving the vaginal environment.

Microbiota Dysbiosis in VVC and Interventions

Vulvovaginal candidiasis is the most common vaginal fungal infection and typically manifests as mucosal inflammation, including cheese-like vaginal discharge, and vulvovaginal burning, itching, and redness (Sobel, 1992). The standard treatment for VVC is antifungal agents, including oral or intravaginal azole or triazole drugs, which can achieve over 80% cure rate (Nurbhai et al., 2007; Sobel and Sobel, 2018). However, the concomitant side effects (diarrhea, abnormal urination, and vaginal burning, itching, and irritation), drug resistance, and high recurrence rate hinder the recovery and pose a threat to health (Xie et al., 2017).

Studies showed that VVC primarily occurred during vaginal dysbiosis and immune deficiency, and was caused by overgrowth of *C. albicans*, which could cause epithelium destruction by destroying the intercellular linkage and intracellular mitochondrial structure, and elicit inflammation, in particular produce IL-6 and IL-8 cytokines (Niu et al., 2017; Li et al., 2019). As protective *Lactobacillus* can regulate the host immune response, inhibit the proliferation of *C. albicans* by producing metabolites such as lactate, and prevent the colonization of *C. albicans*, therapies aimed at adjusting microbiota can help in VVC recovery (Bradford and Ravel, 2017). *In vivo* study on VVC showed that *Lactobacillus* could regulate the immune response by decreasing T-helper 1 (Th1) cell/Th2 cell ratio and inhibiting the release of proinflammatory cytokines such as interleukin 17 (IL17) and interferon-γ (IFN-γ) (Li et al., 2019). Another *in vitro* study investigated the ability of *L. crispatus* to inhibit *C. albicans* infecting vaginal epithelial cells VK2/E6E7, and found that *L. crispatus* could significantly reduce the adherence of *C. albicans* to VK2/E6E7 cells (Niu et al., 2017). Besides,

many studies suggested that *Lactobacillus* could exert direct antifungal effects by releasing antimicrobials, improving the epithelial barrier by decreasing DNA damage of epithelial cells, and improving the microbiota to prevent *C. albicans* overgrowth and VVC recurrence (Mc and Rosenstein, 2000; Reid et al., 2003; Strus et al., 2006; Yeh et al., 2007). Consequently, antibiotics with probiotics can treat VVC and prevent its onset by improving microbial, inflammatory, and epithelial status.

Microbiota Dysbiosis in Trichomonal Vaginitis and Interventions

Trichomonal vaginitis, which manifests as painful and itching coitus, frothy discharge, and vaginal or cervical bleeding, is the most common STI worldwide and closely linked to PID and infertility (Pastorek et al., 1996; Petrin et al., 1998; Harp and Chowdhury, 2011; Edwards et al., 2016). Currently, the standard treatment for Trichomonal vaginitis is metronidazole or tinidazole, which not only are quite effective but also develop drug resistance (Muzny and Schwebke, 2013; Phukan et al., 2018).

The etiology of trichomonal vaginitis is *T. vaginalis*, which is a flagellated parasite of human genital tract that can cause severe damage to epithelial cells by mediating the lysis of epithelial cells, and elicit the inflammatory response, involving recruitment of neutrophils to infected tissues (Fichorova et al., 2006; Edwards et al., 2016). Studies showed that BV, especially with lack of *Lactobacillus*, could protect *T. vaginalis* from nucleic acid degradation through the production of polyamines and form biofilms to reduce drug sensitivity, thus facilitating *T. vaginalis* infection and increasing drug resistance (Figueroa-Angulo et al., 2012; Balkus et al., 2014; Jung et al., 2017). Therefore, it is suggested that restoring the vaginal microbiota can improve the anti-trichomoniasis treatment effect. A randomized clinical study showed that patients taking probiotics in addition to metronidazole showed earlier clinical resolution compared with the patients taking placebo. Besides, reduced leukocyte/epithelial cell ratio, decreased pH, and increased redox potential of the vaginal fluid were detected in the probiotic group, underlining the beneficial mechanisms of *Lactobacillus* to relieve inflammation, inhibit *T. vaginalis* growth, and damage T. vaginalis DNA, respectively (Sgibnev and Kremleva, 2020). Another *in vitro* study showed that the aggregation-promoting factor (APF)-2 of *L. gasseri* could significantly inhibit the adhering of *T. vaginalis* to human vaginal ectocervical cells (Phukan et al., 2018). Thus, antibiotics with probiotics can prevent and treat *T. vaginalis* infection via adjusting vaginal microbiota, inhibiting *T. vaginalis* growth, relieving inflammation, and preventing *T. vaginalis* colonization.

Microbiota Dysbiosis in AV and Interventions

Atrophic vaginitis, caused by the reduction of estrogen and local immunity after menopause, is prevalent among postmenopausal women and is characterized by vulvovaginal dryness, dyspareunia, abnormal vaginal discharge, etc. (Stika, 2010). At present, the treatment principles of AV are giving estrogen to improve the vaginal immunity, and antibiotics (norfloxacin) to inhibit the pathogen growth (Paladine and Desai, 2018).

Estrogen deficiency in menopause leads to vaginal atrophy, resulting in reduced epithelial barrier function and facilitation of pathogen colonization (Jaisamrarn et al., 2013). Brotman et al. (2014) showed that women with AV had lower level of *Lactobacillus* and increased bacterial diversity, involving *Anaerococcus*, *Peptoniphilus*, *Prevotella*, and *Streptococcus*. Since *Lactobacillus* has been shown to improve the overall vaginal environment such as the vaginal immunity and epithelial barrier, probiotics have been used in combination with estrogen to treat AV. A randomized clinical study showed that long-term use of this combination was sufficient to improve the related clinical parameters, maintain the improved maturation of vaginal epithelium, and prevent symptomatic AV relapse (Jaisamrarn et al., 2013). Besides, it is suggested that *Lactobacillus*-dominated vaginal microbiota is significant in protecting postmenopausal women from AV and is considered to be a marker of successful AV treatment (Shen et al., 2016). Thus, antibiotics and probiotics can be used in combination with estrogen to prevent and treat AV by improving the vaginal microbiota and enhancing the epithelial barrier function and the overall vaginal environment.

Microbiota Dysbiosis and Interventions in Viral Infection

Genital HPV, especially HPV-16 and 18 strains, are common sextually transmitted viruses and major causes of cervical cancer (Stanley, 2010). Though over 50% of HPV infections are cleared within a half year, persistent infections can cause symptoms including abnormal vaginal bleeding such as sextual intercourse bleeding, and abnormal vaginal discharge (Mitra et al., 2016; Kashyap et al., 2018). Conventional treatments for cervical cancer include surgery, chemotherapy, and radiotherapy, but they cannot prevent recurrence and have various side effects, such as menstrual change and vaginal pain (Waggoner, 2003).

Studies showed that vaginal microbiota disturbance with reduced *Lactobacillus* and increased microbial diversity was closely linked to HPV infection pathogenesis (Mitra et al., 2016). A cohort study of 32 sextually active American women showed that women with high level of *Atopobium*, *Prevotella*, and *Gardnerella* were most likely to be infected with HPV and had the slowest viral clearance (Brotman et al., 2014). Besides, CST-IV bacteria were shown to increase the severity of cervical lesions, promote the neoplastic progression by producing nitrosamines and ROS to induce DNA damage, and facilitate HPV infection by damaging the barrier and eliciting chronic inflammation (Mhatre et al., 2012; Borgdorff et al., 2016; Piyathilake et al., 2016). Thus, improving the microbiota composition is a feasible approach to prevent and treat HPV infection. A semi-randomized study of 54 HPV infected women showed that women treated with oral *Lactobacillus caseii* had greater clearance of HPV infection and cervical lesions than untreated patients (Verhoeven et al., 2013). Mitra et al. reviewed the currently accepted mechanisms of *Lactobacillus*-mediated protection to cervical health and showed that low vaginal pH (which could decrease around 10% risk of HPV positivity), lactate (which could increase the vaginal mucus viscosity and enhance the viral trapping), and bacteriocins (which could directly interfere the pathogen growth) were significant

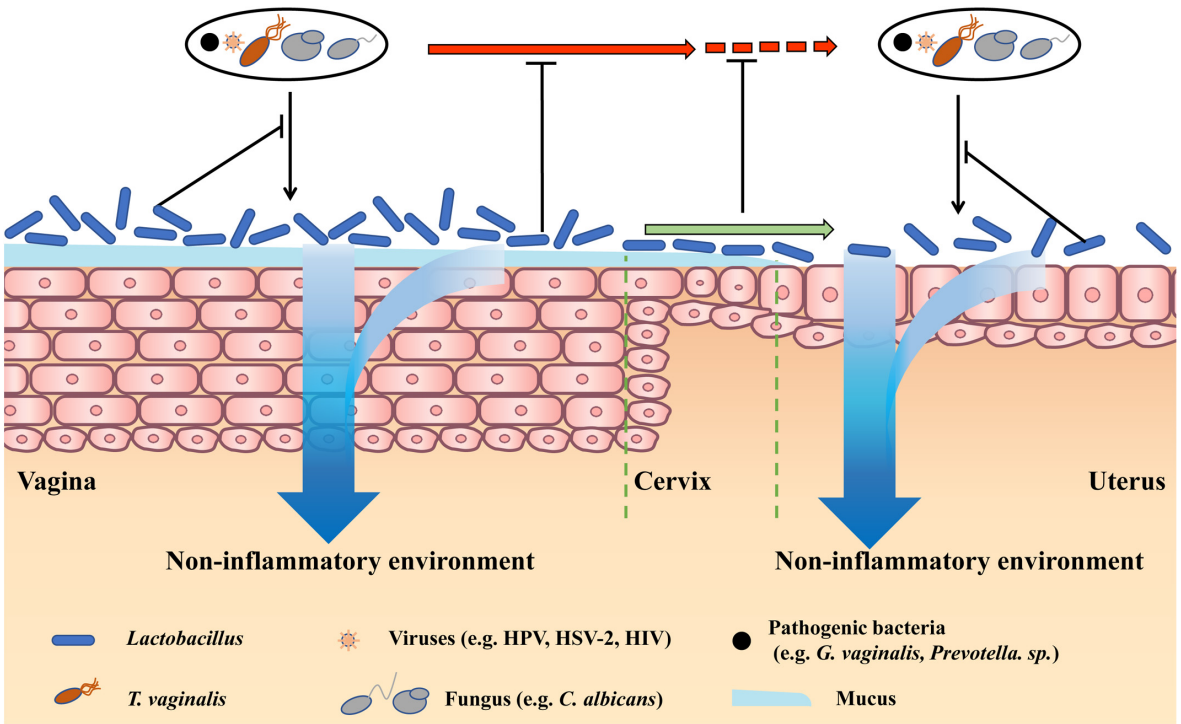

FIGURE 2 | Therapy effects of restoring *Lactobacillus*-dominated vaginal microbiota in non-infectious diseases. *Lactobacillus*-dominated vaginal microbiota cannot only benefit vaginal health by preventing vaginal infections and creating a non-inflammatory environment but also prevent pathogens in the vagina moving to the cervix and uterus. Besides, vaginal *Lactobacillus* can move to the upper reproductive tract, preventing pathogens infecting the cervix and uterus, and creating a non-inflammatory cervical and uterine environment.

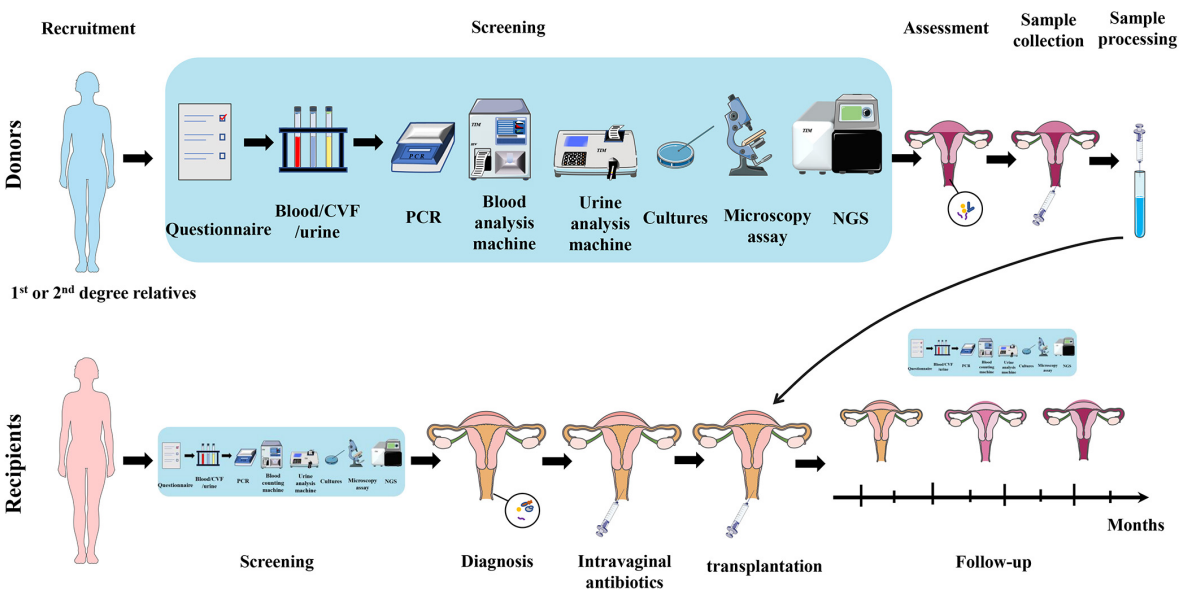

FIGURE 3 | Schematic diagram of VMT operation. As for donors, first, donors are recruited, preferably from the recipients' first and second relatives. Second, collect blood/CVF/urine samples of donors and conduct a series of screening by questionnaire, PCR, blood, and urine analysis machines, cultures, microscopy, and NGS. Third, collect CVF sample from qualified healthy donor and process it. It is then transplanted into the recipient's vagina. As for recipients, first, recipients undergo the same screening process for diagnosis and basic health assessment. Second, recipients are given intravaginal antibiotics to prepare for transplantation. Third, transplant the prepared CVF solution from healthy donor into the recipient's vagina. Fourth, follow-up studies are carried out on recipients to assess the treatment outcome and adverse effects. VMT, vaginal microbiota transplantation; CVF, cervicovaginal fluid; PCR, polymerase chain reaction; NGS, next-generation sequencing.

protective principles, and improvement in local immunity and inflammation was also suggested (Mitra et al., 2016). In addition, Palma et al. (2018) explored the effects of long- and short-term probiotic implementation in clearing HPV infection, and they found that patients with long-term probiotic treatment had significantly higher viral clearance rate, suggesting that long-term healthy vaginal microbiota was required to exert the optimal treatment effect. Therefore, antibiotics and probiotics can prevent and aid treatment of HPV infection by improving the microbial balance.

Other common viral agents that infect the reproductive tract are HSV-2 and HIV, which can cause genital ulcers and AIDS, respectively. Since these viruses cannot be completely eliminated by traditional antiviral therapy, prevention is particularly important for health maintenance. Studies showed that vaginal dysbiosis, especially BV, and lack of *Lactobacillus* could facilitate HSV-2 infection, and a protective vaginal microbiota could prevent and counteract HSV-2 infection by inhibiting HSV-2 replication, producing antimicrobials, and trapping HSV-2 particles (Cherpes et al., 2003; Evans et al., 2003; Conti et al., 2009; Mousavi et al., 2018; Torcia, 2019). As for HIV, many studies showed that women with CST-IV bacteria had a higher HIV infection rate than women with CST-I bacteria, and a *Lactobacillus*-dominated vaginal microbiota could protect the vagina from HIV infection by maintaining acidic environment, producing lactic acid, and reducing the viability of HIV particles (Gosmann et al., 2017; Nahui Palomino et al., 2017). Therefore, antibiotics with probiotics can prevent HIV and HSV-2 infection by correcting the microbial disturbance and creating an unfavorable vaginal environment for viruses.

Microbiota Dysbiosis and Interventions in Other Infections

Neisseria gonorrhoeae, the causative agent of gonorrhea, is continuously developing resistance to antimicrobial treatment (ceftriaxone and azithromycin) and impedes the recovery (Morgan and Decker, 2016; Unemo et al., 2019). An *in vitro* study showed that *Lactobacillus* could significantly reduce *Neisseria gonococcus* viability by creating acidic environment, producing bacteriocins, releasing biosurfactants, and co-aggregating with gonococci, and reduce gonococci adhering to epithelial cells (Foschi et al., 2017). Thus, probiotics can be an adjuvant therapy of antibiotics to treat *N. gonorrhoeae* infection by improving the vaginal microbiota.

Mycoplasma genitalium is a sextually transmitted pathogen that can lead to PID and cervicitis (Cazanave et al., 2012; Onderdonk et al., 2016), and its first line treatment with antibiotics (doxycycline and azithromycin) is compromised by drug resistance (Pinto-Sander and Soni, 2019). Studies showed that BV could favor *M. genitalium* infection (Brotman et al., 2010; Molenaar et al., 2018), and a protective vaginal microbiota dominated by *Lactobacillus* could counteract the infection by producing antimicrobials and maintaining acidic environment (Molenaar et al., 2018). Therefore, probiotics with antibiotics can prevent and treat *M. genitalium* infection by adjusting the microbial structure and improving the vaginal environment.

Chlamydia trachomatis is a common cause of PID (Haggerty et al., 2010; Mestrovic and Ljubin-Sternak, 2018), and its treatment with azithromycin or doxycycline also faces the challenge of antimicrobial resistance (O'Connell and Ferone, 2016; Zhang et al., 2017; Mestrovic and Ljubin-Sternak, 2018). *In vitro* studies showed that *Lactobacillus* could prevent *Chlamydia* colonization by maintaining acidic environment and consuming glucose (Nardini et al., 2016), inhibit *Chlamydia* multiplication at all infection stages, and inhibit the chronic infection by preventing the development of persistent *trachomatis* forms (Mastromarino et al., 2014). Therefore, antibiotics with probiotics can exert a conducive treatment effect on *C. trachomatis* infection by improving the vaginal microbiota.

ROLE OF MICROBIOTA DYSBIOSIS IN NON-INFECTIOUS DISEASES AND INTERVENTIONS

The role of microbiota in non-infectious gynecological diseases was long underestimated, until recently when mounting evidence showed its significance. Herein, we introduce the common non-infectious diseases that were caused by physical injury, fertility problems, and endocrine disorders, and discuss the treatment effects of restoring *Lactobacillus*-dominated vaginal microbiota by antibiotic and probiotic interventions (**Figure 2**).

Microbiota Dysbiosis and Interventions in Diseases Caused by Physical Injury

Induced abortion is a fairly common gynecological operation worldwide, and whether it is drug-induced or surgery-induced, it can cause a great damage to the female reproductive tract and predispose to serious complications such as incomplete abortion, heavy bleeding, infection, scarring of endometrium, adhesions of the uterine cavity and cervix, and endometriosis. Among these, upper genital tract infection is the most concerned and common clinical problem, which can further cause endometritis, salpingitis, and infertility (Mary and Mahmood, 2010; Carlsson et al., 2018).

Studies showed that postabortal infection was usually caused by pathogens from the lower genital tract, such as *Chlamydia*, *N. gonorrhoeae*, *Mycoplasma*, and BV-related bacteria, moving through the cervix to the uterus and even to fallopian tubes, causing infections and inflammation of the entire reproductive system (Bjartling et al., 2010). In this regard, World Health Organization (WHO) recommended the use of antibiotic prophylaxis to prevent the abortion-induced infection, and a meta-analysis of randomized clinical studies showed that perioperative antibiotics (metronidazole, nitroimidazoles, etc.) could effectively reduce the risk of postabortal infection by 50% (Sawaya et al., 1996; Carlsson et al., 2018). However, if the homeostasis of the uterus is not fully restored and is still conducive to microbial disorders, antibiotics cannot protect the women from being reinfected (Low et al., 2012). Therefore, as probiotics have a great potential in restoring the normal

vaginal microbiota and improving the uterine environment, perioperative use of antibiotics and probiotics can prevent the postabortal infection.

Intrauterine adhesions is a condition in which the scar tissues build up inside the uterine cavity, which in many cases will cause adhesion of the opposing endometrium (Chi et al., 2018). Though the adhesions can be removed through the transcervical resection, the postoperative recurrence is high (Pabuccu et al., 2008). A clinical study showed that IUA patients had disturbed vaginal microbiota, characterized by obviously reduced probiotic *Lactobacillus*, and increased pathogenic *Gardnerella* and *Prevotella*, which may promote the uterine pathology and cause recurrence (Liu et al., 2019). Therefore, antibiotics and/or probiotics can promote the recovery and reduce the recurrence of IUA by correcting the vaginal microbiota.

Microbiota Dysbiosis and Interventions in Diseases Caused by Fertility Problems

Miscarriage, defined as a spontaneous pregnancy loss before the expected point, is the most prevalent pregnancy complication (Smith et al., 2019). The etiology is multifactorial and usually secondary to other disorders, such as uterine malformation, infections, chromosomal abnormalities, and hormone deficiency (progestogen) (Haas et al., 2019). In this regard, the preventive and curative measures are always aimed at addressing the primary causes (Haas et al., 2019).

Previous studies showed that pregnant women with BV had around two-fold higher risk of miscarriage than those without BV, which was thought to be caused by ascending of the BV-related bacteria from the vagina to the uterus, leading to endometritis, deciduitis, chorioamnionitis, and amniotic fluid infection (Ralph et al., 1999; Goldenberg et al., 2000). Studies exploring the specific mechanisms of BV favoring miscarriage showed that BV-related bacteria could produce lytic enzymes (proteases, phospholipases, etc.) to cause lysis of the fetal membranes, and induce the formation of prostaglandin, which could promote the uterine muscle contraction, decrease the cervical resistance, and induce the release of metalloproteinases (MMPs) to degrade the chorioamniotic membranes (Isik et al., 2016). Besides, the level of inflammatory cytokines IL-6 and IL-8 was also elevated in the amniotic fluid of pregnant women with BV (Keelan et al., 1997). A randomized controlled trial showed that pregnant women treated with clindamycin for BV were five times less likely to miscarry than those given placebo (Ugwumadu et al., 2003). This suggests that early screening and treatment of BV can prevent the infection-induced miscarriage. In addition, a clinical study suggested that hydrogen peroxide producing *Lactobacillus* in the vagina could not only benefit the vaginal health by improving the microbial and inflammatory status, but also create a favorable uterine environment for implantation and placentation (Eckert et al., 2003). Thus, antibiotics and probiotics could prevent and treat infection-induced miscarriage by restoring the vaginal microbiota and improving the intrauterine environment.

Plenty of evidence showed that BV could also increase the risk of preterm and infertility, mainly via facilitating STI and eliciting the intrauterine inflammation (Peelen et al., 2019; Hong et al., 2020a). Recent studies showed that *Lactobacillus*-dominated vaginal microbiota was negatively associated with preterm and infertility, and could prevent women from adverse fertility outcome by modulating vaginal microbiota and inflammatory cytokines IL-4 and IL-10 (Vitali et al., 2012; Hong et al., 2020a). Therefore, antibiotics and probiotics can prevent the preterm and infertility by improving the vaginal and uterine microbiota and eubiosis.

Microbiota Dysbiosis and Interventions in Diseases Caused by Endocrine Disorders

Polycystic ovarian syndrome is one of the most prevalent endocrine disorders in reproductive women, which usually manifests as menstrual disorder, hirsutism, and infertility (Hong et al., 2020b). Though current treatments are various, such as oral contraceptives to inhibit the maturation of ovarian follicles as a long-term PCOS management, and ovulation induction for PCOS patients with fertility requirement, they cannot cure it basically and lifestyle modification (e.g., loss weight) is still the first-line and mainstream treatment (Jin and Xie, 2018).

A case–control study of 39 PCOS patients and 40 healthy people showed that the vaginal microbiota of PCOS patients was significantly different from that of healthy people, characterized by increased diversity and increased relative abundance of *Mycoplasma* and *Prevotella*, and decreased relative abundance of *L. crispatus* (Hong et al., 2020b). This suggests that vaginal microbiota dysbiosis may participate or contribute to the PCOS pathology, and therapies targeted at improving the vaginal microbiota are promising. A systemic review involving 855 PCOS patients investigated the effects of probiotics (*Lactobacillus*) in treating PCOS, and the results showed that probiotic supplementation in PCOS women significantly improved their hormonal index by reducing free androgen index (FAI) and increasing sex hormone binding globulin (SHBG), and their inflammatory index by increasing plasma nitric oxide (NO) and reducing blood malondialdehyde (MDA) (Shamasbi et al., 2020). Besides, the authors also observed that patients given probiotics had increased total glutathione (GSH) and total antioxidant capacity (TAC) levels, and reduced testosterone, dehydroepiandrosterone sulfate (DHEAS, hormonal index), high sensitive C reactive protein (hsCRP, inflammatory index), and hirsutism score compared to those given placebo. As antibiotics and probiotics are aimed at restoring the normal vaginal microbiota and improving the environment of the reproductive system and beyond, they can be used to treat the PCOS symptoms and promote the recovery by improving the hormonal and inflammatory levels.

Recently, microbiota disturbance has also been implicated in the uterine fibroid (benign tumors in the uterus) and menstrual disorders (e.g., menorrhagia and dysmenorrhea), characterized by increased relative abundance of vaginal *L. iners*, and increased relative abundance of uterine *Gardnerella*, *Prevotella*, *Sneathia*, and *Veillonella*, respectively (Chen et al., 2017; Pelzer et al., 2018).

Thus, antibiotics and/or probiotics are also promising in treating uterine fibroid and menstrual disorders.

FRONTIERS AND CONCLUSION IN TREATING VAGINAL DYSBACTERIOSIS

Inspired by the similarity of the intestinal and vaginal microbiota, and the success of the fecal microbiota transplantation (FMT), VMT has also been proposed for the treatment of vaginal dysbacteriosis, which involves transplanting the entire vaginal microbiota of a healthy donor into the vagina of the patient to restore the overall diversity, stability, and normal composition of the microbiota (DeLong et al., 2019). The procedures of VMT are shown in **Figure 3**. The research of our group in 2017 showed that transplantation of healthy rat vaginal microbiota into the vagina of BV model rats restored the morphology of uterine tissue and reduced the serum inflammatory factors such as IL-6, IL-8, and TNF-α, showing obvious recovery effects on vaginal infections caused by dysregulation of vaginal microbiota. In 2019, the clinical study conducted by Lev-Sagie et al. (2019) further showed that VMT had a great effect on long-term recovery from recurrent, antibiotic unresponsive, and refractory BV. In this study, four of the five BV patients treated with VMT recovered effectively after 5–21 months of VMT treatment, showing significant improvements in symptoms, negative Amsel criteria, and *Lactobacillus*-dominated vaginal fluid under the microscopy, with a cure rate up to 80% and no observed adverse effect. Besides, the authors also found that patients with long-term resolution of BV had a dramatic change in microbial composition in the first month after VMT, which was dominated by increase of *Lactobacillus* and decrease of *Bifidobacterium* (closely related to *Gardnerella*), accompanied with reduced *Fannyhessea* and *Prevotella*. In 2021, our group verified the feasibility of VMT in animal models and explored the specific mechanisms (Chen et al., 2021). The results showed that vaginal secretions from healthy rats can be used to treat vaginal microbiota imbalance and prevent the recurrence in rats, which specifically manifested as the decrease of inflammatory cells, pro-inflammatory cytokines, and apoptotic factors in the uterine wall and the restoration of the diversity of vaginal microbiota.

Preliminary studies of VMT have demonstrated the feasibility of VMT to treat BV, showing favorable therapeutic effects. Compared to other treatments for BV, VMT can completely restore the vaginal microbiota to a healthy state, thus showing better curative effects than conventional antibiotics and probiotics, while addressing the drug resistance, recurrence, and side effects associated with antibiotic treatment. Considering that besides BV, vaginal microbiota dysbiosis is also comprehensively involved in the progression of other gynecological diseases, and improving vaginal microbiota by antibiotics and probiotics shows good therapy effects, restoration of vaginal microbiota by VMT may also have favorable therapeutic effects in the treatment of various gynecological infectious and non-infectious diseases.

However, the clinical implementation of VMT still faces many problems, such as insufficient VMT clinical trial (only one research with five subjects), lacking standard protocol, transmission of unidentifiable and antimicrobial-resistance pathogens, unintended pregnancy, immune rejection, and unclear long-term effects. Therefore, the improvement of the VMT requires multi-disciplinary cooperation. Relevant personnel should formulate VMT screening guidelines as soon as possible, continue to explore the application potential of VMT in the treatment of BV and other gynecological diseases, develop a safe and effective new treatment regimen, and develop safety evaluation criteria. We have reasons to believe that safe, standard, and efficient VMT will bring new hope to patients with gynecological diseases and have a good prospect of application.

AUTHOR CONTRIBUTIONS

TC and ZL provided ideas of this review and designed its framework. YH conducted the research and wrote the manuscript. All authors edited the manuscript. All authors read and approved the final manuscript.

FUNDING

This study was supported by the National Natural Science Foundation of China (Grant No. 82060638), Academic and technical leaders of major disciplines in Jiangxi Province (Grant No. 20194BCJ22032), and Double thousand plan of Jiangxi Province (high end Talents Project of scientific and technological innovation).

REFERENCES

Aldunate, M., Srbinovski, D., Hearps, A. C., Latham, C. F., Ramsland, P. A., Gugasyan, R., et al. (2015). Antimicrobial and immune modulatory effects of lactic acid and short chain fatty acids produced by vaginal microbiota associated with eubiosis and bacterial vaginosis. *Front. Physiol.* 6:164. doi: 10.3389/fphys.2015.00164

Balkus, J. E., Richardson, B. A., Rabe, L. K., Taha, T. E., Mgodi, N., Kasaro, M. P., et al. (2014). Bacterial vaginosis and the risk of trichomonas vaginalis acquisition among HIV-1-negative women. *Sex. Transm. Dis.* 41, 123–128. doi: 10.1097/olq.0000000000000075

Bjartling, C., Osser, S., and Persson, K. (2010). The association between *Mycoplasma genitalium* and pelvic inflammatory disease after termination of pregnancy. *BJOG* 117, 361–364. doi: 10.1111/j.1471-0528.2009.02455.x

Borgdorff, H., Gautam, R., Armstrong, S. D., Xia, D., Ndayisaba, G. F., van Teijlingen, N. H., et al. (2016). Cervicovaginal microbiome dysbiosis is associated with proteome changes related to alterations of the cervicovaginal mucosal barrier. *Mucosal Immunol.* 9, 621–633. doi: 10.1038/mi.2015.86

Bradford, L. L., and Ravel, J. (2017). The vaginal mycobiome: a contemporary perspective on fungi in women's health and diseases. *Virulence* 8, 342–351. doi: 10.1080/21505594.2016.1237332

Bradshaw, C. S., Morton, A. N., Hocking, J., Garland, S. M., Morris, M. B., Moss, L. M., et al. (2006). High recurrence rates of bacterial vaginosis over the course of 12 months after oral metronidazole therapy and factors associated with recurrence. *J. Infect. Dis.* 193, 1478–1486. doi: 10.1086/503780

Brotman, R. M., Klebanoff, M. A., Nansel, T. R., Yu, K. F., Andrews, W. W., Zhang, J., et al. (2010). Bacterial vaginosis assessed by gram stain and diminished

colonization resistance to incident gonococcal, chlamydial, and trichomonal genital infection. *J. Infect. Dis.* 202, 1907–1915. doi: 10.1086/657320

Brotman, R. M., Shardell, M. D., Gajer, P., Fadrosh, D., Chang, K., Silver, M. I., et al. (2014). Association between the vaginal microbiota, menopause status, and signs of vulvovaginal atrophy. *Menopause* 21, 450–458. doi: 10.1097/GME.0b013e3182a4690b

Carlsson, I., Breding, K., and Larsson, P. G. (2018). Complications related to induced abortion: a combined retrospective and longitudinal follow-up study. *BMC Womens Health* 18:158. doi: 10.1186/s12905-018-0645-6

Cazanave, C., Manhart, L. E., and Bebear, C. (2012). *Mycoplasma genitalium*, an emerging sexually transmitted pathogen. *Med. Mal. Infect.* 42, 381–392. doi: 10.1016/j.medmal.2012.05.006

Chen, C., Song, X., Wei, W., Zhong, H., Dai, J., Lan, Z., et al. (2017). The microbiota continuum along the female reproductive tract and its relation to uterine-related diseases. *Nat. Commun.* 8:875. doi: 10.1038/s41467-017-00901-0

Chen, T., Xia, C., Hu, H., Wang, H., Tan, B., Tian, P., et al. (2021). Dysbiosis of the rat vagina is efficiently rescued by vaginal microbiota transplantation or probiotic combination. *Int. J. Antimicrob. Agents* 57:106277. doi: 10.1016/j.ijantimicag.2021.106277

Cherpes, T. L., Meyn, L. A., Krohn, M. A., and Hillier, S. L. (2003). Risk factors for infection with herpes simplex virus type 2: role of smoking, douching, uncircumcised males, and vaginal flora. *Sex. Transm. Dis.* 30, 405–410. doi: 10.1097/00007435-200305000-00006

Chi, Y., He, P., Lei, L., Lan, Y., Hu, J., Meng, Y., et al. (2018). Transdermal estrogen gel and oral aspirin combination therapy improves fertility prognosis via the promotion of endometrial receptivity in moderate to severe intrauterine adhesion. *Mol. Med. Rep.* 17, 6337–6344. doi: 10.3892/mmr.2018.8685

Conti, C., Malacrino, C., and Mastromarino, P. (2009). Inhibition of herpes simplex virus type 2 by vaginal lactobacilli. *J. Physiol. Pharmacol.* 60(Suppl. 6), 19–26.

Cudmore, S. L., Delgaty, K. L., Hayward-McClelland, S. F., Petrin, D. P., and Garber, G. E. (2004). Treatment of infections caused by metronidazole-resistant Trichomonas vaginalis. *Clin. Microbiol. Rev.* 17, 783–793, table of contents. doi: 10.1128/CMR.17.4.783-793.2004

DeLong, K., Zulfiqar, F., Hoffmann, D. E., Tarzian, A. J., and Ensign, L. M. (2019). Vaginal microbiota transplantation: the next frontier. *J. Law Med. Ethics* 47, 555–567. doi: 10.1177/1073110519897731

Eckert, L. O., Moore, D. E., Patton, D. L., Agnew, K. J., and Eschenbach, D. A. (2003). Relationship of vaginal bacteria and inflammation with conception and early pregnancy loss following in-vitro fertilization. *Infect. Dis. Obstet. Gynecol.* 11, 11–17. doi: 10.1155/S1064744903000024

Edwards, T., Burke, P., Smalley, H., and Hobbs, G. (2016). Trichomonas vaginalis: clinical relevance, pathogenicity and diagnosis. *Crit. Rev. Microbiol.* 42, 406–417. doi: 10.3109/1040841X.2014.958050

Evans, B. A., Kell, P. D., Bond, R. A., MacRae, K. D., Slomka, M. J., and Brown, D. W. (2003). Predictors of seropositivity to herpes simplex virus type 2 in women. *Int. J. STD AIDS* 14, 30–36. doi: 10.1258/095646203321043237

Farage, M., and Maibach, H. (2006). Lifetime changes in the vulva and vagina. *Arch. Gynecol. Obstet.* 273, 195–202. doi: 10.1007/s00404-005-0079-x

Faught, B. M., and Reyes, S. (2019). Characterization and treatment of recurrent bacterial vaginosis. *J. Womens Health (Larchmt)* 28, 1218–1226. doi: 10.1089/jwh.2018.7383

Fichorova, R. N., Trifonova, R. T., Gilbert, R. O., Costello, C. E., Hayes, G. R., Lucas, J. J., et al. (2006). *Trichomonas vaginalis* lipophosphoglycan triggers a selective upregulation of cytokines by human female reproductive tract epithelial cells. *Infect. Immun.* 74, 5773–5779. doi: 10.1128/IAI.00631-06

Figueroa-Angulo, E. E., Rendon-Gandarilla, F. J., Puente-Rivera, J., Calla-Choque, J. S., Cardenas-Guerra, R. E., Ortega-Lopez, J., et al. (2012). The effects of environmental factors on the virulence of *Trichomonas vaginalis*. *Microbes Infect.* 14, 1411–1427. doi: 10.1016/j.micinf.2012.09.004

Foschi, C., Salvo, M., Cevenini, R., Parolin, C., Vitali, B., and Marangoni, A. (2017). Vaginal lactobacilli reduce *Neisseria gonorrhoeae* viability through multiple strategies: an in vitro study. *Front. Cell. Infect. Microbiol.* 7:502. doi: 10.3389/fcimb.2017.00502

Gajer, P., Brotman, R. M., Bai, G., Sakamoto, J., Schutte, U. M., Zhong, X., et al. (2012). Temporal dynamics of the human vaginal microbiota. *Sci. Transl. Med.* 4:132ra152. doi: 10.1126/scitranslmed.3003605

Goldenberg, R. L., Hauth, J. C., and Andrews, W. W. (2000). Intrauterine infection and preterm delivery. *N. Engl. J. Med.* 342, 1500–1507. doi: 10.1056/NEJM200005183422007

Gosmann, C., Anahtar, M. N., Handley, S. A., Farcasanu, M., Abu-Ali, G., Bowman, B. A., et al. (2017). *Lactobacillus*-deficient cervicovaginal bacterial communities are associated with increased HIV acquisition in young South African women. *Immunity* 46, 29–37. doi: 10.1016/j.immuni.2016.12.013

Gupta, S., Kakkar, V., and Bhushan, I. (2019). Crosstalk between vaginal microbiome and female health: a review. *Microb. Pathog.* 136:103696. doi: 10.1016/j.micpath.2019.103696

Haas, D. M., Hathaway, T. J., and Ramsey, P. S. (2019). Progestogen for preventing miscarriage in women with recurrent miscarriage of unclear etiology. *Cochrane Database Syst. Rev.* 2019:CD003511. doi: 10.1002/14651858.CD003511.pub5

Haggerty, C. L., Gottlieb, S. L., Taylor, B. D., Low, N., Xu, F., and Ness, R. B. (2010). Risk of sequelae after *Chlamydia trachomatis* genital infection in women. *J. Infect. Dis.* 201(Suppl. 2), S134–S155. doi: 10.1086/652395

Hanson, L., VandeVusse, L., Jerme, M., Abad, C. L., and Safdar, N. (2016). Probiotics for treatment and prevention of urogenital infections in women: a systematic review. *J. Midwifery Womens Health* 61, 339–355. doi: 10.1111/jmwh.12472

Harp, D. F., and Chowdhury, I. (2011). Trichomoniasis: evaluation to execution. *Eur. J. Obstet. Gynecol. Reprod. Biol.* 157, 3–9. doi: 10.1016/j.ejogrb.2011.02.024

Hay, P. E. (2004). Bacterial vaginosis and miscarriage. *Curr. Opin. Infect. Dis.* 17, 41–44. doi: 10.1097/00001432-200402000-00008

Hemalatha, R., Mastromarino, P., Ramalaxmi, B. A., Balakrishna, N. V., and Sesikeran, B. (2012). Effectiveness of vaginal tablets containing lactobacilli versus pH tablets on vaginal health and inflammatory cytokines: a randomized, double-blind study. *Eur. J. Clin. Microbiol. Infect. Dis.* 31, 3097–3105. doi: 10.1007/s10096-012-1671-1

Hong, X., Ma, J., Yin, J., Fang, S., Geng, J., Zhao, H., et al. (2020a). The association between vaginal microbiota and female infertility: a systematic review and meta-analysis. *Arch. Gynecol. Obstet.* 302, 569–578. doi: 10.1007/s00404-020-05675-3

Hong, X., Qin, P., Huang, K., Ding, X., Ma, J., Xuan, Y., et al. (2020b). Association between polycystic ovary syndrome and the vaginal microbiome: a case-control study. *Clin. Endocrinol.* 93, 52–60. doi: 10.1111/cen.14198

Isik, G., Demirezen, S., Donmez, H. G., and Beksac, M. S. (2016). Bacterial vaginosis in association with spontaneous abortion and recurrent pregnancy losses. *J. Cytol.* 33, 135–140. doi: 10.4103/0970-9371.188050

Jaisamrarn, U., Triratanachat, S., Chaikittisilpa, S., Grob, P., Prasauskas, V., and Taechakraichana, N. (2013). Ultra-low-dose estriol and lactobacilli in the local treatment of postmenopausal vaginal atrophy. *Climacteric* 16, 347–355. doi: 10.3109/13697137.2013.769097

Jin, P., and Xie, Y. (2018). Treatment strategies for women with polycystic ovary syndrome. *Gynecol. Endocrinol.* 34, 272–277. doi: 10.1080/09513590.2017.1395841

Jung, H. S., Ehlers, M. M., Lombaard, H., Redelinghuys, M. J., and Kock, M. M. (2017). Etiology of bacterial vaginosis and polymicrobial biofilm formation. *Crit. Rev. Microbiol.* 43, 651–667. doi: 10.1080/1040841X.2017.1291579

Kashyap, N., Krishnan, N., Kaur, S., and Ghai, S. (2018). Assessment of sign and symptoms of cervical cancer amongst the patient : a case control study. *Nurs. Midwifery Res. J.* 14, 19–25.

Keelan, J. A., Sato, T., and Mitchell, M. D. (1997). Interleukin (IL)-6 and IL-8 production by human amnion: regulation by cytokines, growth factors, glucocorticoids, phorbol esters, and bacterial lipopolysaccharide. *Biol. Reprod.* 57, 1438–1444. doi: 10.1095/biolreprod57.6.1438

Khosropour, C. M., Bell, T. R., Hughes, J. P., Manhart, L. E., and Golden, M. R. (2018). A population-based study to compare treatment outcomes among women with urogenital chlamydial infection in Washington State, 1992 to 2015. *Sex. Transm. Dis.* 45, 319–324. doi: 10.1097/OLQ.0000000000000764

Kim, J. M., and Park, Y. J. (2017). Probiotics in the prevention and treatment of postmenopausal vaginal infections: review article. *J. Menopausal Med.* 23, 139–145. doi: 10.6118/jmm.2017.23.3.139

Leitich, H., and Kiss, H. (2007). Asymptomatic bacterial vaginosis and intermediate flora as risk factors for adverse pregnancy outcome. *Best Pract. Res. Clin. Obstet. Gynaecol.* 21, 375–390. doi: 10.1016/j.bpobgyn.2006.12.005

Lev-Sagie, A., Goldman-Wohl, D., Cohen, Y., Dori-Bachash, M., Leshem, A., Mor, U., et al. (2019). Vaginal microbiome transplantation in women with intractable bacterial vaginosis. *Nat. Med.* 25, 1500–1504. doi: 10.1038/s41591-019-0600-6

Lewis, F. M., Bernstein, K. T., and Aral, S. O. (2017). Vaginal microbiome and its relationship to behavior, sexual health, and sexually transmitted diseases. *Obstet. Gynecol.* 129, 643–654. doi: 10.1097/AOG.0000000000001932

Li, T., Liu, Z., Zhang, X., Chen, X., and Wang, S. (2019). Local probiotic *Lactobacillus crispatus* and *Lactobacillus delbrueckii* exhibit strong antifungal effects against vulvovaginal candidiasis in a rat model. *Front. Microbiol.* 10:1033. doi: 10.3389/fmicb.2019.01033

Ling, Z., Kong, J., Liu, F., Zhu, H., Chen, X., Wang, Y., et al. (2010). Molecular analysis of the diversity of vaginal microbiota associated with bacterial vaginosis. *BMC Genomics* 11:488. doi: 10.1186/1471-2164-11-488

Liu, Z., Kong, Y., Gao, Y., Ren, Y., Zheng, C., Deng, X., et al. (2019). Revealing the interaction between intrauterine adhesion and vaginal microbiota using high-throughput sequencing. *Mol. Med. Rep.* 19, 4167–4174. doi: 10.3892/mmr.2019.10092

Lopez-Moreno, A., and Aguilera, M. (2020). Probiotics dietary supplementation for modulating endocrine and fertility microbiota dysbiosis. *Nutrients* 12:757. doi: 10.3390/nu12030757

Low, N., Mueller, M., Van Vliet, H. A., and Kapp, N. (2012). Perioperative antibiotics to prevent infection after first-trimester abortion. *Cochrane Database Syst. Rev.* 2012:CD005217. doi: 10.1002/14651858.CD005217.pub2

Ma, B., Forney, L. J., and Ravel, J. (2012). Vaginal microbiome: rethinking health and disease. *Annu. Rev. Microbiol.* 66, 371–389. doi: 10.1146/annurev-micro-092611-150157

Ma, D., Chen, Y., and Chen, T. (2019). Vaginal microbiota transplantation for the treatment of bacterial vaginosis: a conceptual analysis. *FEMS Microbiol. Lett.* 366:fnz025. doi: 10.1093/femsle/fnz025

Mary, N., and Mahmood, T. A. (2010). Preventing infective complications relating to induced abortion. *Best Pract. Res. Clin. Obstet. Gynaecol.* 24, 539–549. doi: 10.1016/j.bpobgyn.2010.03.005

Mastromarino, P., Di Pietro, M., Schiavoni, G., Nardis, C., Gentile, M., and Sessa, R. (2014). Effects of vaginal lactobacilli in *Chlamydia trachomatis* infection. *Int. J. Med. Microbiol.* 304, 654–661. doi: 10.1016/j.ijmm.2014.04.006

Mc, L. N., and Rosenstein, I. J. (2000). Characterisation and selection of a *Lactobacillus* species to re-colonise the vagina of women with recurrent bacterial vaginosis. *J. Med. Microbiol.* 49, 543–552. doi: 10.1099/0022-1317-49-6-543

Mestrovic, T., and Ljubin-Sternak, S. (2018). Molecular mechanisms of *Chlamydia trachomatis* resistance to antimicrobial drugs. *Front. Biosci. (Landmark Ed.)* 23:656–670. doi: 10.2741/4611

Mhatre, M., McAndrew, T., Carpenter, C., Burk, R. D., Einstein, M. H., and Herold, B. C. (2012). Cervical intraepithelial neoplasia is associated with genital tract mucosal inflammation. *Sex. Transm. Dis.* 39, 591–597. doi: 10.1097/OLQ.0b013e318255aeef

Mitra, A., MacIntyre, D. A., Marchesi, J. R., Lee, Y. S., Bennett, P. R., and Kyrgiou, M. (2016). The vaginal microbiota, human papillomavirus infection and cervical intraepithelial neoplasia: what do we know and where are we going next? *Microbiome* 4:58. doi: 10.1186/s40168-016-0203-0

Molenaar, M. C., Singer, M., and Ouburg, S. (2018). The two-sided role of the vaginal microbiome in Chlamydia trachomatis and Mycoplasma genitalium pathogenesis. *J. Reprod. Immunol.* 130, 11–17. doi: 10.1016/j.jri.2018.08.006

Morgan, M. K., and Decker, C. F. (2016). Gonorrhea. *Di.s Mon.* 62, 260–268. doi: 10.1016/j.disamonth.2016.03.009

Mousavi, E., Makvandi, M., Teimoori, A., Ataei, A., Ghafari, S., and Samarbaf-Zadeh, A. (2018). Antiviral effects of Lactobacillus crispatus against HSV-2 in mammalian cell lines. *J. Chin. Med. Assoc.* 81, 262–267. doi: 10.1016/j.jcma.2017.07.010

Muzny, C. A., and Schwebke, J. R. (2013). The clinical spectrum of *Trichomonas vaginalis* infection and challenges to management. *Sex. Transm. Infect.* 89, 423–425. doi: 10.1136/sextrans-2012-050893

Nahui Palomino, R. A., Zicari, S., Vanpouille, C., Vitali, B., and Margolis, L. (2017). Vaginal *Lactobacillus* inhibits HIV-1 replication in human tissues ex vivo. *Front. Microbiol.* 8:906. doi: 10.3389/fmicb.2017.00906

Nardini, P., Nahui Palomino, R. A., Parolin, C., Laghi, L., Foschi, C., Cevenini, R., et al. (2016). *Lactobacillus crispatus* inhibits the infectivity of *Chlamydia trachomatis* elementary bodies, in vitro study. *Sci. Rep.* 6:29024. doi: 10.1038/srep29024

Nasioudis, D., Linhares, I. M., Ledger, W. J., and Witkin, S. S. (2017). Bacterial vaginosis: a critical analysis of current knowledge. *BJOG* 124, 61–69. doi: 10.1111/1471-0528.14209

Niu, X. X., Li, T., Zhang, X., Wang, S. X., and Liu, Z. H. (2017). *Lactobacillus crispatus* modulates vaginal epithelial cell innate response to *Candida albicans*. *Chin. Med. J. (Engl.)* 130, 273–279. doi: 10.4103/0366-6999.198927

Nurbhai, M., Grimshaw, J., Watson, M., Bond, C., Mollison, J., and Ludbrook, A. (2007). Oral versus intra-vaginal imidazole and triazole anti-fungal treatment of uncomplicated vulvovaginal candidiasis (thrush). *Cochrane Database Syst. Rev.* 4:Cd002845. doi: 10.1002/14651858.CD002845.pub2

O'Connell, C. M., and Ferone, M. E. (2016). Chlamydia trachomatis genital infections. *Microb. Cell* 3, 390–403. doi: 10.15698/mic2016.09.525

Onderdonk, A. B., Delaney, M. L., and Fichorova, R. N. (2016). The human microbiome during bacterial vaginosis. *Clin. Microbiol. Rev.* 29, 223–238. doi: 10.1128/CMR.00075-15

Pabuccu, R., Onalan, G., Kaya, C., Selam, B., Ceyhan, T., Ornek, T., et al. (2008). Efficiency and pregnancy outcome of serial intrauterine device-guided hysteroscopic adhesiolysis of intrauterine synechiae. *Fertil. Steril.* 90, 1973–1977. doi: 10.1016/j.fertnstert.2007.06.074

Paez-Canro, C., Alzate, J. P., Gonzalez, L. M., Rubio-Romero, J. A., Lethaby, A., and Gaitan, H. G. (2019). Antibiotics for treating urogenital *Chlamydia trachomatis* infection in men and non-pregnant women. *Cochrane Database Syst. Rev.* 1:CD010871. doi: 10.1002/14651858.CD010871.pub2

Paladine, H. L., and Desai, U. A. (2018). Vaginitis: diagnosis and treatment. *Am. Fam. Physician* 97, 321–329.

Palma, E., Recine, N., Domenici, L., Giorgini, M., Pierangeli, A., and Panici, P. B. (2018). Long-term *Lactobacillus rhamnosus* BMX 54 application to restore a balanced vaginal ecosystem: a promising solution against HPV-infection. *BMC Infect. Dis.* 18:13. doi: 10.1186/s12879-017-2938-z

Pastorek, J. G. II, Cotch, M. F., Martin, D. H., and Eschenbach, D. A. (1996). Clinical and microbiological correlates of vaginal trichomoniasis during pregnancy. The vaginal infections and prematurity study group. *Clin. Infect. Dis.* 23, 1075–1080. doi: 10.1093/clinids/23.5.1075

Peelen, M. J., Luef, B. M., Lamont, R. F., de Milliano, I., Jensen, J. S., Limpens, J., et al. (2019). The influence of the vaginal microbiota on preterm birth: a systematic review and recommendations for a minimum dataset for future research. *Placenta* 79, 30–39. doi: 10.1016/j.placenta.2019.03.011

Pelzer, E. S., Willner, D., Buttini, M., and Huygens, F. (2018). A role for the endometrial microbiome in dysfunctional menstrual bleeding. *Antonie van Leeuwenhoek* 111, 933–943. doi: 10.1007/s10482-017-0992-6

Petrin, D., Delgaty, K., Bhatt, R., and Garber, G. (1998). Clinical and microbiological aspects of Trichomonas vaginalis. *Clin. Microbiol. Rev.* 11, 300–317.

Phukan, N., Brooks, A. E. S., and Simoes-Barbosa, A. (2018). A cell surface aggregation-promoting factor from *Lactobacillus gasseri* contributes to inhibition of *Trichomonas vaginalis* adhesion to human vaginal ectocervical cells. *Infect. Immun.* 86:e00907-17. doi: 10.1128/IAI.00907-17

Pinto-Sander, N., and Soni, S. (2019). Mycoplasma genitalium infection. *BMJ* 367, l5820. doi: 10.1136/bmj.l5820

Piyathilake, C. J., Ollberding, N. J., Kumar, R., Macaluso, M., Alvarez, R. D., and Morrow, C. D. (2016). Cervical microbiota associated with higher grade cervical intraepithelial neoplasia in women infected with high-risk human papillomaviruses. *Cancer Prev. Res. (Phila)* 9, 357–366. doi: 10.1158/1940-6207.CAPR-15-0350

Ralph, S. G., Rutherford, A. J., and Wilson, J. D. (1999). Influence of bacterial vaginosis on conception and miscarriage in the first trimester: cohort study. *BMJ* 319, 220–223. doi: 10.1136/bmj.319.7204.220

Ravel, J., Gajer, P., Abdo, Z., Schneider, G. M., Koenig, S. S., McCulle, S. L., et al. (2011). Vaginal microbiome of reproductive-age women. *Proc. Natl. Acad. Sci. U.S.A.* 108(Suppl. 1), 4680–4687. doi: 10.1073/pnas.1002611107

Reid, G., Jass, J., Sebulsky, M. T., and McCormick, J. K. (2003). Potential uses of probiotics in clinical practice. *Clin. Microbiol. Rev.* 16, 658–672. doi: 10.1128/cmr.16.4.658-672.2003

Sawaya, G. F., Grady, D., Kerlikowske, K., and Grimes, D. A. (1996). Antibiotics at the time of induced abortion: the case for universal prophylaxis based on a meta-analysis. *Obstet. Gynecol.* 87(5 Pt 2), 884–890.

Sgibnev, A., and Kremleva, E. (2020). Probiotics in addition to metronidazole for treatment *Trichomonas vaginalis* in the presence of BV: a randomized, placebo-controlled, double-blind study. *Eur. J. Clin. Microbiol. Infect. Dis.* 39, 345–351. doi: 10.1007/s10096-019-03731-8

Shamasbi, S. G., Ghanbari-Homayi, S., and Mirghafourvand, M. (2020). The effect of probiotics, prebiotics, and synbiotics on hormonal and inflammatory indices in women with polycystic ovary syndrome: a systematic review and meta-analysis. *Eur. J. Nutr.* 59, 433–450. doi: 10.1007/s00394-019-02033-1

Shen, J., Song, N., Williams, C. J., Brown, C. J., Yan, Z., Xu, C., et al. (2016). Effects of low dose estrogen therapy on the vaginal microbiomes of women with atrophic vaginitis. *Sci. Rep.* 6:24380. doi: 10.1038/srep24380

Smith, P. P., Dhillon-Smith, R. K., O'Toole, E., Cooper, N., Coomarasamy, A., and Clark, T. J. (2019). Outcomes in prevention and management of miscarriage trials: a systematic review. *BJOG* 126, 176–189. doi: 10.1111/1471-0528.15528

Smith, S. B., and Ravel, J. (2017). The vaginal microbiota, host defence and reproductive physiology. *J. Physiol.* 595, 451–463. doi: 10.1113/JP271694

Sobel, J. D. (1992). Pathogenesis and treatment of recurrent vulvovaginal candidiasis. *Clin. Infect. Dis.* 14(Suppl. 1), S148–S153. doi: 10.1093/clinids/14.supplement_1.s148

Sobel, J. D., and Sobel, R. (2018). Current treatment options for vulvovaginal candidiasis caused by azole-resistant Candida species. *Expert Opin. Pharmacother.* 19, 971–977. doi: 10.1080/14656566.2018.1476490

Srinivasan, S., Hoffman, N. G., Morgan, M. T., Matsen, F. A., Fiedler, T. L., Hall, R. W., et al. (2012). Bacterial communities in women with bacterial vaginosis: high resolution phylogenetic analyses reveal relationships of microbiota to clinical criteria. *PLoS One* 7:e37818. doi: 10.1371/journal.pone.0037818

Stanley, M. (2010). Pathology and epidemiology of HPV infection in females. *Gynecol. Oncol.* 117(Suppl. 2), S5–S10. doi: 10.1016/j.ygyno.2010.01.024

Stika, C. S. (2010). Atrophic vaginitis. *Dermatol. Ther.* 23, 514–522. doi: 10.1111/j.1529-8019.2010.01354.x

Strus, M., Brzychczy-Włoch, M., Gosiewski, T., Kochan, P., and Heczko, P. B. (2006). The in vitro effect of hydrogen peroxide on vaginal microbial communities. *FEMS Immunol. Med. Microbiol.* 48, 56–63. doi: 10.1111/j.1574-695X.2006.00120.x

Torcia, M. G. (2019). Interplay among vaginal microbiome, immune response and sexually transmitted viral infections. *Int. J. Mol. Sci.* 20:266. doi: 10.3390/ijms20020266

Ugwumadu, A., Manyonda, I., Reid, F., and Hay, P. (2003). Effect of early oral clindamycin on late miscarriage and preterm delivery in asymptomatic women with abnormal vaginal flora and bacterial vaginosis: a randomised controlled trial. *Lancet* 361, 983–988. doi: 10.1016/S0140-6736(03)12823-1

Unemo, M., Golparian, D., and Eyre, D. W. (2019). Antimicrobial Resistance in *Neisseria gonorrhoeae* and treatment of gonorrhea. *Methods Mol. Biol.* 1997, 37–58. doi: 10.1007/978-1-4939-9496-0_3

van de Wijgert, J., and Jespers, V. (2017). The global health impact of vaginal dysbiosis. *Res. Microbiol.* 168, 859–864. doi: 10.1016/j.resmic.2017.02.003

van Oostrum, N., De Sutter, P., Meys, J., and Verstraelen, H. (2013). Risks associated with bacterial vaginosis in infertility patients: a systematic review and meta-analysis. *Hum. Reprod.* 28, 1809–1815. doi: 10.1093/humrep/det096

Verhoeven, V., Renard, N., Makar, A., Van Royen, P., Bogers, J. P., Lardon, F., et al. (2013). Probiotics enhance the clearance of human papillomavirus-related cervical lesions: a prospective controlled pilot study. *Eur. J. Cancer Prev.* 22, 46–51. doi: 10.1097/CEJ.0b013e328355ed23

Vitali, B., Cruciani, F., Baldassarre, M. E., Capursi, T., Spisni, E., Valerii, M. C., et al. (2012). Dietary supplementation with probiotics during late pregnancy: outcome on vaginal microbiota and cytokine secretion. *BMC Microbiol.* 12:236. doi: 10.1186/1471-2180-12-236

Waggoner, S. E. (2003). Cervical cancer. *Lancet* 361, 2217–2225. doi: 10.1016/s0140-6736(03)13778-6

Wang, Z., He, Y., and Zheng, Y. (2019). Probiotics for the treatment of bacterial vaginosis: a meta-analysis. *Int. J. Environ. Res. Public Health* 16:3859. doi: 10.3390/ijerph16203859

Xie, H. Y., Feng, D., Wei, D. M., Mei, L., Chen, H., Wang, X., et al. (2017). Probiotics for vulvovaginal candidiasis in non-pregnant women. *Cochrane Database Syst. Rev.* 11:CD010496. doi: 10.1002/14651858.CD010496.pub2

Yeh, S. L., Lin, M. S., and Chen, H. L. (2007). Inhibitory effects of a soluble dietary fiber from *Amorphophallus konjac* on cytotoxicity and DNA damage induced by fecal water in Caco-2 cells. *Planta Med.* 73, 1384–1388. doi: 10.1055/s-2007-990228

Zhang, H., Kunadia, A., Lin, Y., Fondell, J. D., Seidel, D., and Fan, H. (2017). Identification of a strong and specific antichlamydial N-acylhydrazone. *PLoS One* 12:e0185783. doi: 10.1371/journal.pone.0185783

Conflict of Interest: The authors declare that the research was conducted in the absence of any commercial or financial relationships that could be construed as a potential conflict of interest.

frontiers in Microbiology

ORIGINAL RESEARCH
published: 08 July 2021
doi: 10.3389/fmicb.2021.685549

Prioritizing Disease-Related Microbes Based on the Topological Properties of a Comprehensive Network

Haixiu Yang[1†], Fan Tong[2†], Changlu Qi[1], Ping Wang[1], Jiangyu Li[2] and Liang Cheng[1,3*]*

[1] College of Bioinformatics Science and Technology, Harbin Medical University, Harbin, China, [2] Academy of Military Medical Science, Beijing, China, [3] NHC and CAMS Key Laboratory of Molecular Probe and Targeted Theranostics, Harbin Medical University, Harbin, China

Many microbes are parasitic within the human body, engaging in various physiological processes and playing an important role in human diseases. The discovery of new microbe–disease associations aids our understanding of disease pathogenesis. Computational methods can be applied in such investigations, thereby avoiding the time-consuming and laborious nature of experimental methods. In this study, we constructed a comprehensive microbe–disease network by integrating known microbe–disease associations from three large-scale databases (Peryton, Disbiome, and gutMDisorder), and extended the random walk with restart to the network for prioritizing unknown microbe–disease associations. The area under the curve values of the leave-one-out cross-validation and the fivefold cross-validation exceeded 0.9370 and 0.9366, respectively, indicating the high performance of this method. Despite being widely studied diseases, in case studies of inflammatory bowel disease, asthma, and obesity, some prioritized disease-related microbes were validated by recent literature. This suggested that our method is effective at prioritizing novel disease-related microbes and may offer further insight into disease pathogenesis.

Keywords: microbe, disease, heterogeneous network, random walk with restart, microbe-disease associations

OPEN ACCESS

Edited by:
Jialiang Yang,
Geneis (Beijing) Co., Ltd., China

Reviewed by:
Hui Ding,
University of Electronic Science and Technology of China, China
Hui Liu,
Changzhou University, China

***Correspondence:**
Jiangyu Li
lijiangyu@bmi.ac.cn
Liang Cheng
liangcheng@hrbmu.edu.cn

[†] These authors have contributed equally to this work

Specialty section:
This article was submitted to Systems Microbiology, a section of the journal Frontiers in Microbiology

Received: *25 March 2021*
Accepted: *10 May 2021*
Published: *08 July 2021*

Citation:
Yang H, Tong F, Qi C, Wang P, Li J and Cheng L (2021) Prioritizing Disease-Related Microbes Based on the Topological Properties of a Comprehensive Network. Front. Microbiol. 12:685549. doi: 10.3389/fmicb.2021.685549

INTRODUCTION

Microbial communities, including fungi, archaea, protozoa, bacteria, and viruses, are distributed across various organs of the human body, such as the skin, oral cavity, respiratory tract, and intestine (Cheng et al., 2020; Qi et al., 2021; Sommer and Backhed, 2013). It is reported that about 10^{14} microbial cells reside in the adult intestine, nearly 10 times the number of human cells. Therefore, microbes play an important role in the human body, engaging in various physiological processes, including metabolism regulation and immune defense (Das and Nair, 2019), and disorders relating to microbial communities within the human body have been linked to various human diseases (Huang et al., 2020; Yang et al., 2016). For example, Qin et al. (2010) found that inflammatory bowel disease (IBD), mainly in the forms of ulcerative colitis and Crohn's disease, was usually caused by low microbial diversity. The diversity of the gut microbiota has also been associated with obesity, and the microbial-community composition can be intentionally manipulated to regulate the energy balance of obese individuals (Ley et al., 2005).

Chen and Blaser (2007) found that colonization with *Helicobacter pylori* was inversely associated with asthma and allergy occurrence, and childhood acquisition of *H. pylori* can reduce these risks. The imbalance of microbial communities has also been associated with various types of cancer, including oral cancer (Zhang L. et al., 2019), colorectal cancer (Kim D.J. et al., 2020), and lung cancer (Zheng et al., 2020). Microbe-based disease pathogenesis is complex and can be influenced by environmental factors such as diet, smoking, and antibiotics therapy (Human Microbiome Project Consortium, 2012; Althani et al., 2016; Chen H. et al., 2017; Liu W. et al., 2020). Exploring and understanding microbe-disease associations, therefore, presents a significant challenge (Cheng et al., 2019; Cheng, 2019).

With the development of high-throughput sequencing technologies, such as 16S ribosomal RNA (16S rRNA), an increasing number of microbes have been identified, accelerating human disease research. Furthermore, projects such as the Human Microbiome Project (HMP) (Gevers et al., 2012; Nadia, and Ramana, 2020) and the Metagenomics of the Human Intestinal Tract (MetaHIT) Project[1] were initiated to reveal the relationships between microbes and human diseases. However, traditional experimental methods for investigating microorganism-based pathogenesis are laborious and time-consuming, hindering progress in this field. In recent years, many computational methods have been successfully applied to the prediction of new associations, for example, miRNA–target association prediction (Deng et al., 2019; Yousef et al., 2007), lncRNA–target association prediction (Wang et al., 2019a; Zhang J. et al., 2019; Zhang Z. et al., 2019; Zhao et al., 2020), drug–target association prediction (Liu H. et al., 2020; Luo et al., 2017; Munir et al., 2019; Wang et al., 2020), drug–ncRNA association prediction (Yang et al., 2020), and association prediction between physical examination indicators with diabetes (Yang et al., 2021). However, these computational methods were only extended to the field of microbe–disease association prediction when the Human Microbe–Disease Association Database (HMDAD) became available (Ma et al., 2017). The HMDAD is the first resource that collects human microbe–disease associations through manual curation from 61 microbiota publications before July 2014. HMDAD documents 483 microbe–disease entries, including 39 diseases and 292 microbes, providing the foundation for subsequent computational–based microbe–disease association predictions.

Based on HMDAD, Chen X. et al. (2017) constructed a microbe–disease network and developed the KATZHMDA model for microbe–disease association prediction using the KATZ measurement and Gaussian interaction profile kernel similarity for microbes and diseases. Then, a series of computational methods were proposed to infer potential microbe–disease associations (Qu et al., 2019; Yang and Zou, 2020; Zhou et al., 2020). For example, Shen et al. (2017) extended the random walk to the microbe–disease heterogeneous network to compute the possibilities of microbe–disease associations. Huang et al. (2017) proposed NGRHMDA, which adopted neighbor-based collaborative filtering and a graph-based scoring method, to infer potential microbe–disease associations. Wang et al. developed a prediction model, NBLPIHMDA, to predict new microbe–disease associations. This model applied bidirectional label propagation on the disease similarity network and the microbe similarity network (Wang et al., 2019b). Liu Y. et al. (2020) proposed a deep matrix factorization microbe–disease association (DMFMDA) model, which combined the linear modeling ability of matrix factorization and the non-linear modeling ability of multi-layer perceptron to infer potential microbe–disease associations. To our knowledge, current computational methods for potential microbe–disease association predictions are all based on known microbe–disease associations from HMDAD. However, HMDAD documents the microbe–disease entries of only 61 publications before July 2014 and has not been updated. In recent years, research into microbe–disease associations have increased exponentially. Accordingly, some online repositories have been developed to record highly credible microbe–disease associations, such as Peryton (Skoufos et al., 2021), Disbiome (Janssens et al., 2018), and gutMDisorder (Cheng et al., 2020), which include thousands of curated microbe–disease associations.

In this study, we constructed a two-layer heterogeneous network by integrating large-scale known microbe–disease associations from the Peryton, Disbiome, and gutMDisorder databases, then extending the random walk with restart (RWR) to the network to prioritize candidate microbe–disease associations. The method fully considered the topological properties of the comprehensive network and achieved reasonable efficacy. Exploring microbe–disease relationships may not only help to reveal the mechanisms of disease pathogenesis but also provide insights to aid the prevention, diagnosis, and prognosis of various diseases.

MATERIALS AND METHODS

Dataset Collection

The known microbe–disease associations used in this study were downloaded from the Peryton database[2] (Skoufos et al., 2021), the Disbiome database[3] (Janssens et al., 2018), and the gutMDisorder database[4] (Cheng et al., 2020). Peryton is a novel resource that hosts more than 7,900 experimentally supported microbe–disease associations through manual curation of 314 publications. The database incorporates 43 diseases and 1,396 microorganisms, which are standardized *via* Medical Subject Headings (MeSH) and the NCBI Taxonomy database, respectively. Disbiome is a comprehensive database that collects microbe–disease associations from nearly 1,200 publications. Disbiome records 372 diseases and 1,622 organisms. The diseases are classified using the Medical Dictionary for Regulatory Activities (MedDRA) classification system and the microorganisms are normalized using NCBI and SILVA taxonomies. The gutMDisorder database provides a

[1] http://www.metahit.eu/

[2] https://dianalab.e-ce.uth.gr/peryton/

[3] https://disbiome.ugent.be/home

[4] http://bio-annotation.cn/gutMDisorder/home.dhtml

comprehensive resource for dysbiosis of the gut microbiota in disorders and interventions. gutMDisorder documents 2,263 experimentally supported microbe–disease associations between 579 gut microbes and 123 disorders or 77 intervention measures in humans. The microbes and diseases are standardized *via* the NCBI Taxonomy database and Disease Ontology (DO), respectively. The human microbe–disease associations were collected from the databases mentioned above to construct the composite heterogeneous network.

Microbe–Disease Associations

The human microbe–disease associations were collected from the three databases mentioned above. Since the identifiers of diseases and microbes were inconsistent between different databases, we standardized the diseases and microbes *via* MeSH and the NCBI Taxonomy database, respectively. Finally, we obtained 7,810 microbe–disease associations (1,389 microbes and 41 diseases) from the Peryton database, 7,378 microbe–disease associations (1,439 microbes and 251 diseases) from the Disbiome database, and 1,249 microbe–disease associations (412 microbes and 84 diseases) from the gutMDisorder database (see **Figure 1**). We removed any repeated microbe–disease associations from different resources, and finally obtained 11,037 distinct microbe–disease associations involving 287 human diseases and 2,106 microbes, which were used to construct the microbe–disease network.

Microbe Similarity

Based on the assumption that microbes with similar functions tend to share similar interactions or non-interaction patterns with diseases (Chen X. et al., 2017), we obtained the microbe similarity *via* known human microbe–disease associations using the Gaussian interaction profile kernel. The interaction profile (IP) of a microbe represented the associations between this microbe and 287 human diseases. The IP of microbe m_i was denoted as a vector, IP(m_i), in which the jth element was set to be 1 when the disease d_j was confirmed to be associated with m_i; otherwise, it was set as 0. According to the interaction profiles, the Gaussian interaction profile kernel microbe similarity was defined as follows:

$$KM\left(m_i, m_j\right) = exp\left(-\gamma_m ||IP\left(m_i\right) - IP(m_j)||^2\right) \quad (1)$$

$$\gamma_m = \gamma'_m \Big/ \left(\frac{1}{n_m}\sum_{k=1}^{n_m} ||IP(m_k)||^2\right) \quad (2)$$

In the formula mentioned above, $\boldsymbol{\gamma_m}$ denotes the normalized kernel bandwidth, which can be calculated by a new bandwidth $\boldsymbol{\gamma'_m}$. In this study, we set $\boldsymbol{\gamma'_m}$=1 according to previous relevant research (Chen X. et al., 2017). $\mathbf{n_m}$ denotes the number of microbes in this study. KM(m_i,m_j) denotes the Gaussian interaction profile kernel similarity between two microbes, m_i and m_j. We constructed a microbe–microbe network, in which 2,106 microbes and the similarity between them were represented by nodes and edges, respectively.

Disease Similarity

Compared with microbe similarity, disease similarity has been widely investigated. A variety of disease similarity in Cheng's study (Cheng et al., 2018) and the Gaussian interaction profile kernel disease similarity were used in this study to obtain the disease similarity. Firstly, we calculated the Gaussian interaction profile kernel similarity between disease d_i and d_j as follows:

$$KD\left(d_i, d_j\right) = exp\left(-\gamma_d ||IP\left(d_i\right) - IP(d_j)||^2\right) \quad (3)$$

$$\gamma_d = \gamma'_d \Big/ \left(\frac{1}{n_d}\sum_{k=1}^{n_d} ||IP(d_k)||^2\right) \quad (4)$$

In the formula mentioned above, $\boldsymbol{\gamma'_d}$ was also set to be 1 and $\mathbf{n_d}$ denotes the number of diseases in this study. KD(d_i,d_j) denotes the Gaussian interaction profile kernel similarity between two diseases, d_i and d_j.

Cheng et al. (2018) provided DincRNA, a comprehensive bioinformatics resource for disease similarity calculation and non-coding RNA functional analysis. They utilized five methods, i.e., those of Wang et al. (2007), Resnik (1995), Lin (1998), PSB (Mathur and Dinakarpandian, 2012), and SemFunSim (Cheng et al., 2014) to calculate the similarity of pairwise diseases (SPWD). These methods took into consideration semantic associations, information content (IC), biological processes, and functional associations. The disease similarity score between d_i and d_j in Cheng's study was defined as SPWD(d_i,d_j). Finally, the average value of Gaussian interaction profile kernel similarity as well as Cheng's SPWD was taken as disease similarity, which is shown as follows:

$$SD\left(d_i, d_j\right) = \frac{KD\left(d_i, d_j\right) + SPWD\left(d_i, d_j\right)}{2} \quad (5)$$

Finally, we constructed a disease–disease network, comprising 287 human diseases, and the similarity between them was represented by edges.

Construction of the Composite Heterogeneous Weighted Network

We constructed a composite heterogeneous weighted network by integrating the microbe–disease, microbe–microbe, and disease–disease associations mentioned above. In the composite network, there were two types of nodes, 2,106 microbes and 287 human diseases. The edges between microbes and diseases represented 11,042 distinct microbe–disease associations, and the edge weight was set to be 1 when the microbe m_i was confirmed to be associated with disease d_j; otherwise, it was 0. The edges between different microbes were based on microbe similarity, and the edge weight between node m_i and m_j was denoted by KM(m_i,m_j). The edges between different diseases were based on disease similarity, and the edge weight between nodes d_i and d_j was denoted by SD(d_i,d_j).

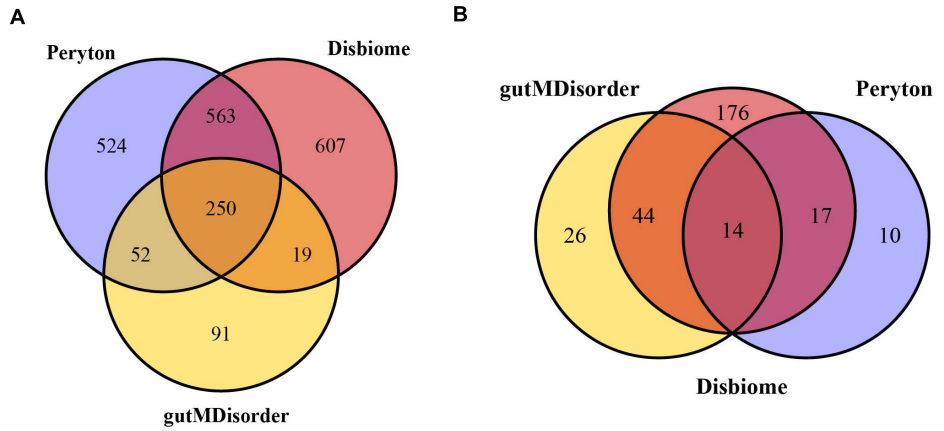

FIGURE 1 | Venn diagram of overlapping microbes **(A)** and diseases **(B)** from the Peryton, Disbiome, and gutMDisorder databases.

Prioritizing Candidate Disease-Related Microbes Based on the Composite Network

Based on the composite heterogeneous weighted network, we used the RWR to prioritize candidate disease-related microbes by fully exploiting the heterogeneous biological associations. The RWR algorithm simulates a random walker that starts from the seed nodes and then moves to their immediate neighbors or stays at the current nodes according to the probability transition matrix. The iterative transition is repeated until all vertices achieve a steady state. In this study, the formula of RWR is defined as:

$$P_{t+1} = (1 - r)\, WP_t + rP_0 \tag{6}$$

In the abovementioned formula, $r \in (0,1)$ denotes the restart probability. P_t denotes a vector in which the ith element holds the probability of being at node i at step t. W denotes the transition matrix, which is a column-normalized adjacency matrix of the composite network. Here, we defined the adjacency matrix W as follows:

$$W = \begin{bmatrix} A_M & B \\ B^T & A_D \end{bmatrix} \tag{7}$$

B is a probability transition matrix from microbe network to disease network. Accordingly, B^T is the transpose of B. Let λ be the probability of the random walker jumping from microbe network to disease network or vice versa. We defined the transition probability from microbe network to disease network as follows:

$$B_{(i,j)} = p\left(d_j \mid m_i\right) = \begin{cases} \lambda B_{ij} / \sum_j B_{ij}, & if \ \sum_j B_{ij} \neq 0 \\ 0, & \text{otherwise} \end{cases} \tag{8}$$

A_M is the microbe network transition matrix. The element of $A_{M(i,j)}$ represents the probability of the random walker transition from m_i to m_j, which is defined as follows:

$$A_{M(i,j)} = \begin{cases} (1 - \lambda) M_{(i,j)} / \sum_j M_{(i,j)}, & if \ \sum_j B_{ij} \neq 0 \\ M_{(i,j)} / \sum_j M_{(i,j)}, & \text{otherwise} \end{cases} \tag{9}$$

Similarly, A_D is the disease network transition matrix. The element of A_D represents the probability of the random walker transition from d_i to d_j, which is defined as follows:

$$A_{D(i,j)} = \begin{cases} (1 - \lambda) D_{(i,j)} / \sum_j D_{(i,j)}, & if \ \sum_j B_{ij} \neq 0 \\ D_{(i,j)} / \sum_j D_{(i,j)}, & otherwise \end{cases} \tag{10}$$

P_0 denotes the initial probability vector, which is a normalized unit vector. $P_0 = \begin{bmatrix} m_0 \\ d_0 \end{bmatrix}$ represents the initial probability vector for the heterogeneous network. m_0 and d_0 represent the initial probabilities of the microbe network and the disease network, respectively. After many iterations, when the difference between P_t and P_{t+1} falls below 10^{-10}, it achieves a steady state. Then, microbes and diseases are ranked based on the steady probability. The flowchart of this work is shown in **Figure 2**.

RESULTS

Performance Evaluation

To assess the performance of our method, we determined its ability to identify known disease-related microbes. The leave-one-out cross-validation (LOOCV) and fivefold cross-validation (fivefold CV) methods (Dao et al., 2020; Wang et al., 2021) were applied on known microbe–disease associations for 236 diseases, which included at least five known microbes. The receiver operating characteristic curve (ROC) plots the true-positive rate (sensitivity) versus false-positive rate (1 - specificity) at different cutoffs, and the area under the curve (AUC) was used to represent the results of cross-validation (Feng et al., 2019; Lv et al., 2020).

For LOOCV, for every disease, each known disease-related microbe was considered as one test sample, the remaining known disease-related microbes were considered as training samples, and all other unknown disease-related microbes in the composite network were considered as candidate samples. Then, we obtained a rank list of the test samples and all candidate

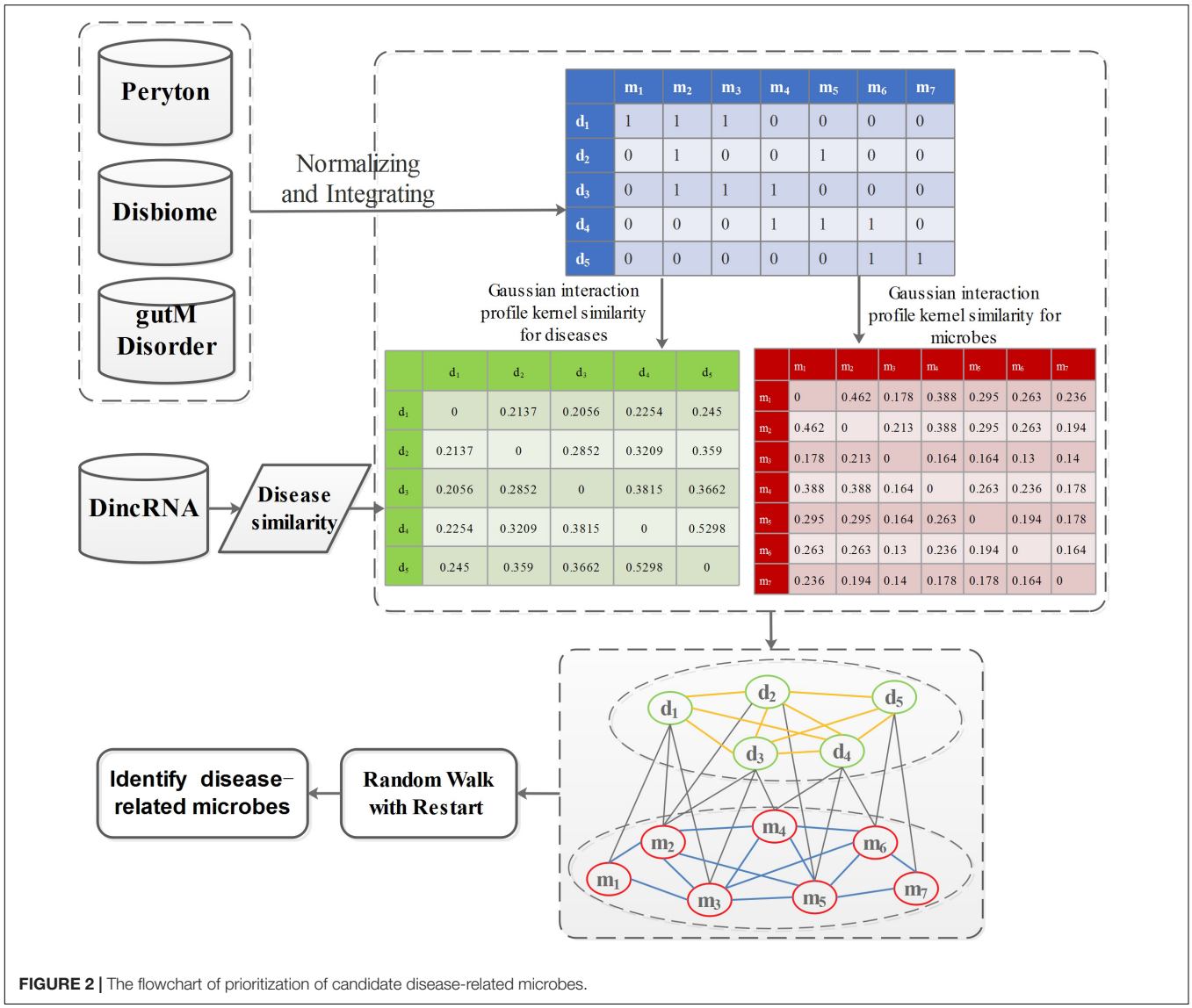

FIGURE 2 | The flowchart of prioritization of candidate disease-related microbes.

samples according to prediction scores by performing our method. The model would achieve high prediction performance when the test samples ranked higher than the given threshold. The ROC and AUC values indicated the performance of the method. In our study, we found that all diseases achieved high predictive performance and the AUC values of LOOCV ranged from 0.9370 to 1 (see **Supplementary Table 1**).

For fivefold CV, for every disease, a set of known disease-related microbes was equally and randomly divided into five subparts. Each subpart was considered as the test sample in turn, and the other four subparts were considered as training samples; all of the other unknown disease-related microbes in the composite network were considered as candidate samples. Considering the potential bias caused by random sample division, we repeated this process 10 times to obtain an average AUC. Similar to LOOCV, we found that the AUC values of fivefold CV ranged from 0.9366 to 1 (**Supplementary Table 2**). The high predictive power indicated that the approach utilizing integrated interactions from the composite two-layer network was highly efficient in prioritizing candidate disease-related microbes.

There are two parameters in our method, one is the restart probability denoted as *r*, and the other is the probability of the random walker jumping between different networks denoted as λ. We set various values under the framework of LOOCV and fivefold CV to evaluate the impact of these parameters and found that the method achieved its best performance when *r* was set as 0.1 and λ was set as 0.5.

Case Studies

We integrated a composite network that included 2,393 nodes (2,106 microbes and 287 human diseases) and 11,037 edges. The RWR algorithm, which makes full use of the network topology, was applied to identify candidate microbes involved in diseases among the composite network of 236 diseases. To verify the ability of our method to discover unknown associations, we implemented case studies on IBD, asthma, and obesity. The

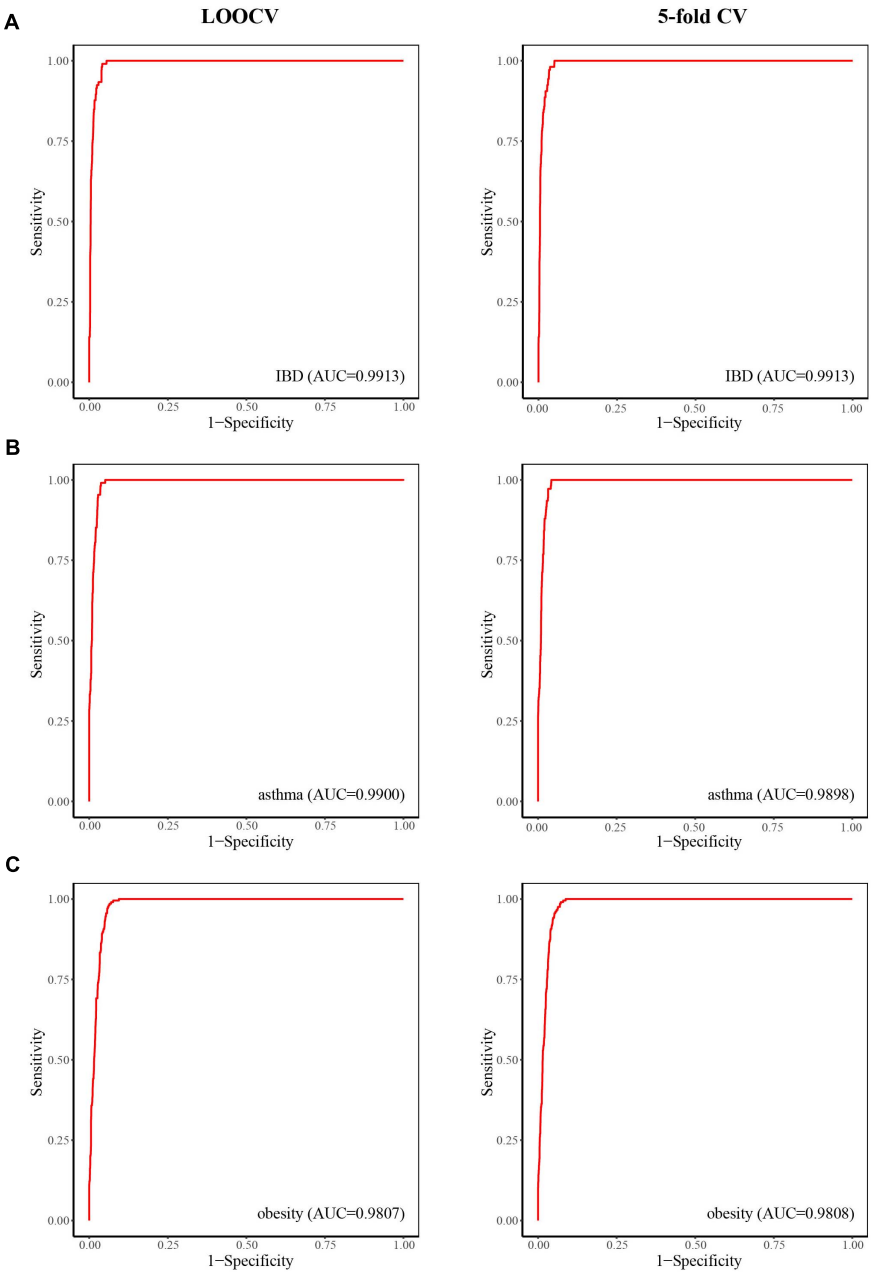

FIGURE 3 | The predictive power of LOOCV (left) and fivefold CV (right) for IBD **(A)**, asthma **(B)**, and obesity **(C)**.

resulting list of the top 30 candidate microbes associated with these diseases is shown in **Supplementary Table 3**.

Inflammatory Bowel Disease

Inflammatory bowel disease, mainly in the form of ulcerative colitis and Crohn's disease, is a chronic relapsing inflammatory disease of the colon and small intestine that affects an increasing number of people (Jostins et al., 2012). When considering case studies of IBD, ROC curves were obtained (**Figure 3A**) and the AUC values of LOOCV and fivefold CV for IBD were both 0.9913. Although there have been many studies on IBD–microbe associations (with 106 known IBD-related microbes), 16 of the top 30 prioritized IBD–microbe associations were manually confirmed by newly published literature (**Table 1**). For example, *Roseburia* is a top-ranked microbe in the prioritized IBD–related microbe list. Kim E.S. et al. (2020) found higher fecal calprotectin (FC) levels in pregnant patients with IBD through pregnancy, and *Roseburia* was positively correlated with maternal FC levels at T3. Sokol et al. (2018) found that IBD patients with *Clostridium difficile* infection (CDI) had more pronounced dysbiosis of *Dorea*, which was also a top-ranked microbe in the prioritized IBD-related microbe list. Toyonaga et al. (2015) found that compared

with IL-10 knockout mice, the level of *Clostridium* cluster XVIII was significantly higher in OPN/IL-10 double knockout mice, when the role of osteopontin in the pathophysiology of IBD was investigated.

Asthma

Asthma is a common chronic inflammatory disease caused by a variety of factors, including genetic and environment factors. Microorganisms may also play a role in the pathogenesis of asthma. Here, we considered asthma case studies, the ROC curves for which are displayed in **Figure 3B**, and the AUC values of LOOCV and fivefold CV for asthma were 0.9900 and 0.9898, respectively. Since asthma and its related microbes have been widely studied (with 108 known asthma-related microbes), seven of the top 30 prioritized asthma–microbe associations were manually confirmed by newly published literature (**Table 2**). *Blautia*, a top-ranked microbe in the prioritized IBD-related microbe list, was found to be present at high concentration in asthma patients (Fu et al., 2021). Dong et al. (2020) showed that treatment with Gu–Ben–Fang–Xiao Decoction (GBFXD) increased the abundance of Lachnospiraceae in asthmatic mice, which consequently led to elevated levels of short-chain fatty acids. Patricia et al. found that the abundance of *Epicoccum* was negatively associated with male asthma patients (Segura-Medina et al., 2019).

Obesity

Obesity is a disease associated with a body mass index of 30 kg/m^2 or higher. It is prevalent in both adults and children worldwide and has been linked to health complications such as rheumatoid arthritis, nonallergic rhinitis, and cancer (Apovian, 2016). Here, we considered obesity case studies, the ROC curves for which are displayed in **Figure 3C**, and the AUC values of LOOCV and fivefold CV for obesity were 0.9807 and 0.9808, respectively. Although obesity and its related microbes have been widely studied (with 204 known obesity-related microbes), seven of the top 30 prioritized obesity–microbe associations were manually confirmed by newly published literature (**Table 3**). Raman et al. (2013) found that *Robinsoniella*, a top-ranked microbe in the obesity-related microbe list, was present at higher levels in nonalcoholic fatty liver disease patients and was implicated in the etiology of, and complications related to, obesity. Zeng et al. (2019) showed that *Dorea* was positively correlated with bodyweight and serum lipids, which were two significant clinical indicators of obesity.

TABLE 1 | Literature verification of the predicted IBD-related microbes.

Microbe	Literature
Helotiales	PMID:27811291
Roseburia	PMID:33307026
Lactobacillus sp.	PMID:30565527
Lachnospira	PMID:33604319
Mycobacteriaceae	PMID:32635236
Streptococcus sp.	PMID:19095961
Erysipelotrichaceae	PMID:33059653
Dorea	PMID:28786749
Bacteroides fragilis group	PMID:17897884
Bacteroides stercoris	PMID:32765449
Akkermansia	PMID:31892611
Klebsiella	PMID:32758418
Clostridium cluster XVIII	PMID:26274807
Megamonas	PMID:31776537
Clostridium sp.	PMID:20552029
Fusobacterium mortiferum	PMID:17607724

DISCUSSION

A wide variety of microbes have been found to be parasitic within the human body. Such microbes play important roles in various physiological processes, such as metabolism regulation and immune defense. Research has also revealed that imbalances in microbial communities are closely associated with human diseases. Thus, identifying novel disease-related microbes is vital when investigating disease pathogenesis, and computational methods have been effective in achieving this. To date, the computational methods that have been applied to identify novel microbe–disease associations have all been based on the HMDAD database, which only recorded 483 microbe–disease entries from 61 publications before July 2014. In this study, we constructed a comprehensive microbe–disease network by integrating known microbe–disease associations from three novel large-scale databases (Peryton, Disbiome, and gutMDisorder), and extended the RWR to the network for prioritizing candidate disease-related microbes. The AUC values of the LOOCV and fivefold CV for 236 human diseases exceeded 0.9370 and 0.9366,

TABLE 2 | Literature verification of the predicted asthma–related microbes.

Microbe	Literature
Epicoccum	PMID:30961954
Galactomyces	PMID:27711990
Citrobacter koseri	PMID:29062711
Blautia	PMID:33221308
Clostridium sp.	PMID:32009325
Lachnospiraceae	PMID:32431609
Unclassified Lactobacillales	PMID:27838347

TABLE 3 | Literature verification of the predicted obesity-related microbes.

Microbe	Literature
Unclassified Lachnospiraceae	PMID:32784721
Dialister succinatiphilus	PMID:28261164
Clostridium cluster XVIII	PMID:31281460
rc4-4	PMID:27304513
Dorea	PMID:31530820
Robinsoniella	PMID:23454028
Enterobacteriaceae	PMID:32805279

The case studies mentioned above indicate that our method is effective for prioritizing novel disease-related microbes, and the prioritized microbes may be used as biomarkers for disease prevention, diagnosis, and prognosis.

respectively, indicating the high performance of our method. Furthermore, we considered case studies of IBD, asthma, and obesity. Although these three diseases have been widely studied, some prioritized disease-related microbes were validated by new publications. This finding suggested that our method is an effective method for prioritizing novel disease-related microbes, thereby aiding our understanding of disease pathogenesis.

There were some limitations in our current study. Firstly, the number of diseases considered in our study was small. This reflects the fact that large-scale microbe studies across a wide range of diseases are lacking, although the development of high-throughput sequencing technologies, such as 16S rRNA, may address this. Secondly, the microbe similarity used in this study was only based on known human microbe–disease associations using a Gaussian interaction profile kernel, which may lead to a defective heterogeneous network. This limitation may be addressed by further research into microbial functions and by integrating the functional similarities of microbes.

DATA AVAILABILITY STATEMENT

The known microbe-disease associations used in this study were downloaded from Peryton database (https://dianalab.e-ce.uth.gr/peryton/#/associations), Disbiome database (https://disbiome.ugent.be/export), and gutMDisorder database (http://bio-annotation.cn/gutMDisorder/resource.dhtml). The raw data used in this study were downloaded from the databases mentioned above, which is open source without any accession number. Other dataset presented in the study are included in the article/**Supplementary Material**.

AUTHOR CONTRIBUTIONS

LC and JL conceived and designed the study. HY and CQ collected and processed the data. HY and PW performed the experiments. HY and FT wrote the manuscript. All authors read and approved the final manuscript.

FUNDING

This work was supported by the Tou-Yan Innovation Team Program of the Heilongjiang Province (2019–15), the National Natural Science Foundation of China (61902095 and 61871160), the Heilongjiang Province Postdoctoral Fund (LBH-Q20030), and the Young Innovative Talents in Colleges and Universities of Heilongjiang Province (2018–69).

SUPPLEMENTARY MATERIAL

The Supplementary Material for this article can be found online at: https://www.frontiersin.org/articles/10.3389/fmicb.2021.685549/full#supplementary-material

REFERENCES

Althani, A. A., Marei, H. E., Hamdi, W. S., Nasrallah, G. K., El Zowalaty, M. E., Al Khodor, S., et al. (2016). Human microbiome and its association with health and diseases. *J. Cell Physiol.* 231, 1688–1694. doi: 10.1002/jcp.25284

Apovian, C. M. (2016). Obesity: definition, comorbidities, causes, and burden. *Am. J. Manag. Care* 22(Suppl. 7), s176–s185.

Chen, H., Peng, S., Dai, S., Zou, Q., Yi, B., Yang, X., et al. (2017a). Oral microbial community assembly under the influence of periodontitis. *Plos One* 12:e0182259. doi: 10.1371/journal.pone.0182259

Chen, X., Huang, Y. A., You, Z. H., Yan, G. Y., and Wang, X. S. (2017b). A novel approach based on KATZ measure to predict associations of human microbiota with non-infectious diseases. *Bioinformatics* 33, 733–739.

Chen, Y., and Blaser, M. J. (2007). Inverse associations of helicobacter pylori with asthma and allergy. *Arch. Intern. Med.* 167, 821–827. doi: 10.1001/archinte.167.8.821

Cheng, L. (2019). Computational and biological methods for gene therapy. *Curr. Gene Ther.* 19:210. doi: 10.2174/1566523219041910221133307

Cheng, L., Hu, Y., Sun, J., Zhou, M., and Jiang, Q. (2018). DincRNA: a comprehensive web-based bioinformatics toolkit for exploring disease associations and ncRNA function. *Bioinformatics* 34, 1953–1956. doi: 10.1093/bioinformatics/bty002

Cheng, L., Li, J., Ju, P., Peng, J., and Wang, Y. (2014). SemFunSim: a new method for measuring disease similarity by integrating semantic and gene functional association. *PLoS One* 9:e99415. doi: 10.1371/journal.pone.0099415

Cheng, L., Qi, C., Zhuang, H., Fu, T., and Zhang, X. (2020). gutMDisorder: a comprehensive database for dysbiosis of the gut microbiota in disorders and interventions. *Nucleic Acids Res.* 48, D554–D560.

Cheng, L., Zhao, H., Wang, P., Zhou, W., Luo, M., Li, T., et al. (2019). Computational methods for identifying similar diseases. *Mol. Ther. Nucleic Acids* 18, 590–604. doi: 10.1016/j.omtn.2019.09.019

Dao, F. Y., Lv, H., Zhang, D., Zhang, Z. M., Liu, L., Lin, H., et al. (2020). DeepYY1: a deep learning approach to identify YY1-mediated chromatin loops. *Brief. Bioinform.* bbaa356. [Epub ahead of print].

Das, B., and Nair, G. B. (2019). Homeostasis and dysbiosis of the gut microbiome in health and disease. *J. Biosci.* 44:117.

Deng, L., Wang, J., and Zhang, J. (2019). Predicting gene ontology function of human microRNAs by integrating multiple networks. *Front. Genet.* 10:3. doi: 10.3389/fgene.2019.00003

Dong, Y., Yan, H., Zhao, X., Lin, R., Lin, L., Ding, Y., et al. (2020). Gu-Ben-Fang-Xiao decoction ameliorated murine asthma in remission stage by modulating microbiota-acetate-tregs axis. *Front. Pharmacol.* 11:549. doi: 10.3389/fphar.2020.00549

Feng, C. Q., Zhang, Z. Y., Zhu, X. J., Lin, Y., Chen, W., Tang, H., et al. (2019). iTerm-PseKNC: a sequence-based tool for predicting bacterial transcriptional terminators. *Bioinformatics* 35, 1469–1477. doi: 10.1093/bioinformatics/bty827

Fu, X., Li, Y., Meng, Y., Yuan, Q., Zhang, Z., Wen, H., et al. (2021). Derived habitats of indoor microbes are associated with asthma symptoms in Chinese university dormitories. *Environ. Res.* 194:110501. doi: 10.1016/j.envres.2020.110501

Gevers, D., Knight, R., Petrosino, J. F., Huang, K., McGuire, A. L., Birren, B. W., et al. (2012). The human microbiome project: a community resource for the healthy human microbiome. *PLoS Biol.* 10:e1001377. doi: 10.1371/journal.pbio.1001377

Huang, S. Y., Xiang, X., Qiu, L., Wang, L., Zhu, B., Guo, R., et al. (2020). Transfection of TGF-beta shRNA by using ultrasound-targeted microbubble destruction to inhibit the early adhesion repair of rats wounded achilles tendon in vitro and in vivo. *Curr. Gene Ther.* 20, 71–81. doi: 10.2174/1566523220666200516165828

Huang, Y. A., You, Z. H., Chen, X., Huang, Z. A., Zhang, S., Yan, G. Y., et al. (2017). Prediction of microbe-disease association from the integration of neighbor and graph with collaborative recommendation model. *J. Transl. Med.* 15:209.

Human Microbiome Project Consortium (2012). Structure, function and diversity of the healthy human microbiome. *Nature* 486, 207–214. doi: 10.1038/nature11234

Janssens, Y., Nielandt, J., Bronselaer, A., Debunne, N., Verbeke, F., Verbeke, F., et al. (2018). Disbiome database: linking the microbiome to disease. *BMC Microbiol.* 18:50. doi: 10.1186/s12866-018-1197-5

Jostins, L., Ripke, S., Weersma, R. K., Duerr, R. H., McGovern, D. P., Hui, K. Y., et al. (2012). Host-microbe interactions have shaped the genetic architecture of inflammatory bowel disease. *Nature* 491, 119–124.

Kim, D. J., Yang, J., Seo, H., Lee, W. H., Lee, D. H., Lee, S., et al. (2020b). Colorectal cancer diagnostic model utilizing metagenomic and metabolomic data of stool microbial extracellular vesicles. *Sci. Rep.* 10:2860.

Kim, E. S., Tarassishin, L., Eisele, C., Barre, A., Nair, N., Rendon, A., et al. (2020a). Longitudinal changes in fecal calprotectin levels among pregnant women with and without inflammatory bowel disease and their babies. *Gastroenterology* 160, 1118–1130.e3.

Ley, R. E., Bäckhed, F., Turnbaugh, P., Lozupone, C. A., Knight, R. D., Gordon, J. I., et al. (2005). Obesity alters gut microbial ecology. *Proc. Natl. Acad. Sci. U. S. A.* 102, 11070–11075.

Lin, D. (1998). "An information-theoretic definition of similarity, in *Proceedings of the 15th International Conference on Machine Learning*, ed M. Kaufman (San Francisco, CA), 296–304.

Liu, H., Zhang, W., Zou, B., and Wang, J. (2020a). DrugCombDB: a comprehensive database of drug combinations toward the discovery of combinatorial therapy. *Nucleic Acids Res.* 48, D871–D881.

Liu, W., Haran, J. P., Allison, J. J., Ye, S., Tjia, J., Bucci, V., et al. (2020b). High-dimensional causal mediation analysis with a large number of mediators clumping at zero to assess the contribution of the microbiome to the risk of bacterial pathogen colonization in older adults. *Curr. Bioinform.* 15, 671–696. doi: 10.2174/1574893614666191115123219

Liu, Y., Wang, S., Zhang, J., and Zhang, W. (2020c). DMFMDA: prediction of microbe-disease associations based on deep matrix factorization using bayesian personalized ranking. *IEEE/ACM Trans. Comput. Biol. Bioinform.* [Epub ahead of print].

Luo, Y., Zhao, X., Zhou, J., Yang, J., Zhang, Y., Kuang, W., et al. (2017). A network integration approach for drug-target interaction prediction and computational drug repositioning from heterogeneous information. *Nat. Commun.* 8:573.

Lv, H., Dao, F. Y., Guan, Z. X., Li, Y. W., Lin, H., Yang, H., et al. (2020). Deep-Kcr: accurate detection of lysine crotonylation sites using deep learning method. *Brief. Bioinform.* bbaa255. [Epub ahead of print].

Ma, W., Zhang, L., Zeng, P., Huang, C., Li, J., Geng, B., et al. (2017). An analysis of human microbe-disease associations. *Brief. Bioinform.* 18, 85–97.

Mathur, S., and Dinakarpandian, D. (2012). Finding disease similarity based on implicit semantic similarity. *J. Biomed. Inform.* 45, 363–371. doi: 10.1016/j.jbi.2011.11.017

Munir, A., Malik, S. I., and Malik, K. A. (2019). Proteome mining for the identification of putative drug targets for human pathogen clostridium tetani. *Curr. Bioinform.* 14, 532–540. doi: 10.2174/1574893613666181114095736

Nadia, and Ramana, J. (2020). The human oncobiome database: a database of cancer microbiome datasets. *Curr. Bioinform.* 15, 472–477. doi: 10.2174/1574893614666190902152727

Qi, C., Wang, P., Fu, T., Lu, M., Cai, Y., Chen, X., et al. (2021). A comprehensive review for gut microbes: technologies, interventions, metabolites and diseases. *Brief. Funct. Genomics* 20, 42–60. doi: 10.1093/bfgp/elaa029

Qin, J., Li, R., Raes, J., Arumugam, M., Burgdorf, K. S., Manichanh, C., et al. (2010). A human gut microbial gene catalogue established by metagenomic sequencing. *Nature* 464, 59–65.

Qu, K., Guo, F., Liu, X., Lin, Y., and Zou, Q. (2019). Application of machine learning in microbiology. *Front. Microbiol.* 10:827. doi: 10.3389/fmicb.2019.00827

Raman, M., Ahmed, I., Gillevet, P. M., Probert, C. S., Ratcliffe, N. M., Smith, S., et al. (2013). Fecal microbiome and volatile organic compound metabolome in obese humans with nonalcoholic fatty liver disease. *Clin. Gastroenterol. Hepatol.* 11,868-75.e1-3.

Resnik, P. (1995). Using information content to evaluate semantic similarity in a taxonomy. *arXiv* [Preprint]. **cmp-lg/9511007**.

Segura-Medina, P., Vargas, M. H., Aguilar-Romero, J. M., Arreola-Ramírez, J. L., Miguel-Reyes, J. L., and Salas-Hernández, J. (2019). Mold burden in house dust and its relationship with asthma control. *Respir. Med.* 150, 74–80. doi: 10.1016/j.rmed.2019.02.014

Shen, X., Chen, Y., Jiang, X., Hu, X., He, T., Yang, J., et al. (2017). Prioritizing disease-causing microbes based on random walking on the heterogeneous network. *Methods* 124, 120–125. doi: 10.1016/j.ymeth.2017.06.014

Skoufos, G., Alexiou, A., Kavakiotis, L., Lambropoulou, A., Kotsira, V., Tastsoglou, S., et al. (2021). Peryton: a manual collection of experimentally supported microbe-disease associations. *Nucleic Acids Res.* 49. 1328–1333. doi: 10.1093/nar/gkaa902

Sokol, H., Jegou, S., McQuitty, C., Straub, M., Leducq, V., Landman, C., et al. (2018). Specificities of the intestinal microbiota in patients with inflammatory bowel disease and Clostridium difficile infection. *Gut Microbes* 9, 55–60. doi: 10.1080/19490976.2017.1361092

Sommer, F., and Backhed, F. (2013). The gut microbiota–masters of host development and physiology. *Nat. Rev. Microbiol.* 11, 227–238. doi: 10.1038/nrmicro2974

Toyonaga, T., Nakase, H., Ueno, S., Matsuura, M., Yoshino, T., Honzawa, Y., et al. (2015). Osteopontin deficiency accelerates spontaneous colitis in mice with disrupted gut microbiota and macrophage phagocytic activity. *PLoS One* 10:e0135552. doi: 10.1371/journal.pone.0135552

Wang, D., Jiang, Y., Wang, D., Zhang, Z., Mao, Z., Lin, H., et al. (2021). DM3Loc: multi-label mRNA subcellular localization prediction and analysis based on multi-head self-attention mechanism. *Nucleic Acids Res.* 49:e46. doi: 10.1093/nar/gkab016

Wang, J., Wang, H., Wang, X., and Chang, H. (2020). Predicting drug-target interactions via FM-DNN learning. *Curr. Bioinform.* 15, 68–76. doi: 10.2174/1574893614666190227160538

Wang, J. Z., Du, Z., Payattakool, R., Yu, P. S., and Yu, P. S. (2007). A new method to measure the semantic similarity of GO terms. *Bioinformatics* 23, 1274–1281. doi: 10.1093/bioinformatics/btm087

Wang, L., Wang, Y., Li, H., Feng, X., Yuan, D., and Yang, J. (2019b). A bidirectional label propagation based computational model for potential microbe-disease association prediction. *Front. Microbiol.* 10:684. doi: 10.3389/fmicb.2019.00684

Wang, L., Xuan, Z., Zhou, S., Kuang, L., and Pei, T. (2019a). A novel model for predicting LncRNA-disease associations based on the LncRNA-MiRNA-disease interactive network. *Curr. Bioinform.* 14, 269–278. doi: 10.2174/1574893613666180703105258

Yang, F., and Zou, Q. (2020). mAML: an automated machine learning pipeline with a microbiome repository for human disease classification. *Database* 2020:baaa050.

Yang, H., Luo, Y., Ren, X., Wu, M., He, X., Peng, B., et al. (2021). Risk prediction of diabetes: big data mining with fusion of multifarious physical examination indicators. *Inf. Fusion* 75, 140–149. doi: 10.1016/j.inffus.2021.02.015

Yang, H., Tang, H., Chen, X. X., Zhang, C. J., Zhu, P. P., Ding, H., et al. (2016). Identification of secretory proteins in mycobacterium tuberculosis using pseudo amino acid composition. *Biomed. Res. Int.* 2016:5413903.

Yang, H., Xu, Y., Shang, D., Shi, H., Zhang, C., Dong, Q., et al. (2020). ncDRMarker: a computational method for identifying non-coding RNA signatures of drug resistance based on heterogeneous network. *Ann. Transl. Med.* 8:1395. doi: 10.21037/atm-20-603

Yousef, M., Jung, S., Kossenkov, A. V., Showe, L. C., and Showe, M. K. (2007). Naive bayes for microRNA target predictions–machine learning for microRNA targets. *Bioinformatics* 23, 2987–2992. doi: 10.1093/bioinformatics/btm484

Zeng, Q., Li, D., He, Y., Li, Y., Yang, Z., Zhao, X., et al. (2019). Discrepant gut microbiota markers for the classification of obesity-related metabolic abnormalities. *Sci. Rep.* 9:13424.

Zhang, J., Zhang, Z., Chen, Z., and Deng, L. (2019a). Integrating multiple heterogeneous networks for novel lncrna-disease association inference. *IEEE/ACM Trans. Comput. Biol. Bioinform.* 16, 396–406. doi: 10.1109/tcbb.2017.2701379

Zhang, L., Liu, Y., Zheng, H. J., and Zhang, C. P. (2019b). The oral microbiota may have influence on oral cancer. *Front. Cell Infect. Microbiol.* 9:476. doi: 10.3389/fcimb.2019.00476

Zhang, Z., Zhang, J., Fan, C., Tang, Y., and Deng, L. (2019c). KATZLGO: large-scale prediction of LncRNA functions by using the KATZ measure based on multiple networks. *IEEE/ACM Trans. Comput. Biol. Bioinform.* 16, 407–416. doi: 10.1109/tcbb.2017.2704587

Zhao, T., Hu, Y., Peng, J., and Cheng, L. (2020). DeepLGP: a novel deep learning method for prioritizing lncRNA target genes. *Bioinformatics* 36, 4466–4472. doi: 10.1093/bioinformatics/btaa428

Zheng, Y., Fang, Z., Xue, Y., Zhang, J., Zhu, J., Gao, R., et al. (2020). Specific gut microbiome signature predicts the early-stage lung cancer. *Gut Microbes* 11, 1030–1042. doi: 10.1080/19490976.2020.1737487

Zhou, J., Wang, Y., and Lei, Q. (2020). Using bioinformatics to quantify the variability and diversity of the microbial community structure in pond ecosystems of a subtropical catchment. *Curr. Bioinform.* 15, 1178–1186. doi: 10.2174/1574893615999200422120819

Conflict of Interest: The authors declare that the research was conducted in the absence of any commercial or financial relationships that could be construed as a potential conflict of interest.

frontiers in Microbiology

ORIGINAL RESEARCH
published: 19 August 2021
doi: 10.3389/fmicb.2021.737066

Development and Validation of a Nomogram for the Prediction of Hospital Mortality of Patients With Encephalopathy Caused by Microbial Infection: A Retrospective Cohort Study

Lina Zhao[1,2†], Yun Li[3†], Yunying Wang[2], Qian Gao[4], Zengzheng Ge[1], Xibo Sun[4] and Yi Li[1*]*

[1] *Emergency Department, State Key Laboratory of Complex Severe and Rare Diseases, Peking Union Medical College Hospital, Peking Union Medical College, Chinese Academy of Medical Sciences, Beijing, China,* [2] *Department of Critical Care Medicine, Chifeng Municipal Hospital, Chifeng Clinical Medical College of Inner Mongolia Medical University, Chifeng, China,* [3] *Department of Anesthesiology, Chifeng Municipal Hospital, Chifeng Clinical Medical College of Inner Mongolia Medical University, Chifeng, China,* [4] *Department of Neurology, Yidu Central Hospital Affiliated to Weifang Medical University, Weifang, China*

OPEN ACCESS

Edited by:
Jialiang Yang,
Genesis (Beijing) Co., Ltd., China

Reviewed by:
Lihong Peng,
Hunan University of Technology, China
Xiao-zheng Zou,
China Medical University, China

***Correspondence:**
Yi Li
billliyi@126.com
orcid.org/0000-0002-7158-3624
Xibo Sun
sunxibo92@sina.com

† These authors have contributed equally to this work

Specialty section:
This article was submitted to Systems Microbiology, a section of the journal Frontiers in Microbiology

Received: *06 July 2021*
Accepted: *02 August 2021*
Published: *19 August 2021*

Citation:
Zhao L, Li Y, Wang Y, Gao Q, Ge Z, Sun X and Li Y (2021) Development and Validation of a Nomogram for the Prediction of Hospital Mortality of Patients With Encephalopathy Caused by Microbial Infection: A Retrospective Cohort Study. Front. Microbiol. 12:737066. doi: 10.3389/fmicb.2021.737066

Background: Hospital mortality is high for patients with encephalopathy caused by microbial infection. Microbial infections often induce sepsis. The damage to the central nervous system (CNS) is defined as sepsis-associated encephalopathy (SAE). However, the relationship between pathogenic microorganisms and the prognosis of SAE patients is still unclear, especially gut microbiota, and there is no clinical tool to predict hospital mortality for SAE patients. The study aimed to explore the relationship between pathogenic microorganisms and the hospital mortality of SAE patients and develop a nomogram for the prediction of hospital mortality in SAE patients.

Methods: The study is a retrospective cohort study. The lasso regression model was used for data dimension reduction and feature selection. Model of hospital mortality of SAE patients was developed by multivariable Cox regression analysis. Calibration and discrimination were used to assess the performance of the nomogram. Decision curve analysis (DCA) to evaluate the clinical utility of the model.

Results: Unfortunately, the results of our study did not find intestinal infection and microorganisms of the gastrointestinal (such as: Escherichia coli) that are related to the prognosis of SAE. Lasso regression and multivariate Cox regression indicated that factors including respiratory failure, lactate, international normalized ratio (INR), albumin, SpO_2, temperature, and renal replacement therapy were significantly correlated with hospital mortality. The AUC of 0.812 under the nomogram was more than that of the Simplified Acute Physiology Score (0.745), indicating excellent discrimination. DCA demonstrated that using the nomogram or including the prognostic signature score

status was better than without the nomogram or using the SAPS II at predicting hospital mortality.

Conclusion: The prognosis of SAE patients has nothing to do with intestinal and microbial infections. We developed a nomogram that predicts hospital mortality in patients with SAE according to clinical data. The nomogram exhibited excellent discrimination and calibration capacity, favoring its clinical utility.

Keywords: sepsis associated encephalopathy, prognosis, hospital mortality, nomogram, microbial infection

INTRODUCTION

Sepsis is defined as a life-threatening organ dysfunction with host response imbalance caused by infection (Singer et al., 2016). Sepsis-associated encephalopathy (SAE) is defined as diffuse brain dysfunction without the central nervous system (CNS) infection in sepsis patients. Metabolic encephalopathy, drug intoxication, structural brain lesions, cerebrovascular events, encephalitis, meningitis, and non-convulsive status epilepticus need to be ruled out in sepsis patients before a diagnosis of SAE (Eidelman et al., 1996). SAE develops in up to 70% of septic patients (Gofton and Young, 2012; Fraser et al., 2014).

SAE is related to increased mortality, extensive costs, prolonged hospitalization, followed by persistent cognitive impairment (Iwashyna et al., 2010; Sonneville et al., 2017). The mortality rates of SAE patients over 60% in sepsis patients (Eidelman et al., 1996; Schuler et al., 2018). At hospital discharge, 45% of patients are related to the development of dementia (Annane and Sharshar, 2015). Early recognition of brain injury and prompt management are of great importance for the survival and prognosis of septic patients. Intestinal microbial infection is one of the important sites of infection in patients with sepsis. Intestinal microbes are not only related to infections. Studies have found that can have an impact on the brain through the microbiota-gut-brain axis, included depression, anxiety, dementia, and other diseases (Grochowska et al., 2018). Li et al. (2018) found that intestinal flora can affect SAE through the vagus nerve. The relationship between intestinal flora and the prognosis of SAE patients is still unclear.

Therefore, further studies for identifying the relationship between intestinal flora and the prognosis of SAE patients, and the predictors of the prognosis of SAE patients, especially accurate and measurable prediction models for hospital mortality, are pivotal for risk-optimized therapeutic strategies and to improve the prognosis of sepsis patients. This study aimed to investigate the predictors associated with hospital mortality in patients with SAE and establish a comprehensive visual predictive nomogram of hospital mortality, calculating a probabilistic estimate that could be of use to clinicians these patients.

Abbreviations: SAE, sepsis-associated encephalopathy; SAPS II, simplified acute physiology score; SOFA, sequential organ failure assessment; qSOFA, quick sequential organ failure assessment; GCS, Glasgow coma scale; ICU, intensive care unit; MIMIC-III, Medical Information Mart for Intensive Care III; ICD-9, International Classification of Diseases, Ninth Revision; ROC, receiver operating characteristic curve; INR, international normalized ratio.

MATERIALS AND METHODS

Data Source

Data were obtained from the Medical Information Mart for Intensive Care (MIMIC-III, Version 1.4), which contains 46,520 patients admitted to the Beth Israel Deaconess Medical Center (Boston, MA, United States) from 2001 to 2012 (Johnson et al., 2016). The database documents included charted events such as demographics, vital signs, microbiology events, medication prescriptions, laboratory tests, etc. International Classification of Diseases, Ninth Revision (ICD-9) codes were also documented by hospital staff on patient discharge. The following CITI program course was completed: CITI 33690380. The raw data were extracted using a structure query language (SQL) using Navicat and further processed with R software.

Patient Population

Inclusion criteria were as follows: Patients with (1) sepsis 3.0. (2) age $\geq$ 18 years-old. (3) at least 24 h stay in the ICU. Sepsis was defined as an infected patient on discharge according to ICD-9 codes and microbial culture positive. According to the definition of sepsis 3.0, we included patients with SOFA score $\geq$ 2.

Exclusion criteria (Sonneville et al., 2017; Yang Y. et al., 2020): (1) Patients without SAE. (2) Primary brain injury including traumatic brain injury, intracerebral hemorrhage, cerebral embolism, ischemic stroke, epilepsy, or intracranial infection, and other cerebrovascular diseases according to ICD-9 codes. (**Supplementary Materials 1–5**); (3) Mental disorders and neurological disease (**Supplementary Material 6**); (4) Chronic alcohol or drug abuse (**Supplementary Material 7**); (5) Encephalopathy caused by other causes including metabolic encephalopathy, hepatic encephalopathy, hypertensive encephalopathy, hypoglycemic coma, and other liver disease or kidney disease affecting consciousness (**Supplementary Material 8**); (6) Severe electrolyte imbalances or blood glucose disturbances, including hyponatremia (<120 mmol/l), hyperglycemia (>180 mg/dl), or hypoglycemia (<54 mg/dl); (7) Partial pressure of CO_2 (PCO_2) $\geq$ 80 mmHg; (8)Without an evaluation of a Glasgow Coma Scale (GCS) score; (9) Patients who have been sedated by tracheal intubation at the time of admission.

Sepsis-Associated Encephalopathy

Sepsis-associated encephalopathy was defined as (1) patients with GCS < 15. (2) The patient was diagnosed with delirium,

cognitive impairment, altered mental status according to the ICD-9 code. (3) The patient was treated with haloperidol during hospitalization. (4) Exclude consciousness disorders caused by other reasons. Many studies use GCS score as an essential tool for evaluating SAE patients (Iwashyna et al., 2010).

Data Extraction and Management

The following data was extracted from the MIMIC III database using R statistical software (R Foundation for Statistical Computing, Vienna, Austria): basic patient demographical data, vital signs (mean value) during the first 24 h of intensive care unit (ICU) stay, the first laboratory data since ICU admission and severity scores (including SAPS II, quick sequential organ failure assessment (qSOFA) score, sequential organ failure assessment (SOFA) score), comorbidity index at discharge according to the ICD-9 code (**Supplementary Material 9**), site of infection and types of microbial infections (**Supplementary Material 10**), organ failure (**Supplementary Material 11**). A matrix diagram of missing data is illustrated in the Data Profiling report (**Supplementary Material 12**). The percentage of missing values of partial thromboplastin time (0.47%), platelet (0.57%), aspartate aminotransferase (0.66%), alanine aminotransferase (0.47%), resprate (0.85%), heartrate (0.85%), blood urea nitrogen (1.14%), dysbp (1.14%), diasbp (1.23%), tempc (1.52%), glucose_min (1.42%), albumin (5.02%), lactate (3.6%), and hemoglobin (3.03%) were <6%. To facilitate statistical analysis, missing individual values were substituted with their mean values.

Statistical Analysis

The Shapiro–Wilk test for the sample distribution was used. Continuous variables with normal distribution were expressed as the mean ± standard deviation (SD), and continuous non-normal distributed variables were expressed as the median (interquartile range, IQR), categorical variables were expressed as frequency and percentage, as appropriate. A non-parametric test (Mann–Whitney *U* test or Kruskal–Wallis test) was applied for data with non-normal distribution or heterogeneity of variances. Pearson Chi-squared test was applied to categorize variables.

Patients were randomly assigned to either the training cohort (80%) or the validation cohort (20%). The selection of predictive features of the nomogram used the least absolute shrinkage and selection operator (Lasso) regression model (Sauerbrei et al., 2007; Sun et al., 2013; Wang et al., 2020). A multivariate COX regression analysis was performed on the selected variables, and a nomogram was constructed based on the results of the multivariate COX regression analysis ($P < 0.05$). We applied a bootstrapped resample with 1,000 iterations to verify the accuracy of the nomogram. The C-index was employed as an indicator to determine the discrimination ability of the nomogram through receiver operating characteristic (ROC) curve analysis and area under the curve (AUC). The calibration was performed by plotting the calibration curve to analyze the association between the observed incidence and the predicted probability. We evaluated the clinical usefulness and net benefit of the new predictive models by using decision curve analysis (DCA).

Statistical analysis was conducted with R software (version 3.4.3). Statistical significance was defined as $p < 0.05$.

RESULTS

Demographic Baseline Characteristics

1,055 patients with SAE were identified from the MIMIC database after applying the inclusion and exclusion criteria. We randomly assigned 80% and 20% of the patients to the training (n = 844) and validation (n = 211) cohorts. The recruitment process is illustrated in **Figure 1**.

Table 1 shows the patient characteristics in the primary and validation cohorts. SAE patients who were older, had urinary tract infection or yeast infection were more likely to die. Circulatory failure was more common in non-survivors [Heartrate, 112 (96–132) vs. 109 (94–125), P = 0.008; Dysbp, 77 (64.8–86) vs. 85 (77–94), $P < 0.001$; Diasbp, 35 (26–41) vs. 39 (33–47), $P < 0.001$; Lactate, 2.3 (1.6–4.4) vs. 1.8 (1.2–2.7), $P < 0.001$] than survivors. Patients in the non-survival group had worse liver function [Alanine aminotransferase, 33 (17–84) vs. 24 (14–51.3), P = 0.001; Aspartate aminotransferase, 49 (25–139) vs. 31.5 (20–64), $P < 0.001$; Albumin, 2.8 (2.2–3.0) vs. 2.9 (2.5–3.3), $P < 0.001$], worse renal function [Creatinine, 1.1 (0.8–1.9) vs. 1.5 (0.9–2.6), $P < 0.001$; Blood urea nitrogen, 24 (16–41) vs. 33 (20–50.3), $P < 0.001$], and worse coagulation [Partial time, 14.3 (13.0–16.4) vs. 15.5 (13.8–19.6), $P < 0.001$; Partial thromboplastin time, 30.5 (26.9–36.9) vs. 36.7 (30.2–49.6), $P < 0.001$; INR 1.3 (1.1–1.5) vs. 1.5 (1.2–2.0), $P < 0.001$], and more serious infections [White blood cell count, 10.7 (7.2–15.3) vs. 11.9 (7.9–16.9), P = 0.061]. Patients in the non-survival group also had a higher incidence of anemia (53.2 vs. 67.8%). Non-surviving patients have more severe disease [SOFA 6.0 (9.0–12.0) vs. 6.0 (4.0–8.0), $p < 0.001$; qSOFA 2.0 (2.0–3.0) vs. 2.0 (2.0–3.0) $p < 0.001$; SAPS II 56 (45–72) vs. 42 (32–51), $p < 0.001$].

Patient Outcomes

Table 2 shows the outcomes for the survival group and non-survival group. Among non-survivors, there was a higher incidence of multiple organ failure including respiratory failure (63.6 vs. 32.9%), renal failure (69.4 vs. 57.3%), hepatic failure (10.5 vs. 3.3%), cardiovascular failure (58.1 vs. 8.5%), and hematological failure (26.7 vs. 21.2%). This led to a higher rate of mechanical ventilation (52.7 vs. 35.2%) and renal replacement therapy (12.0 vs. 2.0%) among non-survivors.

Feature Selection

Using the LASSO regression model, among the non-survivors of SAE, we identified 89 features which reduced to 13 potential predictors. They include SAPS II, renal replacement therapy, temperature, SpO_2, albumin, INR, lactate, respiratory failure, urinary tract infection, anemia, systolic blood pressure (sysbp), partial thromboplastin time (**Supplementary Material 13**: Data supplement) (**Figures 2A,B**).

Multivariate Cox Regression

Furthermore, we performed a univariate, and multivariate cox regression analysis of these 13 potential predictors, sex, and admission type. According to our results, SAPS II, renal replacement therapy, temperature, SpO_2, albumin, international

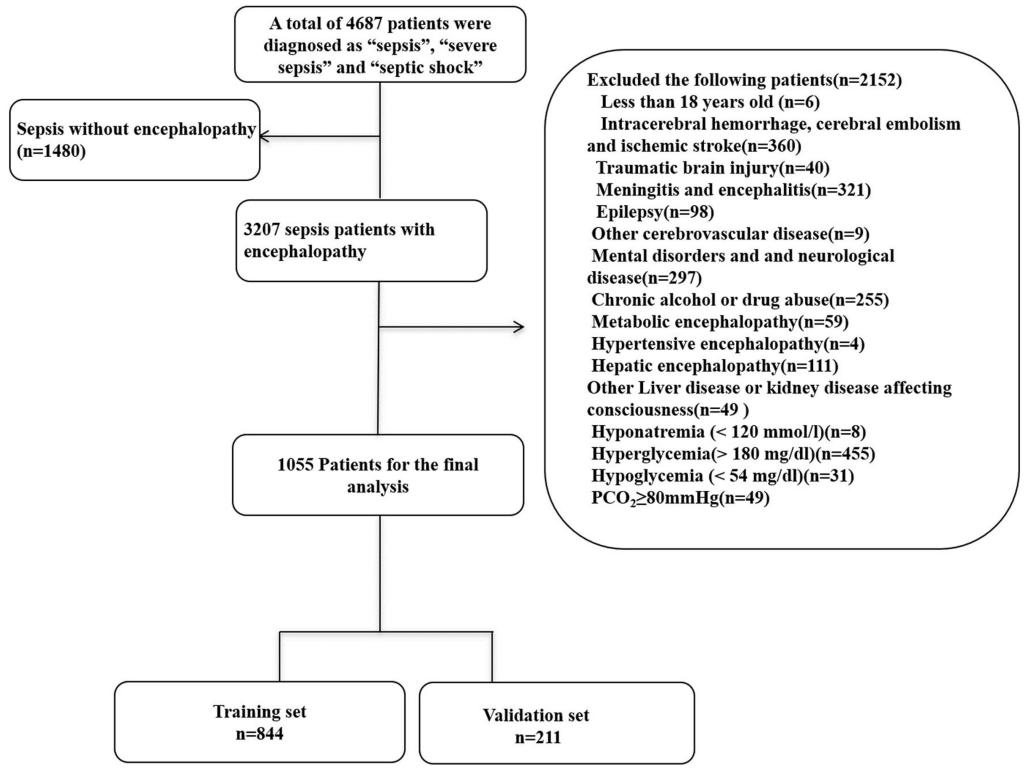

FIGURE 1 | Flow chart of the enrolled patients. MIMIC-III, Medical Information Mart for Intensive Care III.

normalized ratio (INR), lactate, and respiratory failure were independent prognostic factors for SAE patients ($p < 0.01$ or $p < 0.05$) (**Table 3**).

Predictive Nomogram Development

A Lasso regression model and multivariate cox regression analysis identified SAPS II, renal replacement therapy, temperature, SpO_2, albumin, INR, lactate, and respiratory failure as independent prognostic factors for SAE patients in the training cohort. These factors can be used to predict the hospital mortality of patients with SAE (**Table 3**), which was presented as the visualization nomogram (**Figure 3**). The hazard ratio values of these risk factors were established and scored for each level of prognostication. By adding up the scores associated with each variable to assess the hospital mortality of SAE patients.

Discrimination and Calibration

The AUC for the hospital mortality prediction nomogram was 0.812 (95% CI, 0.780–0.843) in the training cohort, which is greater than the SAPS II score of 0.745 (95% CI, 0.708–0.783) (**Figure 4**). The predictive accuracy of the nomogram was shown with a sensitivity of 0.601 and a specificity of 0.867. Our study employed the bootstrap resampling method for internal validation of the model. The calibration plot of hospital mortality of SAE patients revealed good agreement between the observed and predicted values (**Figure 5**).

Clinical Utility

The DCA of the nomograms and SAPS II for the hospital mortality of patients with SAE are illustrated in **Figure 6**. The results showed that the nomogram provided a greater net benefit in predicting hospital mortality compared to that of SAPS II.

DISCUSSION

In our study, patients with SAE have a hospitalized mortality rate of 30.5%. Intestinal infections and microbial infections were not found to be related to the prognosis of SAE patients. We identified independent factors for the prognosis of SAE patients, which included SAPS II, renal replacement therapy, albumin, INR, lactate, temperature, SpO_2, and respiratory failure. We further developed and validated a comprehensive visual nomogram to predict the prognosis of SAE patients. The nomogram showed a high degree of validity, discrimination, and clinical utility.

Microorganisms in the body are related to many diseases. Li-Hong Peng and Lihong Peng et al. (2018, 2020a) established a model to predict the association of microorganisms with various diseases through microorganisms, and the model showed excellent performance. Probiotics can change the types of intestinal microflora and affect patients' mood and memory function (Bagga et al., 2018). Xia et al. (2018) found that probiotics can improve the cognitive function of

TABLE 1 | Characteristics of patients in the primary and validation cohorts.

	Primary cohort			Validation cohort		
	Survive group *n* = 586	**Non-survival group *n* = 258**	***P***	**Survive group *n* = 147**	**Non-survival group *n* = 64**	***P***
Age, median	72 (59.0–82.4)	76.7 (64–84.4)	0.003	70.0 (56.8–81.7)	75.2 (65.2–83.7)	0.068
Sex n (%)						
Female	299 (51.0)	118 (45.7)	0.721	63 (42.9)	33 (51.6)	0.243
Male	287 (49.0)	140 (54.3)		84 (57.1)	31 (48.4)	
Admission_type (%)						
Emergency	535 (92.0)	248 (91.0)	0.043	136 (92.5)	59 (92.2)	0.014
Elective	38 (6.1)	8 (7.2)		9 (6.1)	4 (6.3)	
Urgent	13 (1.9)	2 (1.9)		2 (1.4)	1 (1.5)	
Comorbidity, n (%)						
Hypertension	365 (62.3)	146 (56.6)	<0.001	91 (61.9)	40 (62.5)	0.935
Diabetes	179 (30.5)	88 (34.1)	<0.001	41 (27.9)	19 (29.7)	0.790
Cardiovascular diseases	388 (66.2)	176 (68.2)	0.569	93 (63.3)	47 (73.4)	0.151
Chronic pulmonary disease	122 (20.8)	57 (22.1)	0.677	25 (17.0)	14 (21.9)	0.402
Liver disease	51 (8.7)	27 (10.5)	0.415	17 (11.6)	11 (17.2)	0.268
Anemias	312 (53.2)	175 (67.8)	<0.001	80 (54.4)	49 (76.6)	0.002
Infection site, n (%)						
Lung	235 (40.1)	98 (38.0)	0.562	66 (44.9)	27 (42.2)	0.715
Intestinal	108 (18.4)	41 (15.9)	0.373	30 (20.4)	11 (17.2)	0.587
Urinary system	238 (40.6)	61 (23.6)	<0.001	58 (39.5)	16 (25)	0.043
Catheter related	98 (16.7)	29 (11.2)	0.040	25 (17.0)	7 (10.9)	0.259
Skin and soft tissue	81 (13.8)	31 (12.0)	0.476	19 (12.9)	11 (17.2)	0.415
Abdominal cavity	135 (23.0)	60 (23.3)	0.945	31 (21.1)	17 (26.6)	0.383
Microorganisms, n (%)						
Escherichia coli	122 (20.8)	31 (12.0)	0.002	32 (21.8)	11 (17.2)	0.448
Klebsiella oxytoca	8 (1.4)	6 (2.3)	0.314	7 (4.8)	0 (0)	0.076
Acinetobacter baumannii	10 (1.7)	4 (1.6)	0.870	2 (1.4)	2 (3.1)	0.388
Enterobacter	28 (4.8)	7 (2.7)	0.166	1 (0.68)	2 (3.1)	0.168
Staphylococcus aureus coag	137 (23.4)	71 (27.5)	0.198	38 (25.9)	14 (21.9)	0.538
Pseudomonas aeruginosa	78 (13.3)	22 (8.5)	0.048	16 (10.9)	10 (15.6)	0.336
Enterococcus sp.	130 (22.2)	45 (17.4)	0.034	43 (29.3)	10 (15.6)	0.036
Streptococcus	21 (3.6)	7 (2.7)	0.515	7 (4.8)	1 (1.5)	0.263
Candida albicans	20 (3.4)	13 (5.0)	0.262	11 (7.5)	3 (4.7)	0.453
Yeast	178 (30.4)	101 (39.1)	0.013	64 (43.5)	32 (5.0)	0.386
Aspergillus fumigatus	14 (2.4)	6 (2.3)	0.955	0 (0)	1 (1.5)	0.129
Positive for methicillin resistant *Staphylococcus aureus*	41 (7.0)	8 (3.1)	0.026	8 (5.4)	4 (6.3)	0.816
Staphylococcus coagulase negative	140 (23.9)	51 (19.8)	0.187	32 (21.8)	10 (15.6)	0.304
Virus	3 (0.51)	3 (1.2)	0.300	4 (2.7)	0 (0)	0.183
Vital signs, median						
Heartrate (bpm)	109 (94–125)	112 (96–132)	0.008	111.9 ± 22.7	117.4 ± 22.7	0.055
Dysbp (mmHg)	85 (77–94)	77 (64.8–86)	<0.001	83.5 (75–94.8)	78 (62–89)	0.009
Diasbp (mmHg)	39 (33–47)	35 (26–41)	<0.001	39.5 ± 10.9	36.4 ± 13.8	0.047
Resprate (bpm)	28 (24–32)	29 (25–35)	0.021	29 (25–33.5)	29 (26–34)	0.283
Tempc (°C)	37.6 (36.9–38.3)	37.4 (36.7–38.0)	0.002	37.7 (37.0–38.3)	37.3 (36.7–38.2)	0.042
Laboratory parameters						
Lactate (mmol/L)	1.8 (1.2–2.7)	2.3 (1.6–4.4)	<0.001	1.9 (1.3–2.6)	2.3 (1.3–4.2)	0.088
PCO_2 (mmHg)	40 (36–42)	40 (32–45)	0.874	40 (36–44)	40 (35–44)	0.592
PO_2 (mmHg)	92 (90–95)	91 (83.8–93)	<0.001	93 (89.5–95)	89 (80–95)	0.018
PH	7.34 (7.34–7.39)	7.34 (7.28–7.41)	0.142	7.34 (7.32–7.42)	7.34 (7.25–7.40)	0.229
Glucose_min (mg/dL)	101 (85–120)	99 (75–122)	0.053	104.1 ± 30.5	99.0 ± 31.4	0.378

(Continued)

TABLE 1 | Continued

	Primary cohort			Validation cohort		
	Survive group *n* = 586	**Non-survival group *n* = 258**	***P***	**Survive group *n* = 147**	**Non-survival group *n* = 64**	***P***
Glucose_max (mg/dL)	122 (156–200)	165 (139–205.3)	0.116	147 (124–202.5)	183.5 (147.5–234.5)	0.001
Creatinine (mg/dL)	1.1 (0.8–1.9)	1.5 (0.9–2.6)	<0.001	1.0 (0.7–1.4)	1.4 (0.7–2.5)	0.050
Blood urea nitrogen (mg/dL)	24 (16–41)	33 (20–50.3)	<0.001	22 (13–36)	29.0 (18.3–54.8)	0.005
Alanine aminotransferase (IU/L)	24 (14–51.3)	33 (17–84)	0.001	26.5 (15–43.5)	31 (15.8–49.3)	0.608
Aspartate aminotransferase (IU/L)	31.5 (20–64)	49 (25–139)	<0.001	31 (18–51)	35 (23.8–70.3)	0.090
Albumin (g/dL)	2.9 (2.5–3.3)	2.8 (2.2–3.0)	<0.001	2.9 (2.5–3.2)	2.8 (2.2–3.3)	0.532
Hemoglobin (g/dL)	9.6 (8.5–10.7)	9.7 (8.6–10.8)	0.728	9.7 (8.6–11.1)	9.6 (8.9–11.3)	0.630
Platelet (K/uL)	182.5 (122–272.3)	171 (110.8–246)	0.082	174.0 (106–246)	181.0 (118–271)	0.269
Potassium (mEq/L)	4.0 (3.6–4.4)	4.1 (3.8–4.6)	0.005	4.0 (3.7–4.2)	4.3 (3.8–4.5)	0.010
Sodium (mEq/L)	139 (136–142)	139 (134–142)	0.027	139 (136–142)	138 (135–141)	0.200
Partial time (s)	14.3 (13.0–16.4)	15.5 (13.8–19.6)	<0.001	14.1 (13.0–16.3)	14.7 (13.4–18.2)	0.080
Partial hromboplastin time	30.5 (26.9–36.9)	36.7 (30.2–49.6)	<0.001	29.7 (26.1–36.3)	33.5 (28.9–40.3)	0.004
INR	1.3 (1.1–1.5)	1.5 (1.2–2.0)	<0.001	1.3 (1.1–1.5)	1.4 (1.2–1.9)	0.030
White blood cell count (K/uL)	10.7 (7.2–15.3)	11.9 (7.9–16.9)	0.061	10.2 (6.6–14.3)	11.8 (8.8–15.3)	0.029
Lymphocyte (%)	9.8 (5.4–16.4)	8.0 (5.0–14.0)	0.017	11.2 (6.3–17.6)	10.3 (5.1–16.7)	0.557
Neutrophil (%)	80.1 (70.0–87.5)	80.8 (71.2–88)	0.426	80.0 (70.1–87.8)	82.3 (69.8–89.0)	0.445
Monocytes (%)	4.0 (2.5–6.0)	4.0 (2.0–6.4)	0.776	4.1 (2.7–6.0)	3.9 (2.5–5.2)	0.393
Eosinophils (%)	0.6 (0.0–2.0)	0.2 (0.0–1.2)	0.001	0.55 (0.08–1.4)	0.3 (0.0–1.4)	0.423
Severe Score						
SOFA	6.0 (4.0–8.0)	6.0 (9.0–12.0)	<0.001	5.0 (3.0–8.0)	9.5 (6.0–12.8)	<0.001
qSOFA	2.0 (2.0–3.0)	2.0 (2.0–3.0)	<0.001	2.0 (2.0–3.0)	2.5 (2.0–3.0)	0.003
SAPSII	42 (32–51)	56 (45–72)	<0.001	41 (32–50)	58 (45–70)	<0.001
GCS	14 (11–14)	13 (8–14)	<0.001	14 (10–14)	13 (14–8.25)	0.056

SAPSII, patients' simplified acute physiology score; SOFA, sequential organ failure assessment; qSOFA, quick sequential organ failure assessment; GCS, Glasgow coma scale; INR: international normalized ratio.

patients with hepatic encephalopathy. Wei et al. (2020) found that Enterobacteriaceae can improve patients' mild cognitive impairment. Although the study of Li et al. (2018) has proved that the intestinal flora could affect SAE through the vagus nerve. Unfortunately, our study found that intestinal infections and microbes have nothing to do with the prognosis of SAE patients. It may require further experimental study in the future.

The SAPS II was developed from a European/North American study. Patients included in that study were from medical and surgical wards, as well as ICUs, in ten European and two North American countries. The authors showed that SAPS II demonstrated a high level of predictivity on the death of hospitalized patients (Le Gall et al., 1993). Although later studies have suggested better predictive tools than SAPS II (Norrie,

TABLE 2 | Patients' Outcome in the primary and validation cohorts.

	Primary cohort			Validation cohort		
	Survive group *n* = 586	**Non-survival group *n* = 258**	***P***	**Survive group *n* = 147**	**Non-survival group *n* = 64**	***P***
Mechanical ventilation, n (%)	206 (35.2)	136 (52.7)	<0.001	60 (40.8)	36 (56.3)	0.038
Renal replacement therapy, n (%)	12 (2.0)	31 (12.0)	<0.001	9 (6.1)	5 (7.8)	0.650
Organ failure (%)						
Respiratory	193 (32.9)	164 (63.6)	<0.001	58 (39.5)	45 (70.3)	<0.001
Cardiovascular	50 (8.5)	150 (58.1)	<0.001	59 (40.1)	40 (62.5)	0.003
Renal	336 (57.3)	179 (69.4)	<0.001	78 (53.1)	44 (68.8)	0.034
Hepatic	29 (3.3)	27 (10.5)	<0.001	6 (4.1)	7 (10.9)	0.057
Hematologic	124 (21.2)	69 (26.7)	<0.001	31 (21.1)	25 (39.1)	0.007
ICU stay time, days	2.8 (1.7–5.6)	3.4 (1.8–8.7)	<0.001	3.0 (1.8–6.8)	2.7 (1.1–7.2)	0.234

ICU, intensive care unit.

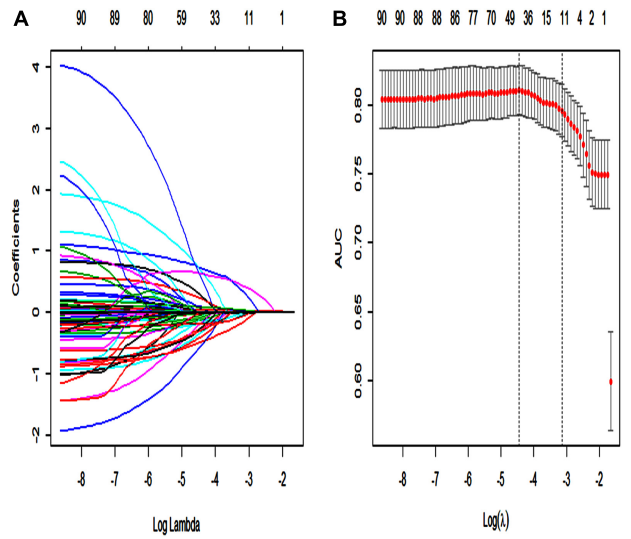

FIGURE 2 | Texture feature selection using the least absolute shrinkage and selection operator (LASSO) binary logistic regression model. **(A)** Each curve in the figure represents the change trajectory of each independent variable coefficient. The ordinate is the value of the coefficient, the lower abscissa is log(λ), and the upper abscissa is the number of non-zero coefficients in the model at this time. **(B)** 10-fold cross-cross validation fitting and then select the model, and at the same time have a more accurate estimate of the performance of the model. For each λ value, around the mean value of the target parameter shown by the red dot, we can get a confidence interval for the target parameter. The two dashed lines indicate two special λ values:c (cvfit$lambda.min, cvfit$lambda.1se). The area under the receiver operating characteristic (AUC) curve was plotted vs. log(λ).

2015), our cohort study showed that the SAPS II score of non-surviving patients was significantly higher than that of patients in the survival group, which further supports the accuracy of SAPS II as an independent predictive factor for hospital mortality in SAE patients.

Our cohort study demonstrated that the incidence of renal replacement therapy in the non-survival group was significantly higher than that in the survival group. After LASSO and multivariate Cox regression analyses, it was found to be an independent risk factor for the death of SAE. However, the use of renal replacement therapy cannot be assumed to be an independent factor for death. Patients who were given renal replacement therapy were more likely to be severely ill with worse kidney function, more serious infection, and a higher incidence of multiple organ dysfunction, and internal environmental disorders (Palevsky, 2008; Bagshaw and Wald, 2018; Tandukar and Palevsky, 2018). This, in turn, leads to a higher mortality rate. Our cohort study also showed that SAE patients with respiratory failure, worse coagulation function, and lower albumin levels were more likely to die. The mechanism of multiple organ dysfunction in patients with SAE is consistent with sepsis patients, and it may be attributed to the immune response to sepsis (Nolt et al., 2018); circulatory abnormalities (De Backer et al., 2013; Finfer et al., 2013), organ ischemia; hypoxia endothelial permeability increases (Kopterides et al., 2011; Opal and van der Poll, 2015); cell death (Pinheiro da Silva and Nizet, 2009); and mitochondrial dysfunction (Yang et al., 2015; Sun et al., 2019). We should promptly correct the respiratory failure, give component blood transfusions, correct coagulation function, supplement albumin, and reduce the mortality of SAE patients.

Lactate is a vital laboratory indicator that affects the prognosis of patients with sepsis. It is widely known, the higher the lactate level, the worse the patient's prognosis (Suetrong and Walley, 2016; Liu et al., 2019). Serum lactate is also an independent risk factor for the prognosis of SAE patients in our cohort study. In patients with septic shock, fluid resuscitation guided by monitoring the serum lactate is still the most effective method for reducing the mortality of septic shock (Hernández et al., 2019). Serum lactate is used to evaluate disease severity, guide treatment plan, and predict patient prognosis (Suetrong and Walley, 2016). Lower serum lactate levels are associated with reduced patient mortality (Puskarich et al., 2013; Vincent et al., 2016). Therefore, serum lactate is an important indicator for evaluating the prognosis of patients with sepsis and SAE. The results of previous studies further support our conclusion. Patients with lactate acidosis and hyperlactic acidosis, we should timely rehydration and other treatments to reduce lactate levels and improve the survival rate of SAE patients.

There is currently a lack of effective tools for predicting hospital mortality in SAE patients. By exploring the clinical indicators for evaluating the prognosis of SAE patients,

TABLE 3 | Multivariate COX analysis of risk factors to hospital mortality.

	Multivariate analysis			
	RR	95.0% CI		*p*-values
		Lower	Upper	
Sex *n* (%)	1.018	0.857	1.207	0.842
Female				
Male				
Admission_type (%)				
Emergency	1.000			
Elective	1.209	0.546	2.676	0.639
Urgent	1.924	0.950	3.897	0.069
Urinary tract Infection (%)	1.022	0.849	1.230	0.817
Anemias (%)	0.363	0.912	1.286	0.363
SAPSII	1.013	1.008	1.018	<0.001
Renal replacement therapy, *n* (%)	2.282	1.598	3.258	<0.001
Sysbp (mmHg)	0.998	0.992	1.004	0.462
Tempc (°C)	0.776	0.703	0.857	<0.001
SpO_2 (mmHg)	0.989	0.980	0.997	0.012
Albumin (g/dL)	1.182	1.040	1.343	0.011
INR	1.140	1.064	1.222	<0.001
Partial time (s)	0.997	0.987	1.008	0.645
lactate (mmol/l)	1.070	1.039	1.103	<0.001
Respiratory failure (%)	1.847	1.540	2.215	<0.001

SAPSII, patients' simplified acute physiology score; INR, international normalized ratio.

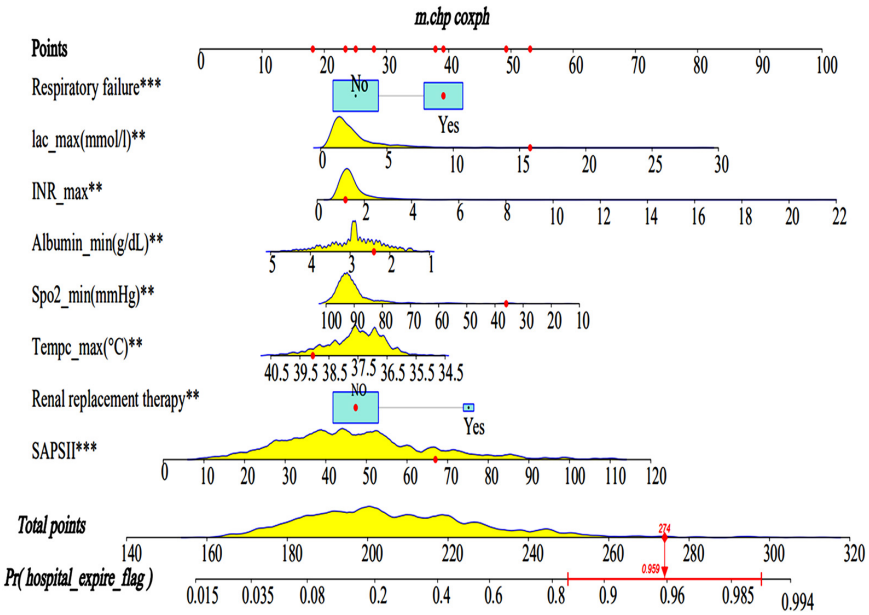

FIGURE 3 | Nomograms for the prediction of the hospital mortality of SAE patients. The line segment corresponding to each variable is marked with a scale, which represents the value range of the variable, and the length of the line segment reflects the contribution of the factor to the hospital mortality of SAE patients. The Point in the figure represents the individual score corresponding to each variable under different values, and the total score, namely Total Point, represents the total score of the sum of the corresponding individual scores after all the variables are valued. SAPS II, simplified acute physiology score; Lac, lactate. ** < 0.05, *** < 0.01.

through Lasso and Cox regression analysis, eight potential predictors, including SAPS II, renal replacement therapy, albumin, INR, lactate, body temperature, SpO_2, respiratory failure were identified and used to establish a comprehensive visual nomogram for predicting hospital mortality of SAE patient. The nomogram demonstrated excellent discrimination (AUC, 0.812; 95%CI: 0.780–0.843) that was better than SAPS II (AUC, 0.745; 95%CI: 0.708–0.783) in the primary cohort. The validation cohort is used to verify the calibration function of the nomogram and has good consistency with the model (**Figure 5**). In terms of clinical application, the net benefit of patients using nomogram is better than that of SAPS II (**Figure 6**), and the nomogram shows good performance in predicting hospital mortality of SAE patients. For the evaluation of nomograms, in addition to the above-mentioned AUC value and other methods, some new methods may be needed to evaluate in the future (Zhou et al., 2019; Liu F. et al., 2020).

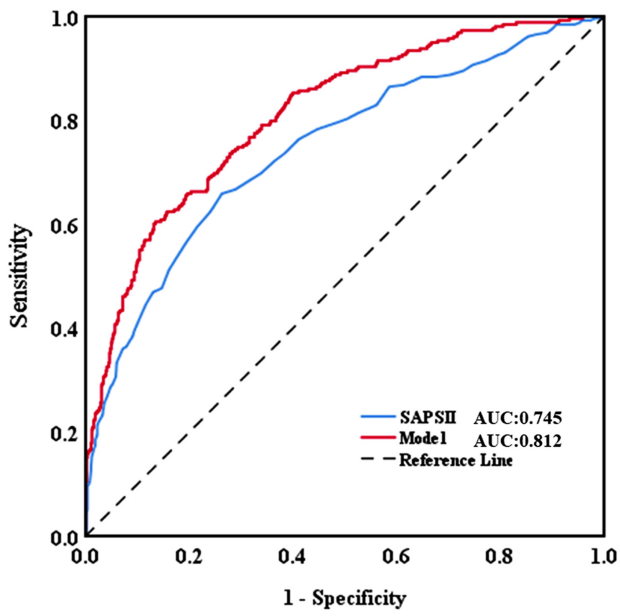

FIGURE 4 | Discriminatory accuracy for predicting the incidence of SAE assessed by receiver operator characteristics (ROC) analysis calculating area under the curve (AUC). SAPS II, simplified acute physiology score.

Several limitations must be acknowledged. Firstly, our study is retrospective based on the MIMIC database, which has its inherent limitations. For instance, our study identified septic patients using the definition from the ICD-9 diagnostic code, which may be different from the Sepsis-3 definition. However, this small discrepancy does not deny the clinical application value of our study. Although our nomogram has excellent performance, our data is older and we need new data to verify in the future. Secondly, we included ICU patients for analysis, which enhanced the heterogeneity of the study population, and thus our results may not be suitable for patients outside the ICU. Third, there are a lot of more widely used methods in feature selection and classification than Lasso, such as elastic net, random forest, and deep neural network (Huang et al., 2017; He et al., 2020a,b; Liang et al., 2020; Liu C. et al., 2020; Yang J. et al., 2020). Model development only uses the general

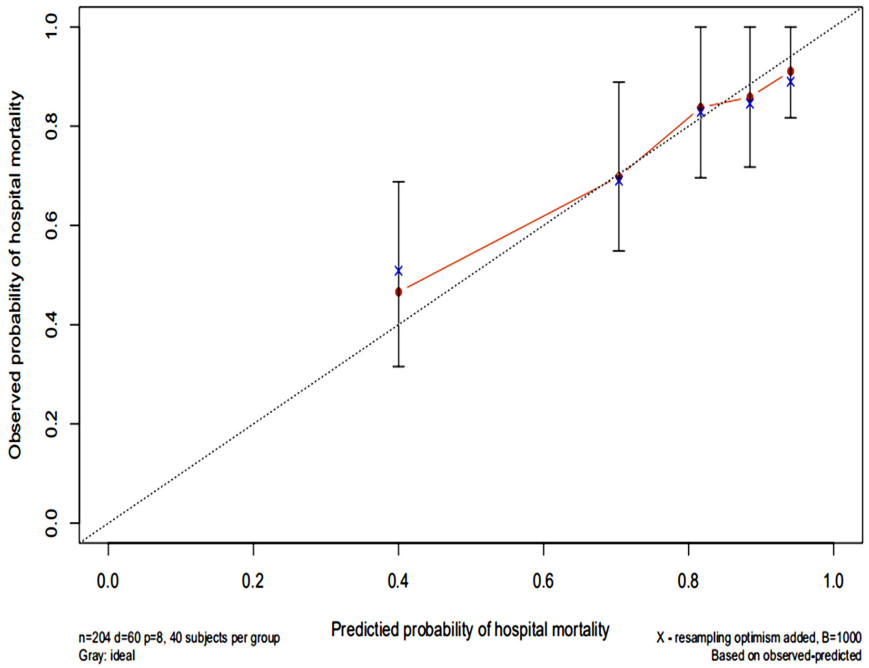

FIGURE 5 | Calibration curves of a nomogram estimating the hospital mortality of SAE patients. The x-axis represents the predicted risk of hospital death in patients with SAE. The y-axis represents the actual risk of hospital death in patients with SAE. The dotted line represents the perfect prediction of the ideal model. The closer the red solid line is to the dotted line, the better the performance of this nomogram.

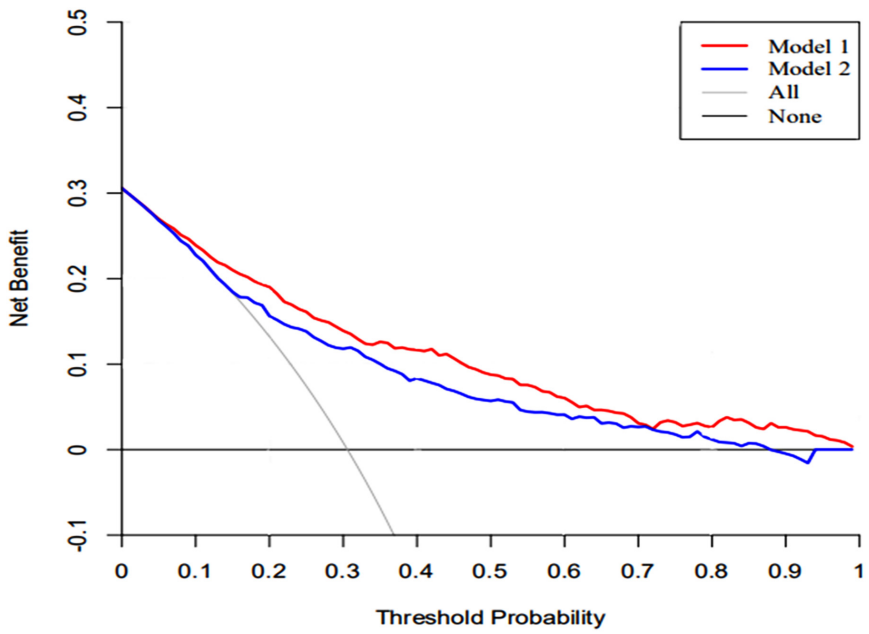

FIGURE 6 | The DCA curve of medical intervention in patients with the nomogram and SAPS II. Model 1: nomogram; Model 2: SAPS II. Solid line: The patient does not apply the nomogram, and the net income is zero; Gray line: All patients used the nomogram. The further the red solid line and blue solid line are from the dotted line, the greater the clinical application value.

linear regression method, fusing various biological information by multi-information fusion (Peng et al., 2017), bipartite local model (Peng et al., 2020b), and the KATZ method (Zhou et al., 2020) should be further studied in the future. We will apply these methods to further improve the performance of our model. Finally, the Model establishment was only verified internally, and

further external verification is required in the future to illustrate its extrapolation.

CONCLUSION

A nomogram was established for predicting hospital mortality of SAE patients, which was accurate and clinically useful. The nomogram also performed better than the SAPS II with a higher net benefit.

DATA AVAILABILITY STATEMENT

The original contributions presented in the study are included in the article/**Supplementary Material**, further inquiries can be directed to the corresponding author/s.

ETHICS STATEMENT

The studies involving human participants were reviewed and approved by the establishment of the database was approved by the Massachusetts Institute of Technology (Cambridge, MA, United States) and the Institutional Review Boards of Beth Israel Deaconess Medical Center (Boston, MA, United States). Written informed consent for participation was not required for this study in accordance with the national legislation and the institutional requirements.

AUTHOR CONTRIBUTIONS

LZ, YL, XS, and YL developed this manuscript central ideas. YW and ZG collected the data regarding the manuscript. LZ wrote the first draft of the manuscript. YL and XS revised the manuscript, worked on the English, and made the final version of the manuscript. All authors read and approved the final manuscript.

FUNDING

This work was supported by the CAMS Innovation Fund for Medical Sciences (CIFMS, serial number 2020-I2M-C&T-B-014).

SUPPLEMENTARY MATERIAL

The Supplementary Material for this article can be found online at: https://www.frontiersin.org/articles/10.3389/fmicb.2021.737066/full#supplementary-material

Supplementary Material 1 | Exclusion of patients with traumatic injury from the MIMIC III database according to ICD-9 codes.

Supplementary Material 2 | Exclusion of patients with intracerebral hemorrhage, cerebral embolism, and ischemic stroke disease from the MIMIC III database according to ICD-9 codes.

Supplementary Material 3 | Exclusion of patients with meningitis and encephalitis from the MIMIC III database according to ICD-9 codes.

Supplementary Material 4 | Exclusion of patients with Epilepsy disease from the MIMIC III database according to ICD-9 codes.

Supplementary Material 5 | Exclusion of patients with other cerebrovascular disease from the MIMIC III database according to ICD-9 codes.

Supplementary Material 6 | Exclusion of patients with mental disorders and neurological disease from the MIMIC III database according to ICD-9 codes.

Supplementary Material 7 | Exclusion of patients with alcohol intoxication/abuse or drug abuse from the MIMIC III database according to ICD-9 codes.

Supplementary Material 8 | Exclusion of patients with metabolic encephalopathy, hepatic encephalopathy, hypertensive encephalopathy, diabetes with coma, disorders of the urea cycle, hypernatremia from the MIMIC III database according to ICD-9 codes.

Supplementary Material 9 | Type of disease and ICD-9 codes.

Supplementary Material 10 | Infection site and ICD-9 codes.

Supplementary Material 11 | Organ failure was defined by a combination of ICD-9-CM and Current Procedural Terminology (CPT) codes.

Supplementary Material 12 | Data profiling report.

Supplementary Material 13 | Data supplement, potential predictors by LASSO logistic regression model.

REFERENCES

Annane, D., and Sharshar, T. (2015). Cognitive decline after sepsis. *Lancet Respir. Med.* 3, 61–69. doi: 10.1016/s2213-2600(14)70246-2

Bagga, D., Reichert, J. L., Koschutnig, K., Aigner, C. S., Holzer, P., Koskinen, K., et al. (2018). Probiotics drive gut microbiome triggering emotional brain signatures. *Gut Microbes* 9, 486–496.

Bagshaw, S. M., and Wald, R. (2018). Indications and timing of continuous renal replacement therapy application. *Contrib. Nephrol.* 194, 25–37. doi: 10.1159/000485598

De Backer, D., Donadello, K., Sakr, Y., Ospina-Tascon, G., Salgado, D., Scolletta, S., et al. (2013). Microcirculatory alterations in patients with severe sepsis: impact of time of assessment and relationship with outcome. *Crit. Care Med.* 41, 791–799. doi: 10.1097/ccm.0b013e3182742e8b

Eidelman, L. A., Putterman, D., Putterman, C., and Sprung, C. L. (1996). The spectrum of septic encephalopathy. Definitions, etiologies, and mortalities. *JAMA* 275, 470–473. doi: 10.1001/jama.1996.03530300054040

Finfer, S. R., Vincent, J. L., Vincent, J. L., and De Backer, D. (2013). Circulatory shock. *N. Engl. J. Med.* 369, 1726–1734.

Fraser, G. L., Riker, R. R., and Coursin, D. C. (2014). Long-term cognitive impairment after critical illness. *N. Engl. J. Med.* 370:184. doi: 10.1056/nejmc1313886

Gofton, T. E., and Young, G. B. (2012). Sepsis-associated encephalopathy. *Nat. Rev. Neurol.* 8, 557–566.

Grochowska, M., Wojnar, M., and Radkowski, M. (2018). The gut microbiota in neuropsychiatric disorders. *Acta Neurobiol. Exp.* 78, 69–81. doi: 10.21307/ane-2018-008

He, B., Dai, C., Lang, J., Bing, P., Tian, G., Wang, B., et al. (2020a). A machine learning framework to trace tumor tissue-of-origin of 13 types of cancer based on DNA somatic mutation. *Biochim. Biophys. Acta Mol. Basis Dis.* 1866:165916. doi: 10.1016/j.bbadis.2020.165916

He, B., Lang, J., Wang, B., Liu, X., Lu, Q., He, J., et al. (2020b). TOOme: a novel computational framework to infer cancer tissue-of-origin by integrating both gene mutation and expression. *Front. Bioeng. Biotechnol.* 8:394. doi: 10.3389/fbioe.2020.00394

Hernández, G., Ospina-Tascón, G. A., Damiani, L. P., Estenssoro, E., Dubin, A., Hurtado, J., et al. (2019). Effect of a resuscitation strategy targeting peripheral perfusion status vs serum lactate levels on 28-day mortality among patients with septic shock: the andromeda-shock randomized clinical trial. *JAMA* 321, 654–664. doi: 10.1001/jama.2019.0071

Huang, L., Li, X., Guo, P., Yao, Y., Liao, B., Zhang, W., et al. (2017). Matrix completion with side information and its applications in predicting the antigenicity of influenza viruses. *Bioinformatics* 33, 3195–3201. doi: 10.1093/bioinformatics/btx390

Iwashyna, T. J., Ely, E. W., Smith, D. M., and Langa, K. M. (2010). long-term cognitive impairment and functional disability among survivors of severe sepsis. *JAMA* 304, 1787–1794. doi: 10.1001/jama.2010.1553

Johnson, A. E., Pollard, T. J., Shen, L., Lehman, L. W., Feng, M., Ghassemi, M., et al. (2016). MIMIC-III, a freely accessible critical care database. *Sci. Data* 3:160035.

Kopterides, P., Nikitas, N., Vassiliadi, D., Orfanos, S. E., Theodorakopoulou, M., Ilias, I., et al. (2011). Microdialysis-assessed interstitium alterations during sepsis: relationship to stage, infection, and pathogen. *Intensive Care Med.* 37, 1756–1764.

Le Gall, J. R., Lemeshow, S., and Saulnier, F. (1993). A new Simplified Acute Physiology Score (SAPS II) based on a European/North American multicenter study. *JAMA* 270, 2957–2963. doi: 10.1001/jama.270.24.2957

Li, S., Lv, J., Li, J., Zhao, Z., Guo, H., Zhang, Y., et al. (2018). Intestinal microbiota impact sepsis associated encephalopathy via the vagus nerve. *Neurosci. Lett.* 662, 98–104. doi: 10.1016/j.neulet.2017.10.008

Liang, Y., Wang, H., Yang, J., Li, X., Dai, C., Shao, P., et al. (2020). A deep learning framework to predict tumor tissue-of-origin based on copy number alteration. *Front. Bioeng. Biotechnol.* 8:701. doi: 10.3389/fbioe.2020.00701

Liu, C., Wei, D., Xiang, J., Ren, F., Huang, L., Lang, J., et al. (2020). An improved anticancer drug-response prediction based on an ensemble method integrating matrix completion and ridge regression. *Mol. Ther. Nucleic Acids* 21, 676–686. doi: 10.1016/j.omtn.2020.07.003

Liu, F., Peng, L., Tian, G., Yang, J., Chen, H., Hu, Q., et al. (2020). Identifying small molecule-miRNA associations based on credible negative sample selection and random walk. *Front. Bioeng. Biotechnol.* 8:131. doi: 10.3389/fbioe.2020.00131

Liu, Z., Meng, Z., Li, Y., Zhao, J., Wu, S., Gou, S., et al. (2019). Prognostic accuracy of the serum lactate level, the SOFA score and the qSOFA score for mortality among adults with Sepsis. *Scand. J. Trauma Resuc. Emerg. Med.* 27:51.

Nolt, B., Tu, F., Wang, X., Ha, T., Winter, R., Williams, D. L., et al. (2018). Lactate and immunosuppression in sepsis. *Shock* 49, 120–125. doi: 10.1097/shk.0000000000000958

Norrie, J. (2015). Mortality prediction in ICU: a methodological advance. *Lancet Respir. Med.* 3, 5–6. doi: 10.1016/s2213-2600(14)70268-1

Opal, S. M., and van der Poll, T. (2015). Endothelial barrier dysfunction in septic shock. *J. Intern. Med.* 277, 277–293. doi: 10.1111/joim.12331

Palevsky, P. M. (2008). Indications and timing of renal replacement therapy in acute kidney injury. *Crit. Care Med.* 36(4 Suppl.), S224–S228.

Peng, L. H., Yin, J., Zhou, L., Liu, M. X., and Zhao, Y. (2018). Human microbe-disease association prediction based on adaptive boosting. *Front. Microbiol.* 9:2440. doi: 10.3389/fmicb.2018.02440

Peng, L., Bo, L., Wen, Z., Li, Z., and Li, K. (2017). Predicting drug–target interactions with multi-information fusion. *IEEE J. Biomed. Health Inf.* 21, 561–572. doi: 10.1109/jbhi.2015.2513200

Peng, L., Shen, L., Liao, L., Liu, G., and Zhou, L. (2020a). RNMFMDA: a microbe-disease association identification method based on reliable negative sample selection and logistic matrix factorization with neighborhood regularization. *Front. Microbiol.* 11:592430. doi: 10.3389/fmicb.2020.592430

Peng, L., Tian, X., Shen, L., Kuang, M., and Zhou, L. (2020b). Identifying effective antiviral drugs against SARS-CoV-2 by drug repositioning through virus-drug association prediction. *Front. Genet.* 11:577387. doi: 10.3389/fgene.2020.577387

Pinheiro da Silva, F., and Nizet, V. (2009). Cell death during sepsis: integration of disintegration in the inflammatory response to overwhelming infection. *Apoptosis* 14, 509–521. doi: 10.1007/s10495-009-0320-3

Puskarich, M. A., Trzeciak, S., Shapiro, N. I., Albers, A. B., Heffner, A. C., Kline, J. A., et al. (2013). Whole blood lactate kinetics in patients undergoing quantitative resuscitation for severe sepsis and septic shock. *Chest* 143, 1548–1553. doi: 10.1378/chest.12-0878

Sauerbrei, W., Royston, P., Binder, and H. (2007). Selection of important variables and determination of functional form for continuous predictors in multivariable model building. *Stat. Med.* 26, 5512–5528. doi: 10.1002/sim.3148

Schuler, A., Wulf, D. A., Lu, Y., Iwashyna, T. J., Escobar, G. J., and Shah, N. H. (2018). The impact of acute organ dysfunction on long-term survival in sepsis. *Crit. Care Med.* 46, 843–849. doi: 10.1097/ccm.0000000000003023

Singer, M., Deutschman, C. S., Seymour, C. W., Shankar-Hari, M., Annane, D., Bauer, M., et al. (2016). The third international consensus definitions for sepsis and septic shock (Sepsis-3). *JAMA* 315, 801–810.

Sonneville, R., De Montmollin, E., Poujade, J., Garrouste-Orgeas, M., Souweine, B., Darmon, M., et al. (2017). Potentially modifiable factors contributing to sepsis-associated encephalopathy. *Intensive Care Med.* 43, 1075–1084. doi: 10.1007/s00134-017-4807-z

Suetrong, B., and Walley, K. R. (2016). Lactic Acidosis in sepsis: it's not all anaerobic implications for diagnosis and management related systems. *Chest* 149, 252–261. doi: 10.1378/chest.15-1703

Sun, H., Yang, J., Zhang, T., Long, L. P., Jia, K., Yang, G., et al. (2013). Using sequence data to infer the antigenicity of influenza virus. *mBio* 4, e00230–13.

Sun, J., Zhang, J., Tian, J., Virzi, G. M., Digvijay, K., Cueto, L., et al. (2019). Mitochondria in sepsis-induced AKI. *J. Am. Soc. Nephrol.* 30, 1151–1161.

Tandukar, S., and Palevsky, P. M. (2018). Continuous renal replacement therapy - who, when, why and how. *Chest* 155, 626–638.

Vincent, J. L., Quintairos, E. S. A., Couto, L. Jr., and Taccone, F. S. (2016). The value of blood lactate kinetics in critically ill patients: a systematic review. *Crit. Care* 20:257.

Wang, F., Yang, J., Lin, H., Li, Q., Ye, Z., Lu, Q., et al. (2020). Improved human age prediction by using gene expression profiles from multiple tissues. *Front. Genet.* 11:1025. doi: 10.3389/fgene.2020.01025

Wei, W., Miao, L. V., Ng, T., Lei, F., and Lee, Y. K. (2020). Mental awareness improved mild cognitive impairment and modulated gut microbiome. *Aging* 12, 24371–24393. doi: 10.18632/aging.202277

Xia, X., Chen, J., Xia, J., Wang, B., Liu, H., Yang, L., et al. (2018). Role of probiotics in the treatment of minimal hepatic encephalopathy in patients with HBV-induced liver cirrhosis. *J. Int. Med. Res.* 46, 3596–3604. doi: 10.1177/0300060518776064

Yang, J., Huang, T., Petralia, F., Long, Q., Zhang, B., Argmann, C., et al. (2015). Synchronized age-related gene expression changes across multiple tissues in human and the link to complex diseases. *Sci. Rep.* 5:15145.

Yang, J., Peng, S., Zhang, B., Houten, S., Schadt, E., Zhu, J., et al. (2020). Human geroprotector discovery by targeting the converging subnetworks of aging and age-related diseases. *Geroscience* 42, 353–372. doi: 10.1007/s11357-019-00106-x

Yang, Y., Liang, S., Geng, J., Wang, Q., Wang, P., Cao, Y., et al. (2020). Development of a nomogram to predict 30-day mortality of patients with sepsis-associatwed encephalopathy: a retrospective cohort study. *J. Intensive Care* 8:45.

Zhou, L., Li, Z., Yang, J., Tian, G., Liu, F., Wen, H., et al. (2019). Revealing drug-target interactions with computational models and algorithms. *Molecules* 24:1714. doi: 10.3390/molecules24091714

Zhou, L., Wang, J., Liu, G., Lu, Q., and Peng, L. (2020). Probing antiviral drugs against SARS-CoV-2 through virus-drug association prediction based on the KATZ method. *Genomics* 112, 4427–4434. doi: 10.1016/j.ygeno.2020.07.044

Conflict of Interest: The authors declare that the research was conducted in the absence of any commercial or financial relationships that could be construed as a potential conflict of interest.

Publisher's Note: All claims expressed in this article are solely those of the authors and do not necessarily represent those of their affiliated organizations, or those of the publisher, the editors and the reviewers. Any product that may be evaluated in this article, or claim that may be made by its manufacturer, is not guaranteed or endorsed by the publisher.

frontiers in Microbiology

CORRECTION
published: 03 November 2021
doi: 10.3389/fmicb.2021.773499

Corrigendum: Development and Validation of a Nomogram for the Prediction of Hospital Mortality of Patients With Encephalopathy Caused by Microbial Infection: A Retrospective Cohort Study

Lina Zhao[1,2†], Yun Li[3†], Yunying Wang[2], Qian Gao[4], Zengzheng Ge[1], Xibo Sun[4] and Yi Li[1*]*

[1] Emergency Department, State Key Laboratory of Complex Severe and Rare Diseases, Peking Union Medical College Hospital, Peking Union Medical College, Chinese Academy of Medical Sciences, Beijing, China, [2] Department of Critical Care Medicine, Chifeng Municipal Hospital, Chifeng Clinical Medical College of Inner Mongolia Medical University, Chifeng, China, [3] Department of Anesthesiology, Chifeng Municipal Hospital, Chifeng Clinical Medical College of Inner Mongolia Medical University, Chifeng, China, [4] Department of Neurology, Yidu Central Hospital Affiliated to Weifang Medical University, Weifang, China

OPEN ACCESS

Edited and reviewed by:
George Tsiamis,
University of Patras, Greece

***Correspondence:**
Yi Li
billliyi@126.com
orcid.org/0000-0002-7158-3624
Xibo Sun
sunxibo92@sina.com

[†]These authors have contributed equally to this work

Specialty section:
This article was submitted to Systems Microbiology, a section of the journal Frontiers in Microbiology

Received: 10 September 2021
Accepted: 11 October 2021
Published: 03 November 2021

Citation:
Zhao L, Li Y, Wang Y, Gao Q, Ge Z, Sun X and Li Y (2021) Corrigendum: Development and Validation of a Nomogram for the Prediction of Hospital Mortality of Patients With Encephalopathy Caused by Microbial Infection: A Retrospective Cohort Study. Front. Microbiol. 12:773499. doi: 10.3389/fmicb.2021.773499

Keywords: sepsis associated encephalopathy, prognosis, hospital mortality, nomogram, microbial infection

A Corrigendum on

Development and Validation of a Nomogram for the Prediction of Hospital Mortality of Patients With Encephalopathy Caused by Microbial Infection: A Retrospective Cohort Study
by Zhao, L., Li, Y., Wang, Y., Gao, Q., Ge, Z., Sun, X., and Li, Y. (2021). Front. Microbiol. 12:737066. doi: 10.3389/fmicb.2021.737066

In the original article, there was a mistake in **Figure 1** as published. Patients with sepsis without encephalopathy should be 1480. We wrote this as 1408 by error. Therefore 3279 patients for the final analysis should be modified to 3207. In the excluded patients, all excluded patients add up to 2152, not 3560. Therefore, there are three numbers in Figure 1 that need to be changed. (1) "sepsis without encephalopathy (n=1408)" changed to "sepsis without encephalopathy (n=1480)." (2) "3279 patients for the final analysis" changed to "3207 patients for the final analysis." (3) "Exclude the following patients (n=3560)" changed to "Exclude the following patients (n=2152)." The corrected **Figure 1** appears below.

We apologize for this error and state that this does not change the scientific conclusions of the article in any way. The original article has been updated.

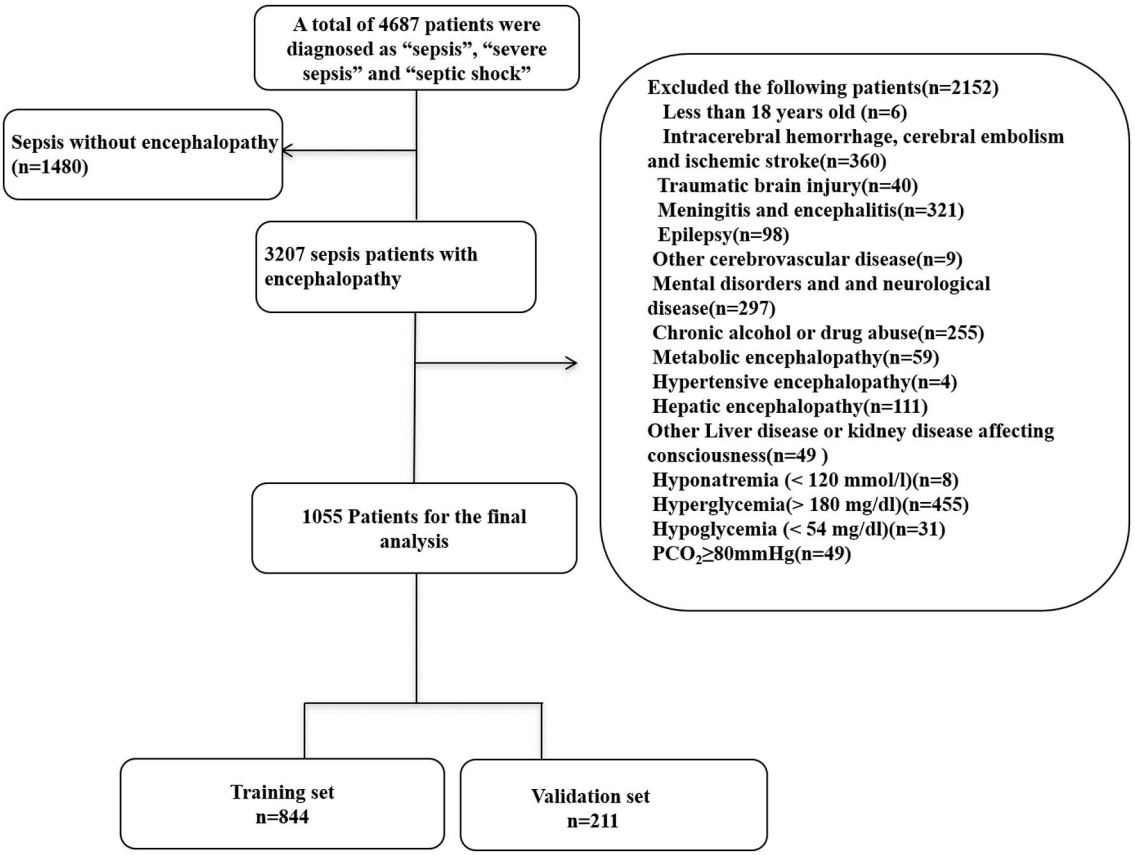

FIGURE 1 | Flow chart of the enrolled patients. MIMIC-III, Medical Information Mart for Intensive Care III.

frontiers in Microbiology

ORIGINAL RESEARCH
published: 26 August 2021
doi: 10.3389/fmicb.2021.738796

Altered Fecal Microbiome and Metabolome in a Mouse Model of Choroidal Neovascularization

*Yun Li[1,2], Yuting Cai[1,2], Qian Huang[1,2], Wei Tan[1,2], Bingyan Li[1,2], Haixiang Zhou[1,2], Zicong Wang[1,2], Jingling Zou[1,2], Chun Ding[1,2], Bing Jiang[1,2], Shigeo Yoshida[3] and Yedi Zhou[1,2]**

[1] Department of Ophthalmology, The Second Xiangya Hospital, Central South University, Changsha, China, [2] Hunan Clinical Research Center of Ophthalmic Disease, Changsha, China, [3] Department of Ophthalmology, Kurume University School of Medicine, Kurume, Japan

OPEN ACCESS

Edited by:
Zhangran Chen,
Xiamen University, China

Reviewed by:
Yan Gong,
Wuhan University, China
Fuxiang Ye,
Shanghai First People's Hospital, China

***Correspondence:**
Yedi Zhou
zhouyedi@csu.edu.cn

Specialty section:
This article was submitted to Systems Microbiology, a section of the journal Frontiers in Microbiology

Received: 09 July 2021
Accepted: 30 July 2021
Published: 26 August 2021

Citation:
Li Y, Cai Y, Huang Q, Tan W, Li B, Zhou H, Wang Z, Zou J, Ding C, Jiang B, Yoshida S and Zhou Y (2021) Altered Fecal Microbiome and Metabolome in a Mouse Model of Choroidal Neovascularization. Front. Microbiol. 12:738796. doi: 10.3389/fmicb.2021.738796

Purpose: Choroidal neovascularization (CNV) is the defining feature of neovascular age-related macular degeneration (nAMD). Gut microbiota might be deeply involved in the pathogenesis of nAMD. This study aimed to reveal the roles of the gut microbiome and fecal metabolome in a mouse model of laser-induced CNV.

Methods: The feces of C57BL/6J mice with or without laser-induced CNV were collected. Multi-omics analyses, including 16S rRNA gene sequencing and untargeted metabolomics, were conducted to analyze the changes in the gut microbial composition and the fecal metabolomic profiles in CNV mice.

Results: The gut microbiota was significantly altered in CNV mice. The abundance of *Candidatus_Saccharimonas* was significantly upregulated in the feces of CNV mice, while 16 genera, including *Prevotellaceae_NK3B31_group*, *Candidatus_Soleaferrea*, and *Truepera,* were significantly more abundant in the controls than in the CNV group. Fecal metabolomics identified 73 altered metabolites (including 52 strongly significantly altered metabolites) in CNV mice compared to control mice. Correlation analysis indicated significant correlations between the altered fecal metabolites and gut microbiota genera, such as *Lachnospiraceae_UCG-001* and *Candidatus_Saccharimonas*. Moreover, KEGG analysis revealed six pathways associated with these altered metabolites, such as the ABC transporter, primary bile acid biosynthesis and steroid hormone biosynthesis pathways.

Conclusion: The study identified an altered fecal microbiome and metabolome in a CNV mouse model. The altered microbes, metabolites and the involved pathways might be associated with the pathogenesis of nAMD.

Keywords: choroidal neovascularization, age-related macular degeneration, gut microbiome, metabolomics, mouse model

INTRODUCTION

Age-related macular degeneration (AMD) is one of the main causes of vision loss and blindness worldwide, and its incidence has dramatically increased in the population worldwide (Mitchell et al., 2018). The presence of choroidal neovascularization (CNV) is the defining feature of wet or neovascular AMD (nAMD), which is one of the two advanced forms of AMD (Patel and Sheth, 2021). As a first-line therapy, intravitreal injection of anti-vascular endothelial growth factor (VEGF) agents is effective in patients with nAMD because it targets pathological CNV (Kovach et al., 2012; Ferrara and Adamis, 2016). However, the limitations of anti-VEGF therapy should not be ignored, such as the side effects of the injection (Xi, 2020) and the unsatisfactory duration of the therapeutic effect (Ehlken et al., 2019). In addition, long-term use of anti-VEGF therapy may lead to serious economic burdens, especially in developing countries and regions (Ruiz-Moreno et al., 2021). Therefore, thorough investigation of the mechanisms of nAMD pathogenesis beyond VEGF is urgently needed.

As an *in vivo* model, laser-induced CNV in mice is widely used to investigate the mechanisms of nAMD (Lambert et al., 2013). We have previously reported the expression profiles of mRNA and various types of non-coding RNAs in a CNV mouse model (Zhang et al., 2019, 2020; Liu et al., 2020) and indicated the importance of inflammatory cytokines and immune cells in AMD pathogenesis (Zhou Y. et al., 2017; Zhou Y. D. et al., 2017; Li and Zhou, 2019; Tan et al., 2020).

Changes in the intestinal microbiota significantly affect barrier function and metabolic pathways and gradually regulate the host immune system (Cerf-Bensussan and Gaboriau-Routhiau, 2010), and loss of gut microbiota diversity affects age-related changes (O'Toole and Jeffery, 2015). Recently, numerous studies have indicated that the gut microbiome is involved in ophthalmic diseases, such as diabetic retinopathy (DR) (Huang et al., 2021), Vogt-Koyanagi-Harada disease (Ye et al., 2020), and glaucoma (Gong et al., 2020).

Zinkernagel et al. (2017) revealed enrichment of the genera *Anaerotruncus* and *Oscillibacter* as well as *Ruminococcus torques* and *Eubacterium ventriosum* in nAMD patients; on the other hand, *Bacteroides eggerthii* was enriched in controls compared to patients. However, an intestinal metagenomic study with a larger number of included cases demonstrated elevated abundance of the class *Negativicutes* in patients with nAMD, while the genus *Oscillibacter* and *Bacteroides* species were more abundant in healthy controls without AMD (Zysset-Burri et al., 2020). Therefore, further explorations and verifications in more research centers are necessary to identify changes in the gut microbiota in AMD patients.

Overweight and obesity are essential risk factors for AMD (Zhang et al., 2016). High-fat diets (HFD) enhance pathology by inducing gut microbiota alteration, and the heightened intestinal permeability and chronic low-grade inflammation induced by gut dysbiosis have been found to upregulate the production of proinflammatory cytokines and VEGF-A and enhance CNV in a laser-induced mouse model (Andriessen et al., 2016). Therefore, alteration of the gut microbiome might be a potential therapeutic target in patients with AMD. Further investigation of the intestinal microbiome might reveal the mechanisms and metabolic pathways of AMD pathogenesis, which might also generate novel therapeutic strategies for AMD.

To clarify the pathogenesis and consequences of nAMD, in this study, we characterized fecal microbiome and metabolomics profiles in a mouse model of laser-induced CNV via 16S rRNA gene sequencing and untargeted metabolomics analysis.

MATERIALS AND METHODS

Animal Model

Seven-week-old male C57BL/6J mice were obtained from Hunan SJA Laboratory Animal Co., Ltd. (Changsha, China). A model of CNV in the mice was induced by laser photocoagulation as described previously (Zhang et al., 2019). Laser photocoagulation was conducted with a 532-nm diode laser (100 mW, 0.1 s duration, 50 μm), with 25 spots burned on each eye.

Fecal samples were collected 7 days after laser photocoagulation. For control group, we used age-matched mice without laser treatment. Samples were collected from 16 mice with laser-induced CNV and 15 controls. The fecal pellets of each mouse were deposited into a sterile conical tube and stored at −80°C.

The animal experiments were performed according to the ARVO Statement for the Use of Animals in Ophthalmic and Vision Research, and the Institutional Animal Care and Use Committee of The Second Xiangya Hospital of Central South University approved all procedures of the experiments (Approval No. 2021533).

DNA and Metabolite Extraction

DNA was isolated from fecal samples by using an E.Z.N.A.® Soil DNA Kit (Omega Bio-Tek, Inc., Norcross, GA, United States). Assessment of the DNA extract was performed on an agarose gel (1%), and the concentration and purity of the DNA were determined by using a NanoDrop 2000 UV-Vis spectrophotometer (Thermo Fisher Scientific, Wilmington, DE, United States).

A 400 μL methanol:water (4:1, v/v) solution was used for the extraction of the fecal metabolites. The mixture was allowed to settle at −20°C. It was then treated with a Wonbio-96c high-throughput tissue crusher (Shanghai Wanbo Biotechnology Co., Ltd., Shanghai, China) at 50 Hz for 6 min, vortexed for 30 s and ultrasonicated at 40 kHz for 30 min. To precipitate proteins, the samples were placed at −20°C for 30 min. After centrifugation (13000 × *g*, 4°C, 15 min), the supernatant was collected for LC-MS/MS analysis.

16S rRNA Gene Sequencing Analysis

As previously described (Peng et al., 2018, 2019), the V3–V4 region of the bacterial 16S rRNA gene was amplified with the primers 338F (5′-ACTCCTACGGGAGGCAGCAG-3′) and 806R (5′-GGACTACHVGGGTWTCTAAT-3′) in an ABI GeneAmp® 9700 PCR thermocycler (ABI, CA, United States). The purified amplicons were pooled in equimolar amounts and

subjected to paired-end sequencing on an Illumina MiSeq PE300 platform/NovaSeq PE250 platform (Illumina, San Diego, CA, United States). To minimize the effects of sequencing depth on diversity measures, the number of reads from each sample was rarefied to 5567 (the minimum number of sample sequences). The Wilcoxon rank-sum test was used for statistical analysis of 16S rRNA gene sequencing analysis. The different enrichment of specific bacterial taxa was determined by the linear discriminant analysis (LDA) effect size (LEfSe) algorithm with an LDA score threshold of 2.0.

Fecal Metabolomics Analysis

A Thermo UHPLC system equipped with an ACQUITY UPLC HSS T3 (100 mm × 2.1 mm i.d., 1.8 μm; Waters Corporation, Milford, MA, United States) was used for chromatographic separation of the metabolites. A Thermo UHPLC-Q Exactive Mass Spectrometer equipped with an electrospray ionization (ESI) source operating in either positive or negative ion mode was used to collect the mass spectrometric data. Data-dependent acquisition (DDA) mode was used for the data acquisition. Detection was conducted over the mass range of 70–1050 m/z.

After UPLC-MS analyses, the raw data were imported into Progenesis QI 2.3 (Non-linear Dynamics, Waters Corporation, United States) for peak detection and alignment. The mass spectra of these metabolic features were identified by using the accurate masses, MS/MS fragment spectra and isotope ratio differences with searching in the following biochemical databases: the Human Metabolome Database (HMDB)[1] and the METLIN database[2].

[1]www.hmdb.ca

[2]metlin.scripps.edu

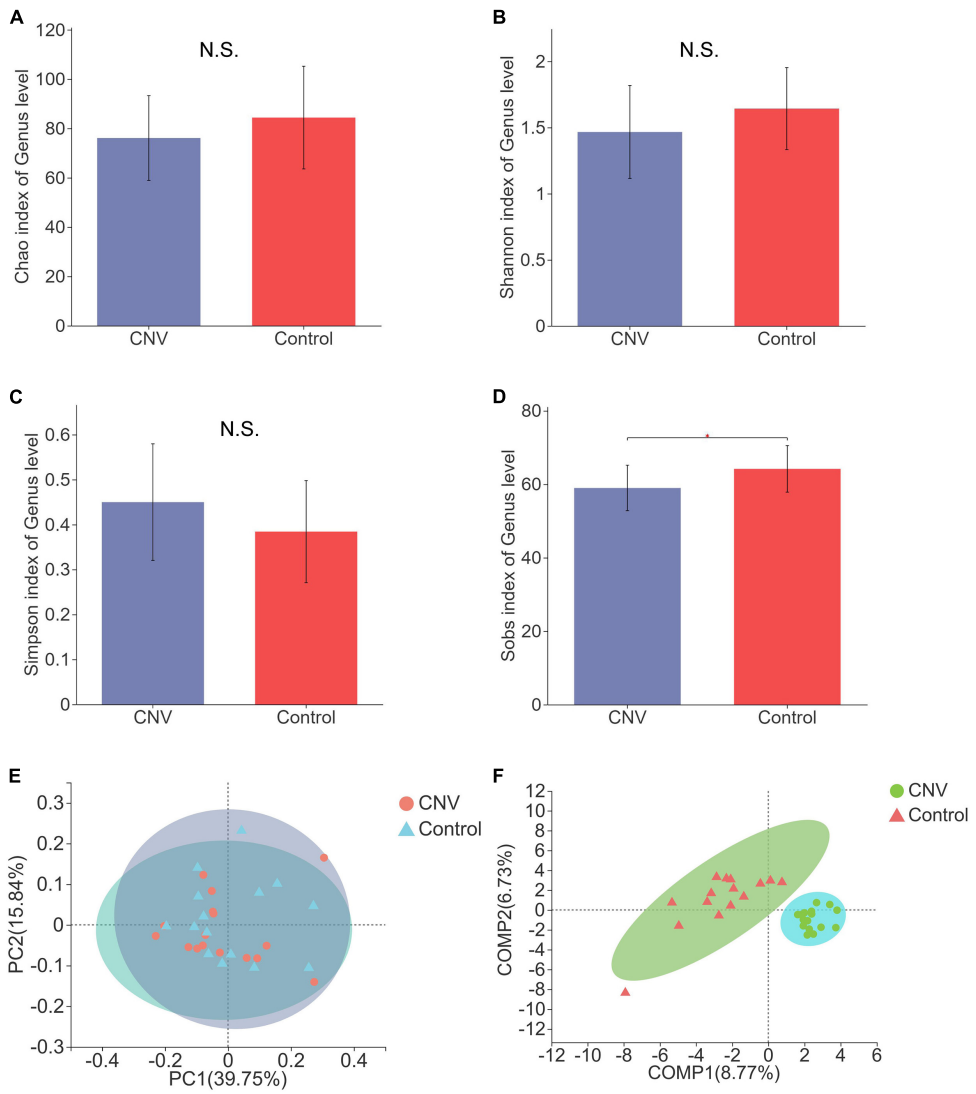

FIGURE 1 | Gut microbial diversity in CNV and control mice. Gut microbial diversity in CNV and control mice. The α-diversity was assessed by the Chao index **(A)**, Shannon index **(B)**, Simpson index **(C)**, and Sobs index **(D)**. $^{*}P < 0.05$. PCoA of the β-diversity **(E)**. PLS-DA of the microbiome at the genus level **(F)**.

Multivariate Statistical Analysis

Variables of all metabolites were scaled to unit variances and then subjected to principal component analysis (PCA) to obtain a visualized overview of the metabolic data, general clustering, trends, and outliers. Orthogonal partial least squares discriminant analysis (OPLS-DA) was used to determine the global alterations of metabolites between the CNV group and the control group. Prior to OPLS-DA, all of the metabolite variables were Pareto-scaled. Variable importance in the projection (VIP) was calculated from the OPLS-DA model. Paired Student's *t*-test was used in calculating *P*-values. Statistically significant differences between CNV group and control group were determined according to $p < 0.05$ and VIP > 1.0.

Bioinformatics Analyses

The Majorbio I-Sanger Cloud Platform[3] was used for the data analyses and bioinformatics analyses. The pathways associated with the altered metabolites were analyzed through metabolic enrichment and pathway analyses according to a database search (KEGG)[4]. Spearman's correlation analysis was conducted to assess the significance of microbiota-metabolite correlations with the threshold values of $|r| \geq 0.50$ and $p < 0.01$.

RESULTS

Diversity of the Gut Microbiota Between CNV Mice and Controls

To reveal the differences in structural diversity of the gut microbiota between CNV mice and controls, microbial α-diversity was assessed using the Chao, Shannon, Simpson, and Sobs indices. Although no significant difference in α-diversity was observed by measurement of the Chao, Shannon, and Simpson indices (**Figures 1A–C**, $p > 0.05$), significantly lower

[3]www.i-sanger.com

[4]www.genome.jp/kegg/

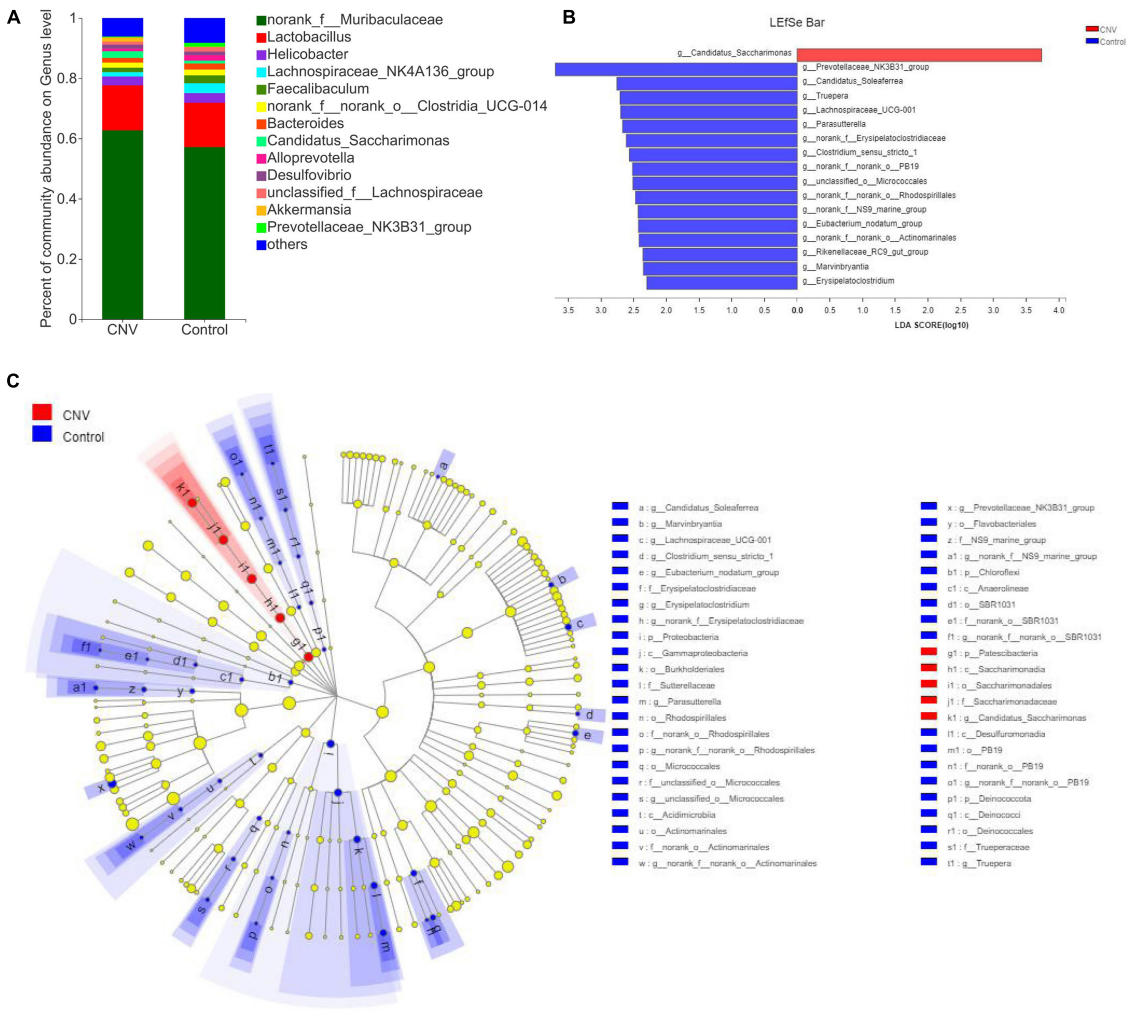

FIGURE 2 | Gut microbiota composition profiles in CNV and control mice. **(A)** Taxonomic distributions of bacteria at the genus level in CNV mice and controls. **(B)** Bar graph of LDA scores to screen altered bacterial genera at the genus level (LDA score ≥2.0). **(C)** Cladogram of the LEfSe analysis from the phylum level to the genus level of the microbiota of CNV mice and controls.

diversity was found in the CNV group than in the control group, as measured by the Sobs index (**Figure 1D**, $p = 0.03079$). For the β-diversity analysis, principal coordinate analysis (PCoA) was used after a genus selection-based bacterial taxonomy analysis was performed, and significant differences were not observed when the CNV group was compared with the control group (**Figure 1E**). However, PLS-DA indicated that the samples derived from the CNV group significantly differed from those collected from the control group (**Figure 1F**), which demonstrated the different compositions of the gut microbiota between these two groups.

Change in the Gut Microbiota Composition in CNV Mice

Taxonomic analysis revealed the differences in relative abundance at the genus level between CNV and control mice (**Figure 2A**). Among the genera, *norank_f_Muribaculaceae* was the predominant genus in both the CNV group (62.7%) and the control group (57.2%). By the LEfSe algorithm, we identified 17 genera as key discriminants (**Figures 2B,C**). *Candidatus_Saccharimonas* was significantly overrepresented in the feces of CNV mice, while 16 genera, including *Prevotellaceae_NK3B31_group*, *Candidatus_Soleaferrea*, and *Truepera,* were significantly more abundant in the control group than in the CNV group. These results demonstrate the different fecal microbiota compositions between these two groups.

Altered Fecal Metabolomic Profiles of CNV Mice

The fecal samples above were also used for identification of metabolites that are altered in CNV by metabolomics. The QC samples clustered closely in both positive and negative ion modes in the PCA (**Figures 3A,B**). OPLS-DA score plots revealed remarkable separation of these two groups under both modes (**Figures 3C,D**).

Metabolites with $p < 0.05$ and VIP > 1 were considered to be significantly altered (**Supplementary Table 1**), and those with $p < 0.05$ and VIP > 1.5 were considered to be strongly significantly altered (**Supplementary Table 2**). In total, 73 significantly altered metabolites (24 in positive ion mode and 49 in negative ion mode) and 52 strongly significantly altered metabolites (21 in positive ion mode and 31 in negative ion mode) were identified between the CNV and control groups. To visualize these 52 strongly significantly altered metabolites,

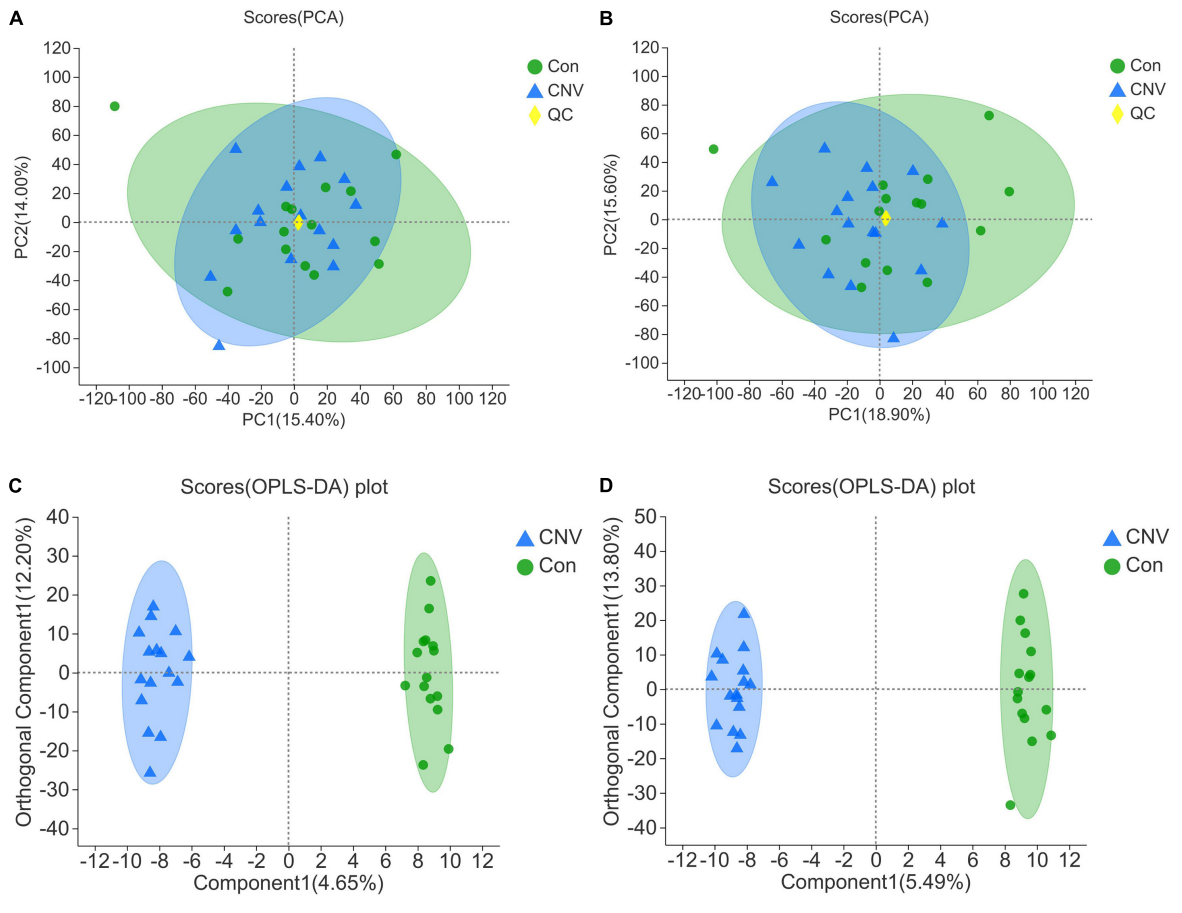

FIGURE 3 | Qualification of the results of fecal metabolomic analysis. PCA of all the samples under the positive **(A)** and negative ion mode **(B)**. OPLS-DA score plots of CNV mice and controls under the positive **(C)** and negative ion mode **(D)**.

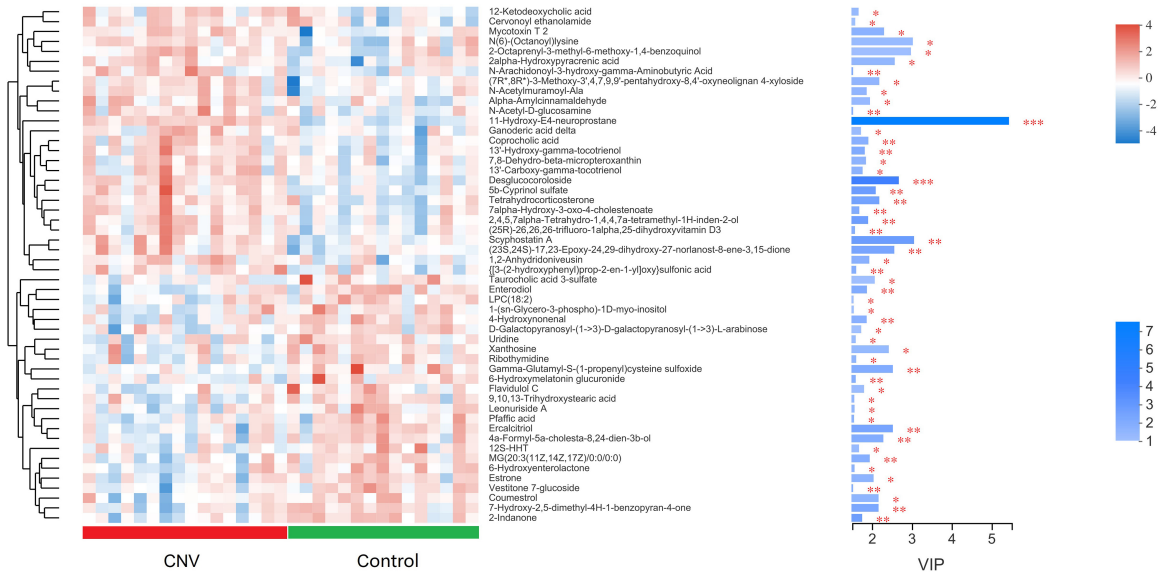

FIGURE 4 | Metabolomic profiles of fecal samples from CNV mice and controls. The hierarchical cluster and heat map show the 52 strongly significantly altered metabolites in each sample. Red and blue colors represent high and low levels of metabolites, respectively. The bar graph shows the VIP scores of each metabolite. $^{*}p < 0.05$, $^{**}p < 0.01$, $^{***}p < 0.001$.

we constructed a heat map (**Figure 4**). Overall, 27 metabolites were significantly increased in CNV mice, while 25 metabolites were significantly decreased in CNV mice. Among them, 25 metabolites belonged to the superclass of lipids and lipid-like molecules, which accounted for the largest proportion of the strongly significantly altered metabolites.

Correlations of the Fecal Metabolome and Gut Microbiota

To explore the functional correlations between the alterations of the gut microbiome and the fecal metabolome, Spearman's correlation coefficient analysis was conducted between the 17 discriminatory genera and 52 strongly significantly altered metabolites ($p < 0.05$ and VIP > 1.5). A total of 24 significant correlations were recognized (**Figure 5**). In particular, both *Lachnospiraceae_UCG-001* and *Candidatus_Saccharimonas* were significantly associated with five fecal metabolites. Moreover, *norank_f__NS9_marine_group*, *Prevotellaceae_NK3B31_group*, and *Eubacterium_nodatum_group* were significantly associated with 4, 3, and 3 metabolites, respectively. The correlations indicated that CNV mice demonstrated significant alterations in their gut microbiomes that may have led to significant changes in their metabolomic profiles.

Pathways Associated With the Altered Fecal Metabolites According to KEGG Analysis

To identify the pathways associated with these metabolites, KEGG pathway enrichment analyses were performed for the 73 significantly altered metabolites. Several essential pathways were detected ($p < 0.05$), as follows: the ATP-binding cassette (ABC) transporter pathway; primary bile acid biosynthesis; steroid hormone biosynthesis; hepatocellular carcinoma; caffeine metabolism; and cutin, suberine, and wax biosynthesis (**Figure 6**).

DISCUSSION

In this study, we characterized the gut microbiome and fecal metabolome in mice with laser-induced CNV, a widely used model of nAMD. The results indicated that the composition of the gut microbiota and the levels of fecal metabolites were significantly altered in CNV mice compared to the age-matched controls.

Linear discriminant analysis effect size revealed *Candidatus_Saccharimonas* as the only dominant genus in the CNV group, while we found 16 genera that were more abundant in the control group than in the CNV group (**Figure 2**). The bacterial genus *Candidatus_Saccharimonas*, which belongs to the phylum *Patescibacteria* (Lemos et al., 2019), was upregulated in CNV mice compared with control mice. Chen et al. (2021) revealed that the probiotic LPPS23 enriches *Candidatus_Saccharimonas* in aged mice. Green tea leaf powder improves lipid metabolism in HFD-fed mice, and gut microbiota reprogramming might be involved in the mechanism. Green tea leaf powder reduces systemic inflammation and the abundance of *Candidatus_Saccharimonas* in HFD-fed mice (Wang et al., 2020). Another study has demonstrated that egg white peptides significantly increase the relative abundance of *Candidatus_Saccharimonas* and inhibit the production of proinflammatory cytokines (Ge et al., 2021). Sang et al. (2020) reported that the

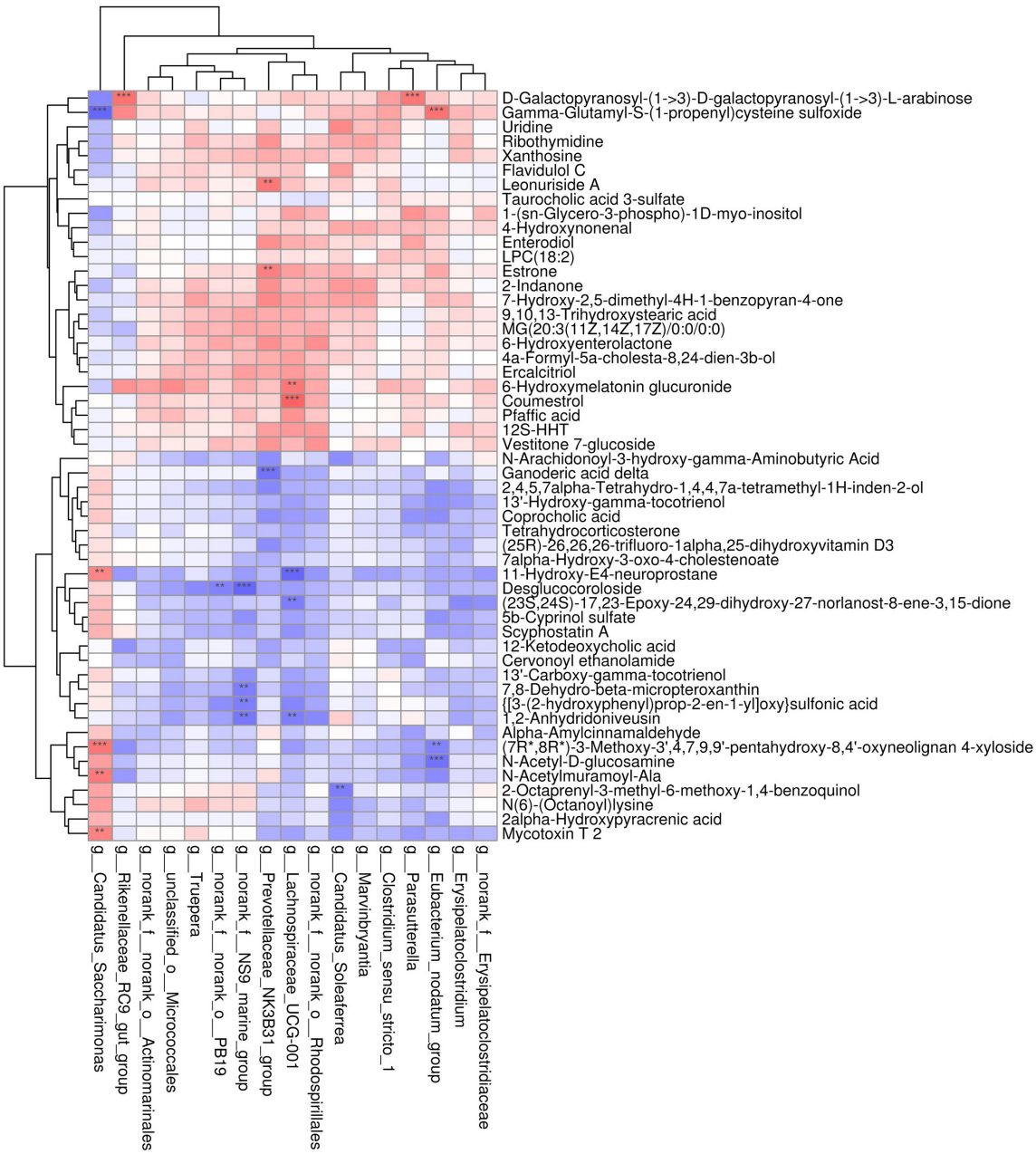

FIGURE 5 | Correlation analysis between the discriminated gut microbiota and the strongly altered fecal metabolites. Red and blue colors represent positive and negative correlations, respectively. Significant correlations were determined according to the threshold values of $|r| > 0.5$ and $P < 0.01$. $^{**}p < 0.01$, $^{***}p < 0.001$.

mushroom *Bulgaria inquinans* reduces the diversity of the gut microbiota and downregulates the abundance of *Candidatus_Saccharimonas* and that *Candidatus_Saccharimonas* is positively correlated with several cytokines (IL-2, IL-4, IL-10, and IFN-γ). Therefore, despite some unclear mechanisms, *Candidatus_Saccharimonas* might be associated with inflammation and the host immunological response. As previously described, inflammation plays an essential role in the pathogenesis of AMD (Tan et al., 2020), and it is worth further clarifying the roles and mechanisms of *Candidatus_Saccharimonas* in inflammation associated with AMD pathogenesis in future studies.

In addition, we identified 73 metabolites that were altered in CNV mice compared to controls and found that 52 of them had strong significant alteration. KEGG analysis revealed six pathways associated with these altered metabolites, such as the ABC transporter pathway. ABC transporter A1 (ABCA1), a gene involved in high-density lipoprotein (HDL) metabolism, mediates the lipid efflux pathway and has functional effects in RPE cells, and it might also contribute to the development and

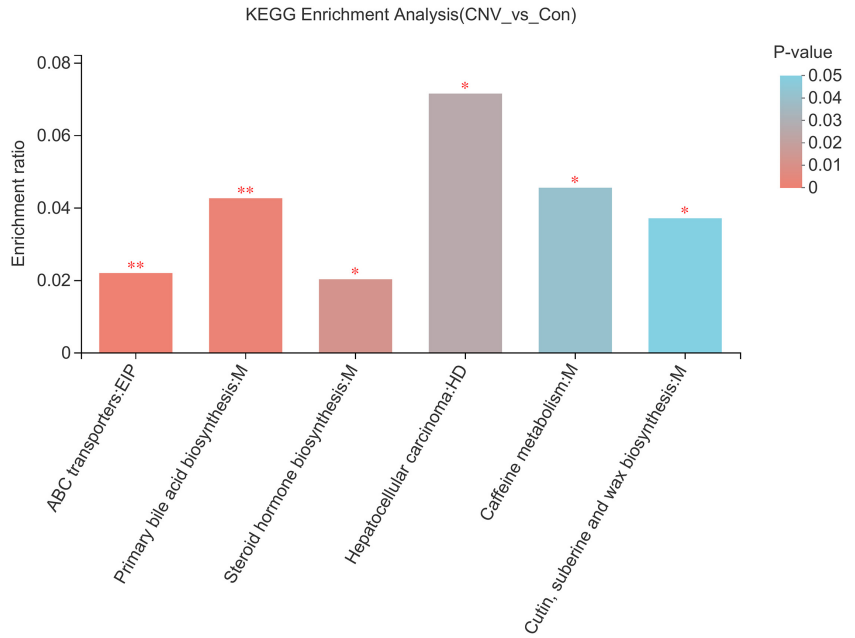

FIGURE 6 | KEGG pathway analysis reveals the pathways associated with the altered fecal metabolites. Colors represent the sizes of the *p*-values. $*p < 0.05$, $**p < 0.01$.

progression of AMD (Storti et al., 2017). Storti and Grimm (2019) reported the essential role of the ABCA1/G1 pathway and the mechanism of active cholesterol efflux in the RPE, rods, and retinal inflammatory cells. Interestingly, in a study we have previously reported, the pathway of ABC transporters was also found to be associated with plasma metabolites that are altered in retinopathy of prematurity, which is another kind of ocular neovascular disease that occurs in premature infants (Zhou et al., 2020). Therefore, the association of mechanisms of ABC transporters with the gut microbiota in AMD needs to be further studied.

Significant correlations were observed between the altered fecal metabolites and gut microbiota genera such as *Lachnospiraceae_UCG-001* and *Candidatus_Saccharimonas*. *Lachnospiraceae UCG-001* produces short-chain fatty acids, and compositional alterations of gut microbiotas including this genera have been found to be associated with inhibition of colon inflammation and tumorigenesis (Guo and Li, 2019). The abundance of *Lachnospiraceae_UCG_001* is lower in rats with ischemic stroke than in sham rats (Wu et al., 2021). Additionally, opposite to the alteration in the abundance of *Candidatus_Saccharimonas*, the abundance of *Lachnospiraceae_UCG-001* is suppressed by the probiotic LPPS23 in aged mice (Chen et al., 2021). These findings indicate that the genera *Lachnospiraceae_UCG-001* and *Candidatus_Saccharimonas* together with their associated altered fecal metabolites might be involved in the pathogenesis of nAMD, which is worth further exploration.

Recent studies demonstrated the alterations and possible application prospects of the gut microbiome in patients with other ocular neovascular diseases, such as DR (Das et al., 2021; Huang et al., 2021) and retinopathy of prematurity (Skondra et al., 2020). Das et al. (2021) recognized a reduction in anti-inflammatory, probiotic and other bacteria that could be pathogenic in the microbiomes of patients with both diabetes mellitus and DR, compared to the healthy controls, and the changes observed in DR patients were more pronounced. Huang et al. (2021) indicated the potential use of gut microbiota as a biomarker of DR, which could be helpful for diagnosis in clinical applications. Moreover, it has been suggested that the effect of antihyperglycemic drugs might be involved in the connection between the gut microbiota and DR, and targeting the gut microbiome could be novel therapeutic strategies in treating DR (Rowan and Taylor, 2018).

There were some limitations of our present study. First, the laser-induced CNV model in mice cannot completely recapitulate the characteristics of clinical samples of nAMD patients; thus, larger cohorts of patients should be investigated in future studies. Second, this study included only one time point (day 7 after laser photocoagulation), which is a representative time point for CNV. However, it is still necessary to assess alterations of the gut microbiota and metabolomics at multiple time points, especially during the period of subretinal fibrosis, which is 3–4 weeks after laser photocoagulation. Third, the roles and regulatory functions of the altered gut microbes and fecal metabolites remain to be further studied. Fecal microbiota transplantation is a novel therapy to restore the gut microbiota and cure diseases, and the investigation of this field is rapidly emerging in many diseases (Vindigni and Surawicz, 2017). Andriessen et al. (2016) confirmed that fecal microbiota transplantation regulates pathological angiogenesis in obesity-driven CNV *in vivo*. Therefore, this method could be used in future studies to

investigate the functions and mechanisms of gut microbes and fecal metabolites in CNV and nAMD.

In conclusion, we demonstrated significant alterations of the gut microbiome and fecal metabolome in CNV mice. Some altered gut microbe genera, such as *Lachnospiraceae_UCG-001* and *Candidatus_Saccharimonas*, were strongly correlated with altered fecal metabolites. Our results demonstrated concurrent alterations of the gut microbiota and fecal metabolites during the pathological process of CNV. Further studies are needed to reveal whether these altered microbiota and metabolites as well as their associated pathways play modulatory roles in CNV and nAMD pathogenesis, which might be helpful in developing novel therapeutic strategies of nAMD.

DATA AVAILABILITY STATEMENT

The raw data of 16S rRNA sequencing was deposited in NCBI Sequence Read Archive (SRA) (accession No. PRJNA744326).

ETHICS STATEMENT

The animal study was reviewed and approved by the Institutional Animal Care and Use Committee of The Second Xiangya Hospital of Central South University.

AUTHOR CONTRIBUTIONS

YZ conceived and designed the study. YZ, YL, and YC wrote the manuscript. YZ, YL, YC, QH, WT, and BL performed the experiments and collected the samples. YZ, HZ, ZW, CD, and JZ analyzed the data. BJ and SY reviewed the manuscript. All authors read and approved the final manuscript.

FUNDING

This work was supported by the National Natural Science Foundation of China (No. 81800855), Natural Science Foundation of Hunan Province (No. 2019JJ50885), and Hunan Provincial Science and Technology Department (No. 2020SK2086).

SUPPLEMENTARY MATERIAL

The Supplementary Material for this article can be found online at: https://www.frontiersin.org/articles/10.3389/fmicb.2021.738796/full#supplementary-material

Supplementary Table 1 | The significantly altered fecal metabolites (Vip > 1 and $p < 0.05$) between Cnv group and control group.

Supplementary Table 2 | The strongly significantly altered fecal metabolites (Vip > 1.5 and $p < 0.05$) between Cnv group and control group.

REFERENCES

Andriessen, E. M., Wilson, A. M., Mawambo, G., Dejda, A., Miloudi, K., Sennlaub, F., et al. (2016). Gut microbiota influences pathological angiogenesis in obesity-driven choroidal neovascularization. *Embo Mol. Med.* 8, 1366–1379. doi: 10.15252/emmm.201606531

Cerf-Bensussan, N., and Gaboriau-Routhiau, V. (2010). The immune system and the gut microbiota: friends or foes? *Nat. Rev. Immunol.* 10, 735–744. doi: 10.1038/nri2850

Chen, L. H., Wang, M. F., Chang, C. C., Huang, S. Y., Pan, C. H., Yeh, Y. T., et al. (2021). *Lacticaseibacillus paracasei* PS23 Effectively modulates gut microbiota composition and improves gastrointestinal function in aged SAMP8 mice. *Nutrients* 13:1116. doi: 10.3390/nu13041116

Das, T., Jayasudha, R., Chakravarthy, S., Prashanthi, G. S., Bhargava, A., Tyagi, M., et al. (2021). Alterations in the gut bacterial microbiome in people with type 2 diabetes mellitus and diabetic retinopathy. *Sci. Rep.* 11:2738. doi: 10.1038/s41598-021-82538-0

Ehlken, C., Guichard, M. M., Schlunck, G., Buhler, A. D., Martin, G., and Agostini, H. T. (2019). Expression of angiogenic and inflammatory factors in choroidal neovascularisation-derived retinal pigment epithelium. *Ophthalmic Res.* 61, 174–182. doi: 10.1159/000481260

Ferrara, N., and Adamis, A. P. (2016). Ten years of anti-vascular endothelial growth factor therapy. *Nat. Rev. Drug Discov.* 15, 385–403. doi: 10.1038/nrd.2015.17

Ge, H., Cai, Z., Chai, J., Liu, J., Liu, B., Yu, Y., et al. (2021). Egg white peptides ameliorate dextran sulfate sodium-induced acute colitis symptoms by inhibiting the production of pro-inflammatory cytokines and modulation of gut microbiota composition. *Food Chem.* 360:129981. doi: 10.1016/j.foodchem.2021.129981

Gong, H., Zhang, S., Li, Q., Zuo, C., Gao, X., Zheng, B., et al. (2020). Gut microbiota compositional profile and serum metabolic phenotype in patients with primary open-angle glaucoma. *Exp. Eye Res.* 191:107921. doi: 10.1016/j.exer.2020.107921

Guo, M., and Li, Z. (2019). Polysaccharides isolated from *Nostoc commune* Vaucher inhibit colitis-associated colon tumorigenesis in mice and modulate gut microbiota. *Food Funct.* 10, 6873–6881. doi: 10.1039/c9fo00296k

Huang, Y., Wang, Z., Ma, H., Ji, S., Chen, Z., Cui, Z., et al. (2021). Dysbiosis and implication of the gut microbiota in diabetic retinopathy. *Front. Cell. Infect. Microbiol.* 11:646348. doi: 10.3389/fcimb.2021.646348

Kovach, J. L., Schwartz, S. G., Flynn, H. W. Jr., and Scott, I. U. (2012). Anti-VEGF treatment strategies for wet AMD. *J. Ophthalmol.* 2012:786870. doi: 10.1155/2012/786870

Lambert, V., Lecomte, J., Hansen, S., Blacher, S., Gonzalez, M. L., Struman, I., et al. (2013). Laser-induced choroidal neovascularization model to study age-related macular degeneration in mice. *Nat. Protoc.* 8, 2197–2211. doi: 10.1038/nprot.2013.135

Lemos, L. N., Medeiros, J. D., Dini-Andreote, F., Fernandes, G. R., Varani, A. M., Oliveira, G., et al. (2019). Genomic signatures and co-occurrence patterns of the ultra-small Saccharimonadia (phylum CPR/Patescibacteria) suggest a symbiotic lifestyle. *Mol. Ecol.* 28, 4259–4271. doi: 10.1111/mec.15208

Li, Y., and Zhou, Y. (2019). Interleukin-17: the role for pathological angiogenesis in ocular neovascular diseases. *Tohoku J. Exp. Med.* 247, 87–98. doi: 10.1620/tjem.247.87

Liu, X., Zhang, L., Wang, J. H., Zeng, H., Zou, J., Tan, W., et al. (2020). Investigation of circRNA expression profiles and analysis of circRNA-miRNA-mRNA networks in an animal (mouse) model of age-related macular degeneration. *Curr. Eye Res.* 45, 1173–1180. doi: 10.1080/02713683.2020.1722179

Mitchell, P., Liew, G., Gopinath, B., and Wong, T. Y. (2018). Age-related macular degeneration. *Lancet* 392, 1147–1159. doi: 10.1016/S0140-6736(18)31550-2

O'Toole, P. W., and Jeffery, I. B. (2015). Gut microbiota and aging. *Science* 350, 1214–1215. doi: 10.1126/science.aac8469

Patel, P., and Sheth, V. (2021). New and innovative treatments for neovascular age-related macular degeneration (nAMD). *J. Clin. Med.* 10, 2436. doi: 10.3390/jcm10112436

Peng, W., Huang, J., Yang, J., Zhang, Z., Yu, R., Fayyaz, S., et al. (2019). Integrated 16S rRNA sequencing, metagenomics, and metabolomics to characterize gut

microbial composition, function, and fecal metabolic phenotype in non-obese type 2 diabetic Goto-Kakizaki Rats. *Front. Microbiol.* 10:3141. doi: 10.3389/fmicb.2019.03141

Peng, W., Yi, P., Yang, J., Xu, P., Wang, Y., Zhang, Z., et al. (2018). Association of gut microbiota composition and function with a senescence-accelerated mouse model of Alzheimer's disease using 16S rRNA gene and metagenomic sequencing analysis. *Aging (Albany NY)* 10, 4054–4065. doi: 10.18632/aging.101693

Rowan, S., and Taylor, A. (2018). The role of microbiota in retinal disease. *Adv. Exp. Med. Biol.* 1074, 429–435. doi: 10.1007/978-3-319-75402-4_53

Ruiz-Moreno, J. M., Arias, L., Abraldes, M. J., Montero, J., Udaondo, P., and Ramdeburs study group. (2021). Economic burden of age-related macular degeneration in routine clinical practice: the RAMDEBURS study. *Int. Ophthalmol.* doi: 10.1007/s10792-021-01906-x [Online ahead of print].

Sang, H., Xie, Y., Su, X., Zhang, M., Zhang, Y., Liu, K., et al. (2020). Mushroom *Bulgaria inquinans* modulates host immunological response and gut microbiota in mice. *Front. Nutr.* 7:144. doi: 10.3389/fnut.2020.00144

Skondra, D., Rodriguez, S. H., Sharma, A., Gilbert, J., Andrews, B., and Claud, E. C. (2020). The early gut microbiome could protect against severe retinopathy of prematurity. *J. AAPOS* 24, 236–238. doi: 10.1016/j.jaapos.2020.03.010

Storti, F., and Grimm, C. (2019). Active cholesterol efflux in the retina and retinal pigment epithelium. *Adv. Exp. Med. Biol.* 1185, 51–55. doi: 10.1007/978-3-030-27378-1_9

Storti, F., Raphael, G., Griesser, V., Klee, K., Drawnel, F., Willburger, C., et al. (2017). Regulated efflux of photoreceptor outer segment-derived cholesterol by human RPE cells. *Exp. Eye Res.* 165, 65–77. doi: 10.1016/j.exer.2017.09.008

Tan, W., Zou, J., Yoshida, S., Jiang, B., and Zhou, Y. (2020). The role of inflammation in age-related macular degeneration. *Int. J. Biol. Sci.* 16, 2989–3001. doi: 10.7150/ijbs.49890

Vindigni, S. M., and Surawicz, C. M. (2017). Fecal microbiota transplantation. *Gastroenterol. Clin. North Am.* 46, 171–185. doi: 10.1016/j.gtc.2016.09.012

Wang, J., Li, P., Liu, S., Zhang, B., Hu, Y., Ma, H., et al. (2020). Green tea leaf powder prevents dyslipidemia in high-fat diet-fed mice by modulating gut microbiota. *Food Nutr. Res.* 64:3672, doi: 10.29219/fnr.v64.3672

Wu, W., Sun, Y., Luo, N., Cheng, C., Jiang, C., Yu, Q., et al. (2021). Integrated 16S rRNA gene sequencing and LC-MS analysis revealed the interplay between gut microbiota and plasma metabolites in rats with ischemic stroke. *J. Mol. Neurosci.* doi: 10.1007/s12031-021-01828-4 [Online ahead of print].

Xi, L. (2020). Pigment epithelium-derived factor as a possible treatment agent for choroidal neovascularization. *Oxid. Med. Cell. Longev.* 2020:8941057. doi: 10.1155/2020/8941057

Ye, Z., Wu, C., Zhang, N., Du, L., Cao, Q., Huang, X., et al. (2020). Altered gut microbiome composition in patients with Vogt-Koyanagi-Harada disease. *Gut Microbes* 11, 539–555. doi: 10.1080/19490976.2019.1700754

Zhang, L., Liu, S., Wang, J. H., Zou, J., Zeng, H., Zhao, H., et al. (2019). Differential expressions of microRNAs and transfer RNA-derived small RNAs: potential targets of choroidal neovascularization. *Curr. Eye Res.* 44, 1226–1235. doi: 10.1080/02713683.2019.1625407

Zhang, L., Zeng, H., Wang, J. H., Zhao, H., Zhang, B., Zou, J., et al. (2020). Altered long non-coding RNAs involved in immunological regulation and associated with choroidal neovascularization in mice. *Int. J. Med. Sci.* 17, 292–301. doi: 10.7150/ijms.37804

Zhang, Q. Y., Tie, L. J., Wu, S. S., Lv, P. L., Huang, H. W., Wang, W. Q., et al. (2016). Overweight, obesity, and risk of age-related macular degeneration. *Invest. Ophthalmol. Vis. Sci.* 57, 1276–1283. doi: 10.1167/iovs.15-18637

Zhou, Y., Xu, Y., Zhang, X., Zhao, P., Gong, X., He, M., et al. (2020). Plasma metabolites in treatment-requiring retinopathy of prematurity: potential biomarkers identified by metabolomics. *Exp. Eye Res.* 199:108198. doi: 10.1016/j.exer.2020.108198

Zhou, Y., Yoshida, S., Kubo, Y., Yoshimura, T., Kobayashi, Y., Nakama, T., et al. (2017). Different distributions of M1 and M2 macrophages in a mouse model of laser-induced choroidal neovascularization. *Mol. Med. Rep.* 15, 3949–3956. doi: 10.3892/mmr.2017.6491

Zhou, Y. D., Yoshida, S., Peng, Y. Q., Kobayashi, Y., Zhang, L. S., and Tang, L. S. (2017). Diverse roles of macrophages in intraocular neovascular diseases: a review. *Int. J. Ophthalmol.* 10, 1902–1908. doi: 10.18240/ijo.2017.12.18

Zinkernagel, M. S., Zysset-Burri, D. C., Keller, I., Berger, L. E., Leichtle, A. B., Largiader, C. R., et al. (2017). Association of the intestinal microbiome with the development of neovascular age-related macular degeneration. *Sci. Rep.* 7:40826. doi: 10.1038/srep40826

Zysset-Burri, D. C., Keller, I., Berger, L. E., Largiader, C. R., Wittwer, M., Wolf, S., et al. (2020). Associations of the intestinal microbiome with the complement system in neovascular age-related macular degeneration. *NPJ Genom. Med.* 5:34. doi: 10.1038/s41525-020-00141-0

Conflict of Interest: The authors declare that the research was conducted in the absence of any commercial or financial relationships that could be construed as a potential conflict of interest.

Publisher's Note: All claims expressed in this article are solely those of the authors and do not necessarily represent those of their affiliated organizations, or those of the publisher, the editors and the reviewers. Any product that may be evaluated in this article, or claim that may be made by its manufacturer, is not guaranteed or endorsed by the publisher.

frontiers in Microbiology

ORIGINAL RESEARCH
published: 16 September 2021
doi: 10.3389/fmicb.2021.724980

Appendectomy Is Associated With Alteration of Human Gut Bacterial and Fungal Communities

Shuntian Cai[1,2†], Yanyun Fan[1,2†], Bangzhou Zhang[1,2†], Jinzhou Lin[1], Xiaoning Yang[1], Yunpeng Liu[1], Jingjing Liu[1,2], Jianlin Ren[1,2] and Hongzhi Xu[1,2*]*

[1] Department of Gastroenterology, Zhongshan Hospital Affiliated to Xiamen University, Xiamen, China, [2] School of Medicine, Institute for Microbial Ecology, Xiamen University, Xiamen, China

Recent research has revealed the importance of the appendix in regulating the intestinal microbiota and mucosal immunity. However, the changes that occur in human gut microbial communities after appendectomy have never been analyzed. We assessed the alterations in gut bacterial and fungal populations associated with a history of appendectomy. In this cross-sectional study, we investigated the association between appendectomy and the gut microbiome using 16S and ITS2 sequencing on fecal samples from 30 healthy individuals with prior appendectomy (HwA) and 30 healthy individuals without appendectomy (HwoA). Analysis showed that the gut bacterial composition of samples from HwA was less diverse than that of samples from HwoA and had a lower abundance of *Roseburia*, *Barnesiella*, *Butyricicoccus*, *Odoribacter*, and *Butyricimonas* species, most of which were short-chain fatty acids-producing microbes. The HwA subgroup analysis indicated a trend toward restoration of the HwoA bacterial microbiome over time after appendectomy. HwA had higher gut fungi composition and diversity than HwoA, even 5 years after appendectomy. Compared with those in samples from HwoA, the abundance correlation networks in samples from HwA displayed more complex fungal–fungal and fungal–bacterial community interactions. This study revealed a marked impact of appendectomy on gut bacteria and fungi, which was particularly durable for fungi.

Keywords: gut bacteria, gut fungi, appendectomy, short-chain fatty acids, community interactions

OPEN ACCESS

Edited by:
Yanling Wei,
Army Medical University, China

Reviewed by:
Hailong Cao,
Tianjin Medical University General Hospital, China
Zikai Wang,
People's Liberation Army General Hospital, China

***Correspondence:**
Jianlin Ren
jianlin.ren@126.com
Hongzhi Xu
xuhongzhi@xmu.edu.cn

† These authors have contributed equally to this work and share first authorship

Specialty section:
This article was submitted to Systems Microbiology, a section of the journal Frontiers in Microbiology

Received: *14 June 2021*
Accepted: *19 August 2021*
Published: *16 September 2021*

Citation:
Cai S, Fan Y, Zhang B, Lin J, Yang X, Liu Y, Liu J, Ren J and Xu H (2021) Appendectomy Is Associated With Alteration of Human Gut Bacterial and Fungal Communities. Front. Microbiol. 12:724980. doi: 10.3389/fmicb.2021.724980

INTRODUCTION

The human appendix was traditionally considered an evolutionary remnant with limited biological function. It is typically removed upon the development of appendicitis or even removed preventatively (D'Souza and Nugent, 2016). However, increasing evidence has revealed that the human appendix plays important biological roles in regulating the intestinal immune system and microbiome (Randal Bollinger et al., 2007; Laurin et al., 2011; Masahata et al., 2014; Kooij et al., 2016; Girard-Madoux et al., 2018; Vitetta et al., 2019). Moreover, studies suggest that prior appendectomy may be associated with increased risk of many diseases, such as sarcoidosis, antibiotic-resistant bacteria-mediated bacteremia caused by biliary tract infection, gallstones, pyogenic liver abscesses, gastrointestinal cancers, Parkinson's disease (PD), and rheumatoid arthritis (Tzeng et al., 2015; Chung et al., 2016; Liao et al., 2016; Song et al., 2016; Kawanishi et al., 2017; Sawahata et al., 2017; Rubin, 2019). However, other studies have indicated no overall increase

in cancer incidence several years after appendectomy (Mellemkjaer et al., 1998; Cope et al., 2003). The role of the appendix must continue to be reevaluated and further investigated to reveal its roles in human health and disease.

Similar to the colon, the healthy appendix is inhabited by diverse microorganisms, predominantly composed of *Firmicutes*, *Bacteroidetes*, *Actinobacteria*, and *Proteobacteria* species (Guinane et al., 2013; Vitetta et al., 2019). Appendicitis is associated with altered microbiota in the appendix. Interestingly, some microbial taxa that are infrequently found in the distal gut, including the oral pathogens *Gemella*, *Parvimonas*, and *Fusobacterium*, have been identified in surgically removed appendices from patients with acute appendicitis (Guinane et al., 2013). Studies have demonstrated differences in the intestinal microbiota of patients with appendicitis and healthy controls, such as a greater abundance of *Fusobacteria* species in the setting of appendicitis (Swidsinski et al., 2011; Zhong et al., 2014; Rogers et al., 2016). However, data about differences in the microbiome based on disease severity are inconsistent (Peeters et al., 2019; The et al., 2019). Using culture methods, the diversity of anaerobes in the appendix differs between individuals with and without appendicitis (Hattori et al., 2019).

Recent studies have demonstrated crucial roles of the appendix in regulating intestinal microecology, possibly acting as a reserve or sanctuary for the gut microbiota that promotes the recovery of gut microecological homeostasis after intestinal perturbation (Randal Bollinger et al., 2007; Vitetta et al., 2019). Appendectomized mice show delayed accumulation of IgA^+ cells in the large intestine with altered fecal microbiota composition compared with sham-operated mice (Masahata et al., 2014). However, few studies have focused on intestinal bacterial changes after appendectomy, with inconsistent results (Goedert et al., 2014; Masahata et al., 2014). To our knowledge, there is no research on the relationship between appendectomy and intestinal fungi (Underhill and Iliev, 2014). Although the gut microbiota is populated mainly by bacteria, it also contains less than 1% of fungi. Intestinal fungal dysbiosis occurs in or contributes to many diseases, including colitis, alcoholic liver disease, primary sclerosing cholangitis, pancreatic cancer, and colon cancer (Iliev et al., 2012; Sokol et al., 2017; Yang et al., 2017; Aykut et al., 2019; Coker et al., 2019; Lemoinne et al., 2020).

To explore the alterations of gut bacterial and fungal communities associated with appendectomy, we firstly recruited and collected fecal samples from 30 healthy individuals with prior appendectomy and 30 healthy individuals without appendectomy. We examined the diversity and community structure of gut bacteria and fungi and evaluated their inter-kingdom interactions using 16S and ITS2 amplicon metagenomics in this study.

STUDY POPULATION AND METHODS

Participants

Healthy individuals with appendectomy (HwA; n = 30, 15 men and 15 women) were recruited from April 2016 to June 2017 from the local population of Xiamen, China. All participants were healthy, not on medication, had no clinically significant disease at the inception of the study, and had undergone appendectomy > 6 months ago. We also enrolled 30 healthy individuals without appendectomy (HwoA, 17 men and 13 women) as controls between February 2018 and May 2018 from the physical examination center in the outpatient department of Zhongshan Hospital Affiliated to Xiamen University (Xiamen, China). Written informed consent was obtained from all participants before stool donation. The study was approved by the local Ethical Review Board of Zhongshan Hospital Affiliated to Xiamen University(IRB2015014).

The exclusion criteria for both groups were as follows: < 18 years of age, antibiotic or proton pump inhibitor (PPI) treatment within 30 days, gastrointestinal surgery (except appendectomy for HwA), or diseases known to affect the gut microbiota. The following clinical data were recorded: age, body mass index (BMI), sex, and years since appendectomy.

Sample Collection, DNA Extraction, and Amplicon Sequencing

Fecal samples from each participant were collected and immediately frozen at −80°C until DNA extraction. The samples were thawed and homogenized, and total DNA was extracted from each sample (0.25 g) using the QIAamp Fast DNA Stool Mini Kit (QIAGEN, Hilden, Germany), according to the manufacturer's protocol. The resulting DNA yield and quality were assessed with a Multiskan^{TM} GO spectrophotometer (Thermo Fisher Scientific, Waltham, MA, United States).

Bacterial and fungal communities were determined by amplicon metagenomics targeting the 16S rRNA gene and ITS2 fragments, respectively. Briefly, the forward primer targeting the 16S rRNA gene V3 and V4 regions was 5′-CCTACGGGNBGCASCAG-3′, and the reverse primer was 5′-GGACTACNVGGGTWTCTAAT-3′. The forward primer targeting ITS2 was 5′-GCATCGATGAAGAACGCAGC-3′, and the reverse primer was 5′-TCCTCCGCTTATTGATATGC-3′. The polymerase chain reaction (PCR) products were purified and assessed with Qubit 3.0 (Thermo Fisher Scientific, Waltham, MA, United States). Sequencing was performed by the Xiamen Treatgut Biotechnology Co., using a 250-bp paired-end sequencing protocol on a HiSeq 2500 platform (Illumina, San Diego, CA, United States). Raw sequences were deposited in the National Center for Biotechnology Information Sequence Read Archive under accession number PRJNA655569.

Bioinformatic Analyses

The raw paired-end reads were assembled and filtered using FLASH with default parameters except parameters of $-M$ = 200 and $-x$ = 0.15 (Magoc and Salzberg, 2011). The resulting high quality reads were checked for chimeras and clustered to generate operational taxonomic units (OTUs) based on 97% similarity cutoff with USEARCH (Edgar, 2013). The representative OTU sequences were classified against the SILVA database for 16S data and against the UNITE database for ITS2 data using RDP Classifier with a confidence threshold of 50% (Wang et al., 2007; Henderson et al., 2019; Nilsson et al., 2019). Bacterial and

fungal data were re-sampled to 31,509 and 30,924 reads/sample, respectively, for downstream analyses.

Statistical Analyses and Visualization

Alpha diversity indices, including richness (observed), Shannon diversity (Shannon), and Pielou's evenness (evenness) were computed based on the OTU table using the vegan package. The significances of differences in the diversity indices and individual taxa were tested using a non-parametric Wilcoxon rank-sum test for two groups or Kruskal–Wallis rank-sum test with Benjamini–Hochberg corrections for multiple groups using the agricolae package. Beta diversity was measured using Bray–Curtis distance, and significance was determined with PERMANOVA with 9,999 permutations using adonis in the R package vegan. Correlations between bacterial and fungal genera were computed and tested using the Hmisc package. Finally, the results were visualized using the custom R script based on ggplot2 or VennDiagram, and the network figures were generated with Gephi v0.9.2. The analyses were performed in R v3.3.2.

RESULTS

Characteristics of the Study Population

The study population included two groups: HwA (n = 30) and HwoA (n = 30). There were no significant differences in the age and sex between the HwA and HwoA groups. The BMI of HwA was less than that of HwoA (20.8 ± 3.0 vs. 22.3 ± 2.5, p = 0.017), but both were within normal limits (18.5 ≤ BMI < 25). The HwA group was further divided into subgroups based on number of years post-appendectomy: cutoff at 2 years (2Y; < 2Y vs. ≥ 2Y), at 2 and 5 years [< 2Y, < 5 years (5Y) to ≥ 2Y, and ≥ 5Y], and at 5 years (< 5Y vs. ≥ 5Y) (**Table 1**).

Gut Bacterial Alterations After Appendectomy

Gut bacterial communities were analyzed by 16S V3–V4 sequencing. Alpha diversity, assessed with the observed, Shannon, and evenness indices, did not significantly differ between the HwA and HwoA groups (**Supplementary Figure 1A**). However, individuals with post-appendectomy periods shorter than 2 years (HwA_ < 2Y) had significantly lower gut bacterial evenness values than HwoA and HwA with a post-appendectomy period longer of at least 2 years (HwA_ ≥ 2Y) (**Figure 1A**; p < 0.05). HwA_ < 2Y also showed marginally lower Shannon diversity (**Figure 1A**; p = 0.08). There were no significant differences in the diversity indices between the other subgroups (**Supplementary Figures 1B,C**). The Venn diagram displays the 314 "universal" OTUs (of 486 total OTUs) shared among the three groups; a larger proportion (15.4%) of OTUs in HwA_ ≥ 2Y than HwA_ < 2Y (5.7%) was shared with the HwoA group (**Figure 1B**). Beta diversity analysis revealed that the gut bacterial communities in the samples from HwoA significantly differed from those in samples from HwA (PERMANOVA, F = 3.1526, p < 0.001) and from the subgroups with a cutoff of 2 years (PERMANOVA, F = 2.1526, p < 0.001). Interestingly, the HwA subgroups (HwA_ < 2Y and HwA_ ≥ 2Y) tended to have greater microbial ecological similarity with HwoA over time (**Figure 1C**), even with no significant differences detected between these two subgroups (PERMANOVA, F = 1.1646, p = 0.184). These results suggest appendectomy disrupted the gut bacteria composition, which was restored over time.

Gut bacteria were dominated by Bacteroidetes, Firmicutes, Proteobacteria, and Fusobacteria at the phylum level (**Figure 2A** and **Supplementary Figure 2A**) and by Bacteroidaceae, Ruminococcaceae, Prevotellaceae, Acidaminococcaceae, Lachnospiraceae, Enterobacteriaceae, and Veillonellaceae at the family level (**Figure 2B** and **Supplementary Figure 2B**). Further analyses at the genus level revealed significantly higher abundances of *Escherichia-Shigella*, *Veillonella*, *Klebsiella*, *Megasphaera*, *Flavonifractor*, the *Ruminococcus gnavus* group, and *Streptococcus* in HwA subgroups than in HwoA (**Supplementary Figure 3**), with a trend toward restoration of the HwoA level with time after appendectomy (**Figure 2C**). On the other hand, *Roseburia*, *Barnesiella*, *Butyricicoccus*, *Odoribacter*, and *Butyricimonas* were significantly more abundant in the HwoA group than in the HwA subgroup (**Supplementary Figure 3**). *Roseburia*, *Butyricicoccus*, *Odoribacter*, and *Butyricimonas* became more abundant over time after appendectomy (**Figure 2C**).

TABLE 1 | Study population characteristics.

Group	HwA	HwoA	p-value
	n = 30	n = 30	
Age (years, mean ± SD)	33.1 ± 6.7	35.1 ± 7.7	0.276
Gender (male/female)	15/15	17/13	0.604
BMI (kg/m^2, mean ± SD)	20.8 ± 3.0	22.3 ± 2.5	0.017
Time after appendectomy (months)[a]	24 (8–180)	–	–
<2 years (n)	12		
2–5 years (n)	12		
≥5 years (n)	6		

[a]*Median (minimum–maximum).*
SD, standard deviation; BMI, body mass index.

Gut Fungal Alterations After Appendectomy

Gut fungal communities were analyzed by ITS2 sequencing. The alpha diversity indices of the gut fungal communities, including the observed, Shannon, and evenness indices, were significantly higher in samples from HwA than those from HwoA (**Supplementary Figure 4A**). This difference was also observed for all HwA subgroups (**Supplementary Figures 4B,C**), even for individuals who had undergone appendectomy at least 5 years prior to the study (HwA_ ≥ 5Y) (**Figure 3A**). The Venn diagram shows a larger proportion of OTUs in HwA_ ≥ 5Y (25.7%) than in HwA_ < 5Y (17.6%) were shared with HwoA. Conversely, HwA_ < 5Y contained a higher proportion (63.7%) of exclusive OTUs than HwA_ ≥ 5Y (31.5%) (**Figure 3B**). Beta diversity analysis showed that the

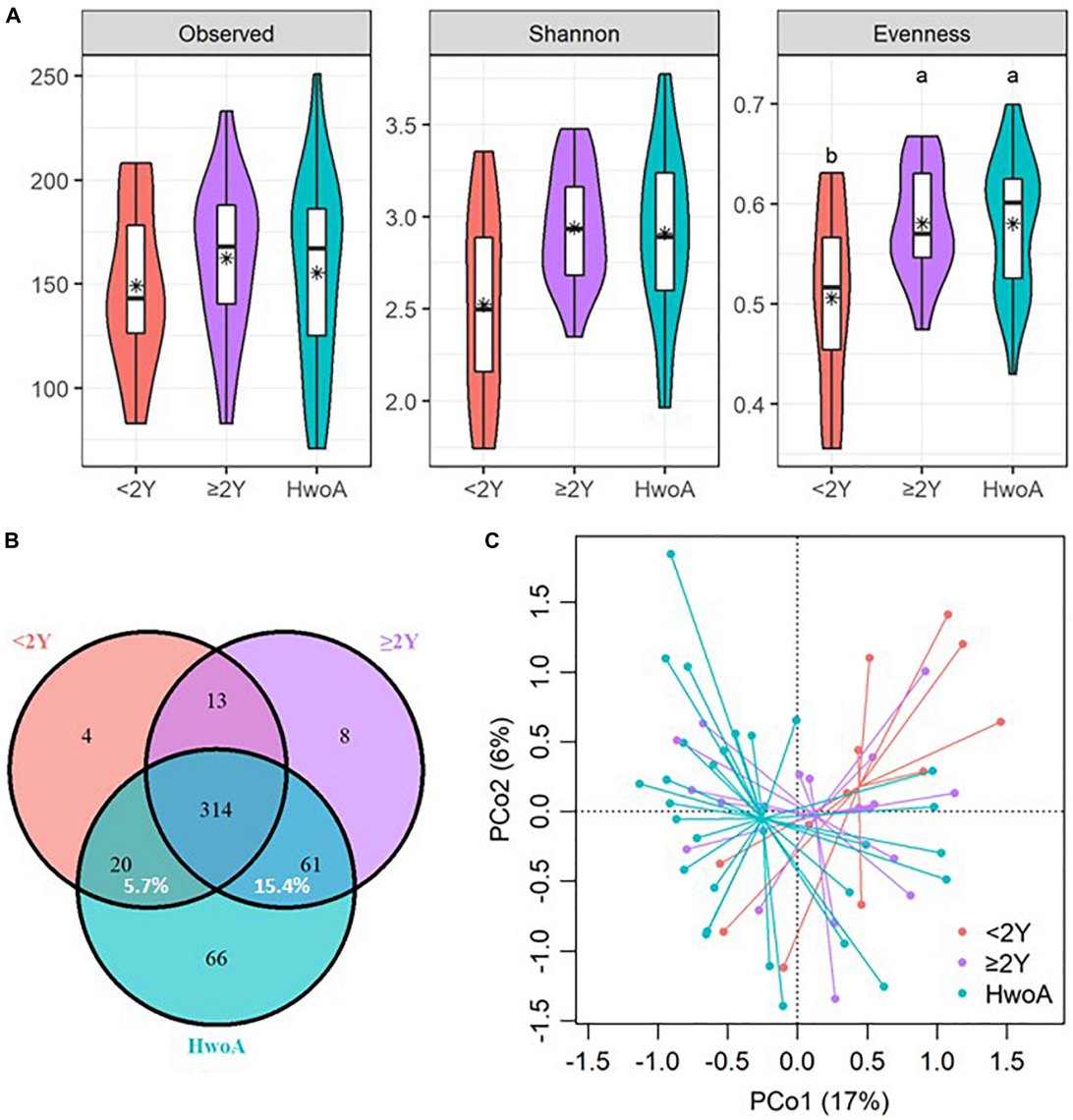

FIGURE 1 | Alterations of gut bacterial diversity and communities, based on 16S V3–V4 sequencing data from HwoA, HwA_ < 2Y, and HwA_ ≥ 2Y. **(A)** Alpha diversity estimated by richness (observed OTUs), Shannon diversity, and Pielou's evenness. Letters indicate the grouping ($p < 0.05$) by Kruskal–Wallis rank-sum test with Benjamini–Hochberg corrections. **(B)** Venn diagram of OTUs shared by and exclusive to the three groups. Corresponding percentages are noted for relevant overlaps. **(C)** Differences in gut bacterial community structures among the groups, assessed by principal coordinate (PCo) analysis of Bray–Curtis distance ($p < 0.001$). OTUs, operational taxonomic units. *Average.

samples from HwoA were clearly separated from those from HwA (PERMANOVA, $F = 4.030$, $p < 0.001$) and from the subgroups divided at 5 years (PERMANOVA, $F = 2.532$, $p < 0.001$). Moreover, the HwA subgroups did not display increasing similarity to HwoA over time (**Figure 3C**). These results suggest that the effects of appendectomy on the gut fungal community persisted for at least 5 years, without obvious restoration over time. The fungal communities were dominated by Ascomycota and Basidiomycota at the phylum level (**Figure 4A**) and by Saccharomycetaceae, Aspergillaceae, and unclassified Ascomycota and Basidiomycetes at the family level (**Figure 4B** and **Supplementary Figure 5**). Further analyses at the genus level revealed that the abundances of many genera were significantly different in HwA and HwoA fecal samples (**Supplementary Figure 6**). Interestingly, the abundances of *Hanseniaspora*, *Alternaria*, *Chaetomium*, *Fusarium*, *Paraphoma*, *Mycosphaerella*, and *Penicillium* decreased with time post-appendectomy (**Figure 4C**), whereas the abundances of *Aspergillus* and unclassified Microascaceae increased over time after appendectomy (**Figure 4C**).

Fungal abundance correlation networks were constructed to evaluate the ecosystem structure. A richer, more complex network of correlations between fungal communities was observed in HwA than in HwoA samples (**Figure 5A**). As

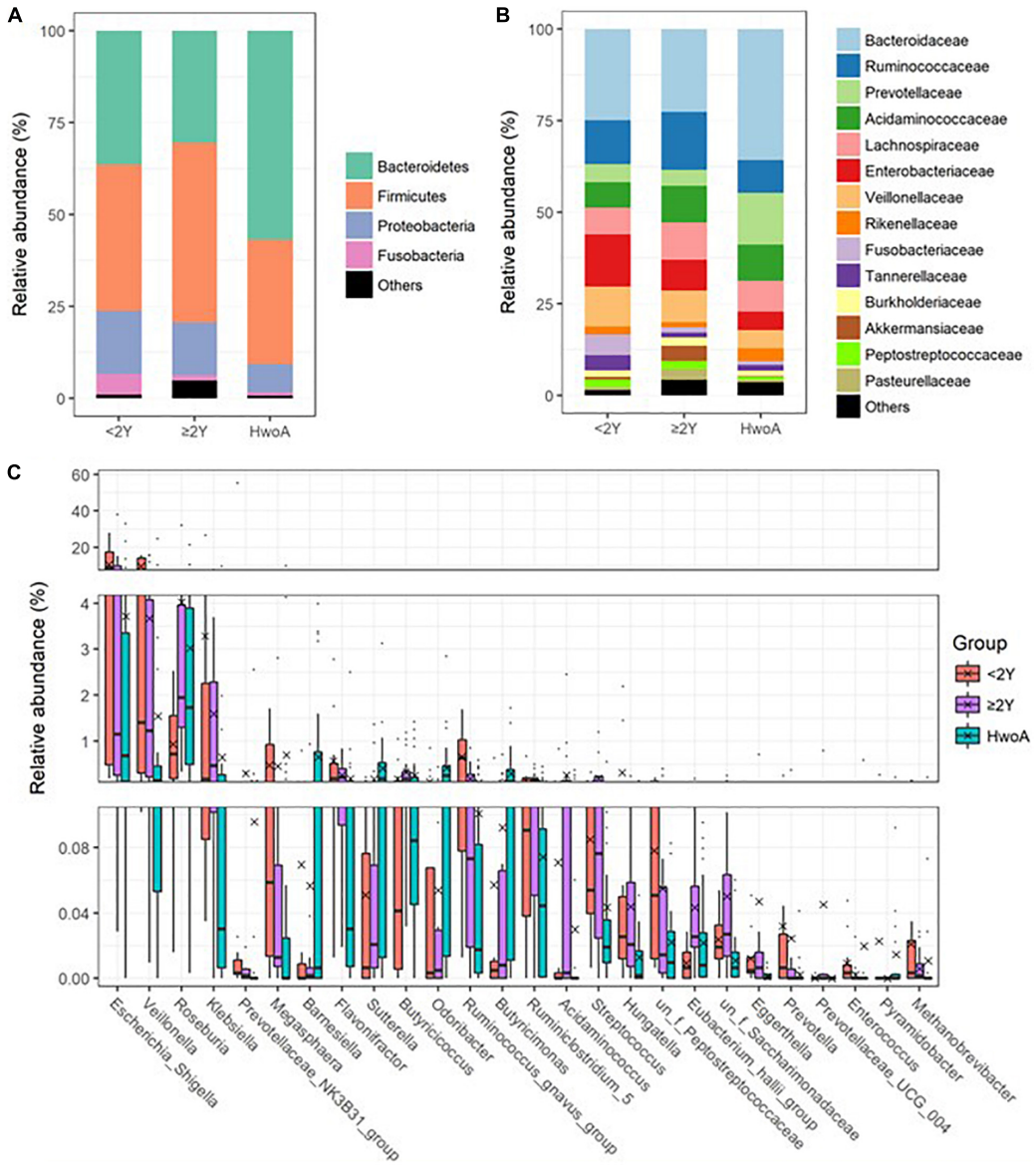

FIGURE 2 | Gut bacteria compositions and differences in the HwoA and HwA subgroups. The overall bacterial structures of the three groups at **(A)** phylum and **(B)** family levels, expressed as the relative abundance of OTUs in each group. **(C)** The relative abundances of major (> 0.01%) bacterial genera significantly differed among HwA subgroups (< 2Y and ≥ 2Y) and HwoA ($p < 0.05$). The "un_f" in bacterial nomenclature means unclassified family at genus level. OTUs, operational taxonomic units.

expected, the density of the fungal correlation network decreased over time in the HwA subgroups, as attested by decreased relative connectedness and fewer neighbors. However, there was a significantly higher density in HwA_ ≥ 5Y samples than in HwoA samples for these two parameters, as well as more nodes (OTUs) and edges (connections) in the networks (**Figures 5A,B**).

Interactions Between the Gut Fungal and Bacterial Communities

To gain an overview of the gut microbial shifts after appendectomy, we first addressed the equilibrium between fungal and bacterial diversity by determining the fungi-to-bacteria diversity ratio. The ratios of the observed, Shannon, and evenness indices were all significantly increased in the HwA group (**Figure 6A**; $p < 0.05$), suggesting a more prominent influence of appendectomy on the fungal community than the bacterial community. Furthermore, abundance correlation networks of bacterial and fungal interactions at the genus level were constructed to explore the interkingdom interactions. Compared with the HwoA group, the HwA group had a denser, obviously disrupted fungi–bacteria network, as illustrated by the increased relative connectedness and more neighbors (**Figure 6B**). Indeed, significantly more neighbors

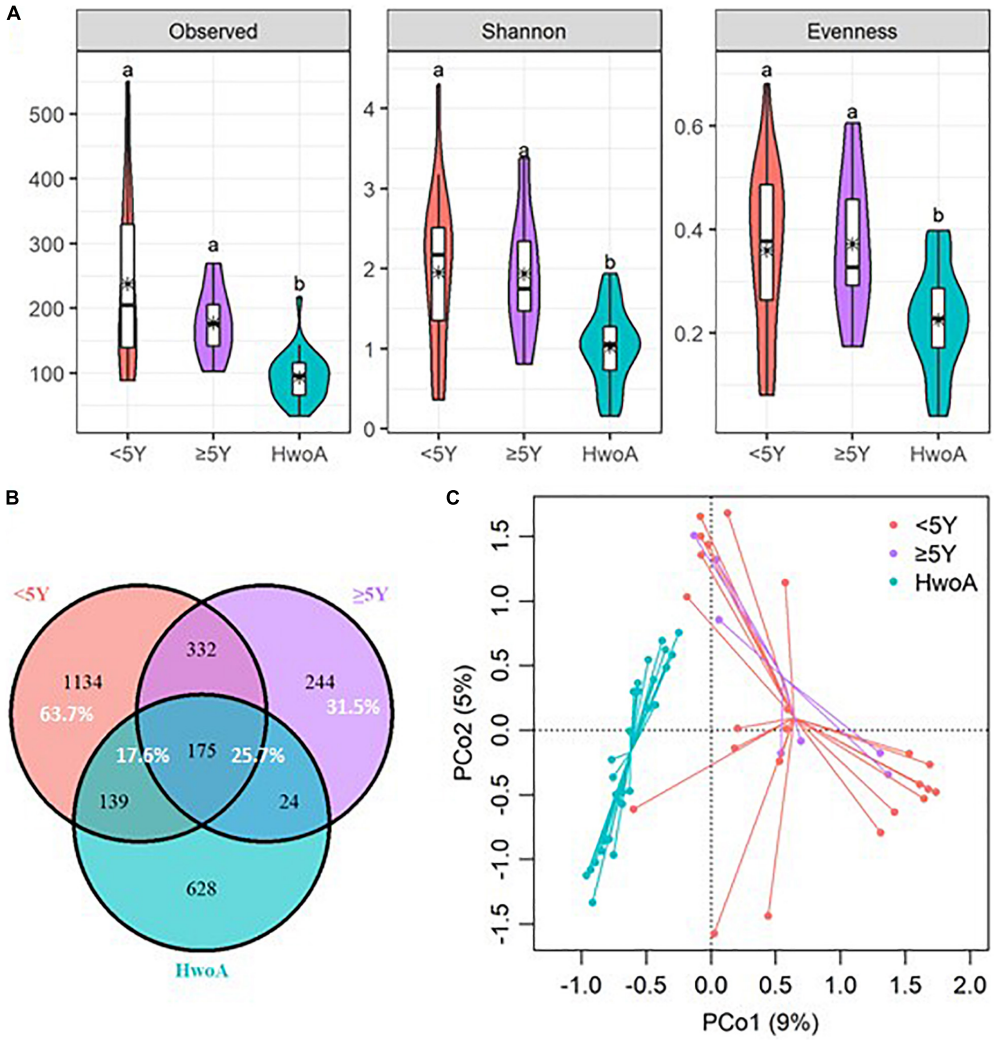

FIGURE 3 | Alterations of gut fungal diversity and communities, based on ITS2 sequencing data of HwoA, HwA_ < 5Y, and HwA_ ≥ 5Y. **(A)** Alpha diversity estimated by the observed, Shannon, and evenness indices. Letters indicate the grouping by Kruskal–Wallis rank-sum test with Benjamini–Hochberg corrections ($p < 0.05$). **(B)** Venn diagram of the OTUs shared by and exclusive to the three groups. Corresponding percentages are noted for relevant overlaps. **(C)** Differences in gut fungal community structures among the groups, assessed by principal coordinate (PCo) analysis of Bray–Curtis distance ($p < 0.001$). OTUs, operational taxonomic units.

were observed for each node in the HwA samples than for those of the HwoA samples (**Figure 6C**). These results indicate that appendectomy is associated with alterations of bacterial–fungal interactions in terms of diversity and taxa relative abundances.

DISCUSSION

In this study, fecal 16S and ITS2 sequences were used to investigate the gut microbiota of individuals with and without a history of appendectomy. We demonstrated that both gut bacterial and fungal communities in healthy subjects with a history of appendectomy are apparently distinct from those in healthy controls. Studies indicated that, 4 weeks after conventionalization, appendectomized germ-free mice have a distinct, less diverse bacterial composition than sham-operated germ-free mice (Masahata et al., 2014). On the contrary, a previous study reported that a history of appendectomy was not associated with beta diversity and that 22 taxa that were more abundant after appendectomy were not statistically different after adjustment (Goedert et al., 2014). In our study, alpha diversity indices did not significantly differ between HwA and HwoA, but beta diversity revealed that the gut bacterial composition of HwA was significantly separated from that of HwoA. Since the literature on this topic is limited, a more complete understanding remains to be gained through additional studies. Notably, in accordance with a previous report, our results suggested that the HwA subgroups tended to gain bacterial ecological similarity to HwoA over time after appendectomy. Similarly, at 8 weeks after conventionalization, the alteration of fecal microbiota composition in appendectomized mice was no longer apparent,

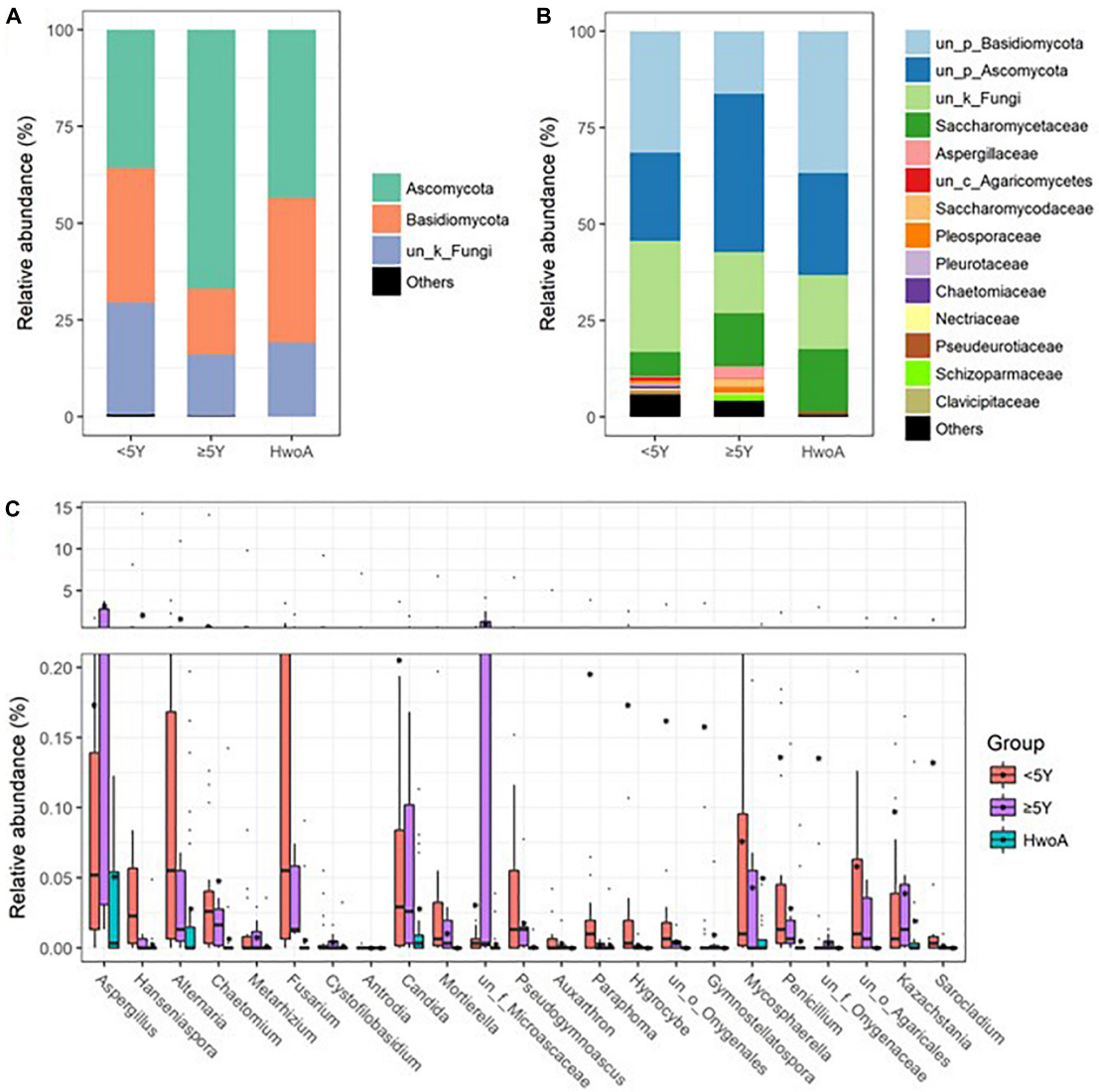

FIGURE 4 | Gut fungal community compositions and differences in the HwoA and HwA subgroups. The overall fungal structures of the three groups at **(A)** phylum and **(B)** family levels, expressed as the relative abundance of OTUs in each group. **(C)** Relative abundances of major (> 0.05%) fungal genera significantly differed among HwA subgroups (< 2Y and ≥ 2Y) and HwoA ($p < 0.05$). OTUs, operational taxonomic units.

and the numbers of colonic IgA-secreting cells normalized (Masahata et al., 2014). Interestingly, our HwA subgroup analysis revealed that gut fungal composition did not shift toward that observed in HwoA over time. Thus, the effect of appendectomy on gut fungi may be more persistent than that on bacteria. Our research indicated that appendectomy had different impact on fecal fungi and bacteria over time.

In our study, gut bacteria were dominated by Bacteroidetes, Firmicutes, Proteobacteria, and Fusobacteria at the phylum level in both HwA and HwoA. Further analyses at the genus level revealed that *Roseburia*, *Barnesiella*, *Butyricicoccus*, *Odoribacter*, and *Butyricimonas* were significantly more abundant in HwoA samples than HwA subgroup samples. Importantly, these more abundant bacteria were identified as short-chain fatty acid (SCFA)-producing microbes (Louis and Flint, 2017). In the gut, SCFAs such as butyric acid, propionic acid, and acetic acid are speculated to play key roles in immune regulation, intestinal mucosal protection, protection against inflammation, and epithelial cell energy provision (Rios-Covian et al., 2016). Some epidemiological studies have shown that removal of the appendix may increase the risk of type 2 diabetes (T2D) and PD (Killinger et al., 2018; Rubin, 2019). Though these associations are controversial and the mechanisms are unclear, alterations in microorganism communities may contribute to post-appendectomy disease occurrence (Killinger et al., 2018; Killinger and Labrie, 2019; Rubin, 2019). Disorders of propionate, an SCFA, in the gut are associated with an increased risk of T2D (Sanna et al., 2019). Studies of fecal microbiota in patients with PD have revealed lower levels of fiber-degrading bacterial strains and less SCFA production than observed in

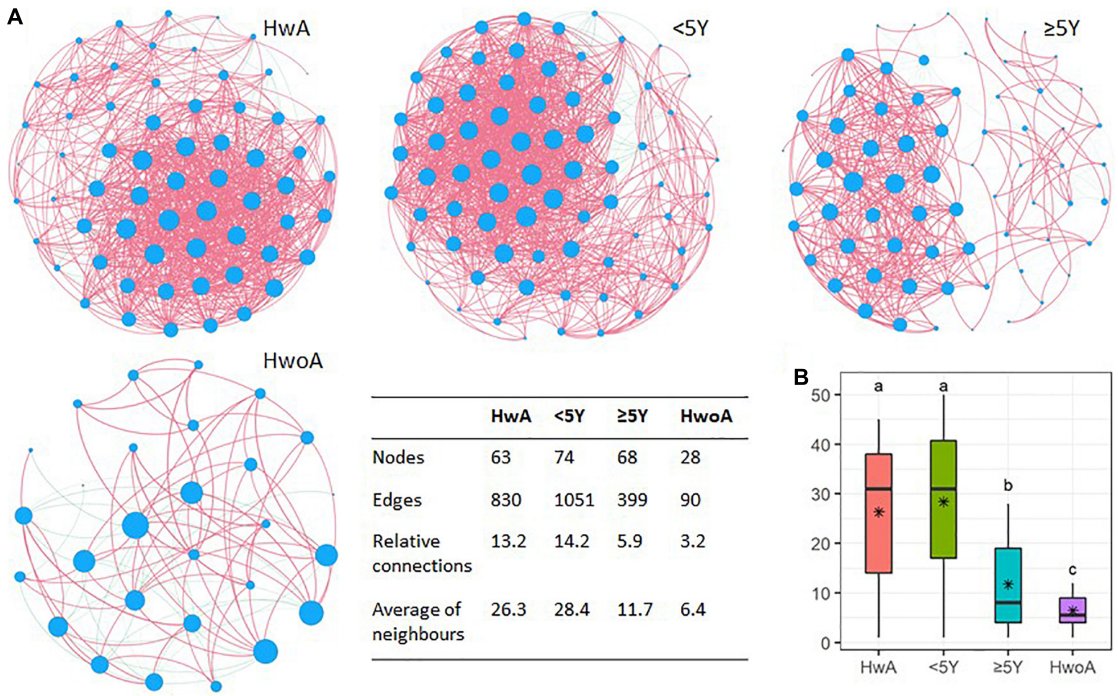

	HwA	<5Y	≥5Y	HwoA
Nodes	63	74	68	28
Edges	830	1051	399	90
Relative connections	13.2	14.2	5.9	3.2
Average of neighbours	26.3	28.4	11.7	6.4

FIGURE 5 | Gut fungal microbiota correlation networks. **(A)** Abundance correlation networks of HwA, HwA subgroups (< 5Y and ≥ 5Y), and HwoA analyzed by Spearman's test with Benjamini–Hochberg corrections. Each node represents an OTU, and its size is scaled to the number of indirect edges within each network. Edges indicate correlations (positive in red and negative in green). Only OTUs present in > 50% of samples in the group were considered, and only significant correlations ($p < 0.05$) are shown. The table in the inset shows the network parameters. The relative connectedness is the ratio between the number of edges and the number of nodes in the network. **(B)** Neighbors of each node within the network. Black stars indicate mean values. Letters indicate the grouping by Kruskal–Wallis rank-sum test with Benjamini–Hochberg corrections ($p < 0.05$). OTUs, operational taxonomic units. *Average.

matched healthy controls (Unger et al., 2016; Li et al., 2017). Moreover, the long-term side effects of antibiotics can decrease the concentration of SCFAs (Holota et al., 2019). However, the roles of SCFA production are contradictory, as they can both benefit the host and lead to metabolic diseases (Schwiertz et al., 2010; Zhao et al., 2018; Pingitore et al., 2019). These results suggest that increasing SCFA-producing microbes due to appendectomy could contribute to the development of specific diseases.

Our study also found that, compared with HwoA, HwA had increased fungal biodiversity and relative changes in the abundance of many fungal groups, which lasted for at least 5 years. Ascomycota and Basidiomycota predominated among the intestinal fungi in both the HwA and control groups. The Basidiomycota-to-Ascomycota ratio in HwA was lower than that in HwoA, and the ratio dropped with time after appendectomy. The gut microbiota plays an important role in the pathogenesis of ulcerative colitis (UC) and colorectal cancer (CRC) (Gao et al., 2017; Ni et al., 2017; Raskov et al., 2017; Khan et al., 2019). It has also been reported that undergoing appendectomy in early life, before the onset of UC, may reduce the risk of colectomy and UC-related hospital admissions (Myrelid et al., 2017). However, it is still unclear if patients with UC can benefit from appendectomy (Park et al., 2014; Parian et al., 2017; Sahami et al., 2019). The relationship between appendectomy and CRC is inconclusive (Grobost et al., 1991; Mellemkjaer et al., 1998; Cope et al., 2003; Wu et al., 2015). The roles of immunoregulation and the microbiota in these associations require clarification. The fecal fungal microbiota of UC and CRC patients are also dominated by Ascomycota and Basidiomycota. In contrast to our findings, the Basidiomycota-to-Ascomycota ratio is higher in individuals with active UC and CRC than in healthy individuals, indicating intestinal fungal imbalance. We demonstrated that the correlation networks of fungal–fungal and fungal–bacterial interactions were denser and obviously disrupted in HwA. Alterations of intrafungal and interkingdom bacteria–fungi interactions are also observed in the settings of CRC and UC (Sokol et al., 2017; Coker et al., 2019). Taken together, these clinical observations and our results provide microbial insights in future research on the mechanism of appendectomy and related diseases.

However, there are some limitations to our study. This was a single-center observational study with a relatively small sample size. In addition, changes in gut immunity and microbial metabolism were not investigated. However, we enrolled individuals who were at various stages post-appendectomy, which allowed us to preliminarily analyze the duration of microecological changes after surgery. We also provided a first analysis of the fecal fungal profiles of individuals with a history of appendectomy.

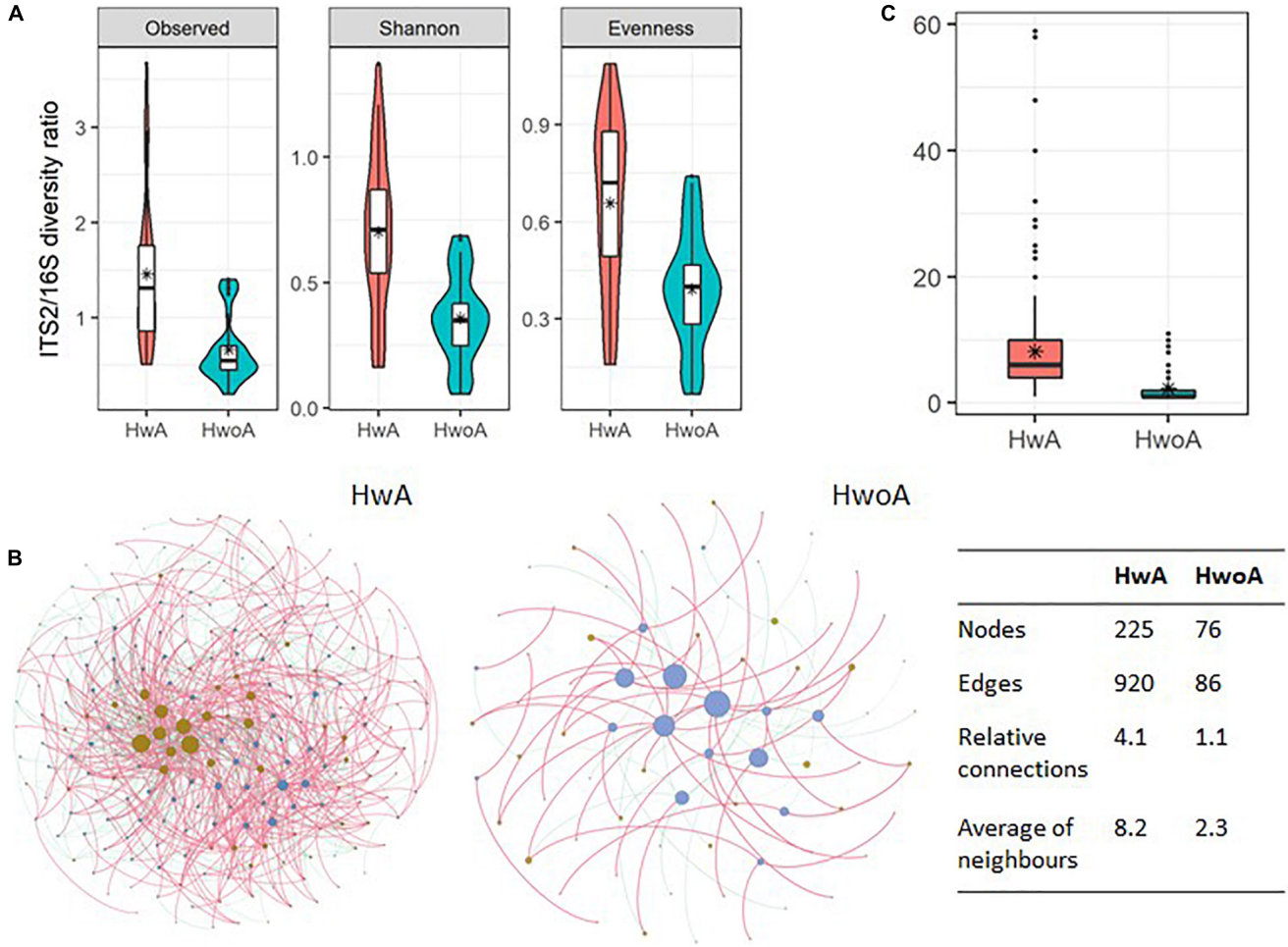

FIGURE 6 | Interactions between gut fungal and bacterial communities. **(A)** Fungi-to-bacteria diversity ratios of the observed, Shannon, and evenness indices. **(B)** Abundance correlation networks of gut fungal and bacterial communities analyzed by Spearman's test. Each node represents a genus, with bacteria in brown and fungi in blue/violet. Node size is scaled to the number of indirect edges within each network. Edges indicate correlations (positive in red and negative in green). Only genera present in ≥ 20% of samples in the group were considered, and only significant correlations ($p < 0.05$) are shown. The table in the inset shows the network parameters. The relative connectedness is the ratio between the number of edges and the number of nodes in the network. **(C)** Neighbors of each node within the network. Black stars are mean values. *Average.

CONCLUSION

We conclude that bacterial and fungal gut microbiota are altered after appendectomy. Moreover, our study elucidates that removal of the appendix alters intrafungal and bacteria–fungi interactions. It appears that the effects of appendectomy on the fecal fungal community are more marked and durable than on bacteria. However, the underlying mechanisms through which appendectomy alters the gut microbiota and the biological consequences of these changes remain to be explored.

DATA AVAILABILITY STATEMENT

The datasets presented in this study can be found in online repositories. The names of the repository/repositories and accession number(s) can be found below: https://www.ncbi.nlm.nih.gov/, PRJNA655569.

ETHICS STATEMENT

The studies involving human participants were reviewed and approved by the Ethical Review Board of Zhongshan Hospital Affiliated to Xiamen University. The patients/participants provided their written informed consent to participate in this study.

AUTHOR CONTRIBUTIONS

SC, YF, HX, JR, JLin, and BZ designed the study, analyzed the data, and wrote the manuscript. JLin, XY, YL, and JLiu undertook

data collection and performed the literature search. All authors read and approved the final manuscript.

FUNDING

This work was supported by the Natural Science Foundation of Fujian Province, China (No. 2020J05286), National Natural Science Foundation of China (No. 81800517), and the China Postdoctoral Science Foundation funded project (No. 2018M632588). The funders had no role in the study design, data collection, data analysis, interpretation, and writing of the report.

ACKNOWLEDGMENTS

We would like to thank all study participants and medical staff for their involvement and support in the study. We thank Editage (www.editage.cn) for English language editing.

SUPPLEMENTARY MATERIAL

The Supplementary Material for this article can be found online at: https://www.frontiersin.org/articles/10.3389/fmicb.2021.724980/full#supplementary-material

REFERENCES

Aykut, B., Pushalkar, S., Chen, R., Li, Q., Abengozar, R., Kim, J. I., et al. (2019). The fungal mycobiome promotes pancreatic oncogenesis via activation of MBL. *Nature* 574, 264–267. doi: 10.1038/s41586-019-1608-2

Chung, S. D., Huang, C. C., Lin, H. C., Tsai, M. C., and Chen, C. H. (2016). Increased Risk of Clinically Significant Gallstones following an Appendectomy: A Five-Year Follow-Up Study. *PLoS One* 11:e0165829. doi: 10.1371/journal.pone.0165829

Coker, O. O., Nakatsu, G., Dai, R. Z., Wu, W. K. K., Wong, S. H., Ng, S. C., et al. (2019). Enteric fungal microbiota dysbiosis and ecological alterations in colorectal cancer. *Gut* 68, 654–662. doi: 10.1136/gutjnl-2018-317178

Cope, J. U., Askling, J., Gridley, G., Mohr, A., Ekbom, A., Nyren, O., et al. (2003). Appendectomy during childhood and adolescence and the subsequent risk of cancer in Sweden. *Pediatrics* 111(6 Pt 1), 1343–1350. doi: 10.1542/peds.111.6.1343

D'Souza, N., and Nugent, K. (2016). Appendicitis. *Am. Fam. Physician.* 93, 142–143.

Edgar, R. C. (2013). UPARSE: highly accurate OTU sequences from microbial amplicon reads. *Nat. Methods* 10, 996–998. doi: 10.1038/nmeth.2604

Gao, R., Gao, Z., Huang, L., and Qin, H. (2017). Gut microbiota and colorectal cancer. *Eur. J. Clin. Microbiol. Infect. Dis.* 36, 757–769. doi: 10.1007/s10096-016-2881-8

Girard-Madoux, M. J. H., Gomez, de Aguero, M., Ganal-Vonarburg, S. C., Mooser, C., Belz, G. T., et al. (2018). The immunological functions of the Appendix: An example of redundancy? *Semin. Immunol.* 36, 31–44. doi: 10.1016/j.smim.2018.02.005

Goedert, J. J., Hua, X., Yu, G., and Shi, J. (2014). Diversity and composition of the adult fecal microbiome associated with history of cesarean birth or appendectomy: Analysis of the American Gut Project. *EBioMed.* 1, 167–172. doi: 10.1016/j.ebiom.2014.11.004

Grobost, O., Boutron, M. C., Arveux, P., Bedenne, L., Chatrenet, P., and Faivre, J. (1991). Appendectomy, cholecystectomy, cholelithiasis and colorectal cancer. A retrospective case control study at the Cote-d'Or. *Gastroenterol. Clin. Biol.* 15, 594–599.

Guinane, C. M., Tadrous, A., Fouhy, F., Ryan, C. A., Dempsey, E. M., Murphy, B., et al. (2013). Microbial composition of human appendices from patients following appendectomy. *mBio* 4:12. doi: 10.1128/mBio.00366-12

Hattori, T., Yuasa, N., Ikegami, S., Nishiyama, H., Takeuchi, E., Miyake, H., et al. (2019). Culture-based bacterial evaluation of the appendix lumen in patients with and without acute appendicitis. *J. Infect. Chemother.* 25, 708–713. doi: 10.1016/j.jiac.2019.03.021

Henderson, G., Yilmaz, P., Kumar, S., Forster, R. J., Kelly, W. J., Leahy, S. C., et al. (2019). Improved taxonomic assignment of rumen bacterial 16S rRNA sequences using a revised SILVA taxonomic framework. *PeerJ.* 7:e6496. doi: 10.7717/peerj.6496

Holota, Y., Dovbynchuk, T., Kaji, I., Vareniuk, I., Dzyubenko, N., Chervinska, T., et al. (2019). The long-term consequences of antibiotic therapy: Role of colonic short-chain fatty acids (SCFA) system and intestinal barrier integrity. *PLoS One* 14:e0220642. doi: 10.1371/journal.pone.0220642

Iliev, I. D., Funari, V. A., Taylor, K. D., Nguyen, Q., Reyes, C. N., Strom, S. P., et al. (2012). Interactions between commensal fungi and the C-type lectin receptor Dectin-1 influence colitis. *Science* 336, 1314–1317. doi: 10.1126/science.1221789

Kawanishi, K., Kinoshita, J., Abe, H., Kakimoto, T., Yasuda, Y., Hara, T., et al. (2017). Appendectomy as a Risk Factor for Bacteremic Biliary Tract Infection Caused by Antibiotic-Resistant Pathogens. *Biomed. Res. Int.* 2017:3276120. doi: 10.1155/2017/3276120

Khan, I., Ullah, N., Zha, L., Bai, Y., Khan, A., Zhao, T., et al. (2019). Alteration of Gut Microbiota in Inflammatory Bowel Disease (IBD): Cause or Consequence? IBD Treatment Targeting the Gut Microbiome. *Pathogens* 8:3. doi: 10.3390/pathogens8030126

Killinger, B., and Labrie, V. (2019). The Appendix in Parkinson's Disease: From Vestigial Remnant to Vital Organ? *J. Parkinsons Dis.* 9, S345–S358. doi: 10.3233/JPD-191703

Killinger, B. A., Madaj, Z., Sikora, J. W., Rey, N., Haas, A. J., Vepa, Y., et al. (2018). The vermiform appendix impacts the risk of developing Parkinson's disease. *Sci. Transl. Med.* 10:465. doi: 10.1126/scitranslmed.aar5280

Kooij, I. A., Sahami, S., Meijer, S. L., Buskens, C. J., and Te Velde, A. A. (2016). The immunology of the vermiform appendix: a review of the literature. *Clin. Exp. Immunol.* 186, 1–9. doi: 10.1111/cei.12821

Laurin, M., Everett, M. L., and Parker, W. (2011). The cecal appendix: one more immune component with a function disturbed by post-industrial culture. *Anat. Rec.* 294, 567–579. doi: 10.1002/ar.21357

Lemoinne, S., Kemgang, A., Ben Belkacem, K., Straube, M., Jegou, S., Corpechot, C., et al. (2020). Fungi participate in the dysbiosis of gut microbiota in patients with primary sclerosing cholangitis. *Gut* 69, 92–102. doi: 10.1136/gutjnl-2018-317791

Li, W., Wu, X., Hu, X., Wang, T., Liang, S., Duan, Y., et al. (2017). Structural changes of gut microbiota in Parkinson's disease and its correlation with clinical features. *Sci. China Life Sci.* 60, 1223–1233. doi: 10.1007/s11427-016-9001-4

Liao, K. F., Lai, S. W., Lin, C. L., and Chien, S. H. (2016). Appendectomy correlates with increased risk of pyogenic liver abscess: A population-based cohort study in Taiwan. *Medicine* 95:e4015. doi: 10.1097/MD.0000000000004015

Louis, P., and Flint, H. J. (2017). Formation of propionate and butyrate by the human colonic microbiota. *Environ. Microbiol.* 19, 29–41. doi: 10.1111/1462-2920.13589

Magoc, T., and Salzberg, S. L. (2011). FLASH: fast length adjustment of short reads to improve genome assemblies. *Bioinformatics* 27, 2957–2963. doi: 10.1093/bioinformatics/btr507

Masahata, K., Umemoto, E., Kayama, H., Kotani, M., Nakamura, S., Kurakawa, T., et al. (2014). Generation of colonic IgA-secreting cells in the caecal patch. *Nat. Commun.* 5:3704. doi: 10.1038/ncomms4704

Mellemkjaer, L., Johansen, C., Linet, M. S., Gridley, G., and Olsen, J. H. (1998). Cancer risk following appendectomy for acute appendicitis (Denmark). *Cancer Causes Control* 9, 183–187. doi: 10.1023/a:1008834311514

Myrelid, P., Landerholm, K., Nordenvall, C., Pinkney, T. D., and Andersson, R. E. (2017). Appendectomy and the Risk of Colectomy in Ulcerative Colitis: A National Cohort Study. *Am. J. Gastroenterol.* 112, 1311–1319. doi: 10.1038/ajg.2017.183

Ni, J., Wu, G. D., Albenberg, L., and Tomov, V. T. (2017). Gut microbiota and IBD: causation or correlation? *Nat. Rev. Gastroenterol. Hepatol.* 14, 573–584. doi: 10.1038/nrgastro.2017.88

Nilsson, R. H., Larsson, K. H., Taylor, A. F. S., Bengtsson-Palme, J., Jeppesen, T. S., Schigel, D., et al. (2019). The UNITE database for molecular identification of fungi: handling dark taxa and parallel taxonomic classifications. *Nucleic Acids Res.* 47, D259–D264. doi: 10.1093/nar/gky1022

Parian, A., Limketkai, B., Koh, J., Brant, S. R., Bitton, A., Cho, J. H., et al. (2017). Appendectomy does not decrease the risk of future colectomy in UC: results from a large cohort and meta-analysis. *Gut* 66, 1390–1397. doi: 10.1136/gutjnl-2016-311550

Park, S. H., Loftus, E. V. Jr., and Yang, S. K. (2014). Appendiceal skip inflammation and ulcerative colitis. *Dig. Dis. Sci.* 59, 2050–2057. doi: 10.1007/s10620-014-3129-z

Peeters, T., Penders, J., Smeekens, S. P., Galazzo, G., Houben, B., Netea, M. G., et al. (2019). The fecal and mucosal microbiome in acute appendicitis patients: an observational study. *Future Microbiol.* 14, 111–127. doi: 10.2217/fmb-2018-0203

Pingitore, A., Gonzalez-Abuin, N., Ruz-Maldonado, I., Huang, G. C., Frost, G., and Persaud, S. J. (2019). Short chain fatty acids stimulate insulin secretion and reduce apoptosis in mouse and human islets in vitro: Role of free fatty acid receptor 2. *Diabetes Obes Metab.* 21, 330–339. doi: 10.1111/dom.13529

Randal Bollinger, R., Barbas, A. S., Bush, E. L., Lin, S. S., and Parker, W. (2007). Biofilms in the large bowel suggest an apparent function of the human vermiform appendix. *J. Theor. Biol.* 249, 826–831. doi: 10.1016/j.jtbi.2007.08.032

Raskov, H., Burcharth, J., and Pommergaard, H. C. (2017). Linking Gut Microbiota to Colorectal Cancer. *J. Cancer* 8, 3378–3395. doi: 10.7150/jca.20497

Rios-Covian, D., Ruas-Madiedo, P., Margolles, A., Gueimonde, M., de Los Reyes-Gavilan, C. G., and Salazar, N. (2016). Intestinal Short Chain Fatty Acids and their Link with Diet and Human Health. *Front. Microbiol.* 7:185. doi: 10.3389/fmicb.2016.00185

Rogers, M. B., Brower-Sinning, R., Firek, B., Zhong, D., and Morowitz, M. J. (2016). Acute Appendicitis in Children Is Associated With a Local Expansion of Fusobacteria. *Clin. Infect. Dis.* 63, 71–78. doi: 10.1093/cid/ciw208

Rubin, R. (2019). Uncovering a Link Between the Appendix and Parkinson Disease Risk. *JAMA* 322, 293–294. doi: 10.1001/jama.2019.9041

Sahami, S., Wildenberg, M. E., Koens, L., Doherty, G., Martin, S., D'Haens, G., et al. (2019). Appendectomy for Therapy-Refractory Ulcerative Colitis Results in Pathological Improvement of Colonic Inflammation: Short-Term Results of the PASSION Study. *J. Crohns Colitis* 13, 165–171. doi: 10.1093/ecco-jcc/jjy127

Sanna, S., van Zuydam, N. R., Mahajan, A., Kurilshikov, A., Vich Vila, A., Vosa, U., et al. (2019). Causal relationships among the gut microbiome, short-chain fatty acids and metabolic diseases. *Nat. Genet.* 51, 600–605. doi: 10.1038/s41588-019-0350-x

Sawahata, M., Nakamura, Y., and Sugiyama, Y. (2017). Appendectomy, tonsillectomy, and risk for sarcoidosis - A hospital-based case-control study in Japan. *Respir. Investig.* 55, 196–202. doi: 10.1016/j.resinv.2016.12.004

Schwiertz, A., Taras, D., Schafer, K., Beijer, S., Bos, N. A., Donus, C., et al. (2010). Microbiota and SCFA in lean and overweight healthy subjects. *Obesity* 18, 190–195. doi: 10.1038/oby.2009.167

Sokol, H., Leducq, V., Aschard, H., Pham, H. P., Jegou, S., Landman, C., et al. (2017). Fungal microbiota dysbiosis in IBD. *Gut* 66, 1039–1048. doi: 10.1136/gutjnl-2015-310746

Song, H., Abnet, C. C., Andren-Sandberg, A., Chaturvedi, A. K., and Ye, W. (2016). Risk of Gastrointestinal Cancers among Patients with Appendectomy: A Large-Scale Swedish Register-Based Cohort Study during 1970-2009. *PLoS One* 11:e0151262. doi: 10.1371/journal.pone.0151262

Swidsinski, A., Dorffel, Y., Loening-Baucke, V., Theissig, F., Ruckert, J. C., Ismail, M., et al. (2011). Acute appendicitis is characterised by local invasion with *Fusobacterium nucleatum*/necrophorum. *Gut* 60, 34–40. doi: 10.1136/gut.2009.191320

The, S. M. L., Bakx, R., Budding, A. E., de Meij, T. G. J., van der Lee, J. H., Bunders, M. J., et al. (2019). Microbiota of Children With Complex Appendicitis: Different Composition and Diversity of The Microbiota in Children With Complex Compared With Simple Appendicitis. *Pediatr. Infect. Dis. J.* 38, 1054–1060. doi: 10.1097/INF.0000000000002434

Tzeng, Y. M., Kao, L. T., Kao, S., Lin, H. C., Tsai, M. C., and Lee, C. Z. (2015). An appendectomy increases the risk of rheumatoid arthritis: a five-year follow-up study. *PLoS One* 10:e0126816. doi: 10.1371/journal.pone.0126816

Underhill, D. M., and Iliev, I. D. (2014). The mycobiota: interactions between commensal fungi and the host immune system. *Nat. Rev. Immunol.* 14, 405–416. doi: 10.1038/nri3684

Unger, M. M., Spiegel, J., Dillmann, K. U., Grundmann, D., Philippeit, H., Burmann, J., et al. (2016). Short chain fatty acids and gut microbiota differ between patients with Parkinson's disease and age-matched controls. *Parkinsonism. Relat. Disord.* 32, 66–72. doi: 10.1016/j.parkreldis.2016.08.019

Vitetta, L., Chen, J., and Clarke, S. (2019). The vermiform appendix: an immunological organ sustaining a microbiome inoculum. *Clin. Sci.* 133, 1–8. doi: 10.1042/CS20180956

Wang, Q., Garrity, G. M., Tiedje, J. M., and Cole, J. R. (2007). Naive Bayesian classifier for rapid assignment of rRNA sequences into the new bacterial taxonomy. *Appl. Environ. Microbiol.* 73, 5261–5267. doi: 10.1128/AEM.00062-07

Wu, S. C., Chen, W. T., Muo, C. H., Ke, T. W., Fang, C. W., and Sung, F. C. (2015). Association between appendectomy and subsequent colorectal cancer development: an Asian population study. *PLoS One* 10:e0118411. doi: 10.1371/journal.pone.0118411

Yang, A. M., Inamine, T., Hochrath, K., Chen, P., Wang, L., Llorente, C., et al. (2017). Intestinal fungi contribute to development of alcoholic liver disease. *J. Clin. Invest.* 127, 2829–2841. doi: 10.1172/JCI90562

Zhao, L., Zhang, F., Ding, X., Wu, G., Lam, Y. Y., Wang, X., et al. (2018). Gut bacteria selectively promoted by dietary fibers alleviate type 2 diabetes. *Science* 359, 1151–1156. doi: 10.1126/science.aao5774

Zhong, D., Brower-Sinning, R., Firek, B., and Morowitz, M. J. (2014). Acute appendicitis in children is associated with an abundance of bacteria from the phylum Fusobacteria. *J. Pediatr. Surg.* 49, 441–446. doi: 10.1016/j.jpedsurg.2013.06.026

Conflict of Interest: The authors declare that the research was conducted in the absence of any commercial or financial relationships that could be construed as a potential conflict of interest.

Publisher's Note: All claims expressed in this article are solely those of the authors and do not necessarily represent those of their affiliated organizations, or those of the publisher, the editors and the reviewers. Any product that may be evaluated in this article, or claim that may be made by its manufacturer, is not guaranteed or endorsed by the publisher.

frontiers in Microbiology

ORIGINAL RESEARCH
published: 27 September 2021
doi: 10.3389/fmicb.2021.729455

Artificial Intelligence Systems for Diagnosis and Clinical Classification of COVID-19

*Lan Yu[1,2], Xiaoli Shi[3,4], Xiaoling Liu[5], Wen Jin[1], Xiaoqing Jia[6], Shuxue Xi[3,4], Ailan Wang[3,4], Tianbao Li[3,4], Xiao Zhang[1], Geng Tian[3,4] and Dejun Sun[7]**

[1] Clinical Medical Research Center/Inner Mongolia Key Laboratory of Gene Regulation of the Metabolic Diseases, Inner Mongolia People's Hospital, Hohhot, China, [2] Department of Endocrinology, Inner Mongolia People's Hospital, Hohhot, China, [3] Geneis (Beijing) Co., Ltd., Beijing, China, [4] Qingdao Geneis Institute of Big Data Mining and Precision Medicine, Qingdao, China, [5] Department of Otolaryngology, Inner Mongolia People's Hospital, Hohhot, China, [6] Baotou City Hospital for Infectious Diseases, Baotou, China, [7] Department of Pulmonary and Critical Care Medicine/Key Laboratory of National Health Commission for the Diagnosis & Treatment of COPD, Inner Mongolia People's Hospital, Hohhot, China

Objectives: COVID-19 is highly infectious and has been widely spread worldwide, with more than 159 million confirmed cases and more than 3 million deaths as of May 11, 2021. It has become a serious public health event threatening people's lives and safety. Due to the rapid transmission and long incubation period, shortage of medical resources would easily occur in the short term of discovering disease cases. Therefore, we aimed to construct an artificial intelligent framework to rapidly distinguish patients with COVID-19 from common pneumonia and non-pneumonia populations based on computed tomography (CT) images. Furthermore, we explored artificial intelligence (AI) algorithms to integrate CT features and laboratory findings on admission to predict the clinical classification of COVID-19. This will ease the burden of doctors in this emergency period and aid them to perform timely and appropriate treatment on patients.

Methods: We collected all CT images and clinical data of novel coronavirus pneumonia cases in Inner Mongolia, including domestic cases and those imported from abroad; then, three models based on transfer learning to distinguish COVID-19 from other pneumonia and non-pneumonia population were developed. In addition, CT features and laboratory findings on admission were combined to predict clinical types of COVID-19 using AI algorithms. Lastly, Spearman's correlation test was applied to study correlations of CT characteristics and laboratory findings.

Results: Among three models to distinguish COVID-19 based on CT, vgg19 showed excellent diagnostic performance, with area under the curve (AUC) of the receiver operating characteristic (ROC) curve at 95%. Together with laboratory findings, we were able to predict clinical types of COVID-19 with AUC of the ROC curve at 90%. Furthermore, biochemical markers, such as C-reactive protein (CRP), LYM, and lactic dehydrogenase (LDH) were identified and correlated with CT features.

Conclusion: We developed an AI model to identify patients who were positive for COVID-19 according to the results of the first CT examination after admission and

OPEN ACCESS

Edited by:
Zhangran Chen,
Xiamen University, China

Reviewed by:
Lei Wang,
Changsha University, China
Jujuan Zhuang,
Dalian Maritime University, China

****Correspondence:***
Dejun Sun
nmresearch@foxmail.com

Specialty section:
This article was submitted to Systems Microbiology, a section of the journal Frontiers in Microbiology

Received: *23 June 2021*
Accepted: *17 August 2021*
Published: *27 September 2021*

Citation:
Yu L, Shi X, Liu X, Jin W, Jia X, Xi S, Wang A, Li T, Zhang X, Tian G and Sun D (2021) Artificial Intelligence Systems for Diagnosis and Clinical Classification of COVID-19. Front. Microbiol. 12:729455. doi: 10.3389/fmicb.2021.729455

predict the progression combined with laboratory findings. In addition, we obtained important clinical characteristics that correlated with the CT image features. Together, our AI system could rapidly diagnose COVID-19 and predict clinical types to assist clinicians perform appropriate clinical management.

Keywords: COVID-19, CT images, laboratory findings, artificial intelligence, correlation analysis

INTRODUCTION

In December 2019, a cluster of patients with unidentified pneumonia disease was discovered. Soon a novel coronavirus was isolated from these patients, which belonged to the beta-coronavirus family and was named severe acute respiratory syndrome coronavirus 2 (SARS-CoV-2) (Zhu et al., 2020). On February 12, 2020, the World Health Organization (WHO) named the disease as Coronavirus Disease 2019 (COVID-19) as it had spread quickly all over the world and developed into a plague (Mahase, 2020). By May 11, 2021, more than 159 million people were confirmed infected with more than 3 million cases of mortality. The crowd was affected easily, and the common clinical manifestations were fever, dry cough, and fatigue (Chen et al., 2020; Huang et al., 2020). Mild patients may have no obvious clinical symptoms, while severe patients may have dyspnea and hypoxemia. The incubation period of COVID-19 was 1–14 days, mostly 3–7 days, and it was infectious even in the incubation period (Sun et al., 2020). The main transmission route was *via* respiratory droplets and close contact (Li et al., 2021). Patients with COVID-19 but with no symptoms may have transmitted the virus to close contacts before a definite diagnosis could be made. Though there are many studies on identifying effective drugs against SARS-CoV-2 (Tang et al., 2020; Peng et al., 2021), most of them need further experimental and clinical validation (Peng et al., 2020; Zhou et al., 2020). Therefore, early diagnosis was extremely important.

According to the current diagnostic criteria, the gold standard of diagnosis was nucleic acid detection, and reverse transcription–polymerase chain reaction (RT-PCR) had become the main test method because of its low cost and high speed compared to complete genome sequencing (Loeffelholz and Tang, 2020). However, due to sampling deviation, with low viral load (the number of virus replications cannot reach the qPCR detection threshold) in the specimen and the accuracy of detection reagents, the detection results may be false negative (Ai et al., 2020; Mei et al., 2020; Rubin et al., 2020), which resulted in suspected patients not being identified and isolated in time. This would lead to further spread of infection, resulting in the epidemic being difficult to control. On the other hand, patients with COVID-19 could not get timely treatment if not identified, so a series of nucleic acid tests may be required to eliminate the possibility of false-negative results in suspected or discharged patients. During the outbreak of a highly infectious epidemic, a novel method for rapid and accurate diagnosis of patients with COVID-19 was urgently needed.

Chest computed tomography (CT) examination was an indispensable method in the diagnosis of COVID-19, and CT could reveal the severity of COVID-19 as well as the disease progression in dynamic monitoring, while nucleic acid detection was only a qualitative test result (Dai et al., 2020). In the critical epidemic situation of Wuhan, China, CT played an important role for patients who had negative nucleic acid tests but with symptoms or close contact with the confirmed patients. The most common CT findings in patients affected by COVID-19 included ground glass opacities (GGO) and consolidation involving the bilateral lungs in a peripheral distribution (Zhang et al., 2020). Pleural effusions, lymphadenopathy, and discrete pulmonary nodules were very rare (Kanne, 2020; Nishiura et al., 2020; Song et al., 2020). Consolidation was considered as a sign of disease progression. However, CT alone was not suitable for independently ruling out SARS-CoV-2 infection to the best of our knowledge because some patients may have normal radiological features at early stages of the disease and doctors could not distinguish by naked eye observation (Chung et al., 2020). During the period of the epidemic, the physicians needed to analyze numerous CT images to judge the condition of patients and integrated them with clinical information to make the final judgment. Thus, developing artificial intelligence (AI)-based imaging analysis methods was crucial to support physicians. Mei et al. (2020) had established an AI algorithm to combine chest CT findings with clinical symptoms, laboratory testing, and exposure history to rapidly diagnose patients with SARS-CoV-2.

In this study, we used AI algorithms to construct a model to attempt to distinguish patients with COVID-19 from common pneumonia and non-pneumonia based on CT images rapidly and accurately, which would greatly reduce the workload of radiologists and also brought huge convenience to the hospitals without experienced radiologists. It was convenient for doctors to take timely and accurate pertinent treatment and improve their prognosis. Furthermore, we could predict the progression of COVID-19 combined with laboratory findings on admission, and this would be very meaningful for medical workers to take appropriate treatment.

MATERIALS AND METHODS

Data Collection

This retrospective study had been approved by the ethics committees of the Inner Mongolia People's Hospital. Further informed consent was waived with approval, as the study only involved de-identified data and had no potential risk to patients.

We collected chest CT images and clinical information from all confirmed COVID-19 patients who were admitted to different hospitals in Inner Mongolia. All patients had been confirmed COVID-19 positive by nucleic acid detection. In addition, novel coronavirus pneumonia cases that entered Inner Mongolia from

overseas were also included in the study. The demographic characteristics, clinical features of first detection, and initial chest CT images were sorted out. Other pneumonia (not COVID-19) and non-pneumonia patients were randomly selected from hospitals within the last 6 months before COVID-19 occurred.

Preprocessing and Image Augmentation

Qualified CT slices were selected by senior radiologists from the original hundreds of images produced by CT scanners. Pulmonary tissue <20% of the size of the body part and the images containing severe artifacts or obvious image resolution reductions were excluded. Finally, we selected 1,041 chest CT images from 150 non-pneumonia patients, 965 CT images from 186 patients with COVID-19, including 61 mild and 125 moderate types, and 852 CT images from 113 other pneumonia patients. The raw CT images with 512 × 512 pixels were rescaled to the size of 224 × 224 pixels, after which we normalized image channels, respectively.

To alleviate an overfitting phenomenon, data augmentation is employed. By applying horizontal flipping image data, we doubled the number of images in the training data set.

Model Construction Using Transfer Learning

To build an automated system with two progressive models, the first model is used for diagnosing COVID-19, and the second is for disease typing. For the first model, a one-vs.-the-rest classification strategy is employed; more specifically, the CT data were divided into one (COVID-19) vs. other two classes that include other pneumonia cases and normal control cases. Fairly, fivefold cross-validation is used for performance evaluation (Kaczorowska et al., 2021). Patients with each disease type were divided into five subgroups with stratified sampling. In our experimental setup, we loaded three pre-trained models (resnet18, vgg19, and vgg16) on the ImageNet database and reset the size of the final fully connected layer. Training was terminated when the validation accuracy did not increase for 10 epochs. Transfer learning was a popular method in computer vision community since it enabled an accurate model to be established in a short time (Rawat and Wang, 2017).

For the model combining CT images and laboratory findings, we applied the global averaging layer to the last layers of the convolutional model described previously to derive a 512 dimensional feature vector for representation. The way we used in multimodal fusion is Compact Bilinear Pooling (CBP). A total of 55 laboratory findings of the same patient were concatenated with this feature vector. A Multi-Layer Perceptron (MLP) took this combined feature vector as the input to predict the status of COVID-19. We used a three-layer MLP; each layer has 64 nodes followed by a batch normalization layer, a fully connected layer, and a ReLU activation function. The MLP was trained with an end-to-end manner. Then, we applied binary cross-entropy loss function to evaluate both MLP and CNN during the feed forward phase. Eventually, we evaluated the performance of models based on four metrics, which include area under the curve (AUC) of receiver operating characteristic (ROC), sensitivity, specificity, and accuracy.

Correlation Analysis Between Imaging Features and Laboratory Findings

Clinical records collected from patients with COVID-19 included demographic characteristics, such as gender and age, clinical data on vital signs and symptoms, as well as dynamic results of laboratory test and imaging data monitored from admission to discharge. Laboratory tests included routine blood tests, liver and kidney biochemical indicators, coagulation function tests, and serum protein levels and activities.

To explore the correlation between lung CT image features and laboratory detection indexes, Spearman's correlation test was applied. A total of 512 CT features and 55 experimental detection indicators were input. The resultant correlation was considered significant when $p < 0.05$ after correction with the Holm–Bonferroni method.

RESULTS

Imaging Protocol

As the methods used in model construction were relatively complex and multiple threads were covered in this study, we drew a flowchart to illustrate the experimental process (**Figure 1**). Firstly, we used three kinds of methods to construct models to distinguish patients with COVID-19, other common pneumonia, and normal controls based on the chest CT scans, then the model was built to further classify the types of COVID-19 based on CT images on admission. Lastly, the laboratory findings were combined with the CT scans to improve the performance of machine-learning models to classify the types of COVID-19.

Image Datasets of Patients

We collected all CT images of 237 patients with COVID-19 from admission to discharge in Inner Mongolia, with 79 domestic cases and 158 imported cases. Among them, seven patients belong to severe novel coronavirus pneumonia, 160 patients were moderate type, and 70 patients were mild type. We finally got 2,858 qualified CT slices taken into model construction after a selection performed by experienced radiologists, which were from 186 patients infected with SARS-CoV-2, 113 other pneumonia patients, and 150 normal control patients (**Table 1**). The severe type of COVID-19 was excluded, as the number of this kind of patients was too low. In addition, the number of mild type was significantly less than the moderate type. In order to get better training effect, we should make the number of CT films as close as possible.

Results of the Diagnostic Model

Normalized CT images were put into the model construction without the preprocessing of lung segmentation or feature selection. To distinguish COVID-19 from other common pneumonia and normal controls, we applied vgg19, resnet18, and vgg16 as a backbone to train the deep learning model, and the performance of the ROC curve of these AI models based

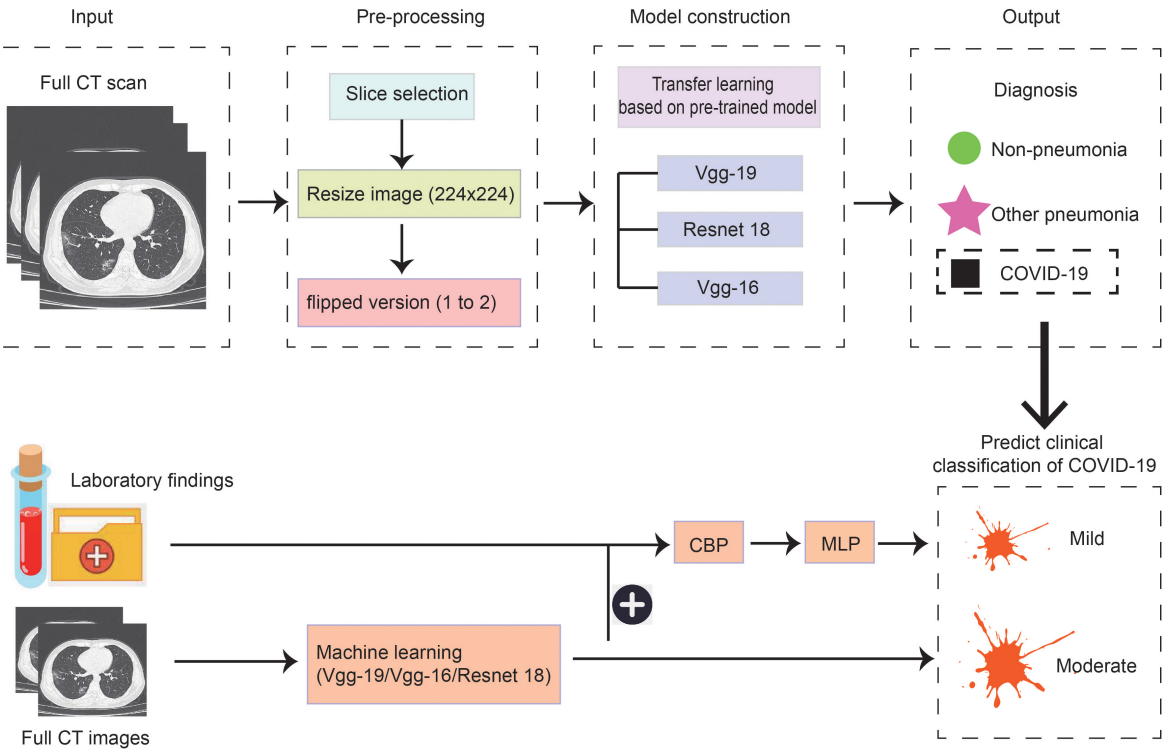

FIGURE 1 | Scheme of our deep learning framework based on the first chest CT images and laboratory findings for the diagnosis and classification of COVID-19. The first row describes the process of constructing the diagnosis model. Full CT images of COVID-19, other pneumonia, and non-pneumonia were taken as input and generated the probability of three disease states with classification networks. The second row indicates predicting the clinical classification of COVID-19 based on CT images only and based on CT images together with laboratory findings.

on test data is demonstrated in **Figure 2A**. All models have achieved superior performance with AUC value of ROC curves between 0.94 and 0.95, and the AUC value of vgg19 presenting the highest. In addition, we calculated and compared the sensitivity, specificity, and accuracy of the three AI models. Among them, the best model vgg19 was able to distinguish COVID-19 from the other two classes with 78.85% accuracy, 98.54% sensitivity, and 59.16% specificity (**Figure 2B**).

In order to make the model better understood, we used the Class Activation Mapping (CAM) method (Zhou et al., 2016) to visualize the important domains resulting in the decision of the model. After preprocessing, such as removing noise and rescale, the region heat maps were fully generated by a deep learning model without manual annotation. We selected a typical image from each of the three disease types to show in **Figure 3**. The first column displays the original image and heat map of normal control patients from top to bottom. The second column demonstrates the original image and heat map of other pneumonia patients and the third column shows images of COVID-19. The heat maps are standard jet color pictures made by OpenCV and are overlapped on the initial image, where dark red highlights the activation regions associated with the classification.

TABLE 1 | Summary of the patients' information.

	Non-pneumonia	Other common pneumonia	COVID-19	
			Mild	Moderate
Patients	150	113	61	125
CT slices	1,041	852	495	470

Performance of Predicting Mild and Moderate Types of COVID-19

After establishing a model that can quickly and accurately diagnose COVID-19, we also want to further establish an automatic classification system so that a truly integrated diagnosis and treatment can be realized, helping doctors determine whether the patient is suffering from COVID-19 at the shortest time possible after receiving the patient. If the person is suffering from COVID-19, what kind of clinical type is it? The most suitable treatment can then be taken on time.

Firstly, we still predicted the clinical classification of patients (mild or moderate) based on the CT images on admission. Since the number of severe patients collected was too low, this type was excluded temporarily. After screening, we collected 495 qualified CT films from 61 mild patients and 470 qualified CT films from 125 moderate patients. The fivefold cross-validation method is still used to construct the classification system based on three

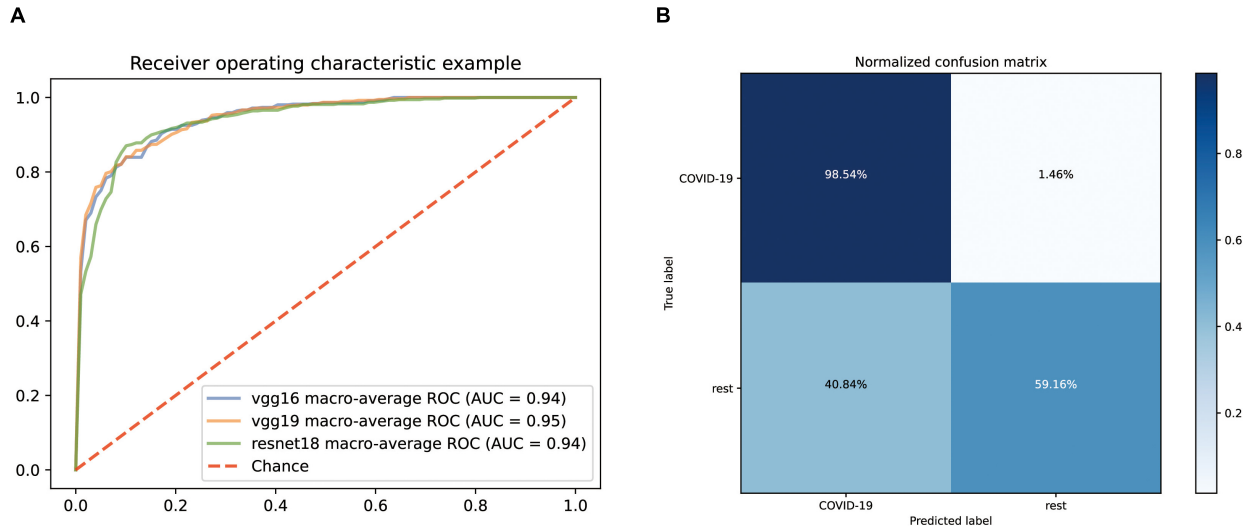

FIGURE 2 | Performance of our AI systems in differentiating COVID-19 from other common pneumonia and normal controls. **(A)** ROC curves of vgg16, vgg19 and resnet18 systems. **(B)** Normalized confusion matrix of vgg19 system.

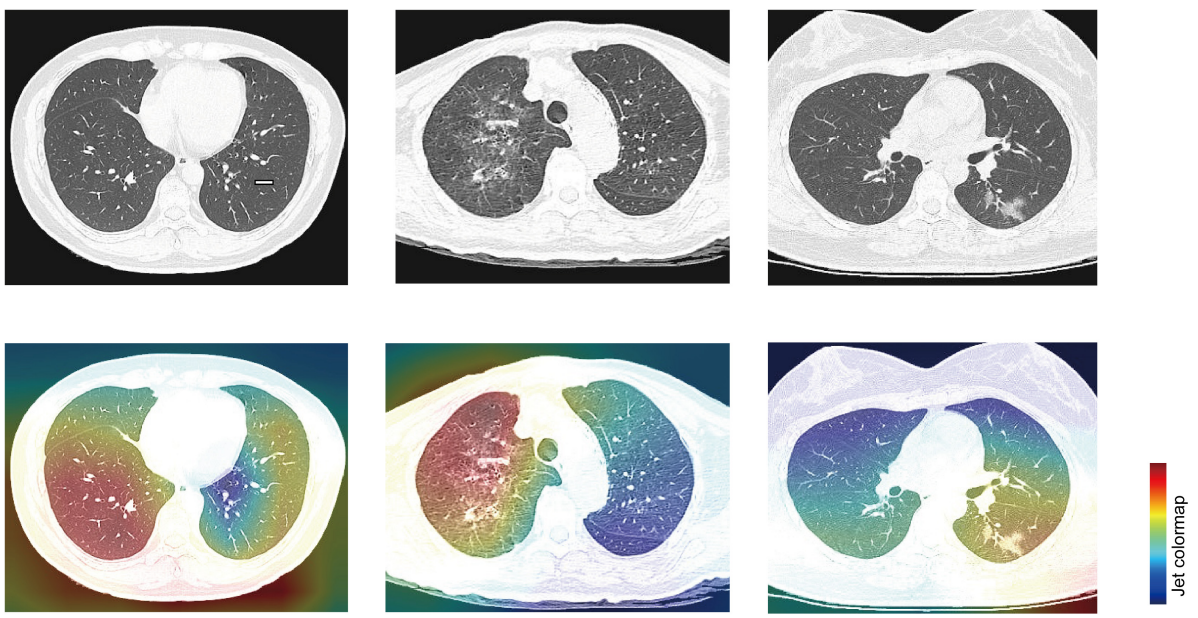

FIGURE 3 | Typical examples of chest CT images of patients and visual features correlated to classification. The first row demonstrates the original images of patients with normal control, other pneumonia, and COVID-19, respectively. The second row demonstrates heat maps corresponding to the first row, showing highly relevant areas of classification.

pre-trained networks (vgg19, vgg16, and resnet18). The ROC curves of the classification systems are shown in **Figure 4A**. Among them, the model based on resnet18 has the highest AUC value (0.75). Its confusion matrix is shown in **Figure 4B**, with a sensitivity of 76.92% and a specificity of 79.17%. The AUC values of the other two models were 0.73 (vgg16) and 0.74 (vgg19), respectively. According to these results, it could be seen that the performance of the model constructed only based on CT images was not good enough for clinical application.

Considering that there was still a lot of routine examination information available on admission, we combined the information and CT images as input to establish a predictive classification model. The ROC curve of these three models we built is shown in **Figure 4C**. The performance of all models greatly improved after combining the laboratory findings, with AUC values ranging from 0.88 to 0.90. The confusion matrix of vgg19, which had the best AUC value, is displayed in **Figure 4D**, with a

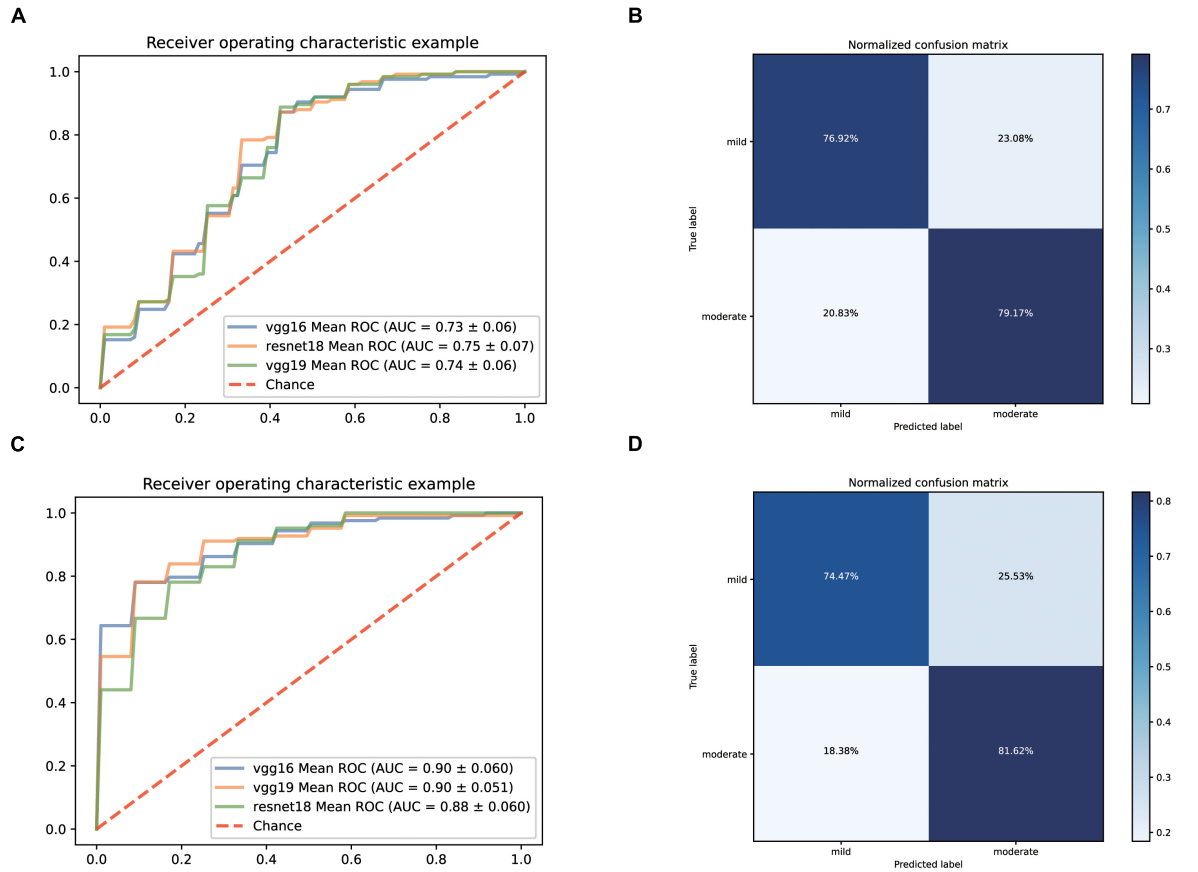

FIGURE 4 | Performance of our AI Systems in predicting mild and moderate types of COVID-19 based on the original CT images and on the original CT images plus biochemical indicators. **(A,B)** ROC curves and normalized confusion matrix of one model (resnet18) based on the original CT images. **(C,D)** ROC curves and normalized confusion matrix (vgg19) based on the original CT images and biochemical indicators.

sensitivity of 74.47% and a specificity of 81.62% on the test set.

Correlations of Lung Imaging Features and Laboratory Findings of COVID-19

Lung imaging features could reflect values of clinical biochemical parameters to some extent. Zhang et al. (2020) also reported that volume lesion ratio of lung was well linearly correlated to clinical parameters, such as C-reactive protein (CRP) and albumin. In order to investigate the association between CT features and biochemical indicators, we performed Spearman's correlation tests and found key biochemical markers. The threshold of significant correlation was $p < 0.05$ after correction with the Holm–Bonferroni method, then the p-value was further refined into $p < 0.001$ (marked as 1), $p < 0.01$ (marked as 2), and $p < 0.05$ (marked as 3), which are labeled in **Figure 5**. In addition, we selected a |correlation value| of CT feature $\geq$0.35 and a |correlation value| of laboratory findings $\geq$0.30 to show in **Figure 5**. Eosinophil ratio (EO%), eosinophils (EOS), and lymphocyte number (LYM_N) showed highly positive correlations with the X370 feature of CT (lesion features). Generally speaking, the increase of eosinophils and lymphocyte number at the same time is considered to be caused by virus infection, which may be reflected on CT images of the lung. Glucose (GLU), red cell distribution width standard deviation (RDW_SD), chlorine (Cl), and mean corpuscular volume (MCV) were highly correlated with the X242 and X89 feature of CT. CRP, γ-glutamyl transpeptidase (GGT), direct bilirubin (DBIL), lactic dehydrogenase (LDH), and total bilirubin (TBIL) were highly correlated with the X402 feature of CT, whereas indirect bilirubin (IBIL), DBIL, and TBIL showed highly negative correlations with the X49 feature of CT.

This means the damage of liver and heart can be reflected in lung imaging as these biochemical indexes are markers of liver and heart function, suggesting that pulmonary lesions are not only related to the function of the respiratory system but also related to the health of other major organs, although we did not know the exact underlying pathogenetic mechanisms.

DISCUSSION

In this study, we collected CT images of all patients with COVID-19 in Inner Mongolia since the outbreak and CT images of other common pneumonia and normal controls who visited the hospital 6 months before the outbreak of COVID-19. Based on these CT images, we applied three network structures to construct

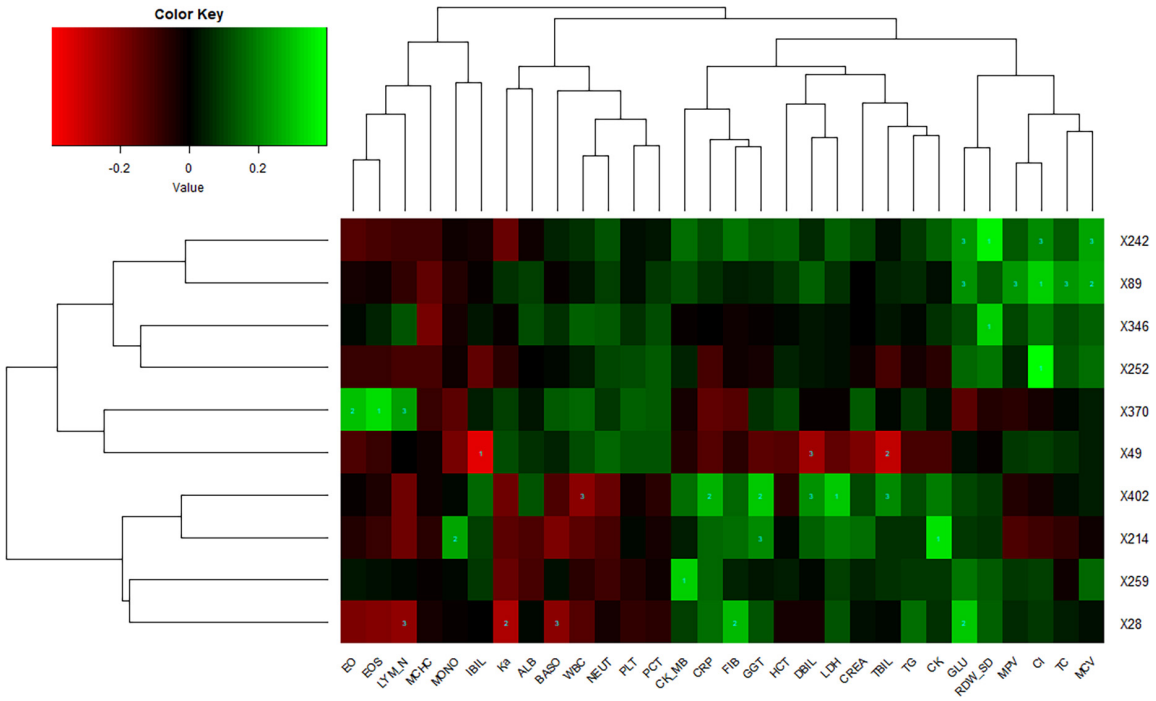

FIGURE 5 | Correlations of lung imaging features and laboratory findings. Horizontal axis represents biochemical index, and vertical axis represents CT features. Number one indicates $p < 0.001$, number two indicates $p < 0.01$, and number three indicates $p < 0.05$.

a deep learning model for disease classification. Among these, vgg19 represented the best performance with an AUC of 0.95, which provided a favorable tool for rapid diagnosis of COVID-19. It was conceivable that if this model was applied to medical units, it would help radiologists and clinicians fight against the pandemic and reduce their burden. Especially in remote areas or communities where there was lack of experienced doctors, it would be an effective complementary measure. For patients with COVID-19, we further developed a deep learning model to predict the clinical classification through CT images of the first examination after admission. However, the classification effect of the prediction model based on three network structures was lower than expected, so the laboratory findings were added to improve the prediction effect and the performance of vgg19 was raised to an AUC of 0.90. This would be conducive to the timely arrangement of an appropriate treatment plan according to the patient's condition to achieve the efficient management of patients. Thus, based on the routine examination items of patients, we built a rapid identification and classification system of COVID-19. In addition, we found that CRP, EOS, LDH, and other indicators were significantly correlated with the CT image features of the lung.

Our research still had some limitations. Firstly, the sample size used to build the model was relatively small. Deep learning typically needed a large number of samples to extract features and the training model in order to achieve wider applicability and higher accuracy. Our model put forward the feasibility of using CT images to predict the trend and classification of COVID-19 disease, and more samples are needed to optimize the model and test the generalizability of the an AI model. The cooperation with more medical centers or hospitals may contribute to the improvement of this work. Secondly, as the number of severe and critical patients was too few, their CT slices were not included in this study. The model still needed to be improved in predictable subtypes and disease severity. If we could collect more CT images of severe patients to train the model, this study will include more comprehensive types of prediction and will be more applicable in clinical practice. Thirdly, we adopted the chest CT slices directly without preprocessing of lung segmentation in order to save time, while lung segmentation preprocessing was generally regarded to improve the accuracy of AI training (Chung et al., 2018; Li et al., 2020; Xu et al., 2020). In weighing the advantages against the disadvantages, we chose transfer learning based on resnet18, vgg19, and vgg16 pre-trained CNN models in the ImageNet data sets (Shin et al., 2016) and fivefold cross-validation. Finally, besides early diagnosis, tracing the origin of SARS-CoV-2 is also critical for understanding and preventing the further outbreak of this virus (Li et al., 2021). There are many methods to identify the evolution of influenza that could be adopted in SARS-CoV-2 (Yang et al., 2013, 2014a). In addition, ideas like antigenic map (Barnett et al., 2012; Huang et al., 2017) and sequence-based virus antigenicity prediction (Sun et al., 2013; Yang et al., 2014b; Yao et al., 2017) are helpful for the vaccine design of SARS-CoV-2. More importantly, drug–target interaction identification (Peng et al., 2017; Zhou et al., 2019) based on the existing two targets (SARS-CoV-2 spike protein and human ACE2) may contribute to the prevention of COVID-19. However, it is out of the scope of this study.

After analyzing the correlation between clinical features and CT image features, we found that there were some features with high positive or negative correlation. As we did not extract and specify image features, such as GGO and consolidation, but chose the pixel feature of the image as the input, we could get a more comprehensive analysis. However, it was difficult to explain how the association was made. In future studies, we will collect more samples from hospitals or public databases to further optimize the performance of AI systems and extend the applicability.

DATA AVAILABILITY STATEMENT

The original contributions presented in the study are included in the article/supplementary material, further inquiries can be directed to the corresponding author.

ETHICS STATEMENT

The studies involving human participants were reviewed and approved by the Medical Research Ethics Committee of Inner Mongolia People's Hospital. Written informed consent from the participants' legal guardian/next of kin was not required to participate in this study in accordance with the national legislation and the institutional requirements.

AUTHOR CONTRIBUTIONS

DS designed the study. LY, XL, WJ, XJ, and SX collected and analyzed the data. LY and XS interpreted the data and wrote the manuscript. AW, TL, XZ, and GT reviewed the manuscript. All authors contributed to the article and approved the submitted version.

FUNDING

This study was partially supported by the Science and Technology Planning Project of Inner Mongolia (No. 2020GG0004) and the talent training plan for the Key Laboratory of Inner Mongolia Science and Technology Department.

REFERENCES

Ai, T., Yang, Z., Hou, H., Zhan, C., Chen, C., Lv, W., et al. (2020). Correlation of chest CT and RT-PCR testing for Coronavirus disease 2019 (COVID-19) in China: a report of 1014 cases. *Radiology* 296, E32–E40.

Barnett, J. L., Yang, J., Cai, Z., Zhang, T., and Wan, X. F. (2012). AntigenMap 3D: an online antigenic cartography resource. *Bioinformatics* 28, 1292–1293. doi: 10.1093/bioinformatics/bts105

Chen, N., Zhou, M., Dong, X., Qu, J., Gong, F., Han, Y., et al. (2020). Epidemiological and clinical characteristics of 99 cases of 2019 novel Coronavirus pneumonia in Wuhan, China: a descriptive study. *Lancet* 395, 507–513. doi: 10.1016/s0140-6736(20)30211-7

Chung, H., Ko, H., Jeon, S. J., Yoon, K. H., and Lee, J. (2018). Automatic lung segmentation with juxta-pleural nodule identification using active contour model and Bayesian approach. *IEEE J. Transl. Eng. Health Med.* 6:180 0513.

Chung, M., Bernheim, A., Mei, X., Zhang, N., Huang, M., Zeng, X., et al. (2020). CT Imaging features of 2019 novel Coronavirus (2019-nCoV). *Radiology* 295, 202–207.

Dai, W. C., Zhang, H. W., Yu, J., Xu, H. J., Chen, H., Luo, S. P., et al. (2020). CT imaging and differential diagnosis of COVID-19. *Can. Assoc. Radiol. J.* 71, 195–200.

Huang, C., Wang, Y., Li, X., Ren, L., Zhao, J., Hu, Y., et al. (2020). Clinical features of patients infected with 2019 novel Coronavirus in Wuhan, China. *Lancet* 395, 497–506.

Huang, L., Li, X., Guo, P., Yao, Y., Liao, B., Zhang, W., et al. (2017). Matrix completion with side information and its applications in predicting the antigenicity of influenza viruses. *Bioinformatics* 33, 3195–3201. doi: 10.1093/bioinformatics/btx390

Kaczorowska, M., Plechawska-Wójcik, M., and Tokovarov, M. (2021). Interpretable machine learning models for three-way classification of cognitive workload levels for eye-tracking features. *Brain Sci.* 11:210. doi: 10.3390/brainsci11020210

Kanne, J. P. (2020). Chest CT findings in 2019 novel Coronavirus (2019-nCoV) infections from Wuhan, China: key points for the radiologist. *Radiology* 295, 16–17. doi: 10.1148/radiol.2020200241

Li, L., Qin, L., Xu, Z., Yin, Y., Wang, X., Kong, B., et al. (2020). Using artificial intelligence to detect COVID-19 and community-acquired pneumonia based on pulmonary CT: evaluation of the diagnostic accuracy. *Radiology* 296, E65–E71.

Li, T., Huang, T., Guo, C., Wang, A., Shi, X., Mo, X., et al. (2021). Genomic variation, origin tracing, and vaccine development of SARS-CoV-2: a systematic review. *Innovation* 2:100116. doi: 10.1016/j.xinn.2021.100116

Loeffelholz, M. J., and Tang, Y. W. (2020). Laboratory diagnosis of emerging human coronavirus infections - the state of the art. *Emerg. Microb. Infect.* 9, 747–756. doi: 10.1080/22221751.2020.1745095

Mahase, E. (2020). Covid-19: WHO declares pandemic because of "alarming levels" of spread, severity, and inaction. *BMJ* 368:m1036. doi: 10.1136/bmj.m1036

Mei, X., Lee, H. C., Diao, K. Y., Huang, M., Lin, B., Liu, C., et al. (2020). Artificial intelligence-enabled rapid diagnosis of patients with COVID-19. *Nat. Med.* 26, 1224–1228.

Nishiura, H., Jung, S. M., Linton, N. M., Kinoshita, R., Yang, Y., Hayashi, K., et al. (2020). The extent of transmission of novel Coronavirus in Wuhan, China, 2020. *J. Clin. Med.* 9:330. doi: 10.3390/jcm9020330

Peng, L., Bo, L., Wen, Z., Li, Z., and Li, K. (2017). Predicting drug–target interactions with multi-information fusion. *IEEE J. Biomed. Health Inform.* 21, 561–572. doi: 10.1109/jbhi.2015.2513200

Peng, L., Shen, L., Xu, J., Tian, X., Liu, F., Wang, J., et al. (2021). Prioritizing antiviral drugs against SARS-CoV-2 by integrating viral complete genome sequences and drug chemical structures. *Sci. Rep.* 11:6248.

Peng, L., Tian, X., Shen, L., Kuang, M., Li, T., Tian, G., et al. (2020). Identifying effective antiviral drugs against SARS-CoV-2 by drug repositioning through virus-drug association prediction. *Front. Genet.* 11:577387. doi: 10.3389/fgene.2020.577387

Rawat, W., and Wang, Z. (2017). Deep convolutional neural networks for image classification: a comprehensive review. *Neural Comput.* 29, 2352–2449. doi: 10.1162/neco_a_00990

Rubin, G. D., Ryerson, C. J., Haramati, L. B., Sverzellati, N., Kanne, J. P., Raoof, S., et al. (2020). The role of chest imaging in patient management during the COVID-19 pandemic: a multinational consensus statement from the fleischner society. *Radiology* 296, 172–180. doi: 10.1148/radiol.2020201365

Shin, H. C., Roth, H. R., Gao, M., Lu, L., Xu, Z., Nogues, I., et al. (2016). Deep convolutional neural networks for computer-aided detection: CNN architectures, dataset characteristics and transfer learning. *IEEE Trans. Med. Imag.* 35, 1285–1298. doi: 10.1109/tmi.2016.2528162

Song, F., Shi, N., Shan, F., Zhang, Z., Shen, J., Lu, H., et al. (2020). Emerging 2019 novel coronavirus (2019-nCoV) pneumonia. *Radiology* 297:E346.

Sun, H., Yang, J., Zhang, T., Long, L. P., Jia, K., Yang, G., et al. (2013). Using sequence data to infer the antigenicity of influenza virus. *mBio* 4:e00230-13.

Sun, K., Chen, J., and Viboud, C. (2020). Early epidemiological analysis of the coronavirus disease 2019 outbreak based on crowdsourced data: a population-level observational study. *Lancet Digit. Health* 2, e201–e208.

Tang, X., Cai, L., Meng, Y., Xu, J., Lu, C., and Yang, J. (2020). Indicator regularized non-negative matrix factorization method-based drug repurposing for COVID-19. *Front. Immunol.* 11:603615. doi: 10.3389/fimmu.2020.603615

Xu, X., Jiang, X., Ma, C., Du, P., Li, X., Lv, S., et al. (2020). A deep learning system to screen novel coronavirus disease 2019 pneumonia. *Engineering* 6, 1122–1129. doi: 10.1016/j.eng.2020.04.010

Yang, J., Grünewald, S., and Wan, X. F. (2013). Quartet-net: a quartet-based method to reconstruct phylogenetic networks. *Mol. Biol. Evol.* 30, 1206–1217. doi: 10.1093/molbev/mst040

Yang, J., Grünewald, S., Xu, Y., and Wan, X. F. (2014a). Quartet-based methods to reconstruct phylogenetic networks. *BMC Syst. Biol.* 8:21. doi: 10.1186/1752-0509-8-21

Yang, J., Zhang, T., and Wan, X. F. (2014b). Sequence-based antigenic change prediction by a sparse learning method incorporating co-evolutionary information. *PLoS One* 9:e106660. doi: 10.1371/journal.pone.0106660

Yao, Y., Li, X., Liao, B., Huang, L., He, P., Wang, F., et al. (2017). Predicting influenza antigenicity from hemagglutintin sequence data based on a joint random forest method. *Sci. Rep.* 7:1545.

Zhang, K., Liu, X., Shen, J., Li, Z., Sang, Y., Wu, X., et al. (2020). Clinically applicable AI system for accurate diagnosis, quantitative measurements, and prognosis of COVID-19 pneumonia using computed tomography. *Cell* 181, 1423–1433.e1411.

Zhou, B., Khosla, A., Lapedriza, A., Oliva, A., and Torralba, A. (2016). "Learning deep features for discriminative localization," in *Proceedings of the IEEE Conference on Computer Vision and Pattern Recognition*, (New York, NY: Springer), 2921–2929.

Zhou, L., Li, Z., Yang, J., Tian, G., Liu, F., Wen, H., et al. (2019). Revealing drug-target interactions with computational models and algorithms. *Molecules* 24:1714. doi: 10.3390/molecules24091714

Zhou, L., Wang, J., Liu, G., Lu, Q., Dong, R., Tian, G., et al. (2020). Probing antiviral drugs against SARS-CoV-2 through virus-drug association prediction based on the KATZ method. *Genomics* 112, 4427–4434. doi: 10.1016/j.ygeno.2020.07.044

Zhu, N., Zhang, D., Wang, W., Li, X., Yang, B., Song, J., et al. (2020). A novel Coronavirus from patients with pneumonia in China, 2019. *N. Engl. J. Med.* 382, 727–733.

Conflict of Interest: XS, SX, AW, TL, and GT were employed by Geneis (Beijing) Co., Ltd.

The remaining authors declare that the research was conducted in the absence of any commercial or financial relationships that could be construed as a potential conflict of interest.

Publisher's Note: All claims expressed in this article are solely those of the authors and do not necessarily represent those of their affiliated organizations, or those of the publisher, the editors and the reviewers. Any product that may be evaluated in this article, or claim that may be made by its manufacturer, is not guaranteed or endorsed by the publisher.

frontiers in Microbiology

ORIGINAL RESEARCH
published: 07 October 2021
doi: 10.3389/fmicb.2021.700718

Fecal Microbiota Transplantation Modulates the Gut Flora Favoring Patients With Functional Constipation

Xueying Zhang, Ning Li, Qiyi Chen and Huanlong Qin**

Intestinal Microenvironment Treatment Center, Shanghai Tenth People's Hospital, Tongji University School of Medicine, Shanghai, China

OPEN ACCESS

Edited by:
Yanling Wei,
Army Medical University, China

Reviewed by:
Dongxu Qiu,
Central South University, China
Wei-Hua Chen,
Huazhong University of Science and Technology, China

***Correspondence:**
Qiyi Chen
qiyichen2011@163.com
Huanlong Qin
qin_huanlong@126.com

Specialty section:
This article was submitted to Systems Microbiology, a section of the journal Frontiers in Microbiology

Received: *26 April 2021*
Accepted: *23 August 2021*
Published: *07 October 2021*

Citation:
Zhang X, Li N, Chen Q and Qin H (2021) Fecal Microbiota Transplantation Modulates the Gut Flora Favoring Patients With Functional Constipation. Front. Microbiol. 12:700718. doi: 10.3389/fmicb.2021.700718

Intestinal dysmotility is common in many diseases and is correlated with gut microbiota dysbiosis and systemic inflammation. Functional constipation (FC) is the most typical manifestation of intestinal hypomotility and reduces patients' quality of life. Some studies have reported that fecal micriobiota transplantation (FMT) may be an effective and safe therapy for FC as it corrects intestinal dysbiosis. This study was conducted to evaluate how FMT remodels the gut microbiome and to determine a possible correlation between certain microbes and clinical symptoms in constipated individuals. Data were retrospectively collected on 18 patients who underwent FMT between January 1, 2019 and June 30, 2020. The fecal bacterial genome was detected by sequencing the V3–V4 hypervariable regions of the 16S rDNA gene. Fecal short chain fatty acids (SCFAs) were detected by gas chromatography-mass spectrometry, and serum inflammatory factor concentrations were detected via enzyme-linked immunosorbent assay. Comparing the changes in fecal microbiome compositions before and after FMT revealed a significant augmentation in the alpha diversity and increased abundances of some flora such as Clostridiales, *Fusicatenibacter,* and *Paraprevotella*. This was consistent with the patients experiencing relief from their clinical symptoms. Abundances of other flora, including *Lachnoanaerobaculum,* were decreased, which might correlate with the severity of patients' constipation. Although no differences were found in SCFA production, the butyric acid concentration was correlated with both bacterial alterations and clinical symptoms. Serum IL-8 levels were significantly lower after FMT than at baseline, but IL-4, IL-6, IL-10, and IL-12p70 levels were not noticeably changed. This study showed how FMT regulates the intestinal microenvironment and affects systemic inflammation in constipated patients, providing direction for further research on the mechanisms of FMT. It also revealed potential microbial targets for precise intervention, which may bring new breakthroughs in treating constipation.

Keywords: fecal microbiota transplantation, gut microbiome, functional constipation, 16S rDNA gene sequencing, short chain fatty acid, serum inflammatory factor

INTRODUCTION

Intestinal motility disorder is common with many diseases such as irritable bowel syndrome (IBS), inflammatory bowel diseases, critical illness, and postsurgical intestinal dysfunction. Intestinal dysmotility alone may lead to poor quality of life for patients, while dysmotility in other diseases may contribute to a worse prognosis (Garrett and Bar-Or, 2008, Shimizu et al., 2011). Thus, gut motility disorder is problematic and requires further study.

Intestinal dysmotility is associated with many factors, including neuroimmune interactions and gut microbiota changes (De Jonge et al., 2005; Zhao and Yu, 2016). The intestinal flora may regulate intestinal motility by releasing bacterial metabolites such as short-chain fatty acids (SCFAs), intestinal neuroendocrine factors, and mediators released by the gut immune response (Barbara et al., 2005). Long durations of intestinal dysmotility, such as with chronic constipation, may alter the microbiome composition and intestinal permeability, which may lead to systemic immune system activation and inflammatory status changes (Khalif et al., 2005; de Jong et al., 2016). Therefore, intestinal motility disorders involve a series of complex pathophysiological processes in which the gut microbiota may play a key role.

Functional constipation (FC) is the most typical manifestation of intestinal hypomotility. According to the ROME IV criteria, FC is a gut-brain interaction disorder (Drossman and Hasler, 2016). Patients have difficulty defecating and may experience depression and/or anxiety. Furthermore, severe constipation can potentially lead to bowel obstruction. The American Gastroenterological Association recommends microbiota-modulating methods, such as dietary control and fiber intake, as the first-line treatment for FC, and probiotics such as *Bifidobacterium lactis* DN-173 010 and *Lactobacillus casei* Shirota are reported to have potential treatment efficacy (Chmielewska and Szajewska, 2010; Mearin et al., 2016). Laxatives and 5-HT4 receptor agonists are also recommended as empiric therapy (Mearin et al., 2016). However, few conservative treatments exist for refractory constipation, and patients whose symptoms are not relieved by the above treatments may require surgery.

Fecal microbiota transplantation (FMT) may help cure constipation that cannot be alleviated by other conservative treatments and may help many patients (Tian et al., 2017; Tian Y. et al., 2020). FMT involves transferring the gut microbiotas from healthy donors to patients to treat diseases and is effective for recurrent or refractory *Clostridium difficile* infections (Cammarota et al., 2017; Mullish et al., 2018). Under approval from the Ethics Committee of Shanghai Tenth People's Hospital of Tongji University, we have been performing FMT on patients with bowel disorders since 2017. As of June 2020, we have treated over 1,000 patients with constipation, with an efficacy rate of $>$ 67%. Most constipated patients have other diseases, such as diabetes, Parkinson's disease and mental disorders, or have histories of drug use or surgeries that contributed or might have contributed to their defecation difficulties. The underlying mechanism by which FMT regulates gut motility remains unclear, especially when combined diseases may also affect the pathophysiological processes of constipation. We conducted this retrospective study to evaluate the clinical efficacy and gut microbiota remodeling ability of FMT on constipated patients and to explore the potential mechanisms underlying FMT and gut motility. We attempted to build an appropriate model of bowel hypomotility by selecting FC patients without combined diseases or surgical histories or histories of using drugs that might influence bowel motility or the gut microbiome. We hypothesized that FMT could relieve constipation symptoms by remodeling the gut microbiota composition and that the possible mechanism might be correlated with altered abundances of key bacteria and altered metabolism of products such as SCFAs. FMT may affect patients' systemic immunity, which might cause and/or result in motility changes.

MATERIALS AND METHODS

Patient Clinical Data and Sample Collection

We retrospectively evaluated 18 patients with refractory constipation who were strictly without other combined diseases and were treated with FMT at Tenth People's Hospital of Tongji University between January 1, 2019 and June 30, 2020. The Ethics Committee of Shanghai Tenth People's Hospital of Tongji University reviewed and approved the study. Patients provided written informed consent to participate.

Patients were eligible for inclusion if they were diagnosed with FC according to the Rome IV criteria (Drossman and Hasler, 2016; Mearin et al., 2016) and had a Bristol Stool Form Scale (BSFS) of 1 or 2 (Lewis and Heaton, 1997). Other inclusion criteria were that patients were aged 18–65 years and had a body mass index (BMI) of 18–25 kg/m^2.

Patients were excluded if they were pregnant or breast-feeding; their constipation was secondary to other diseases (e.g., endocrine, metabolic, or neurological disorders) or intervention (e.g., drugs); they had histories of organic digestive system diseases or disorders (e.g., peptic ulcers, bleeding erosive gastritis, megacolon, cancer, inflammatory bowel disease, intestinal obstruction, or other); they had a history of organ surgery; they had a history of systemic diseases (e.g., endocrine, renal, cardiovascular, respiratory, or other); they were definitively diagnosed with a psychiatric disorder; they had an active infection; they were treated with probiotics, prebiotics, antibiotics, or proton pump inhibitors within the last 3 months; or they had a previous history of FMT within the last year. Patients with depression or anxiety symptoms were also excluded, defined by a Hamilton Depression Scale (HAMD) or Hamilton Anxiety Scale (HAMA) $\geq$ 7. Considering the gut-brain interaction, mood disorders may influence both the gut microbiome and intestinal neurons; thus, mood disorders were considered confounding factors in studying how FMT affects gut motility (Mayer et al., 2015).

Study Design

This was a retrospective single-arm study to evaluate the changes in the gut microbiota and related biomarkers in FC patients who underwent FMT as well as the correlation between specific

bacteria and clinical symptoms. Constipation-related clinical symptoms were evaluated both before and 4 weeks after FMT by complete weekly spontaneous bowel movements (CSBMs), stool consistency (BSFS) (Mearin et al., 2016), Wexner constipation score, the Patient Assessment of Constipation-Symptoms (PAC-SYM), and the Patient Assessment of Constipation Quality of Life (PAC-QOL) questionnaire (Ding et al., 2018; Zhang et al., 2018). Patients were defined as clinically cured if they had an average of three or more CSBMs per week during follow-up (Tian et al., 2017). Stool and blood specimens were collected during clinical evaluation. Feces were stored at −80°C within 20 min after collection. Serum samples were collected between 6 and 8 a.m. and stored at −80°C before use. The efficacy of FMT for treating constipation was evaluated by comparing clinical symptoms before and after FMT. The influence of FMT on gut microbiota profiles and systemic inflammatory conditions was reflected by changes in the fecal flora composition, SCFA concentrations, and serum IL-4, IL-6, IL-8, IL-10, and IL-12p70 levels.

Fecal Micriobiota Transplantation Process

Donor Screening

Unrelated donors were selected under the following conditions: (1) aged 18–30 years; (2) BMI of 18–25 kg/m^2; (3) no pathological signs during physical examination; (4) no history or recent history of infectious diseases or gastrointestinal, metabolic, neurological, or other systematic disorders (Cammarota et al., 2017); (5) no recent use of drugs that can impair the gut microbiota composition (Cammarota et al., 2017); (6) had a regular routine and a healthy diet, appropriate exercise, family harmony, and no smoking or drinking habits; (7) passed blood and stool tests 4 weeks before donation, including general blood and stool testing and tests for possible pathogens or infectious diseases (Cammarota et al., 2017). Four donors met these criteria.

Preparation of Fecal Material

Approximately 100 g of donor feces were collected in a sterile container, mixed with 300 mL of sterile, non-bacteriostatic normal saline, passed through 2.0- and 0.5-mm sieves, amended with sterile glycerol to a final concentration of 10%, and stored frozen at −20°C for 1–8 weeks until use (Hamilton et al., 2012). Samples were prepared anaerobically within 6 h after fecal collection by the donor. The final fecal suspension contained the entire spectrum of the donor fecal microbiome as well as the metabolites and other possible active substances in the donor stool.

TABLE 1 | Patient characteristics.

Characteristics	Eligible patients (n = 18)
Age (years)	45.1 ± 13.3
Gender (female)	13 (72.2%)
BMI (kg/m^2)	22.0 ± 2.6
Disease duration (years)	10.3 ± 7.8
Combined diseases	None
HAMA	3.7 ± 1.8
HAMD	2.3 ± 2.0

TABLE 2 | Evaluation of FC patients' clinical symptoms before and after FMT.

Clinical symptoms	Group before (n = 18)	Group after (n = 18)	P-value
CSBMs/week	0.7 ± 0.8	4.8 ± 2.5	0.0007***
BSFS	1 (1.2)	4 (1.4)	0.0002***
Wexner score	12.7 ± 3.6	6.6 ± 5.6	<0.0001****
PAC-SYM	21.1 ± 6.5	7.9 ± 8.0	<0.0001****
PAC-QOL	50.2 ± 23.1	18.6 ± 18.1	0.0006***

*Group before: patients before FMT; Group after: patients 4 weeks after FMT. ***0.0001 ≤ p < 0.001, ****p < 0.0001.*

Clinical Management and Fecal Delivery

Patients orally received vancomycin for 3 days and underwent bowel lavage with polyethylene glycol 12–24 h before FMT. Fecal suspensions were thawed in a 37°C water bath and infused within 6 h of thawing via an indwelling nasojejunal tube (Cammarota et al., 2017). Each recipient received approximately 33.3 g of donor feces once daily from the same donor for 6 consecutive days (Zhang et al., 2018).

Sample Testing

Fecal Microbiome Testing Based on 16S rDNA Gene Analysis

Patients were asked to empty their bladder, then deliver stool into a sterile container. Approximately 2 g of feces were taken from the central part of the stool that had no contact with the air and placed in sterile cryotubes for storage at −80°C.

The fecal DNA was extracted and quantified using a NanoDrop 2000 spectrophotometer (Thermo Fisher Scientific Inc., MA). The V3-V4 hypervariable regions were amplified

TABLE 3 | Donor-recipient pairs and clinical outcomes.

ID	Donor	Clinical curation
Patient 1	Donor 1	No
Patient 2	Donor 1	No
Patient 3	Donor 1	Yes
Patient 4	Donor 1	No
Patient 5	Donor 2	No
Patient 6	Donor 2	Yes
Patient 7	Donor 2	Yes
Patient 8	Donor 2	Yes
Patient 9	Donor 2	Yes
Patient 10	Donor 2	Yes
Patient 11	Donor 2	Yes
Patient 12	Donor 3	Yes
Patient 13	Donor 3	Yes
Patient 14	Donor 3	Yes
Patient 15	Donor 3	Yes
Patient 16	Donor 4	Yes
Patient 17	Donor 4	Yes
Patient 18	Donor 4	Yes

via polymer chain reaction (PCR) using the universal primers, forward (5′–3′): CCTACGGGRSGCAGCAG (341F) and reverse (5′–3′): GGACTACVVGGGTATCTAATC (806R). The amplicons were purified using an AxyPrep DNA Gel Extraction Kit (Axygen Biosciences, Union City, CA) followed by library quantification using a Qubit™ dsDNA BR Assay Kit (Thermo Fisher Scientific). Finally, the pooled amplicons were paired end sequenced (2 × 250 bp) on an Illumina HiSeq PE250 sequencing platform. The sequencing depth was 42,501 reads per sample.

Fecal Short Chain Fatty Acid Quantification

Fecal SCFAs were quantified as previously described (Zheng et al., 2013). The fecal supernatant samples were quantified using an Agilent 7890A gas chromatograph coupled with an Agilent 5975C mass spectrometric detector (Agilent Technologies, U.S.). The initial oven temperature was 90°C, which was increased to 120°C at 10°C/min, to 150°C at 5°C/min, to 250°C at 25°C/min, and finally held at 250°C for 2 min. The concentrations of acetic acid (3.209 min), propionic acid (3.974 min), isobutyric acid (4.265 min), butyric acid (4.954 min), isovaleric acid (5.511 min), valeric acid (6.394 min), and caproic acid (8.023 min) were separated via a polar DB-WAX capillary column (30 m × 0.25 mm ID* 0.25 μm, Agilent, CA) with helium as the carrier gas at a constant flow rate of 1 mL/min.

Serum Inflammatory Factor Detection

Serum IL-4, IL-6, IL-8, IL-10, and IL-12p70 levels were detected using enzyme-linked immunosorbent assay (ELISA) kits (Neobioscience, China) according to the manufacturer's protocol.

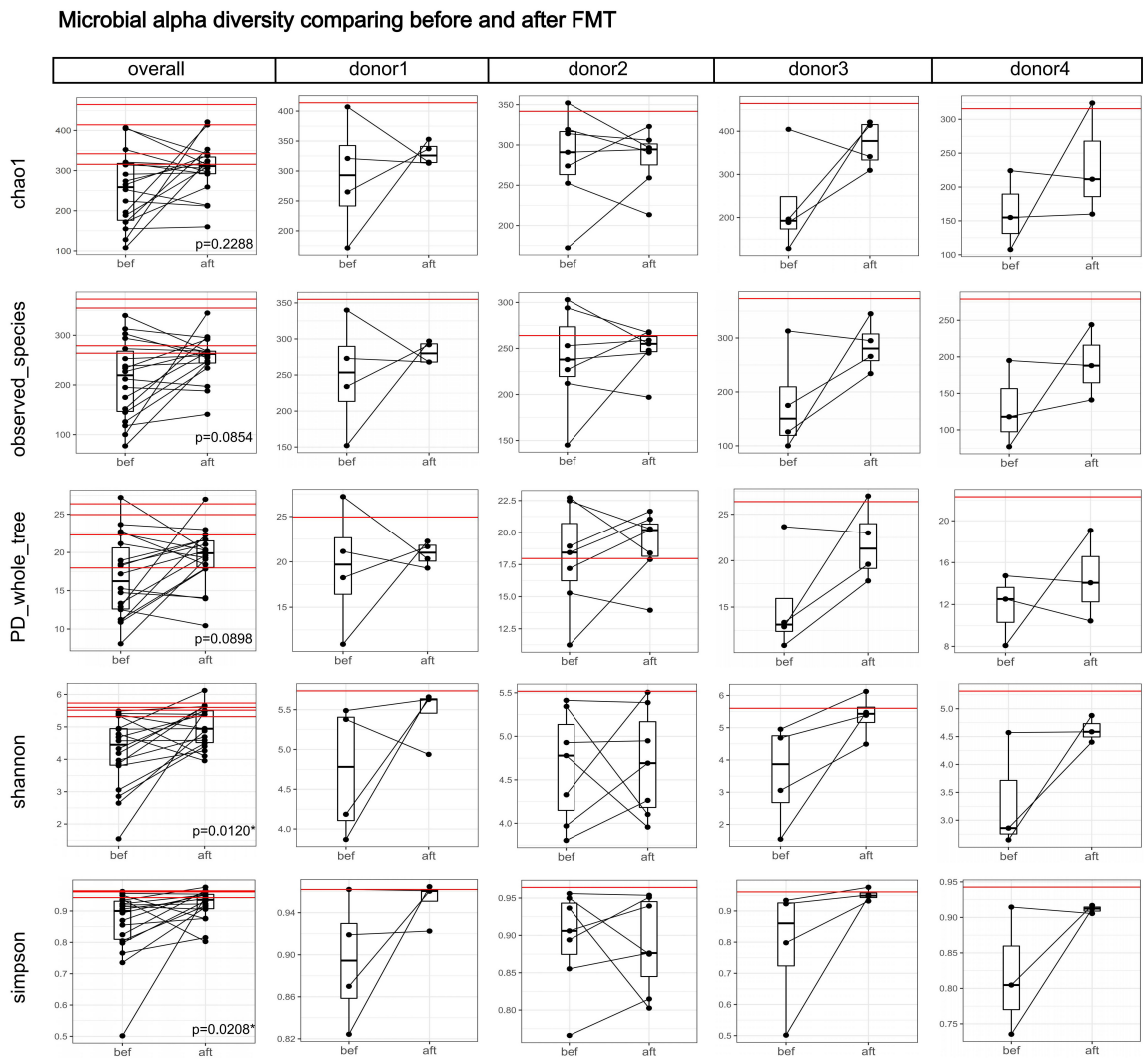

FIGURE 1 | Boxplots comparing the gut microbial alpha diversities before and after FMT. Each black dot represents one sample (patient); pre-FMT and post-FMT samples from the same patient are connected by a black line. Each red horizontal line represents one donor. The "overall" column shows the alpha diversity indexes of the 18 patients and four donors, and the significance test between the before and after groups was a paired-samples Wilcoxon-test ("*" indicates $0.01 \leq p < 0.05$). The Shannon and Simpson indexes increased significantly after FMT. Columns for each donor show the alpha diversity changes in each donor-recipient pair. We did not perform separate significance tests on each donor-recipient pair because of the small sample size.

Statistical Analysis

Analysis of 16S Sequencing Data

Raw FASTQ files were aligned using Pandaseq (version 2.7) and quality-filtered (Masella et al., 2012). The tags were clustered into operational taxonomic units (OTUs) with a 97% similarity cutoff using UPARSE (version7.1) (Edgar, 2013), and 868 OTUs were revealed. The taxonomy of each 16S rDNA gene sequence was analyzed using RDP Classifier[1] and annotated to each classification level (kingdom, phylum, class, order, family, genus, and species). Microbiota richness was analyzed using QIIME.

[1]http://rdp.cme.msu.edu/

Alpha diversity was calculated and compared between the two groups (before and after FMT) using paired Wilcoxon tests. Beta diversity was evaluated by (un)weighted UniFrac distances and analyzed by ANOSIM. Significant differences in microbiota abundances were compared via linear discriminant analysis effect size (LEfSe).

Analysis of Other Data and Correlations With the Microbiota

Continuous data are presented as the mean ± standard deviation, hierarchical data are presented as the medium (minimum, maximum), and categorical data are presented as

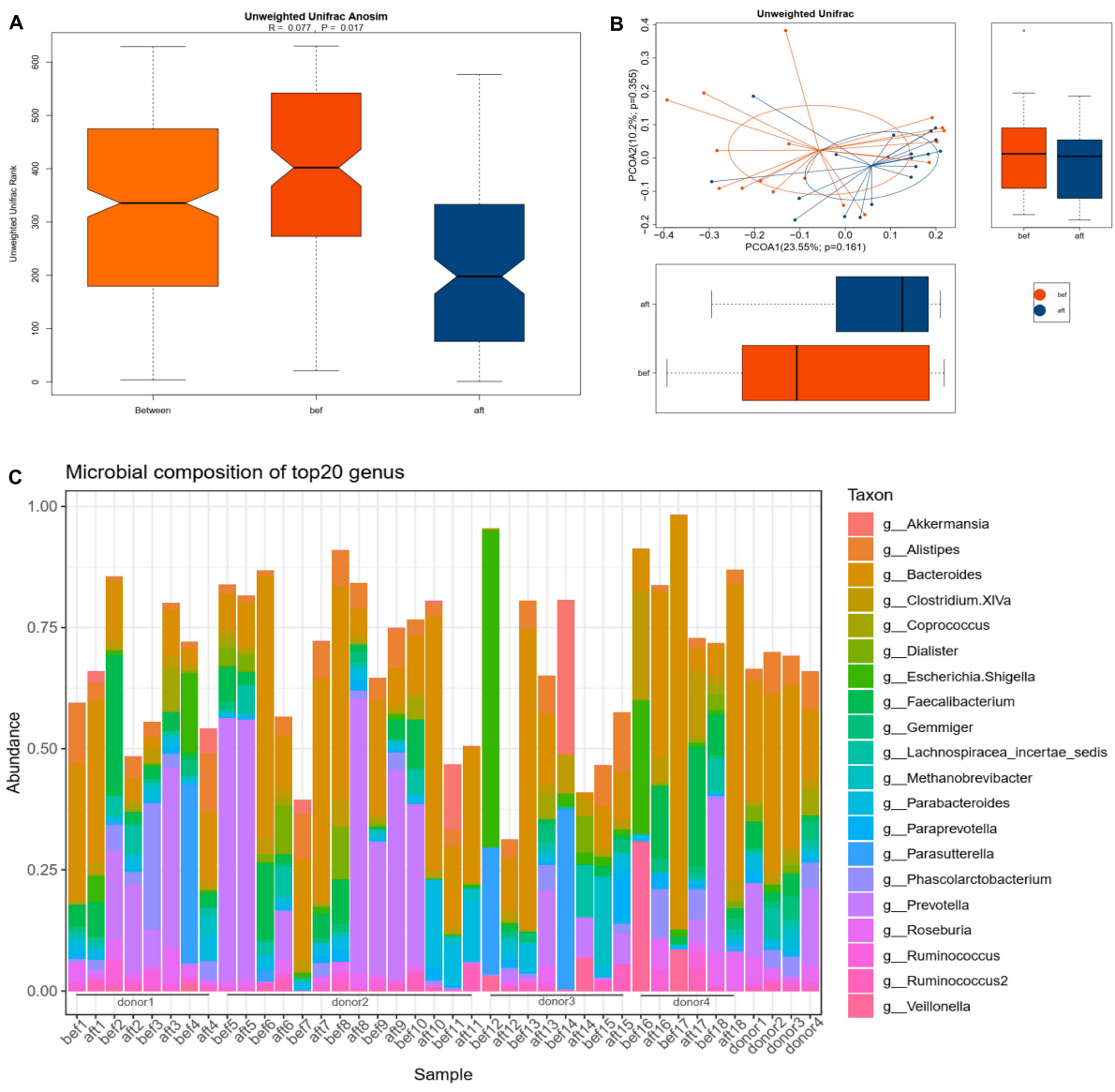

FIGURE 2 | Bacterial community compositions in pre-FMT and post-FMT fecal samples. "Bef" represents pre-FMT samples; "aft" represents post-FMT samples. **(A)** ANOSIM was used to determine the beta diversities of 18 patients' gut microbiomes pre- and post-FMT. The bacterial community compositions differed significantly before and after FMT ($p = 0.017$). **(B)** PCoA showed an overall shift in the 18 patients' gut microbiota compositions after FMT. **(C)** Genus-level microbial compositions of the top 20 abundant taxa in patients' and donors' stool samples.

numbers (%). Paired *t*-tests and paired Wilcoxon tests were performed to determine the differences in clinical symptoms, SCFA concentrations, and inflammatory factors. Spearman correlations were used to identify relationships between the microbiota and other phenotypes. Analyses were performed using R (version 4.0.3). A two-tailed $p < 0.05$ was considered statistically significant.

RESULTS

Patients' Characteristics and Clinical Symptoms

Eighteen patients with constipation who were treated with FMT were included in the analysis. **Table 1** and **Supplementary Table 1** show the patients' clinical characteristics. Patients' constipation symptoms were significantly alleviated 4 weeks post-FMT (**Table 2**). Spontaneous defecation (CSBMs/week) increased from 0.7 ± 0.8 to 4.8 ± 2.5, and the stool form improved from hard to smooth and soft. Objective evaluation (Wexner score) and self-assessment (PAC-SYM, PAC-QOL) of the severity of constipation were significantly alleviated ($p < 0.05$). **Supplementary Table 2** shows patients' detailed clinical scale scores before and after treatment. Of the 18 patients, 14 were clinically cured, while the remaining 4 continue to experience constipation after the FMT; thus, the total success rate was 77.78%. **Table 3** shows the donor-recipient pairs and clinical outcomes.

Microbial Community Diversity and Composition

The microbial alpha diversity was increased 4 weeks post-FMT (**Figure 1**). The Shannon and Simpson indexes were significantly lower in the pre-FMT samples and increased significantly in the post-FMT samples ($p = 0.0120$ and 0.0208, respectively). ANOSIM of the beta diversity revealed that the bacterial community compositions differed significantly between pre-FMT and post-FMT samples ($R = 0.077$, $p = 0.017$; **Figure 2A**).

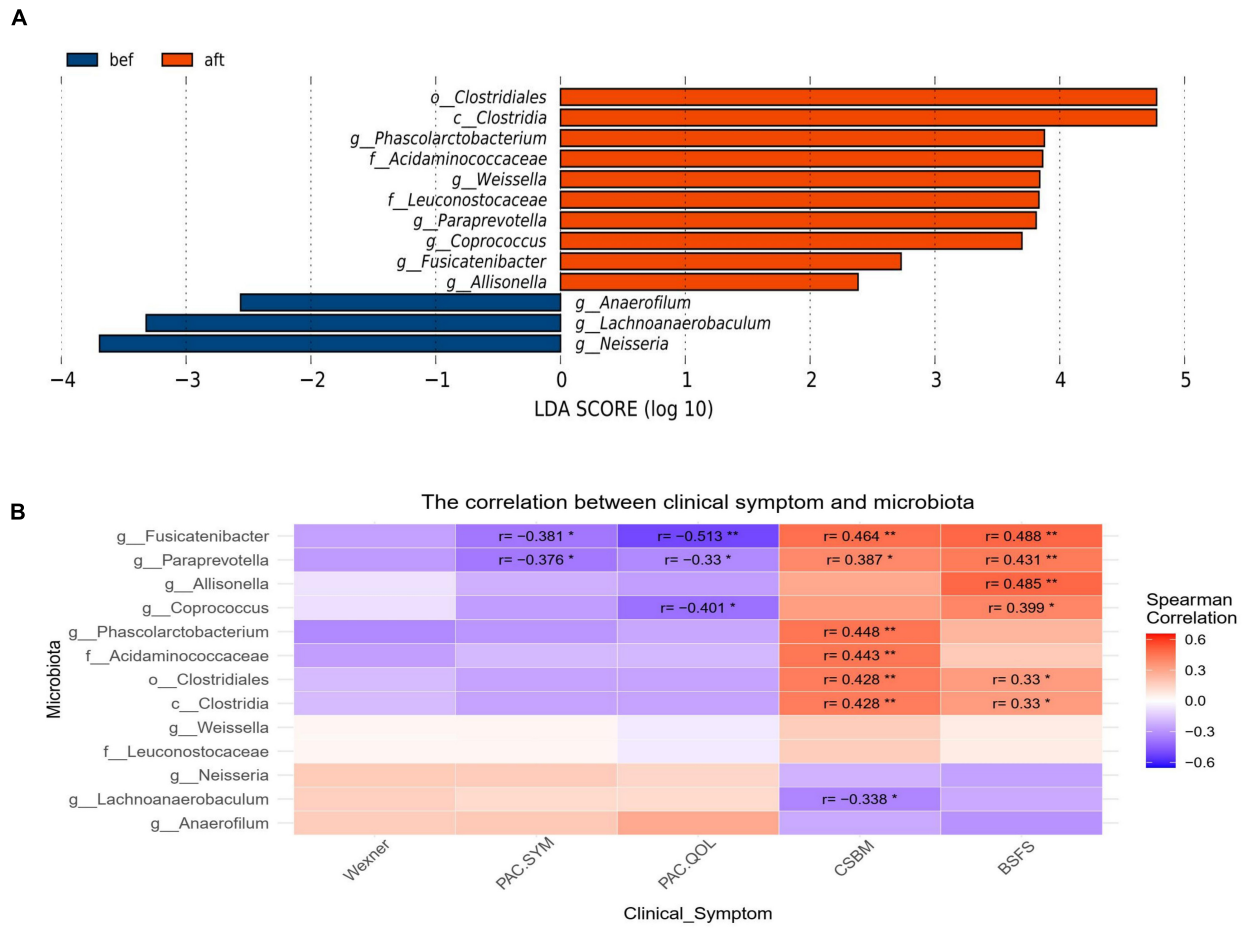

FIGURE 3 | (A) LEfSe analysis revealed significant changes in the fecal microbiota compositions before and after FMT. **(B)** Spearman correlation analysis revealed a correlation between patients' clinical symptoms and the significantly altered bacteria from the LEfSe analysis. *Fusicatenibacter*, *Paraprevotella*, *Allisonella*, *Coprococcus*, *Phascolarctobacterium*, Acidaminococcaceae, Clostridiales, and class Clostridia were correlated with relief of patients' constipation symptoms, and *Lachnoanaerobaculum* may be correlated with constipation severity ("*" represents $0.01 \leq p < 0.05$; "**" represents $0.001 \leq p < 0.01$).

Principal-coordinate analysis (PCoA) revealed an overall shift in the bacterial community compositions of all patients and donors (**Figure 2B**). **Figure 2C** shows the genus-level microbial compositions of the top 20 abundant taxa in both the patient and donor stool samples.

Bacteria Significantly Changed and Were Correlated With Clinical Symptoms

LEfSse analysis revealed significant changes in the fecal microbiota compositions. The genera *Paraprevotella*, *Weissella*, *Coprococcus*, *Phascolarctobacterium*, *Allisonella*, and *Fusicatenibacter;* families Acidaminococcaceae and Leuconostocaceae; class Clostridia and order Clostridiales were more abundant in the post-FMT samples. The genera *Lachnoanaerobaculum*, *Anaerofilum,* and *Neisseria* were more abundant in pre-FMT samples (**Figure 3A**). Spearman correlation analysis revealed that *Fusicatenibacter*, *Paraprevotella*, *Allisonella*, *Coprococcus*, *Phascolarctobacterium*, Acidaminococcaceae, Clostridiales, and Clostridia were correlated with a relief of patients' constipation symptoms, and *Lachnoanaerobaculum* may be correlated with constipation severity (**Figure 3B**). Of the above bacteria, *Fusicatenibacter* and *Paraprevotella* were correlated with more than three clinical scales, which might indicate a possible key role of these genera in the efficacy of FMT. We found no significant or coincident relationship between alpha diversity and clinical scores.

Fecal Micriobiota Transplantation Success Rates Might Be Related to Key Microbiota Abundances

In this study, the success rates of the recipients differed significantly by donor ($p = 0.0252$). The success rates of the four donors were 25% (1/4), 85.71% (6/7), 100% (4/4), and 100% (3/3). Although the small sample size per donor might contribute to bias in the success rates, we attempted to find a relationship between the donor-recipient gut microbiotas and FMT efficacy. We compared the abundances of the significantly altered bacteria (**Figure 3**) among the four donor stool samples and the post-FMT samples of the 14 patients whose symptoms

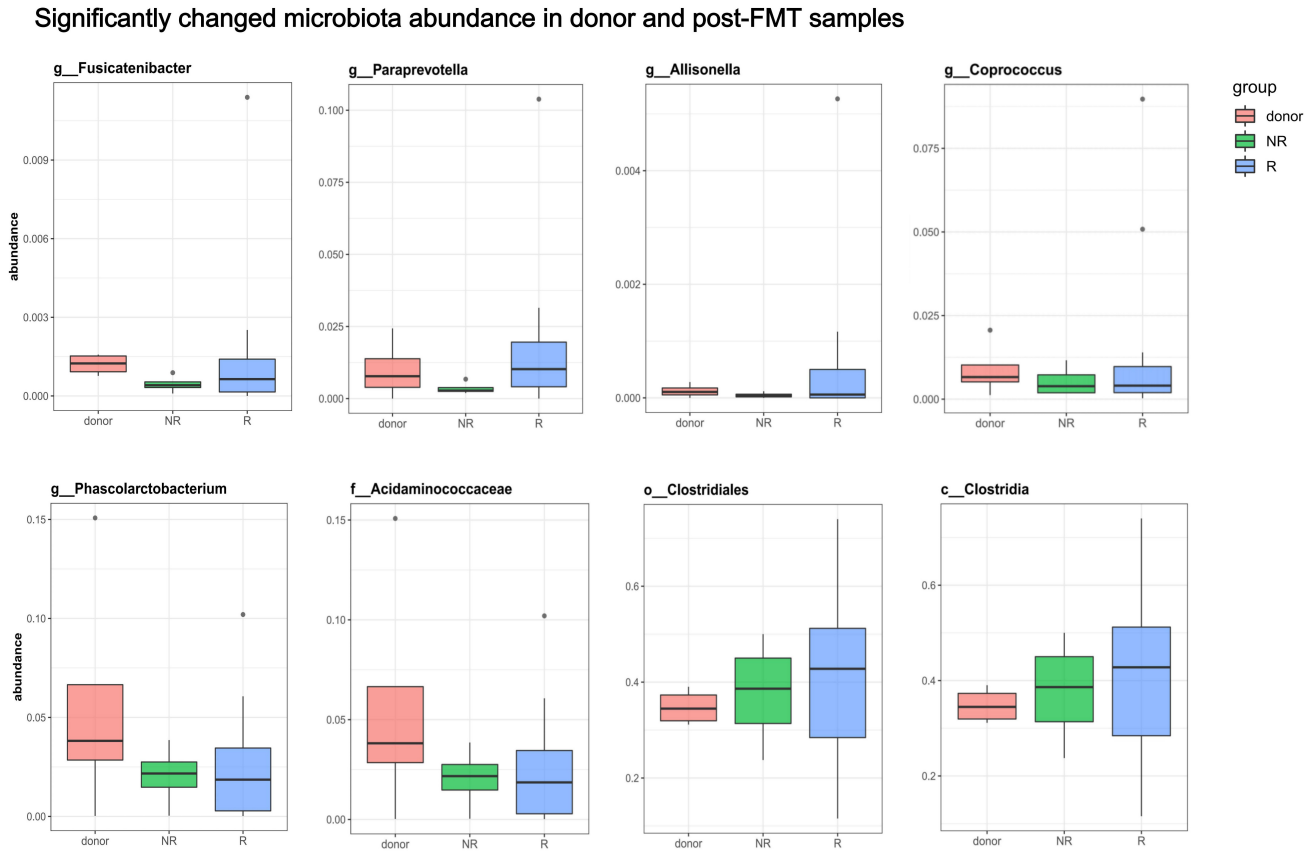

FIGURE 4 | Comparisons of the significantly altered bacterial abundances among donors and post-FMT fecal samples. The compared bacteria were shown to be significantly enriched in post-FMT samples determined by LEFse analysis and meanwhile correlated to clinical symptoms. All 4 donors and 18 patients were included. Group R refers to post-FMT samples from patients who were clinically cured after FMT; Group NR refers to post-FMT samples from patients who were not cured by FMT. Wilcoxon tests showed no significant differences among the groups, but the abundances of *Fusicatenibacter* and *Paraprevotella* were lower in the NR group and higher in the donor and R groups.

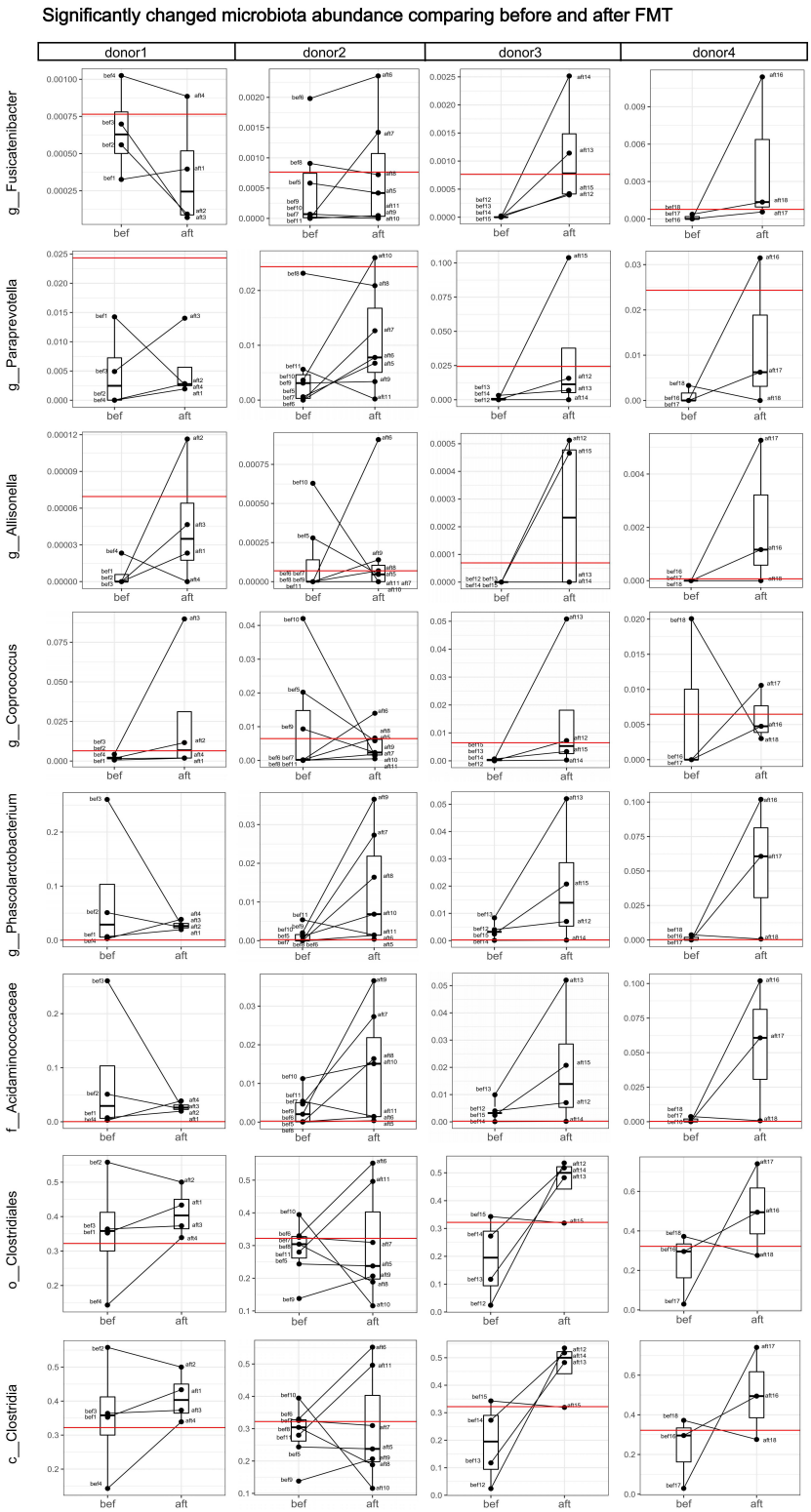

FIGURE 5 | Analyses of abundance changes in post-FMT-enriched bacteria in each donor-recipient pair. Boxplots comparing the bacterial abundances before and after FMT are shown. Each black dot represents one sample (patient); pre-FMT and post-FMT samples from the same patient are connected by a black line. Red horizontal lines represent the donor. One failed patient had a decreased abundance of *Paraprevotella* after FMT, and failed Patients 2, 4, and 5 had decreased abundances of *Fusicatenibacter* after FMT. The recipients of Donors 1 and 2 had more decreased bacterial abundances compared with the increased bacterial abundances in the recipients of Donors 3 and 4.

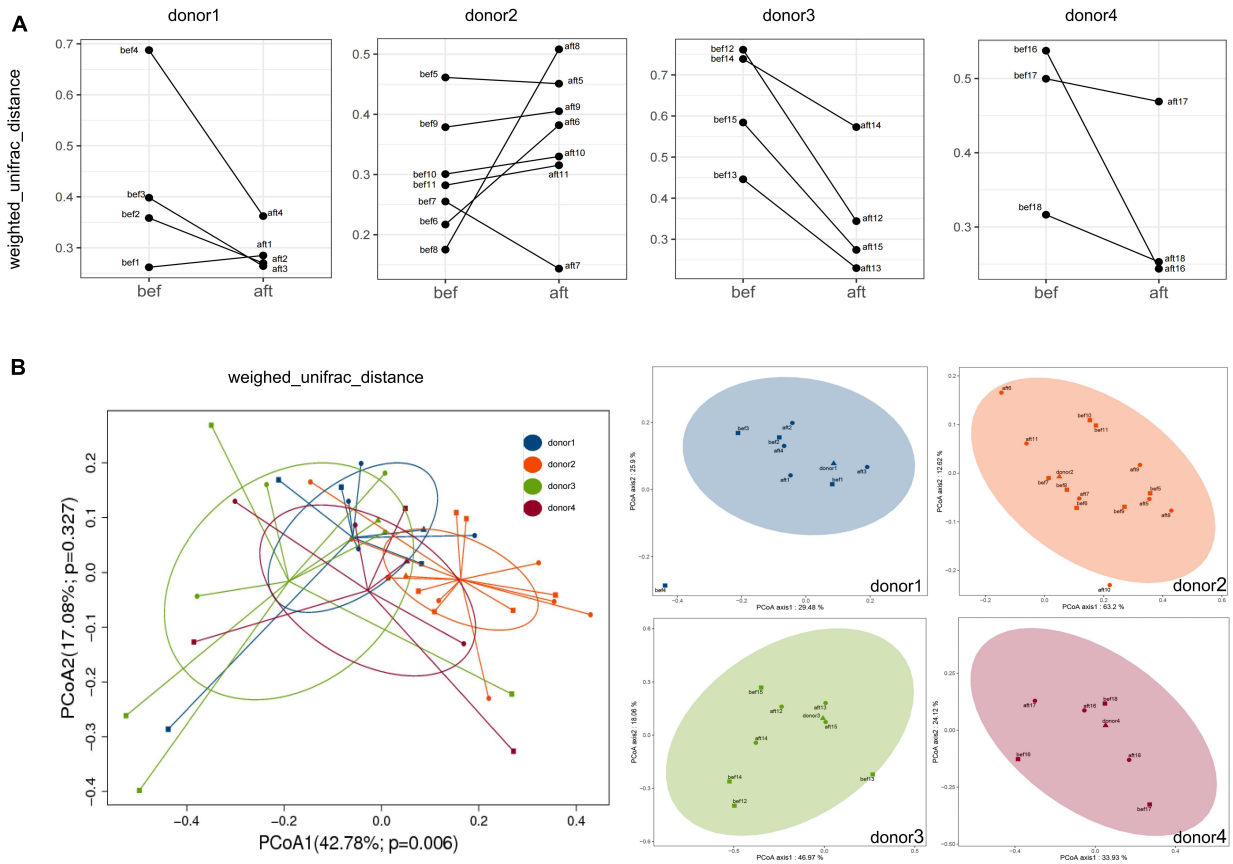

FIGURE 6 | Weighed UniFrac distances of each donor-recipient pair before and after FMT. **(A)** Each graph shows the changes in distance between recipients and their donor. Fecal microbial profiles of most recipients of Donor 1 and all recipients of Donors 3 and 4 became more similar to those of their donor, while most recipients of Donor 2 showed minimal change or became less similar to those of their donor. **(B)** PCoA of the microbiota compositions based on UniFrac distances showed the overall beta diversities of the 4 donors and the pre- and post-FMT samples of the 18 patients (left) and of each donor-recipient group (right).

were alleviated by the FMT (those who were clinically cured; group R) and the post-FMT samples of the four patients who were not cured by FMT (group NR). Wilcoxon tests showed no significant differences among the three groups; however, the abundances of *Fusicatenibacter* and *Paraprevotella* were lower in the NR group and higher in the donors and R group (**Figure 4**). We analyzed the abundance alterations of the post-FMT-enriched bacteria in each donor-recipient pair (**Figure 5**). One NR patient had a decreased abundance of *Paraprevotella* post-FMT, and three NR patients had decreased abundances of *Fusicatenibacter* post-FMT. Compared with the increase trend of those mentioned bacteria abundance in donor 3 and donor 4 recipients, donor 1 and donor 2 seemed to have more decreases. To determine whether the recipients' fecal microbiota profiles were similar or dissimilar to those of the donors post-FMT, we calculated the weighted UniFrac distances between each donor-recipient pair (**Supplementary Table 3**). **Figure 6** shows the changes in weighted UniFrac distance before and after FMT and the PCoAs of the microbiota compositions based on UniFrac distance. Fecal microbial profiles of most recipients of donor 1 and all recipients of donors 3 and 4 became more like those of the donor, while most recipients of donor 2 changed little or became dissimilar to those of the donor. No definitive regularity existed between the donor-recipient distances and FMT efficacy for FC patients.

Changes in Short Chain Fatty Acids, Inflammatory Factors, and Correlations With the Fecal Microbiota

No significant differences were found in SCFA concentrations between the pre-FMT and post-FMT fecal samples; however, the butyric acid concentrations increased after FMT (**Figure 7A**). Serum levels of IL-8 were significantly lower after FMT, while no obvious changes were detected in the IL-4, IL-6, IL-10, or IL-12p70 levels (**Figure 7B**). Correlation analysis showed that IL-4, IL-8, and some SCFAs were correlated with the abundances of some significantly altered bacteria, and the changing trends coincided with severity of patients' clinical symptoms (**Figure 7C**). *Paraprevotella* was positively correlated with propionic acid, butyric acid, and valeric acid. *Fusicatenibacter* was positively correlated with butyric acid and valeric acid and negatively correlated with IL-8. Among these SCFA and inflammatory factors, only IL-8 and butyric

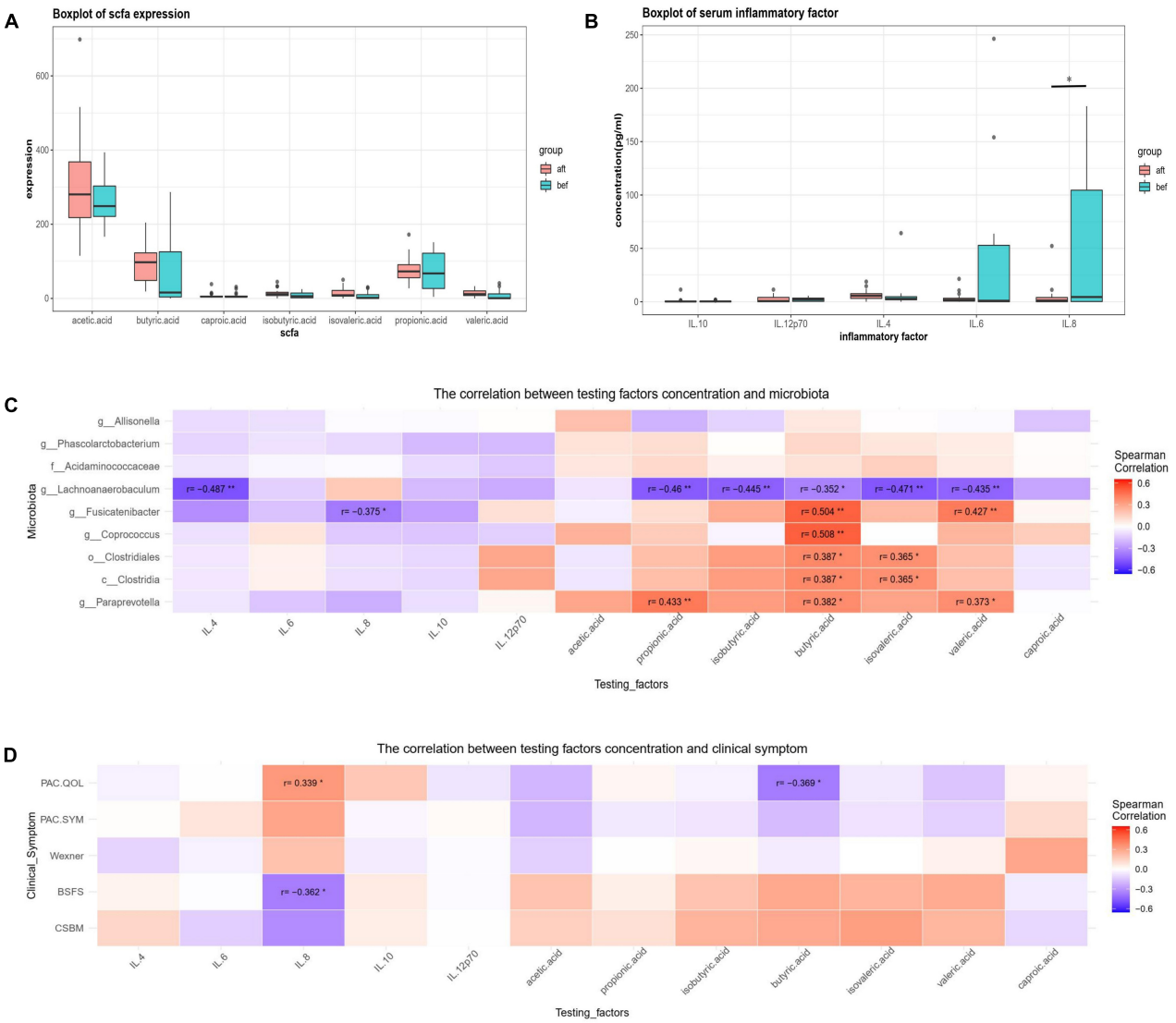

FIGURE 7 | (A) Post-FMT and pre-FMT fecal SCFA concentrations of 18 patients were compared using paired-samples Wilcoxon tests. Butyric acid concentrations increased after FMT but not significantly. **(B)** Post-FMT and pre-FMT serum inflammatory factors of 18 patients were compared using paired-samples Wilcoxon tests. IL-8 levels decreased significantly after FMT. **(C,D)** Spearman correlation analysis of pre-FMT and post-FMT clinical symptoms, fecal microbiotas, SCFAs, and serum inflammatory factors of 18 patients revealed that IL-4, IL-8, and some SCFAs (especially butyric acid) were significantly correlated with some bacterial changes. Only IL-8 and butyric acid were correlated with clinical symptoms ("*" represents $0.01 \leq p < 0.05$; "**" represents $0.001 \leq p < 0.01$).

acid concentrations were significantly correlated with clinical symptoms (**Figure 7D**).

DISCUSSION

This retrospective study was conducted to evaluate the clinical efficacy and remodeling of the gut ecology after FMT for constipation. Several articles have reported that FMT can relieve constipation, but few have reported the changes in the gut microbiota post-FMT (Tian et al., 2017; Ding et al., 2018). Using 16S rRNA amplicon sequencing, Ohara (2019) identified 22 microorganismal species that had colonized in recipients 1 month post-FMT; however, whether the colonization was correlated with clinical improvement is unknown. To our knowledge, our study was the first to characterize the correlation between gut microbiota alterations and relief of clinical symptoms after FMT. We thus proposed the specific bacteria and potential mechanism that might have contributed to the clinical efficacy.

Gut dysbiosis exists in patients with constipation and may play an important role in disturbing colonic motility. Simpson indexes have revealed lower alpha diversities for constipated individuals, which is consistent with our findings that alpha diversity increased after FMT (Huang et al., 2018; Tian H. et al., 2020). Some bacteria, including *Parabacteroides* and *Bifidobacterium*, were more abundant in constipated patients'

fecal samples compared with those of healthy individuals. These bacteria have been consistently reported in constipated patients, and other bacteria, such as *Streptococcus* and *Ruminococcus*, have been sporadically reported (Huang et al., 2018; Tian H. et al., 2020). SCFAs, especially butyrate, are also altered in constipated patients, which may affect gut motility and have important immunomodulatory functions (Martin-Gallausiaux et al., 2021). Gut dysbiosis in patients with FC as well as other functional bowel dysmotility disorders, including IBS, may disturb the intestinal immunity, cause "leaky gut," and affect systemic inflammatory conditions. Some studies reported higher concentrations of proinflammatory cytokines such as IL-6, IL-8, and IL-12 in adult IBS patients. Serum IL-6 and IL-12 levels were also higher in constipated children than in healthy controls. As anti-inflammatory cytokines, IL-10 levels were decreased, and IL-4 levels were increased in IBS patients (Cıralı et al., 2018). In our study, serum IL-8 was decreased in FC patients after FMT, indicating that FMT might have an anti-inflammatory effect that can modulate intestinal motility or may result from recovery of the gut microbiota and motility.

The gut microbiota may cause gut motility disorders via complex mechanisms, and the potential key bacteria differ among studies. Tian Y. et al. (2020) analyzed fecal microbiota changes in constipated patients undergoing FMT and found higher abundances of *Bacteroides* and *Enterobacteriaceae* pre-FMT and increased abundances of *Prevotella* and *Acidaminococcus* post-FMT. Bacteria that were abundant in constipated patients (compared with healthy individuals) or pre-FMT (compared with post-FMT) fecal samples might have a causative effect; however, previous studies did not perform correlation analyses between the abundances of certain microbes and the severity of clinical symptoms. Additionally, some bacteria including *Parabacteroides*, *Bifidobacterium*, *Bacteroides,* and Enterobacteriaceae, were abundant in patients with anxiety and/or depression (Simpson et al., 2021). Because many constipated patients have emotional problems, and these patients were not excluded from the above studies, some of the bacteria may not have played causal roles in colonic motility disturbances during constipation. Further, the bacteria that increased post-FMT may have had no real curative effect on slow colonic motility. In our study, we analyzed the microbiota changes before and after FMT, and examined correlation analyses of certain bacteria, clinical symptom severity scores, and changes in SCFAs and inflammatory factors in constipated patients without symptoms of depression, anxiety, or systemic diseases. Our findings may provide a more compelling hypothesis that certain bacteria, such as *Fusicatenibacter*, *Paraprevotella*, and *Lachnoanaerobaculum,* may help regulate colonic motility, and the mechanism may be related to modulating the fecal butyrate and serum IL-8 concentrations.

FMT is reported to be effective for treating many diseases; however, it is difficult to standardize or improve for disease-specific therapies. We found that colonization of key bacteria, such as *Fusicatenibacter* and *Paraprevotella*, may influence the success of FMT for treating FC, but we found no regularity in donor-recipient distances. Owing to the limitations of a small sample size and short follow-up, other bacteria may be correlated with gut motility regulation; thus, the role of similarity between the donor-recipient pairs requires further research. Functional species screening and mechanistic research are needed to enhance the efficacy of microbial-targeting treatments and make breakthroughs in FMT. Future research should include large datasets, machine learning, and multiomic detection to discover the principles underlying microbiota-host interactions. Mechanistic studies, such as germ-free animal studies, will help verify microbial functions to promote development of improved FMT and precise therapy.

CONCLUSION

In summary, we assessed the clinical efficacy and microbial remodeling ability of FMT on constipated patients, together with changes in the fecal SCFAs and systemic inflammatory conditions. FMT relieved constipation symptoms and altered the fecal microbiota compositions to a higher alpha diversity. *Fusicatenibacter*, *Paraprevotella*, *Allisonella*, *Coprococcus*, *Phascolarctobacterium*, Acidaminococcaceae, Clostridiales, and class Clostridia were more abundant in post-FMT fecal samples, which was consistent and in accord with the relief of constipation symptoms. *Lachnoanaerobaculum* was correlated with constipation severity and might play a role in causing constipation. The efficacy of FMT for treating FC might be correlated with the abundances of key bacteria such as *Fusicatenibacter* and *Paraprevotella*, but we found no decisive role of donor-recipient distances. Regulating butyrate production might be one potential mechanism by which the microbiota modulates gut motility. The potential role of systemic IL-8 and its relationship with the gut microbiota also deserve further study. Microbial multiomics studies based on big data analyses are needed to screen causal and functional bacteria. Further research on potential mechanisms may enable precise treatments for constipation and other gut motility disorders.

DATA AVAILABILITY STATEMENT

The datasets presented in this study can be found in online repositories. The names of the repository/repositories and accession number(s) can be found below: https://www.ncbi.nlm.nih.gov/sra/, PRJNA732583.

ETHICS STATEMENT

The studies involving human participants were reviewed and approved by the Ethics Committee of Shanghai Tenth People's Hospital of Tongji University. The patients/participants provided their written informed consent to participate in this study.

AUTHOR CONTRIBUTIONS

XZ, NL, QC, and HQ conceived, designed the study, and interpreted the results. XZ, NL, and QC collected the samples. XZ and QC performed the laboratory assays and bioinformatics

analyses. XZ performed the statistical analysis and drafted the manuscript. NL, QC, and HQ supervised the work and revised and contributed to the final manuscript. NL and HQ contributed with resources and fundings. All authors read and approved the final manuscript.

FUNDING

This work was supported by the National Natural Science Foundation of China (Nos. 81670493, 81972221, and 81730102), the Clinical Research Plan of SHD (Nos. SHDC12019114, SHDC2020CR4026, and SHDC12017112), the 12th 5-Year Major Program of Army Research (No. AWS12J001), and the Specialized Research Fund for the Combined Traditional Chinese and Western Medicine in the General Hospital of Shanghai (No. ZHYY-ZXYJHZX-1-201704).

ACKNOWLEDGMENTS

We thank Yang Bo, Zhao Di, Tian Hongliang, Lin Zhiliang, Ye Chen, Zhang Shaoyi, Cui Jiaqu, Ma Chunlian, and Lv Xiaoqiong from the Intestinal Microenvironment Treatment Center, Tenth People's Hospital of Tongji University for contributing to patients' clinical management and sample collection. We thank Traci Raley, MS, ELS, from Liwen Bianji, Edanz Editing China (www.liwenbianji.cn/) for editing a draft of this manuscript.

SUPPLEMENTARY MATERIAL

The Supplementary Material for this article can be found online at: https://www.frontiersin.org/articles/10.3389/fmicb.2021.700718/full#supplementary-material

REFERENCES

Barbara, G., Stanghellini, V., Brandi, G., Cremon, C., Di Nardo, G., De Giorgio, R., et al. (2005). Interactions between commensal bacteria and gut sensorimotor function in health and disease. *Am. J. Gastroenterol.* 100, 2560–2568. doi: 10.1111/j.1572-0241.2005.00230.x

Cammarota, G., Ianiro, G., Tilg, H., Rajilić-Stojanović, M., Kump, P., Satokari, R., et al. (2017). European consensus conference on faecal microbiota transplantation in clinical practice. *Gut* 66, 569–580. doi: 10.1136/gutjnl-2016-313017

Chmielewska, A., and Szajewska, H. (2010). Systematic review of randomised controlled trials: probiotics for functional constipation. *World J. Gastroenterol.* 16, 69–75. doi: 10.3748/wjg.v16.i1.69

Cıralı, C., Ulusoy, E., Kume, T., and Arslan, N. (2018). Elevated serum neopterin levels in children with functional constipation: association with systemic proinflammatory cytokines. *World J. Pediatr.* 14, 448–453. doi: 10.1007/s12519-018-0144-8

de Jong, P. R., González-Navajas, J. M., and Jansen, N. J. (2016). The digestive tract as the origin of systemic inflammation. *Crit. Care* 20:279. doi: 10.1186/s13054-016-1458-3

De Jonge, W. J., The, F. O., van der Zanden, E. P., van den Wijngaard, R. M., and Boeckxstaens, G. E. (2005). Inflammation and gut motility; neural control of intestinal immune cell activation. *J. Pediatr. Gastroenterol. Nutr.* 41(Suppl. 1), S10–S11. doi: 10.1097/01.scs.0000180287.58988.86

Ding, C., Fan, W., Gu, L., Tian, H., Ge, X., Gong, J., et al. (2018). Outcomes and prognostic factors of fecal microbiota transplantation in patients with slow transit constipation: results from a prospective study with long-term follow-up. *Gastroenterol. Rep.* 6, 101–107. doi: 10.1093/gastro/gox036

Drossman, D. A., and Hasler, W. L. (2016). Rome IV-functional GI disorders: disorders of gut-brain interaction. *Gastroenterology* 150, 1257–1261. doi: 10.1053/j.gastro.2016.03.035

Edgar, R. (2013). UPARSE: highly accurate OTU sequences from microbial amplicon reads. *Nat. Methods* 10, 996–998. doi: 10.1038/nmeth.2604

Garrett, R. E., and Bar-Or, D. (2008). Constipation, critical illness and mortality: gut-derived toxidromes–real and now imagined. *Crit. Care Med.* 36, 2710–2711. doi: 10.1097/CCM.0b013e318184705b

Hamilton, M. J., Weingarden, A. R., Sadowsky, M. J., and Khoruts, A. (2012). Standardized frozen preparation for transplantation of fecal microbiota for recurrent Clostridium difficile infection. *Am. J. Gastroenterol.* 107, 761–767. doi: 10.1038/ajg.2011.482

Huang, L. S., Kong, C., Gao, R. Y., Yan, X., Yu, H. J., Wen, B., et al. (2018). Analysis of fecal microbiota in patients with functional constipation undergoing treatment with synbiotics. *Eur. J. Clin. Microbiol. Infect. Dis.* 37, 555–563. doi: 10.1007/s10096-017-3149-7

Khalif, I. L., Quigley, E. M., Konovitch, E. A., and Maximova, I. D. (2005). Alterations in the colonic flora and intestinal permeability and evidence of immune activation in chronic constipation. *Dig. Liver Dis.* 37, 838–849. doi: 10.1016/j.dld.2005.06.008

Lewis, S. J., and Heaton, K. W. (1997). Stool form scale as a useful guide to intestinal transit time. *Scand. J. Gastroenterol.* 32, 920–924. doi: 10.3109/00365529709011203

Martin-Gallausiaux, C., Marinelli, L., Blottière, H. M., Larraufie, P., and Lapaque, N. (2021). SCFA: mechanisms and functional importance in the gut. *Proc. Nutr. Soc.* 80, 37–49. doi: 10.1017/s0029665120006916

Masella, A., Bartram, A., Truszkowski, J., Brown, D., and Neufeld, J. (2012). PANDAseq: paired-end assembler for illumina sequences. *BMC Bioinformatics* 13:31. doi: 10.1186/1471-2105-13-31

Mayer, E. A., Tillisch, K., and Gupta, A. (2015). Gut/brain axis and the microbiota. *J. Clin. Invest.* 125, 926–938. doi: 10.1172/jci76304

Mearin, F., Lacy, B. E., Chang, L., Chey, W. D., Lembo, A. J., Simren, M., et al. (2016). Bowel disorders. *Gastroenterology* 150, 1393–1407.e5. doi: 10.1053/j.gastro.2016.02.031

Mullish, B. H., Quraishi, M. N., Segal, J. P., McCune, V. L., Baxter, M., Marsden, G. L., et al. (2018). The use of faecal microbiota transplant as treatment for recurrent or refractory Clostridium difficile infection and other potential indications: joint British Society of Gastroenterology (BSG) and Healthcare Infection Society (HIS) guidelines. *Gut* 67, 1920–1941. doi: 10.1136/gutjnl-2018-316818

Ohara, T. (2019). Identification of the microbial diversity after fecal microbiota transplantation therapy for chronic intractable constipation using 16s rRNA amplicon sequencing. *PLoS One* 14:e0214085. doi: 10.1371/journal.pone.0214085

Shimizu, K., Ogura, H., Asahara, T., Nomoto, K., Morotomi, M., Nakahori, Y., et al. (2011). Gastrointestinal dysmotility is associated with altered gut flora and septic mortality in patients with severe systemic inflammatory response syndrome: a preliminary study. *Neurogastroenterol. Motil.* 23, 330–335.e157. doi: 10.1111/j.1365-2982.2010.01653.x

Simpson, C. A., Diaz-Arteche, C., Eliby, D., Schwartz, O. S., Simmons, J. G., and Cowan, C. S. M. (2021). The gut microbiota in anxiety and depression – A systematic review. *Clin. Psychol. Rev.* 83:101943. doi: 10.1016/j.cpr.2020.101943

Tian, H., Chen, Q., Yang, B., Qin, H., and Li, N. (2020). Analysis of gut microbiome and metabolite characteristics in patients with slow transit constipation. *Dig. Dis. Sci.* 66, 3026–3035. doi: 10.1007/s10620-020-06500-2

Tian, H., Ge, X., Nie, Y., Yang, L., Ding, C., McFarland, L. V., et al. (2017). Fecal microbiota transplantation in patients with slow-transit constipation: a randomized, clinical trial. *PLoS One* 12:e0171308. doi: 10.1371/journal.pone.0171308

Tian, Y., Zuo, L., Guo, Q., Li, J., Hu, Z., Zhao, K., et al. (2020). Potential role of fecal microbiota in patients with constipation. *Therap. Adv. Gastroenterol.* 13:1756284820968423. doi: 10.1177/1756284820968423

Zhang, X., Tian, H., Gu, L., Nie, Y., Ding, C., Ge, X., et al. (2018). Long-term follow-up of the effects of fecal microbiota transplantation in combination with soluble dietary fiber as a therapeutic regimen in slow transit constipation. *Sci. China Life Sci.* 61, 779–786. doi: 10.1007/s11427-017-9229-1

Zhao, Y., and Yu, Y. B. (2016). Intestinal microbiota and chronic constipation. *Springerplus* 5:1130. doi: 10.1186/s40064-016-2821-1

Zheng, X., Qiu, Y., Zhong, W., Baxter, S., Su, M., Li, Q., et al. (2013). A targeted metabolomic protocol for short-chain fatty acids and branched-chain amino acids. *Metabolomics* 9, 818–827. doi: 10.1007/s11306-013-0500-6

Conflict of Interest: The authors declare that the research was conducted in the absence of any commercial or financial relationships that could be construed as a potential conflict of interest.

Publisher's Note: All claims expressed in this article are solely those of the authors and do not necessarily represent those of their affiliated organizations, or those of the publisher, the editors and the reviewers. Any product that may be evaluated in this article, or claim that may be made by its manufacturer, is not guaranteed or endorsed by the publisher.

frontiers in Microbiology

ORIGINAL RESEARCH
published: 18 November 2021
doi: 10.3389/fmicb.2021.773829

Comparative Proteomics Demonstrates Altered Metabolism Pathways in Cotrimoxazole-Resistant and Amikacin-Resistant *Klebsiella pneumoniae* Isolates

Chunmei Shen[1], Ying Shen[1], Hui Zhang[2], Maosuo Xu[2], Leqi He[2] and Jingbo Qie[1,3]**

[1] Department of Hospital Infection Management, The Fifth People's Hospital of Shanghai, Fudan University, Shanghai, China,
[2] Department of Clinical Laboratory Medicine, The Fifth People's Hospital of Shanghai, Fudan University, Shanghai, China,
[3] Institute of Biomedical Sciences, Fudan University, Shanghai, China

Antibiotic resistance (AMR) has always been a hot topic all over the world and its mechanisms are varied and complicated. Previous evidence revealed the metabolic slowdown in resistant bacteria, suggesting the important role of metabolism in antibiotic resistance. However, the molecular mechanism of reduced metabolism remains poorly understood, which inspires us to explore the global proteome change during antibiotic resistance. Here, the sensitive, cotrimoxazole-resistant, amikacin-resistant, and amikacin/cotrimoxazole -both-resistant KPN clinical isolates were collected and subjected to proteome analysis through liquid chromatography coupled with tandem mass spectrometry (LC–MS/MS). A deep coverage of 2,266 proteins were successfully identified and quantified in total, representing the most comprehensive protein quantification data by now. Further bioinformatic analysis showed down-regulation of tricarboxylic acid cycle (TCA) pathway and up-regulation of alcohol metabolic or glutathione metabolism processes, which may contribute to ROS clearance and cell survival, in drug-resistant isolates. These results indicated that metabolic pathway alteration was directly correlated with antibiotic resistance, which could promote the development of antibacterial drugs from "target" to "network." Moreover, combined with minimum inhibitory concentration (MIC) of cotrimoxazole and amikacin on different KPN isolates, we identified nine proteins, including garK, uxaC, exuT, hpaB, fhuA, KPN_01492, fumA, hisC, and aroE, which might contribute mostly to the survival of KPN under drug pressure. In sum, our findings provided novel, non-antibiotic-based therapeutics against resistant KPN.

Keywords: *Klebsiella pneumoniae (K. pneumoniae)*, comparative proteomics, bioinformatics, metabolism, antibiotic resistance

OPEN ACCESS

Edited by:
Jialiang Yang,
Geneis (Beijing) Co., Ltd., China

Reviewed by:
Hu Zhou,
Shanghai Institute of Materia Medica, Chinese Academy of Sciences (CAS), China
Sinosh Skariyachan,
St. Pius X College, India
Ke Xu,
Tongji University, China
Lifang Zou,
Shanghai Jiao Tong University, China

****Correspondence:***
Leqi He
leqi_he@fudan.edu.cn
Jingbo Qie
jingboqie@fudan.edu.cn

Specialty section:
This article was submitted to Systems Microbiology, a section of the journal Frontiers in Microbiology

Received: *10 September 2021*
Accepted: *29 October 2021*
Published: *18 November 2021*

Citation:
Shen C, Shen Y, Zhang H, Xu M, He L and Qie J (2021) Comparative Proteomics Demonstrates Altered Metabolism Pathways in Cotrimoxazole- Resistant and Amikacin-Resistant Klebsiella pneumoniae Isolates. Front. Microbiol. 12:773829. doi: 10.3389/fmicb.2021.773829

INTRODUCTION

Antibiotic resistance (AMR) has always been a hot topic all over the world. The report released by World Health Organization (WHO) revealed that this serious threat is happening in every region of the world and has the potential to affect anyone, of any age, in any country (World Health Organization [WHO], 2014). In-depth research on the causes of bacterial drug resistance can provide effective guidance and support for us to fight against bacterial drug resistance.

Increasing evidences showed that metabolic changes in bacteria can reduce bacterial susceptibility to antibiotics and promote the evolvement of resistance, tolerance and persistence, and the regulation of physiological metabolism of bacteria can restore their sensitivity to antibiotics (Martinez and Rojo, 2011). Meylan et al. (2017) reported that metabolically dormant bacteria were genetically susceptible to antibiotic treatment, which could be reversed by adding glyoxylate into the culture. Mechanistic studies demonstrated that glyoxylate could induce phenotypic resistance of bacteria by inhibiting cellular respiration with acetyl-coenzyme A diversion through the glyoxylate shunt (Meylan et al., 2017). Another empirical study showed that aminoglycosides, such as glucose, mannitol, fructose, and pyruvic acid, improved the sensitivity of *Ataphylococcus aureus* and *Escherichia coli* to gentamicin by promoting glycolysis metabolic pathway (Allison et al., 2011). Barraud et al. (2013) also found that mannitol enhanced antibiotic sensitivity of persister bacteria in *Pseudomonas aeruginosa* biofilms. These findings were confirmed by the studies of other drug-resistant bacteria (Peng et al., 2015; Su et al., 2015, 2018; Koeva et al., 2017), suggesting that metabolic alteration have been a widely used strategy applied by bacteria to adapt the antibiotic pressure. Recently, protein aggresome was introduced into the study of AMR. Bai' group found that the protein aggresome, whose formation is promoted by decreased cellular ATP level, was critical for AMR (Pu et al., 2019; Jing et al., 2020; Jin et al., 2021). These findings prove the important of metabolism in AMR, from another side. However, the specific metabolism-related protein profiles of resistant bacteria are still poorly understood.

Comparative proteomics has been extensively used to illustrate the dynamic changes of bacterial proteomes in the antibiotic stress (Freiberg et al., 2004). Resistant bacteria can revert its internal harmony which is disturbed by antimicrobials via modulating cellular protein expression and related pathways. By mapping the proteome of resistant bacteria, researchers could explain the observed experimental phenomenon and explore novel strategies employed by bacteria to gain antibiotic resistance. By now, proteomic study has been performed in *Escherichia coli*, *Bacillus subtilis,* and other micro-organisms (dos Santos et al., 2010; Hessling et al., 2013; Lata et al., 2015; Qayyum et al., 2016; Keasey et al., 2019).

Klebsiella pneumoniae (KPN) is a gram-negative pathogen, which was first identified in 1882 (Wang G. et al., 2020). In the 1960s, KPN have become one of the most important causes of opportunistic healthcare-associated infections (Paczosa and Mecsas, 2016). Nowadays, cotrimoxazole (CTX) and amikacin (AMI) are the antimicrobial of choice for treating CR-KPN (Ramirez and Tolmasky, 2017). But with the extensive use of cotrimoxazole and amikacin, even abuse, we find increasing cotrimoxazole-resistant, amikacin-resistant, even both-resistant KPN in our hospital, which is of great clinical concern. In this study, the sensitive, cotrimoxazole-resistant, amikacin-resistant, and amikacin/cotrimoxazole -both-resistant KPN clinical isolates in our hospital were collected and subjected to LC-MS/MS analysis. As a result, a deep coverage of 2,266 proteins were successfully identified and quantified in total, representing the most comprehensive protein quantification data by now. We applied comparative proteomics to explore the correlation between pattern characteristics and drug-resistances. The results showed absolute pattern identity between ATCC strains and hospital isolates, as well as altered energy metabolism processes between SEN isolates and drug-resistant isolates. Specifically, proteins involved in tricarboxylic acid cycle (TCA) pathway were down-regulated in both of amikacin- and cotrimoxazole -resistant KPNs, which may restraint the ROS production in drug-resistant isolates. Finally, we identified nine genes involved in metabolism pathways significantly associated with MICs of amikacin/cotrimoxazole, and participated in such an alteration. These results indicated that the alteration of metabolic network was directly correlated with antibiotic resistance, which could promote the development of antibacterial drugs from "target" to "network," and provided novel, non-antibiotic-based therapeutics against resistant bacteria.

MATERIALS AND METHODS

Strain Collection and Drug Susceptibility Testing

Three cotrimoxazole-resistant (CTX), three amikacin-resistant (AMI), three both-resistant (ACB), and three drug-sensitive (SEN) KPN isolates were collected by the microbiology lab at Shanghai Fifth People's Hospital for this study. The KPN type strains (33259, 13883, and 11296) were purchased from American Type Culture Collection (ATCC, United States). Minimum inhibitory concentrations (MICs) were interpreted according to the Performance Standards for Antimicrobial Susceptibility Testing M100 edition 28 (2018) of the Clinical and Laboratory Standards Institute (CLSI) (Gehring et al., 2021).

Culture Scaling and Sample Preparation for Proteome

For each KPN strain, three KPN monoclonals were inoculated in Luria-Bertani (LB) broth to the exponential phase (OD_{600} = 0.8), and KPN cells were collected and washed in PBS and subjected to global protein extraction using 8 M Urea (PH = 8.0) containing protease inhibitor, followed by 3 min of sonication (3 s on, 3 s off, amplitude 25%). Then the protein concentration was quantified through Bradford method and 100 μg protein was digested overnight following filter-acid sample preparation (FASP) method (Wisniewski et al., 2009) with 3.5 μg trypsin in 50 mM ammonium acid carbonate (PH 8.0) overnight at 37°C. Finally, the purified peptides were acquired after extraction with

50% acetonitrile (ACN) and 0.1% formic acid (FA) following desalination in two layers of Empore 3 M C18 disk with 2 mg packing (3 μm, 150 Å, Agela) in a pipet tip and dried in a vacuum concentrator (Thermo Fisher Scientific).

Liquid Chromatography Coupled With Tandem Mass Spectrometry Analysis, Proteome Identification and Quantification With MaxQuant-Based Database Searching

Proteome analysis was processed on Q Exactive HFX mass spectrometer (Thermo Fisher Scientific, Rockford, IL, United States) coupled with Easy-nLC 1,000 nanoflow liquid chromatography system (Thermo Fisher Scientific). The MS raw files were searched against *Klebsiella pneumoniae* subsp. *Pneumoniae* (strain ATCC 700721) database (version 20171126) in the Uniprot Knowledgebase (UniProtKB) using Maxquant (Version 1.5.3.30) (Cox and Mann, 2008). Peptides (minimum length of seven amino acid residues) with 1% FDR and a Mascot ion score greater than 20 were selected for protein identification. Proteins with 1% FDR (with at least one unique peptide) were selected for further analysis. For the proteome quantification, the intensity-based absolute quantification (iBAQ) value was extracted from MaxQuant results and

TABLE 1 | Sample information.

Sample ID	Sample type	MIC_CTX (μ g/ml)	MIC_AMI (μ g/ml)
SEN1	Sputum	8	2
SEN2	Sputum	8	4
SEN3	Sputum	6	2
CTX1	Sputum	340	4
CTX2	Sputum	370	2
CTX3	Sputum	340	4
AMI1	Sputum	6	410
AMI2	Sputum	8	450
AMI3	Sputum	8	360
ACB1	Sputum	380	220
ACB2	Sputum	450	280
ACB3	Sputum	400	240

SEN, drug-sensitive isolate; CTX, cotrimoxazole-resistant isolate; AMI, amikacin-resistant isolate; ACB, both-resistant isolate; MIC, minimum inhibitory concentration.

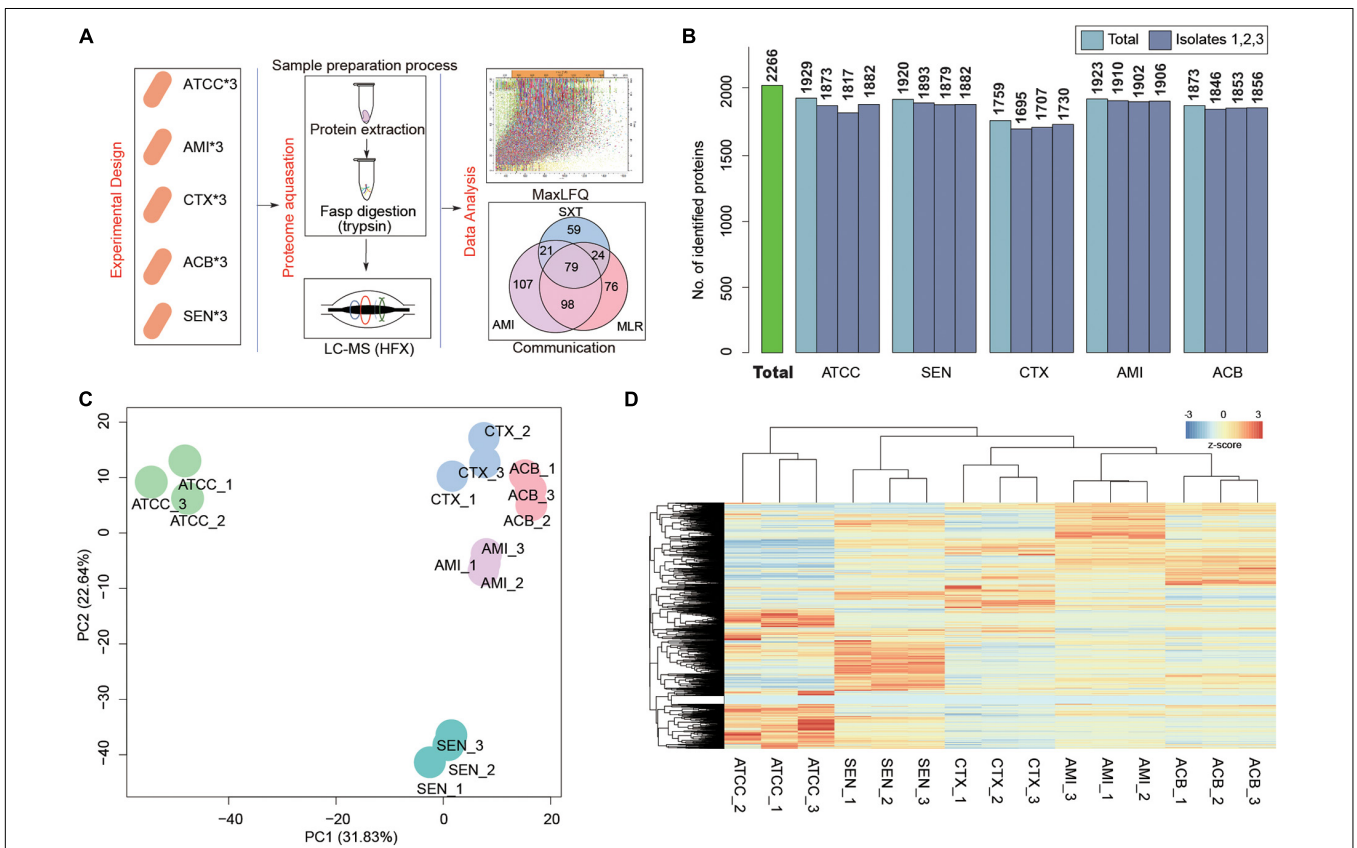

FIGURE 1 | Label-Free Quantitative Proteome identify the pattern characteristics of hospital-derived KPN strains. **(A)** The experimental design and workflow. *Klebsiella pneumoniae* clinical isolates, including SEN, AMI-resistant, CTX-resistant, and ACB-resistant isolates, and ATCC strains were collected. The cells were subjected to LC-MS/MS analysis for label-free proteome following protein extraction and FASP digestion. Protein quantification were finished using Maxquant software with iBAQ algorithm. **(B)** The number of proteins detected in each isolate. **(C,D)** Principal component analysis **(C)** and Unsupervised hierarchical clustering **(D)** of the protein profiling of 15 KPN strains.

subjected to FOT calculation. FOT was defined as protein's iBAQ divided by the total iBAQ of all identified proteins in one experiment. Finally, FOT was multiplied by 10^6 for easy presentation. The geometric mean value of the copy numbers in three proteomic analyses of each macrophage population were calculated and used for protein quantification. The significantly different expressed proteins (DEPs) were filtered with the fold change > 2 and P-value < 0.05 (bilateral Student's t-test).

Hierarchical Clustering and Principal Component Analysis

Unsupervised hierarchical clustering was carried out using R package "pheatmap" (version 1.0.12). The distances between the rows or columns of a data matrix were computed based on the Euclidean distance. The "complete" method was used in agglomeration process. PCA was performed using R package "gmodels" (version 2.18.1) in the statistical analysis environment R version 4.0.0 based on the relative protein quantification values (FOT) of each sample.

Gene Enrichment Analysis

Gene Ontology (GO) enrichment and Kyoto Encyclopedia of Genes and Genomes (KEGG) pathway analyses of the DEPs between sensitive and drug (AMI or CTX)-resistant isolates was performed with the R Bioconductor package "clusterProfiler" (version 4.0.2). Enrichment significance was determined using Fisher's exact test.

RESULTS

Label-Free Quantitative Proteome Identify the Pattern Characteristics of Hospital-Derived *Klebsiella pneumoniae* Strains

To search the global protein patterns of different KPN clinical isolates, a total of 15 KPN strains, including three sensitive (SEN), three amikacin-resistant (AMI), three cotrimoxazole-resistant (CTX), and three amikacin/cotrimoxazole both-drug-resistant (ACB) KPN isolates derived from 12 different patients

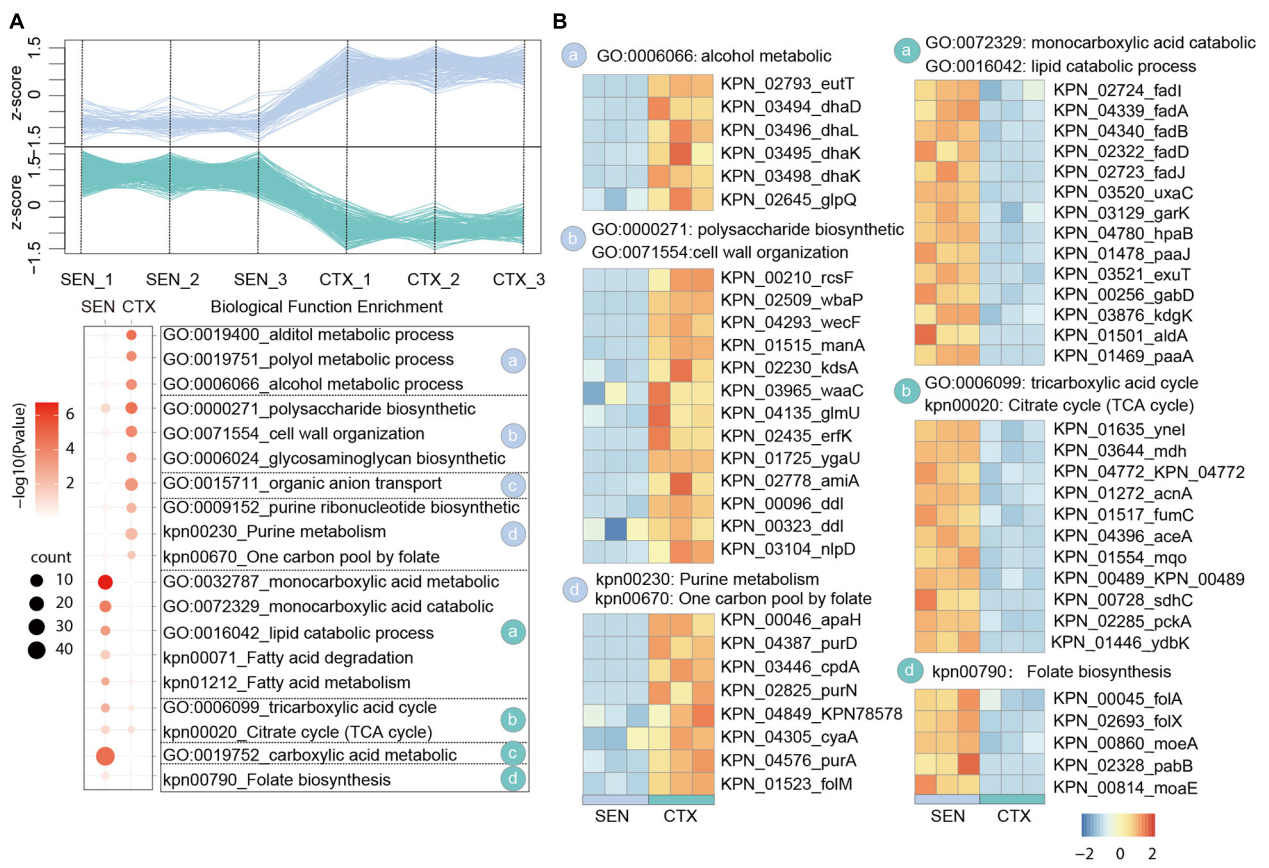

FIGURE 2 | Comparative Proteomics Analyses Revealed the metabolism alteration of CTX-resistant isolates comparing with SEN isolates. **(A)** Expression profiles (up) and representative function enrichment analysis (down) of differentially expressed genes between CTX-resistant isolates and SEN isolates. Each line represents one protein. Functional terms were labeled and color-coded with p-value (Fisher's exact test) according to the legend. **(B)** Expression patterns of proteins participating in the indicated cellular functions/pathways across CTX-resistant or SEN isolates. Values for each protein in all groups are color-coded based on the z-scored protein abundance per cell.

(**Table 1**) in our hospital, as well as three ATCC type strains, were collected and subjected to LC-MS/MS in single runs by a quadrupole Orbitarp instrument after trypsin digestion for label-free proteomics analysis (**Figure 1A**). As a result, a deep coverage of 2,266 proteins were successfully identified and quantified in total (**Figure 1B** and **Supplementary Table 1**), expanding the experimental coverage of the 5,126 predicted bacterial gene products (in KPN database from UniprotKB, strain ATCC 700721) from 23% (1,156) (Sharma et al., 2019), 32% (1,654) (Keasey et al., 2019) to 44%, providing an extended characterization of KPN proteome. The dynamic ranges of protein quantification values in this study spanned over six orders of magnitude (**Supplementary Figure 1A**), with the most abundant proteins being rpsU, HupA, tufa, etc. (**Supplementary Figure 1B**). rpsU, also known as ribosomal protein S21 (rps21), was reported to contribute to fitness, stress-tolerance and host interaction (Koomen et al., 2018). HupA (heat-unstable α, HUα) is a subunit of a heterotypic dimer, Huαβ, resulting in high growth and a lowly pleiotropic phenotype (Abebe et al., 2017). tufA (translational elongation factor EF-Tu) was involved in a change in state or activity of a cell as a result of an antibiotic stimulus (Silk and Wu, 1993). The proteome quantification results of 15 experiments were comparable, as their medians were on the same level (**Supplementary Figure 1C**).

To obtain the proteome identity of different strains systematically, PCA was carried out based on the protein abundance of KPNs. The result showed a very clear separation between ATCC and hospital isolates on the first component level as shown in *x*-axis, and captured the significant differences between sensitive and drug-resistant strains on the second component level as shown in *y*-axis (**Figure 1C**). An unsupervised hierarchical clustering analysis of the proteome patterns further supported the results (**Figure 1D**). Therefore, considering the fundamental differences between standard KPN strains from ATCC and clinical isolates from our hospital, we mainly focused on comparative analysis between proteome of three drug-resistant isolates (CTX, AMI, and ACB) and sensitive isolates for further study.

Comparative Proteomics Analyses Revealed the Metabolism Alteration of Cotrimoxazole-Resistant Isolates Comparing With Sensitive Isolates

Cotrimoxazole is a combination of trimethoprim/sulfamethoxazole, and widely used for treatment of bacterial infections. The drug is extensively used due to the relatively cheap, available over-the-counter, and well tolerated

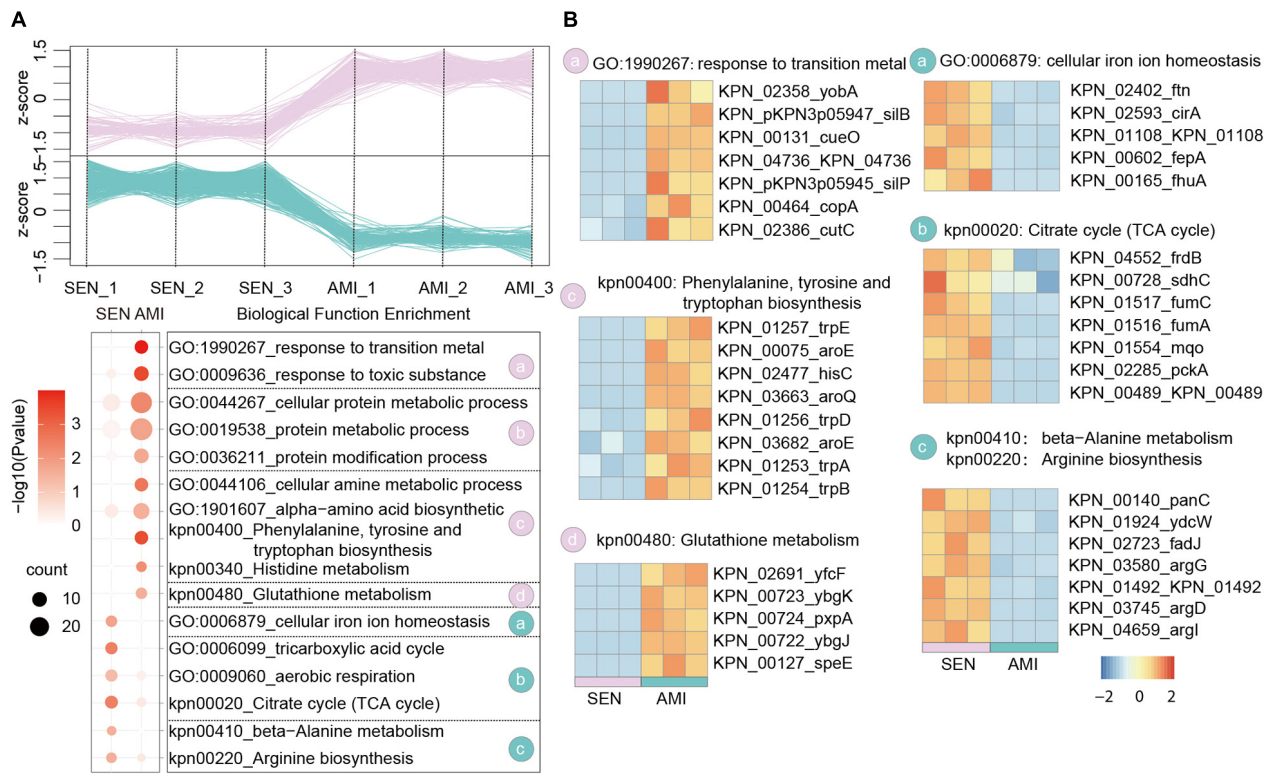

FIGURE 3 | Comparative Proteomics Analyses Revealed the metabolism alteration of AMI-resistant isolates comparing with SEN isolates. **(A)** Expression profiles (up) and representative function enrichment analysis (down) of differentially expressed genes between AMI-resistant isolates and SEN isolates. Each line represents one protein. Functional terms were labeled and color-coded with *p*-value (Fisher's exact test) according to the legend. **(B)** Expression patterns of proteins participating in the indicated cellular functions/pathways across AMI-resistant or SEN isolates. Values for each protein in all groups are color-coded based on the z-scored protein abundance per cell.

(Morgan et al., 2011). Because of the injudicious use, the spread of bacteria with this antibiotic resistance has been a major factor (Okeke et al., 1999). Recent studies from the African continent have reported high rates of cotrimoxazole resistance in gram-negative pathogenic bacteria in the range of 50–96% (Manyahi et al., 2017).

In our comparative proteome analysis between CTX-resistant isolates and SEN isolates, we identified 183 up-regulated proteins and 501 down-regulated proteins, respectively (**Figure 2A** and **Supplementary Figure 2A**). Further gene enrichment analysis showed an activation of alcohol metabolic process (eutT, dhaD, dhal) as well as a restraint of lipid catabolic process (fadl, fadA, fadB) and tricarboxylic acid (TCA) cycle pathway (ynel, mdh, acnA) in CTX-resistant isolates, which may contribute to ROS reduction and cell survival under drug pressure. It's also worth noting that although the folate biosynthesis of cells (folA, folX, morA) was attenuated by CTX administration, the usage rate of one carbon unit was not affected accordingly illustrated by activation of purine ribonucleotide biosynthetic process and "one carbon pool by folate pathway (apaH, purD, cpdA). Besides, proteins in polysaccharide biosynthetic and cell wall organization processes (rcsF, wbaP, wecF), which may protect cell from drug perturbation through the physical safeguards" strategies, were up-regulated in CTX-resistant isolates (**Figure 2B**). There results showed the relative metabolism alteration of CTX-resistant isolates comparing with SEN isolates.

Comparative Proteomics Analyses Revealed the Metabolism Alteration of Amikacin-Resistant Isolates Comparing With Sensitive Isolates

Amikacin shows a particularly broad antimicrobial activity which is used for severe bacterial infections. Nowadays, the emergency of amikacin-resistant KPN occurs dramatically with 20% in Turkey (Gokmen et al., 2016). Based on the proteome dataset, we identified 305 up-regulated proteins and 319 down-regulated proteins, respectively in AMI-resistant isolates comparing with SEN strains (**Figure 3A** and **Supplementary Figure 2B**). Gene enrichment analysis of these differentially expressed proteins

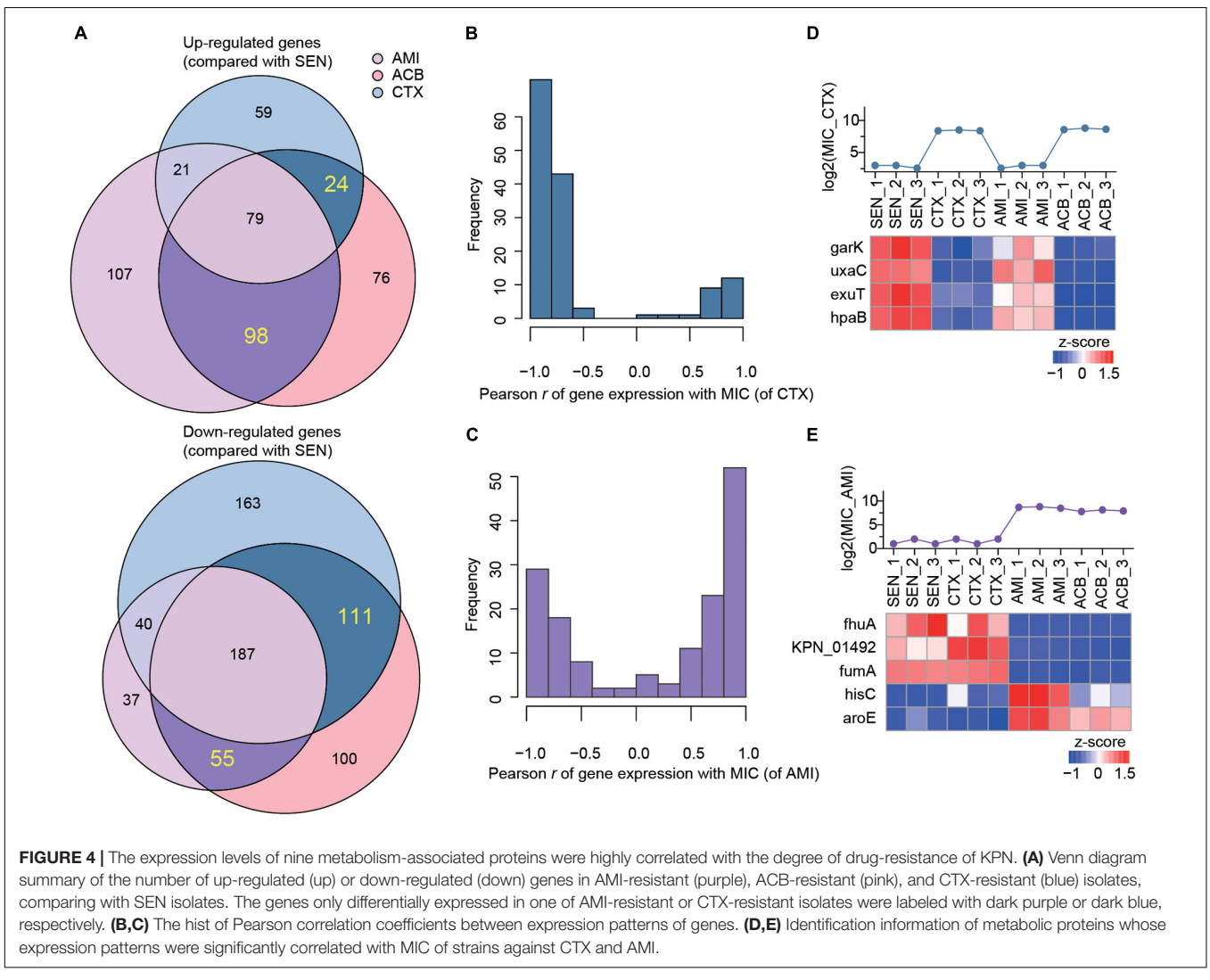

FIGURE 4 | The expression levels of nine metabolism-associated proteins were highly correlated with the degree of drug-resistance of KPN. **(A)** Venn diagram summary of the number of up-regulated (up) or down-regulated (down) genes in AMI-resistant (purple), ACB-resistant (pink), and CTX-resistant (blue) isolates, comparing with SEN isolates. The genes only differentially expressed in one of AMI-resistant or CTX-resistant isolates were labeled with dark purple or dark blue, respectively. **(B,C)** The hist of Pearson correlation coefficients between expression patterns of genes. **(D,E)** Identification information of metabolic proteins whose expression patterns were significantly correlated with MIC of strains against CTX and AMI.

indicated activation of glutathione metabolism pathway (yfcF, ybgK, pxpA) and restraint of TCA cycle pathway (frdB, sdhC, fumC), contributing to ROS clearance and cell survival under drug perturbation, in AMI-resistant isolates. Additionally, protein metabolic process as well as amino acid biosynthesis process was elevated in AMI-resistant isolates, indicating less affection of AMI administration in these isolates (**Figure 3B**).

Of note, combined with the results of CTX-resistant isolates, we found TCA cycle pathway was also inhibited in AMI-resistant isolates, and the downregulated proteins in TCA cycle pathway were high-degree overlapped, such as sdhC, fumC, mqo, pcka, and KPN_00489. These results reveal that restraint of TCA cycle pathway may be a widely used strategy of KPN to gain antibiotic resistance.

The Expression Levels of Nine Metabolism-Associated Proteins Were Highly Correlated With the Degree of Drug-Resistance of *Klebsiella pneumoniae*

Combining with the proteome profiling of ACB-resistant isolates, we screened out a set of candidate proteins that were specifically associated with the mechanism of single antibiotic resistance of KPN. As a result, we identified 24 proteins whose expression were simultaneously up-regulated in CTX-resistant isolates and ACB-resistant isolates but not affected by AMI administration comparing with SEN strains, and 111 proteins on the contrary, as candidate proteins specifically for CTX-resistant isolates. Similarly, a total of 98 and 55 proteins exclusively up-regulated or down-regulated in AMI-resistant isolates, respectively, were identified as candidates specifically for AMI-resistant isolates (**Figure 4A**).

Next, to further identify the proteins closely correlated with mechanism of antibiotic resistance in KPN, we introduced the MICs of cotrimoxazole and amikacin on all the KPN hospital-isolates studied (**Table 1**). The **Figures 4B,C** showed the distribution of Pearson correlation coefficients between MICs and expression of protein sets above, respectively, for CTX-resistant isolates and AMI-resistant isolates. Finally, based on the results of gene enrichment analysis and correlation analysis, we identified nine proteins (**Table 2**), which were not only involved in the metabolic regulation of drug-resistant isolates, but also significantly correlated (positively or negatively) with the degree of drug resistance of KPN isolates (**Figures 4D,E**). Therefore, these enzymes possess important roles in reducing the ROS levels in cytoplasmic of cells. Further investigations need to be processed to determine the precise biological mechanism of the influence of these proteins on isolates resistance.

TABLE 2 | Pearson correlation coefficients between MICs and expression of protein sets.

Gene_ID	Symbol[a]	Pearson *r*[b]	Function	FC[c]	*p*[d]
CTX group					
KPN_03129	garK	−0.9	Monocarboxylic acid catabolic process	0.30	4.72e-2
KPN_03520	uxaC	−0.98	Monocarboxylic acid catabolic process	0.35	1.11e-4
KPN_03521	exuT	−0.91	Monocarboxylic acid catabolic process	0.24	6.67e-4
KPN_04780	hpaB	−0.95	Monocarboxylic acid catabolic process	0.26	3.21e-3
AMI group					
KPN_00165	fhuA	−0.87	Cellular iron ion homeostasis	0.01	1.11e-3
KPN_01492	01492	−0.84	Arginine biosynthesis	0.48	5.20e-4
KPN_01516	fumA	−0.93	Citrate cycle	0.22	1.43e-4
KPN_02477	hisC	0.89	Phe, tyr, and try biosynthesis	48.18	1.16e-4
KPN_03682	aroE	0.95	Phe, tyr, and try biosynthesis	3.34	1.31e-2

[a] *Gene name from Uniprot.*
[b] *Pearson correlation coefficients between MICs and expression of protein.*
[c] *Fold change.*
[d] *P-value.*

DISCUSSION

Previous evidence has shown that bacteria can alter its metabolism to adapt the antibiotic pressure by reducing the accumulation of intracellular antibiotic (Richter et al., 2017). However, the specific metabolism-related protein profiles of drug-resistant bacteria are still largely understood (Liu et al., 2019).

In the present study, we found that proteins in TCA pathway were down-regulated in both CTX- and AMI-resistant KPNs, which may restraint the ROS production in drug-resistant isolates. The proteomics results showed the deficiencies of resistant KPN in central metabolic pathways (TCA cycle), compared with the sensitive KPN. Illuminated by the results from comparative proteomic approaches, our findings provide a mechanism to explain why adding alanine and/or glucose into culture could reduce drug resistance to the antibiotic (Bhargava and Collins, 2015; Peng et al., 2015; Su et al., 2015, 2018; Koeva et al., 2017). By re-analyzing the data reported previously, we found the deficiencies of resistant KPN in central metabolic pathways was a generally existent phenomenon. Briefly, the metabolic process, cellular process and response to stimulus were downregulated in ESBL-producing KPN (Wang Y. et al., 2020), and the Carbohydrate metabolic process, Generation of precursor metabolites and energy, Cellular amino acid metabolic process, Lipid metabolic process, Catabolic process, were all downregulated in carbapenem-resistant KPN (Sharma et al., 2019). These findings showed that restraint of TCA cycle pathway could be a widely used strategy of KPN to gain antibiotic resistance, showing a non-antibiotic based therapeutic method against antibiotic-resistant infections.

Besides the findings of TCA cycle and related pathways in resistant KPN, we also screened out nine resistance-related proteins participating in metabolic pathways, including garK, uxaC, exuT, hpaB, fhuA, KPN_01492, fumA, hisC, aroE, which participate in metabolism-related pathways and are associated with MIC of resistant KPN. garK play a role of glycerate kinase

in phosphorylating glycerate to glycerate-2-phosphate, which is involved in the central metabolism of the cell (Wehrmann et al., 2020). uxaC, working as a D-glucoronate/D-galacturonate isomerase, is report to participate in catabolism of fructuronate (Utz et al., 2004). fumA encodes fumarase A (FumA), which participates in the tricarboxylic acid (TCA) cycle during both aerobic and anaerobic growth (Lin et al., 2012). Therefore, these enzymes possess important roles in the metabolism of KPN. Further investigations need to be processed to determine the precise biological mechanism of the influence of these proteins on isolates resistance.

In sum, proteomics was performed on the sensitive (SEN), cotrimoxazole (CTX)-resistant, amikacin (AMI)-resistant, and amikacin/cotrimoxazole-both (ACB)-resistant *Klebsiella pneumoniae* clinical isolates. A total of 2,266 proteins were identified and further bioinformatic analysis showed down-regulation of TCA pathway and up-regulation of alcohol metabolic or glutathione metabolism processes, which may contribute to ROS clearance and cell survival, in drug-resistant isolates. Finally, combined with MIC of amikacin and cotrimoxazole on different KPN isolates, we identified nine proteins, including garK, uxaC, exuT, hpaB, fhuA, KPN_01492, fumA, hisC, and aroE, that might contribute mostly to the survival of KPN under drug pressure, providing novel, non-antibiotic-based therapeutics against resistant KPN.

DATA AVAILABILITY STATEMENT

All the proteome data generated in this study, including the raw files, quantitative files, and final protein expression matrixes have been deposited to ProteomeXchange (http://www.proteomexchange.org) with accession number PXD028544.

ETHICS STATEMENT

The studies involving human participants were reviewed and approved by the Ethics Committee of Shanghai Fifth People's Hospital. The patients/participants provided their written informed consent to participate in this study.

AUTHOR CONTRIBUTIONS

JQ and LH conceived and supervised the study. JQ designed experiments and wrote the manuscript. CS performed experiments. CS, YS, HZ, and MX analyzed the data. All authors read and approved the manuscript and agreed to be accountable for all aspects of the research in ensuring that the accuracy or integrity of any part of the work are appropriately investigated and resolved.

FUNDING

The present study was supported by the Scientific Research Project funded by the Shanghai Fifth People's Hospital, Fudan University (No. 2019WYZT03).

SUPPLEMENTARY MATERIAL

The Supplementary Material for this article can be found online at: https://www.frontiersin.org/articles/10.3389/fmicb.2021.773829/full#supplementary-material

Supplementary Figure 1 | Overview of Label-Free Quantitative Proteome analysis. **(A)** The dynamic ranges of protein quantification values in this study spanned over six orders of magnitude. **(B)** The abundance of identified proteins with the most abundant proteins being rpsU, HupA, tufa, etc. **(C)** The proteome quantification results of 15 experiments.

Supplementary Figure 2 | Volcano plot showing log2 fold change plotted against −log10 *P*-value. **(A)** For CTX-resistant isolates vs. SEN isolates. **(B)** For AMI-resistant isolates vs. SEN isolates. The red dots and green dots represent the upregulated and downregulated DEPs, respectively.

REFERENCES

Abebe, A. H., Aranovich, A., and Fishov, I. (2017). HU content and dynamics in *Escherichia coli* during the cell cycle and at different growth rates. *FEMS Microbiol. Lett.* 364:fnx195. doi: 10.1093/femsle/fnx195

Allison, K. R., Brynildsen, M. P., and Collins, J. J. (2011). Metabolite-enabled eradication of bacterial persisters by aminoglycosides. *Nature* 473, 216–220. doi: 10.1038/nature10069

Barraud, N., Buson, A., Jarolimek, W., and Rice, S. A. (2013). Mannitol Enhances Antibiotic Sensitivity of Persister Bacteria in *Pseudomonas aeruginosa* Biofilms. *PLoS One* 8:e84220. doi: 10.1371/journal.pone.0084220

Bhargava, P., and Collins, J. J. (2015). Boosting Bacterial Metabolism to Combat Antibiotic Resistance. *Cell Metab.* 21, 154–155. doi: 10.1016/j.cmet.2015.01.012

Cox, J., and Mann, M. (2008). MaxQuant enables high peptide identification rates, individualized p.p.b.-range mass accuracies and proteome-wide protein quantification. *Nat. Biotechnol.* 26, 1367–1372. doi: 10.1038/nbt.1511

dos Santos, K. V., Diniz, C. G., Veloso, L. D., De Andrade, H. M., Giusta, M. D., Pires, S. D., et al. (2010). Proteomic analysis of *Escherichia coli* with experimentally induced resistance to piperacillin/tazobactam. *Res. Microbiol.* 161, 268–275. doi: 10.1016/j.resmic.2010.03.006

Freiberg, C., Brotz-Oesterhelt, H., and Labischinski, H. (2004). The impact of transcriptome and proteome analyses on antibiotic drug discovery. *Curr. Opin. Microbiol.* 7, 451–459. doi: 10.1016/j.mib.2004.08.010

Gehring, T., Kim, H. J., Dibloni, E., Neuenhoff, M., and Buechler, C. (2021). Comparison of Antimicrobial Susceptibility Test Results of Disk Diffusion, Gradient Strip, and Automated Dilution with Broth Microdilution for Piperacillin-Tazobactam. *Microb. Drug Resist.* 27, 1305–1311. doi: 10.1089/mdr.2020.0011

Gokmen, T. G., Nagiyev, T., Meral, M., Onlen, C., Heydari, F., and Koksal, F. (2016). NDM-1 and rmtC-Producing *Klebsiella pneumoniae* Isolates in Turkey. *Jundishapur J. Microbiol.* 9:e33990. doi: 10.5812/jjm.33990

Hessling, B., Bonn, F., Otto, A., Herbst, F. A., Rappen, G. M., Bernhardt, J., et al. (2013). Global proteome analysis of vancomycin stress in Staphylococcus aureus. *Int. J. Med. Microbiol.* 303, 624–634. doi: 10.1016/j.ijmm.2013.08.014

Jin, X., Lee, J. E., Schaefer, C., Luo, X., Wollman, A. J. M., Payne-Dwyer, A. L., et al. (2021). Membraneless organelles formed by liquid-liquid phase separation increase bacterial fitness. *Sci. Adv.* 7:eabh2929. doi: 10.1126/sciadv.abh2929

Jing, H. R., Bai, Q. W., Lin, Y. N., Chang, H. J., Yin, D. X., and Liang, D. H. (2020). Fission and Internal Fusion of Protocell with Membraneless "Organelles"

Formed by Liquid-Liquid Phase Separation. *Langmuir* 36, 8017–8026. doi: 10.1021/acs.langmuir.0c01864

Keasey, S. L., Suh, M. J., Das, S., Blancett, C. D., Zeng, X. K., Andresson, T., et al. (2019). Decreased Antibiotic Susceptibility Driven by Global Remodeling of the *Klebsiella pneumoniae* Proteome. *Mol. Cell. Proteom.* 18, 657–668. doi: 10.1074/mcp.RA118.000739

Koeva, M., Gutu, A. D., Hebert, W., Wager, J. D., Yonker, L. M., O'toole, G. A., et al. (2017). An Antipersister Strategy for Treatment of Chronic *Pseudomonas aeruginosa* Infections. *Antimicrob. Agents Chemother.* 61, e00987–17. doi: 10.1128/AAC.00987-17

Koomen, J., Den Besten, H. M. W., Metselaar, K. I., Tempelaars, M. H., Wijnands, L. M., Zwietering, M. H., et al. (2018). Gene profiling-based phenotyping for identification of cellular parameters that contribute to fitness, stress-tolerance and virulence of Listeria monocytogenes variants. *Int. J. Food Microbiol.* 283, 14–21. doi: 10.1016/j.ijfoodmicro.2018.06.003

Lata, M., Sharma, D., Deo, N., Tiwari, P. K., Bisht, D., and Venkatesan, K. (2015). Proteomic analysis of ofloxacin-mono resistant Mycobacterium tuberculosis isolates. *J. Proteom.* 127, 114–121. doi: 10.1016/j.jprot.2015.07.031

Lin, H. H., Lin, C. H., Hwang, S. M., and Tseng, C. P. (2012). High Growth Rate Downregulates fumA mRNA Transcription but Is Dramatically Compensated by Its mRNA Stability in *Escherichia coli*. *Curr. Microbiol.* 64, 412–417. doi: 10.1007/s00284-012-0087-6

Liu, Y., Li, R. C., Xiao, X., and Wang, Z. Q. (2019). Bacterial metabolism-inspired molecules to modulate antibiotic efficacy. *J. Antimicrob. Chemother.* 74, 3409–3417. doi: 10.1093/jac/dkz230

Manyahi, J., Tellevik, M. G., Ndugulile, F., Moyo, S. J., Langeland, N., and Blomberg, B. (2017). Molecular Characterization of Cotrimoxazole Resistance Genes and Their Associated Integrons in Clinical Isolates of Gram-Negative Bacteria from Tanzania. *Microb. Drug Resist.* 23, 37–43. doi: 10.1089/mdr.2016.0074

Martinez, J. L., and Rojo, F. (2011). Metabolic regulation of antibiotic resistance. *FEMS Microbiol. Rev.* 35, 768–789. doi: 10.1111/j.1574-6976.2011.00282.x

Meylan, S., Porter, C. B. M., Yang, J. H., Belenky, P., Gutierrez, A., Lobritz, M. A., et al. (2017). Carbon Sources Tune Antibiotic Susceptibility in *Pseudomonas aeruginosa* via Tricarboxylic Acid Cycle Control. *Cell Chem. Biol.* 24, 195–206. doi: 10.1016/j.chembiol.2016.12.015

Morgan, D. J., Okeke, I. N., Laxminarayan, R., Perencevich, E. N., and Weisenberg, S. (2011). Non-prescription antimicrobial use worldwide: a systematic review. *Lancet Infect. Dis.* 11, 692–701.

Okeke, I. N., Lamikanra, A., and Edelman, R. (1999). Socioeconomic and behavioral factors leading to acquired bacterial resistance to antibiotics in developing countries. *Emerg. Infect. Dis.* 5, 18–27. doi: 10.3201/eid0501.990103

Paczosa, M. K., and Mecsas, J. (2016). *Klebsiella pneumoniae*: going on the Offense with a Strong Defense. *Microbiol. Mol. Biol. Rev.* 80, 629–661. doi: 10.1128/MMBR.00078-15

Peng, B., Su, Y. B., Li, H., Han, Y., Guo, C., Tian, Y. M., et al. (2015). Exogenous Alanine and/or Glucose plus Kanamycin Kills Antibiotic-Resistant Bacteria. *Cell Metab.* 21, 249–261. doi: 10.1016/j.cmet.2015.01.008

Pu, Y. Y., Li, Y. X., Jin, X., Tian, T., Ma, Q., Zhao, Z. Y., et al. (2019). ATP-Dependent Dynamic Protein Aggregation Regulates Bacterial Dormancy Depth Critical for Antibiotic Tolerance. *Mol. Cell* 73, 143–156.e4. doi: 10.1016/j.molcel.2018.10.022

Qayyum, S., Sharma, D., Bisht, D., and Khan, A. U. (2016). Protein translation machinery holds a key for transition of planktonic cells to biofilm state in Enterococcus faecalis: a proteomic approach. *Biochem. Biophys. Res. Commun.* 474, 652–659. doi: 10.1016/j.bbrc.2016.04.145

Ramirez, M. S., and Tolmasky, M. E. (2017). Amikacin: uses, Resistance, and Prospects for Inhibition. *Molecules* 22:2267. doi: 10.3390/molecules22122267

Richter, M. F., Drown, B. S., Riley, A. P., Garcia, A., Shirai, T., Svec, R. L., et al. (2017). Predictive compound accumulation rules yield a broad-spectrum antibiotic. *Nature* 545, 299–304. doi: 10.1038/nature22308

Sharma, D., Garg, A., Kumar, M., Rashid, F., and Khan, A. U. (2019). Down-Regulation of Flagellar, Fimbriae, and Pili Proteins in Carbapenem-Resistant *Klebsiella pneumoniae* (NDM-4) Clinical Isolates: a Novel Linkage to Drug Resistance. *Front. Microbiol.* 10:2865. doi: 10.3389/fmicb.2019.02865

Silk, G. W., and Wu, M. (1993). Posttranscriptional Accumulation of Chloroplast Tufa (Elongation-Factor Gene) Messenger-Rna during Chloroplast Development in Chlamydomonas-Reinhardtii. *Plant Mol. Biol.* 23, 87–96. doi: 10.1007/BF00021422

Su, Y. B., Peng, B., Han, Y., Li, H., and Peng, X. X. (2015). Fructose restores susceptibility of multidrug-resistant Edwardsiella tarda to kanamycin. *J. Proteome Res.* 14, 1612–1620. doi: 10.1021/pr501285f

Su, Y. B., Peng, B., Li, H., Cheng, Z. X., Zhang, T. T., Zhu, J. X., et al. (2018). Pyruvate cycle increases aminoglycoside efficacy and provides respiratory energy in bacteria. *Proc. Natl. Acad. Sci. U. S. A.* 115, E1578–E1587.

Utz, C. B., Nguyen, A. B., Smalley, D. J., Anderson, A. B., and Conway, T. (2004). GntP Is the *Escherichia coli* Fructuronic Acid Transporter and Belongs to the UxuR Regulon. *J. Bacteriol.* 186, 7690–7696. doi: 10.1128/JB.186.22.7690-7696.2004

Wang, G., Zhao, G., Chao, X., Xie, L., and Wang, H. (2020). The Characteristic of Virulence, Biofilm and Antibiotic Resistance of *Klebsiella pneumoniae*. *Int. J. Environ. Res. Public Health* 17:6278.

Wang, Y., Cong, S., Zhang, Q. H., Li, R. W., and Wang, K. (2020). iTRAQ-Based Proteomics Reveals Potential Anti-Virulence Targets for ESBL-Producing *Klebsiella pneumoniae*. *Infect. Drug Resist.* 13, 2891–2899. doi: 10.2147/IDR.S259894

Wehrmann, M., Toussaint, M., Pfannstiel, J., Billard, P., and Klebensberger, J. (2020). The Cellular Response to Lanthanum Is Substrate Specific and Reveals a Novel Route for Glycerol Metabolism in *Pseudomonas* putida KT2440. *mBio* 11, e516–e520. doi: 10.1128/mBio.00516-20

Wisniewski, J. R., Zougman, A., Nagaraj, N., and Mann, M. (2009). Universal sample preparation method for proteome analysis. *Nat. Methods* 6, 359–362. doi: 10.1038/nmeth.1322

World Health Organization [WHO] (2014). *Antimicrobial Resistance: Global Report on Surveillance*. Geneva: World Health Organization.

Conflict of Interest: The authors declare that the research was conducted in the absence of any commercial or financial relationships that could be construed as a potential conflict of interest.

Publisher's Note: All claims expressed in this article are solely those of the authors and do not necessarily represent those of their affiliated organizations, or those of the publisher, the editors and the reviewers. Any product that may be evaluated in this article, or claim that may be made by its manufacturer, is not guaranteed or endorsed by the publisher.

frontiers in Microbiology

ORIGINAL RESEARCH
published: 18 November 2021
doi: 10.3389/fmicb.2021.752102

Multiomics Study Reveals *Enterococcus* and *Subdoligranulum* Are Beneficial to Necrotizing Enterocolitis

Hao Lin[1,2,3†], Qingqing Guo[4†], Yun Ran[5†], Lijian Lin[6], Pengcheng Chen[7], Jianquan He[8], Ye Chen[1,9] and Jianbo Wen[1,10*]*

[1] State Key Laboratory of Organ Failure Research, Guangdong Provincial Key Laboratory of Gastroenterology, Nanfang Hospital, Southern Medical University, Guangzhou, China, [2] Shengli Clinical Medical College, Fujian Medical University, Fuzhou, China, [3] Department of Gastroenterology, Fujian Provincial Hospital South Branch, Fuzhou, China, [4] Department of Intensive Medicine, The First Affiliated Hospital of Fujian Medical University, Fuzhou, China, [5] Department of Gastroenterology, Kaiping Centre Hospital, Changsha Sanjiang Development Zone, Kaiping, China, [6] Department of Emergency, Fujian Provincial Hospital, Fujian Medical University, Fuzhou, China, [7] Fujian Provincial Hospital South Branch, Department of Health Management, Fuzhou, China, [8] School of Medicine, Xiamen University, Xiamen, China, [9] Department of Gastroenterology, Integrative Microecology Center, Shenzhen Hospital, Southern Medical University, Shenzhen, China, [10] Department of Gastroenterology, Affiliated PingXiang Hospital, Southern Medical University, Pingxiang, China

OPEN ACCESS

Edited by:
Yanling Wei,
Army Medical University, China

Reviewed by:
Suleyman Yildirim,
Istanbul Medipol University, Turkey
Fen Wang,
Central South University, China
Jingnan Li,
Peking Union Medical College Hospital (CAMS), China

***Correspondence:**
Ye Chen
yechen@smu.edu.cn
Jianbo Wen
wenjbpx@126.com

[†]These authors have contributed equally to this work and share first authorship

Specialty section:
This article was submitted to Systems Microbiology, a section of the journal Frontiers in Microbiology

Received: *02 August 2021*
Accepted: *30 September 2021*
Published: *18 November 2021*

Citation:
Lin H, Guo Q, Ran Y, Lin L, Chen P, He J, Chen Y and Wen J (2021) Multiomics Study Reveals Enterococcus and Subdoligranulum Are Beneficial to Necrotizing Enterocolitis. Front. Microbiol. 12:752102. doi: 10.3389/fmicb.2021.752102

Necrotizing enterocolitis (NEC) is a life-threatening disease for premature infants with low body weight. Due to its fragile gut microbiome and successful treatment of fecal microbiota transplantation (FMT) for intestinal disease, we aimed to reveal the multiple-omics changes after FMT and/or sulperazone treatment. In this study, 2-week-old newborn rabbits were used to simulate the NEC model and grouped into healthy control, NEC, sulperazone treatment, FTM treatment, and FMT and sulperazone combination treatment. We evaluated the intestinal pathology and survival to define the benefit from each treatment and performed microbiome and transcriptome analysis to reveal the changes in microcosmic level, which could be helpful to understand the pathogenesis of NEC and develop new strategy. We found NEC rabbits benefit more from the combination of FMT and sulperazone treatment. Combination treatment reverses a lot of microorganisms dysregulated by NEC and showed the most similar transcript profiler with healthy control. Moreover, a combination of FMT and sulperazone significantly prolonged the survival of NEC rabbits. Function enrichment showed that metabolism and viral life cycle are the most significant changes in NEC. FMT is a common therapy method for NEC. Meanwhile, in the severe situation of NEC with intestinal infection, the first therapy strategy is preferred the third-generation cephalosporin, among which sulperazone is used widely and the effect is remarkable. So, we used sulperazone to treat the rabbits with the NEC. In this research, we aim to explore the different effects on NEC between FMT and sulperazone as well as the combination. Considering the microbiome and transcriptome result, we make a conclusion that the *Enterococcus* and *Subdoligranulum* benefits NEC by influencing the bacterial phages and butyrate production, respectively.

Keywords: NEC, FMT, sulperazone, gut microbiome, transcriptome

INTRODUCTION

Necrotizing enterocolitis (NEC) is a life-threatening intestinal disease associated with an increased risk of morbidity and mortality (Papillon et al., 2017; Alganabi et al., 2019). According to epidemiological survey, about 7% of premature infants with body weights less than 1,500 g would be diagnosed as NEC (Papillon et al., 2017). However, etiologies primarily leading to the NEC are complex and unclear including premature delivery, hypoxia, and ischemia of the intestinal mucosa, infection, and gut microbiome chaos (Bi et al., 2019). Antibiotics, surgery, and advanced life support are prevailing treatments for the NEC, but the effect is limited (Bi et al., 2019).

The intestinal lumen of the newborn is considered germ-free before birth. The microorganisms from the mother's vagina, breast milk, food, and environment will shape the gut colonized by microorganisms during the first 2 weeks of life and form the gut microbiome (Plaza-Díaz et al., 2018; Shao et al., 2019; Pilla and Suchodolski, 2020). This process of gut bacteria colonization and diversity is essential for the healthy gut of infants. Because the gut microbiome will interact with TLRs, the gut epithelial cells will develop tolerance and appropriately respond to pro-inflammatory and anti-inflammatory (Plaza-Díaz et al., 2018). The microbiome also helps to resist the pathogenic microorganisms and maintains the balance of gut microorganisms. Intestinal dysbiosis, which refers to loss of microbiome diversity and structure homeostasis in the intestine, has been proven to be associated with premature infants NEC (Papillon et al., 2017). Fecal microbiota transplantation (FMT) is an emerging and beneficial strategy to treat disease caused by gut microbiome chaos, such as chronic diarrhea, by transferring of fecal matter from healthy individuals to patients with dysbiosis to adjust the gut microbiome (Goyal et al., 2018; Antushevich, 2020; Liu et al., 2020). FMT also has been used to treat pseudomembranous colitis and shows high efficiency. Some experiments revealed that FMT is useful for infectious diseases, including NEC (Matson et al., 2018). However, the mechanisms remain to be demonstrated, especially the interactions between the microorganisms and host.

In this study, we performed gut microbiome and transcriptome analysis based on newborn rabbit models and compared among healthy, NEC, and different treatment groups. In the severe situation of NEC with intestinal infection, the first therapy strategy preferred the third-generation cephalosporin, among which sulperazone is used widely, and the effect is remarkable. So, we used sulperazone to treat rabbits with NEC. We found that NEC is characterized by metabolism dysregulation, and the FMT and sulperazone combination treatment showed the highest benefits for the NEC. The proportion of *Enterococcus* showed a significant increase after treatment, particularly after combination treatment of FMT and sulperazone. The bacterial phages carried by *Enterococcus* have been demonstrated to improve T-cell immunity, and several strains of *Enterococcus faecalis* has been proven to reverse NEC pathology (Stewart et al., 2012; Matson et al., 2018). Another significant change was the emerging of *Subdoligranulum* after combination treatment, which produces butyrate to regulate gut function (Chassard et al., 2014). These two genera may have the potential to be developed as a target for NEC treatment.

MATERIALS AND METHODS

Animal Model and Study Design

The 2-week-old newborn rabbits (*Oryctolagus cuniculus*) were used to imitate NEC as the previous with a little change (Choi et al., 2010; Bozeman et al., 2013). Briefly, the newborn rabbits were fed with mother's milk for 3 days before inducing NEC. The healthy controls were fed with mother's milk all the time. The NEC rabbits were fed with homemade hypertonic formula milk (10 g protein powder dissolved in 75 ml Esbilac, 15 ml/kg/per, 3 times/day) and stimulated with hypothermia (10 min/4°C, 2 times/day for 3 days) and hypoxia (95% nitrogen and 5% oxygen. 10 L/min, 10 min/2 times/day for 3 days). The ingredients of sulperazone (cefoperazone sodium and sulbactam sodium for injection) are cefoperazone and sulbactam with a ratio of 2:1. Sulperazone was administrated to the rabbits by intravenous drip of 30 mg/kg/per 12 h. The rabbits of the groups reached 50% lethality as the end point of the experiment. The animal health condition was recorded for 2 weeks after model construction for 3 days. The animal study was reviewed and approved by the Ethics Committee of Southern Medical University (No. 2019R001-F05).

Experimental Groups

The 2-week-old newborn suckling rabbits were selected and divided into five groups randomly, 15 rabbits for each group [Group A: healthy rabbits taken at the end of the experiment; Group B: model control group (with jugular vein venous catheter for nutrition supply); Group C: conventional treatment group: after model building successfully treated with sulperazone; Group D: FMT group (fecal bacteria transplantation treatment group): after model building successfully, healthy rabbits, they were gavaged with feces from healthy rabbits; Group E: conventional treatment and FMT group: after model building successfully, the rabbits were treated with sulperazone and FMT.

Fecal Microbiota Transplantation

The feces of healthy baby rabbits was mixed with physiological saline, centrifuged, filtered, and the stomach was gavaged. Rabeprazole was injected before gavage to inhibit gastric acid secretion and reduce the destruction of bacterial flora in the stomach. During the experiment, fluids and antibiotics were given through the central vein.

Intestinal Pathological Score

The intestinal tube was separated, and 2–3 cm of the ileocecum tissue was retrieved. After H&E staining, the ileocecum pathology score was performed. The pathological severity assessment was performed independently by two pathologists under double-blind conditions. The final pathology score calculation was half of the sum of the two scores. The scoring standard refers to the NADLER scoring standard: 0 points, intestinal villi and epithelium are intact, and the tissue structure is

normal; 1 point, mild submucosal and/or lamina propria swelling and separation; 2 points, moderate submucosal and/or lamina propria swelling and separation, submucosal and/or muscle layer edema; 3 points, severe submucosal and/or lamina propria swelling and separation, submucosal and/or muscle layer edema, local villi loss; 4 points, intestinal villi disappearance with intestinal necrosis. The final pathology score $\geq$ 2 points is determined to be NEC.

16S rRNA Sequencing

DNA Extraction

Feces DNA was extracted using the Omega Stool DNA Kit following the manual. Purity and quality of the genomic DNA were checked by NanoDrop spectrophotometer (Thermo Fisher Scientific).

PCR Amplification

The V3–4 hypervariable region of the bacterial 16S rRNA gene was amplified with the primers 338F (5′-ACTCCTACGGG AGGCAGCAG-3′) and 806R (5′-GGACTACNNGGGTATCT AAT-3′). For each feces sample, an eight-digit barcode sequence was added to the 5′ end of the forward and reverse primers (provided by Allwegene Company, Beijing). The PCR was carried out on a Mastercycler Gradient (Eppendorf, Germany) using 25-μl reaction volumes, containing 12.5 μl 2 × Taq PCR MasterMix, 3 μl of BSA (2 ng/μl), 1 μl of forward primer (5 μM), 1 μl of reverse primer (5 μM), 2 μl of template DNA, and 5.5 μl of ddH_2O. Cycling parameters were 95°C for 5 min, followed by 28 cycles of 95°C for 45 s, 55°C for 50 s, and 72°C for 45 s with a final extension at 72°C for 10min. The PCR products were purified using an Agencourt AMPure XP Kit.

High-Throughput Sequencing

Deep sequencing was performed on Miseq PE300 platform at Allwegene Company (Beijing). After the run, image analysis, base calling, and error estimation were performed using Illumina Analysis Pipeline Version 2.6.

Data Analysis

The raw data were first screened, and sequences were removed from consideration if they were shorter than 230 bp, had a low-quality score ($\leq$20), contained ambiguous bases or did not exactly match the primer sequences and barcode tags, and separated using the sample-specific barcode sequences. Qualified reads were clustered into operational taxonomic units (OTUs) at a similarity level of 97% using the Uparse algorithm of Vsearch (v2.7.1) software. The Ribosomal Database Project (RDP) Classifier tool was used to classify all sequences into different taxonomic groups against the SILVA128 database.

QIIME (v1.8.0) was used to calculate the richness and diversity indices based on the OTU information.

RNA Sequencing

RNA Isolation and Qualification

Small intestine tissue RNA was extracted using the TRIzol method (TIANGEN BIOTECH, Beijing) and treated with RNase-free DNase I (TaKaRa). RNA degradation and contamination was monitored on 1% agarose gels. RNA was quantified using Agilent 2100 Bioanalyzer (Agilent Technologies, CA, United States). The quality and integrity were assessed by NanoDrop spectrophotometer (IMPLEN, CA, United States).

Library Preparation for Transcriptome Sequencing

A total amount of 1.5 μg of RNA per sample was used as input material for the RNA sample preparations. Sequencing libraries were generated using NEBNext® Ultra™ RNA Library Prep Kit for Illumina® (NEB, United States) following the recommendations of the manufacturer, and index codes were added to attribute sequences to each sample. Briefly, mRNA was purified from total RNA using poly-T oligo-attached magnetic beads. Fragmentation was carried out using divalent cations under elevated temperature in NEBNext First Strand Synthesis Reaction Buffer (5X). First-strand cDNA was synthesized using random hexamer primer and M-MuLV Reverse Transcriptase (RNase H). Second-strand cDNA synthesis was subsequently performed using DNA Polymerase I and RNase H. The remaining overhangs were converted into blunt ends *via* exonuclease/polymerase activities. After adenylation of the 3′ ends of DNA fragments, the NEBNext Adaptor with hairpin loop structure was ligated to prepare for hybridization. In order to select cDNA fragments of preferentially 200–250 bp in length, the library fragments were purified with AMPure XP system (Beckman Coulter, Beverly, United States). Then 3 μl of USER Enzyme (NEB, United States) was used with size-selected, adaptor-ligated cDNA at 37°C for 15 min followed by 5 min at 95°C before PCR. Then PCR was performed with Phusion High-Fidelity DNA polymerase, Universal PCR primers, and Index (X) Primer. At last, PCR products were purified (AMPure XP system), and library quality was assessed on the Agilent Bioanalyzer 2100 system. The library preparations were sequenced on an Illumina Hiseq 4000 platform by the Beijing Allwegene Technology Company Limited (Beijing, China), and paired-end 150-bp reads were generated.

Gene Ontology Enrichment a Pathway Enrichment Analysis

Gene Ontology (GO) enrichment analysis of the differentially expressed genes (DEGs) was implemented by the GOseq R packages based on the Wallenius non-central hyper-geometric distribution, which can adjust for gene length bias in DEGs.

RESULTS

Fecal Microbiota Transplantation and Sulperazone Combination Treatment Efficiently Antagonizes Necrotizing Enterocolitis

Gut microbiota structure chaos is one of the leading causes of NEC. Recently, FMT is an emerging strategy to treat digestive tract disease caused by microbiome disorders. To verify whether FMT is beneficial for NEC newborn rabbits in

our experiment, we constructed NEC models as described in "Materials and Methods" section, and NEC rabbits were treated with sulperazone, FMT, and its combination (**Figure 1A**). As shown in the figure, the NEC rabbits showed typical NEC pathology, such as intestinal mucosa destruction, villi shedding, inflammatory cell infiltration, etc. Two pathologists evaluated the sections independently, and the NEC model showed ≥ 2 score, which indicted the model had been constructed successfully. After different treatments, the pathology of NEC showed relief on different levels. However, the combined treatment of FMT and sulperazone could efficiently reverse the NEC symptom and prolong lives (**Figure 1B**).

The Diversity of Microbiome Shared a Similarity With the Healthy Group After Fecal Microbiota Transplantation and Sulperazone Combination Treatment

It is worth noting that the sulperazone and FMT combination shows the most efficiency (**Figures 2A,B**), which indicates that this therapy strategy may be a better choice for NEC treatment. We performed 16s RNA-seq to investigate how the gut microbiome changes. First, we checked the diversities of the different groups by four diversity indexes (**Figure 2A**). The microbiome diversity was lowest in the NEC group compared with the other groups. The microbiome diversity was significantly increased after treatments, and the combination of the sulperazone and FMT group showed the highest efficiency and shared the most similarity with the healthy group (**Figures 2B,C**). This result suggests that microbiome homeostasis and diversity is very important for NEC treatment, and diversity recovery is helpful for NEC treatment (Guo et al., 2021).

Then, we checked the microbiome changes on a genius level. In healthy control, *Bacteroides*, *Akkermansia*, *Ruminococcaceae NK4A214 group*, *Christensenellaceae R-7 group*, *Lachnospiraceae NK4A136 group*, and *Ruminococcus 1* were the top 10 abundant genera (**Figure 2D**). All the above microorganisms were probiotics, involved in food degradation, metabolism regulation, and inhibiting the pathogenic bacteria proliferation. *Ruminococcus 1*, *Marvinbryantia*, *Parabacteroides*, *Kurthia*, *Flavonifractor*, *Lactonifactor*, and *Lachnospiaceae UCG 010* were the signatures of NEC (**Figure 2D**; Esber et al., 2020; Hiippala et al., 2020; Lordan et al., 2020). *Parabacteroides* was reported to be upregulated in NEC (**Figure 2D**). The others were defined as conditional pathogenic bacteria.

Next, we compared the top five abundant microbes among different groups. *Christensenellaceae R-7 group* and *Akkermansia* were not recovered after all treatments, which may indicate that both of them were not the key microorganisms for treatment used in our experiments. *Enterococcus* and *Ruminococcaceae NK4A214 groups* were significantly increased after all treatments. The *Vagococcus* and *Myroides* were the highest in the NEC group. Moreover, they did not exist in healthy control and were downregulated by all treatments, especially by sulperazone

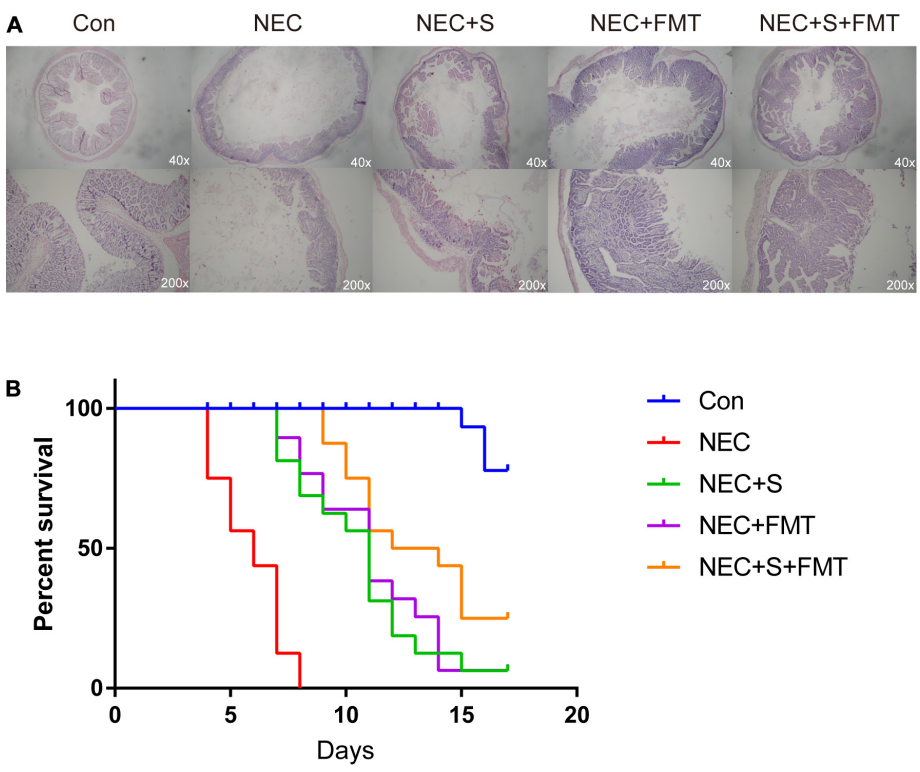

FIGURE 1 | Fecal microbiota transplantation (FMT) and sulperazone combination treatment efficiently antagonizes necrotizing enterocolitis (NEC). **(A)** Pathology pictures and **(B)** survival analysis of different groups. Con, control; NEC, necrotizing enterocolitis; S, sulperazone; FMT, fecal microbiota transplantation.

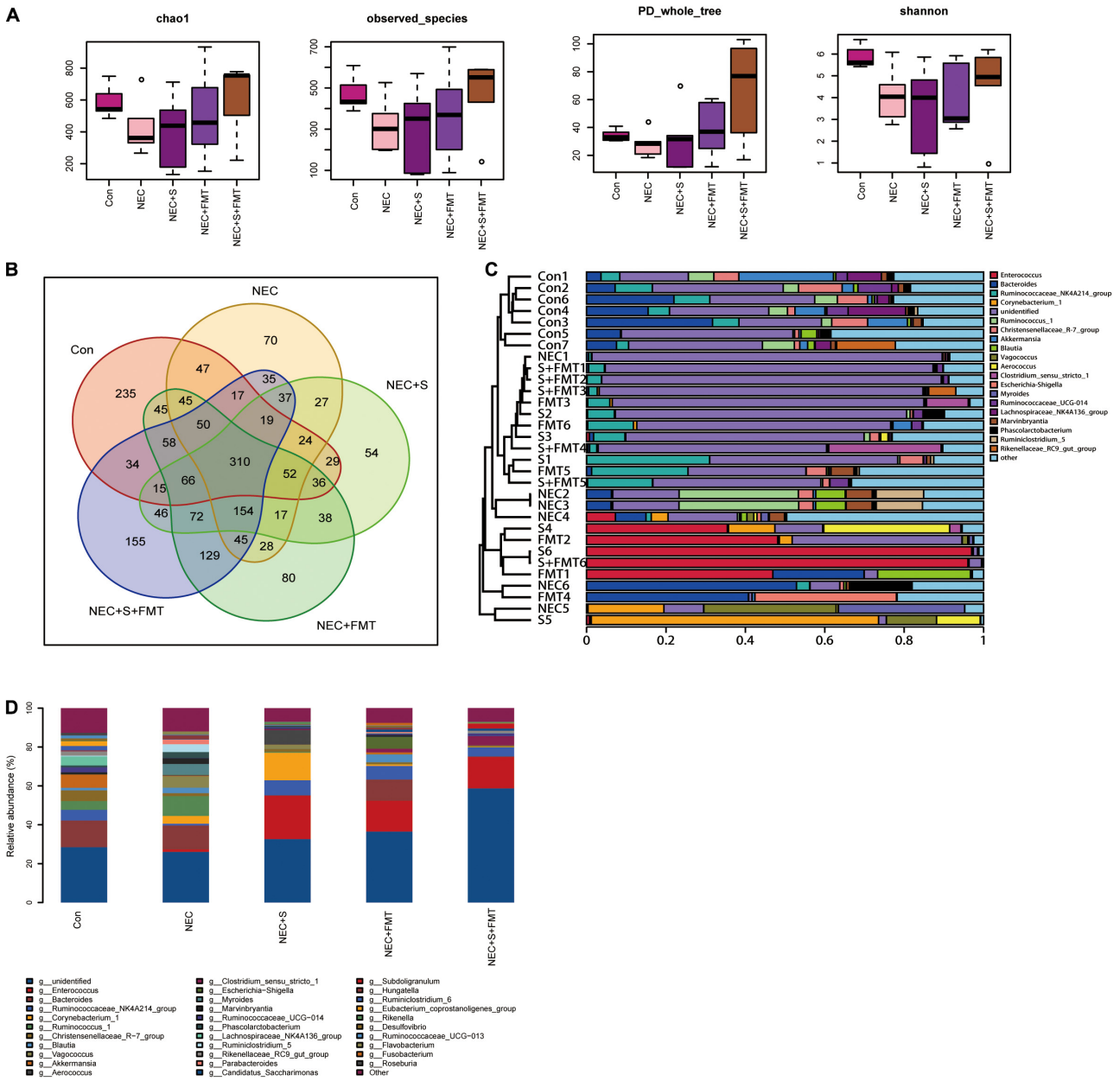

FIGURE 2 | The diversity of microbiome shared a similarity to the healthy group after FMT and sulperazone combination treatment. **(A)** Four methods measured the diversity of microbiome in five groups. **(B)** Venn plot for the five groups. **(C)** Microbiome clusters of five groups. **(D)** Microbiome proportion of five groups. Con, control; NEC, necrotizing enterocolitis; S, sulperazone; FMT, fecal microbiota transplantation.

and FMT combination, and they were discovered first in our study. The hazard of *Vagococcus* was still not clarified. However, it is clear that *Vagococcus* is associated with purulent infection (Altintas et al., 2020). *Myroides* has strong resistance to bactericides such as antibiotics and leads to infection (LaVergne et al., 2019). *Corynebacterium 1* and *Aerococcus* were the unique microorganisms of sulperazone treatment. A lot of studies reported that these two Gram-positive bacteria are conditional pathogenic bacteria (Rasmussen, 2016; Oliveira et al., 2017), and their benefits remain to be revealed. *Escherichia–Shigella* was a unique genus after FMT treatment. The abundance of *Escherichia–Shigella* was negatively correlated with NEC progress (Zhou et al., 2015). One of the mechanisms of FMT treatment to NEC was recovering *Escherichia–Shigella. Clostridium sensu stricto 1* and *Subdoligranulum* were unique genera in sulperazone and FMT combination group. *Clostridium sensu stricto 1* was helpful in promoting gut development and maintaining the gut microbiome diversity (Du et al., 2018). *Subdoligranulum* was one of the producers of butyrate, which is essential for gut health (Chassard et al., 2014). However, it could be detected in maternal

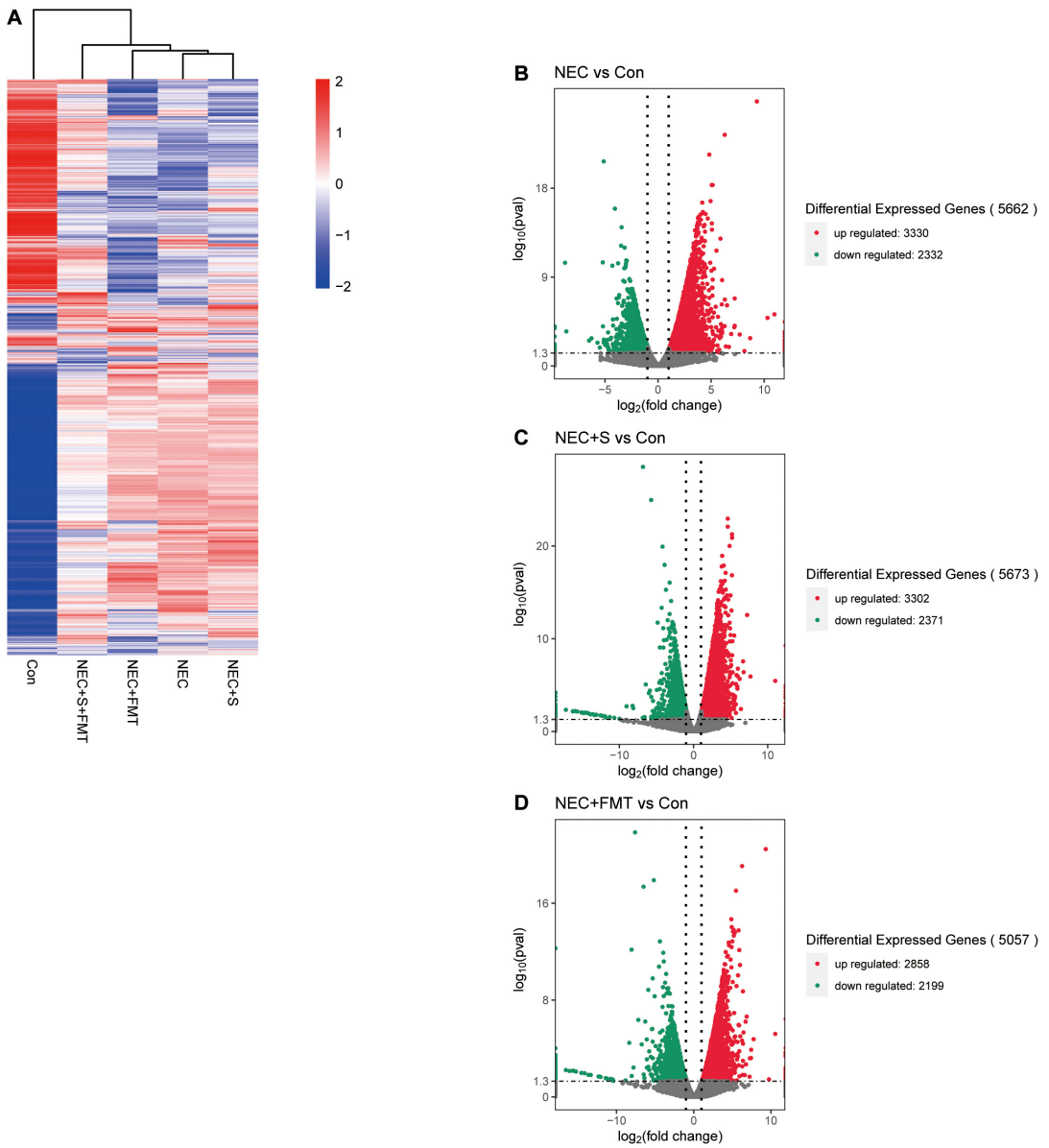

FIGURE 3 | The transcription profiles in five groups. **(A)** Transcription profiles of the different groups. **(B)** Volcano plot differential expression genes between NEC and Con. **(C)** Volcano plot differential expression genes between NEC plus sulperazone and Con. **(D)** Volcano plot differential expression genes between NEC plus FMT and Con. Con, control; NEC, necrotizing enterocolitis; S, Sulperazone; FMT, fecal microbiota transplantation.

feces and breast milk but does not exist in the gut of NEC babies. The combination treatment could fill the deficiency.

Interestingly, *Enterococcus* has a low proportion in NEC and healthy control but increased significantly in all treatment groups (**Figures 2C,D**). *Enterococcus* was classified as an infection source for inpatients and sometimes could be life threatening, but *Enterococcus faecalis*, one species of *Enterococcus*, was a common early colonizer in newborn gut and is associated with relieving NEC (Gao et al., 2018; Delaplain et al., 2019). Furthermore, a recent study showed that *Enterococcus* carries bacteriophage and interacts with human tumor antigen to enhance the T-cell immune response (Delaplain et al., 2019). Whether a similar function of *Enterococcus*, especially the *faecalis* species exists in NEC needs to be further investigated.

The Transcriptome Shared the Similarity With the Healthy Group After Fecal Microbiota Transplantation and Sulperazone Combination Treatment

To investigate gene expression change, we performed transcriptome analysis. The transcript profile of sulperazone and FMT combination treatment showed the highest similarity with the healthy group and the sulperazone treatment showed

the highest similarity with the NEC group, which reminds that the combination of sulperazone and FMT may show a better benefit for NEC (**Figure 3A**). Then, we compared the different groups to define the further changes. We found 3,330 upregulated genes and 2,332 downregulated genes in the NEC group (**Figure 3B**). These genes were enriched in alginic acid metabolism, thermogenesis, oxidative phosphorylation, ribosome, and viral process, suggesting that metabolism and microbiome dysregulation were the most significant molecular changes in NEC (**Figure 4A**). The 3,302 upregulated genes and 2,371 downregulated genes were defined after sulperazone treatment (**Figure 3C**). Function enrichment analysis showed that differentially expressed genes were involved in proteolysis, tryptophan metabolism, and indolakylamine metabolism, which showed that the sulperazone may help to inhibit the necrosis (**Figure 4B**; Cussotto et al., 2020; Yusufu et al., 2021). Interestingly, sulperazone may inhibit the inflammation because the downregulation of tryptophan and indolakylamine could be the signature of downregulation of inflammation. FMT treatment leads to 5,057 genes changed on the expression level (2,858 upregulated and 2,199 downregulated), and they were enriched in cytokine production, proteolysis, lymphocytes and monocytes behaviors, and thermogenesis of GO (**Figures 3D**, **4C**). Finally, we checked the pathway changes of the combination of FMT and sulperazone. Response to lipid, especially cholesterol, was the most significant downregulated pathway in metabolism, and the pathways of cell locomotion were broadly downregulated (**Figure 4D**).

DISCUSSION

Necrotizing enterocolitis is one kind of deadly disease in premature infants characterized by various injuries or damage to the intestine. The defined cause of NEC is unknown. Treatment involves stopping feedings, passing a small tube into the stomach to relieve gas, and giving intravenous fluids and antibiotics. Surgery may be needed if there is perforated or necrotic (dead) bowel tissue. About 60–80% of affected newborns survive the condition (Bi et al., 2019). FMT has showed benefits for a lot of intestinal disease by coordinating the gut microbiome (Goyal et al., 2018). Furthermore, FMT also has additional profits in metabolism and immune adjustment for patients (Lee et al., 2019).

In this study, we aimed to reveal the systematic alteration in different types with FMT and sulperazone treatment. In a multi-omics perspective, NEC was characterized with the gut microbiome and metabolism change. We found that the diversity of microbiome is declined in NEC and is reversed by FMT and/or sulperazone treatment. Interestingly, the combination of FMT and sulperazone showed the most efficiency. However, the mechanism of the results in different groups could be diversified. The FMT has the same function on benefiting the NEC by immunoregulation but from a different way. Sulperazone regulates the NEC immune response by metabolism. Sulperazone elevated microbiome diversity mainly by inhibiting harmful bacteria proliferation and showing less effects on host intrinsic behaviors, but FMT, by regulating cytokines and immune cells, was more direct and effective by supplying beneficial bacteria, and the combination treatment has both function and showed the most efficiency. Some kinds of cholesterol were important for activation of immune cells and also took part in the cell migration (Shahoei and Nelson, 2019). The combination of FMT and sulperazone may regulate the immune cell recruitment by cholesterol metabolism, and this is a different pathway to sulperazone or FMT treatment.

Intriguingly, the *Enterococcus* has a significant increase after treatment. *Enterococcus* is a genus bacterium in the intestine, which can be found under physiological conditions and could ferment carbohydrates, producing lactic acid (Liu et al., 2019). Several studies had reported that *Enterococcus faecalis*, an important species of *Enterococcus*, is decreased in NEC (Stewart et al., 2012), and some strains of *Enterococcus faecalis* is helpful in reversing the NEC pathology (Stewart et al., 2012). It should be noticed that some bacteria of the *Enterococcus* genus also carried bacterial phages, which could regulate T-cell immunity and activate cytotoxicity (Matson et al., 2018). The metabolic products of *Enterococcus* can act as feeds for other bacteria, which could help in maintaining the microbiome homeostasis. We speculate that the *Enterococcus* may have a positive function on NEC. Another genus *Subdoligranulum* is a unique genus in combination treatment, which can produce butyrate that protects the gut function. These two genera play key roles in combination treatment. We inferred based on our data that gut microbiome dysregulation leads to disorder of thermogenesis, oxidative phosphorylation, and transcription, and further metabolic disorders. The dysregulation of these pathways is consistent with the clinical symptoms of NEC. Transcriptome results show that the combination of FMT and sulperazone has the most similar transcript profile with healthy control compared with other treatment groups. Out of our expectation, the viral process is involved in NEC according to the enrichment results (**Figure 4E**). It may be caused by the bacteriophage activity as some reports showed that the microbes behavior could be affected by bacteriophages and further regulates the host immune response (Matson et al., 2018). All treatments could benefit NEC by metabolism and immune regulation. Sulperazone could downregulate tryptophan catabolism, and tryptophan is supposed to help to suppress the hyperinflammation (Cussotto et al., 2020; Yusufu et al., 2021). However, there are no direct evidence to conform the relationship between tryptophan metabolism and indolakylamine metabolism and sulperazone on public research, which should have a further investigation. FMT could influence cytokines production of the intestine and suppress the activation of lymphocytes and monocytes. Moreover, FMT also inhibits proteolysis like sulperazone.

In summary, we found that FMT and sulperazone combination shows the most benefits for NEC, which could significantly reverse the NEC symptoms and prolong the survival of NEC rabbits. Mechanically, the combination treatment shows the most similar transcript profiles with healthy control and could regulate the immune cell recruitment by the

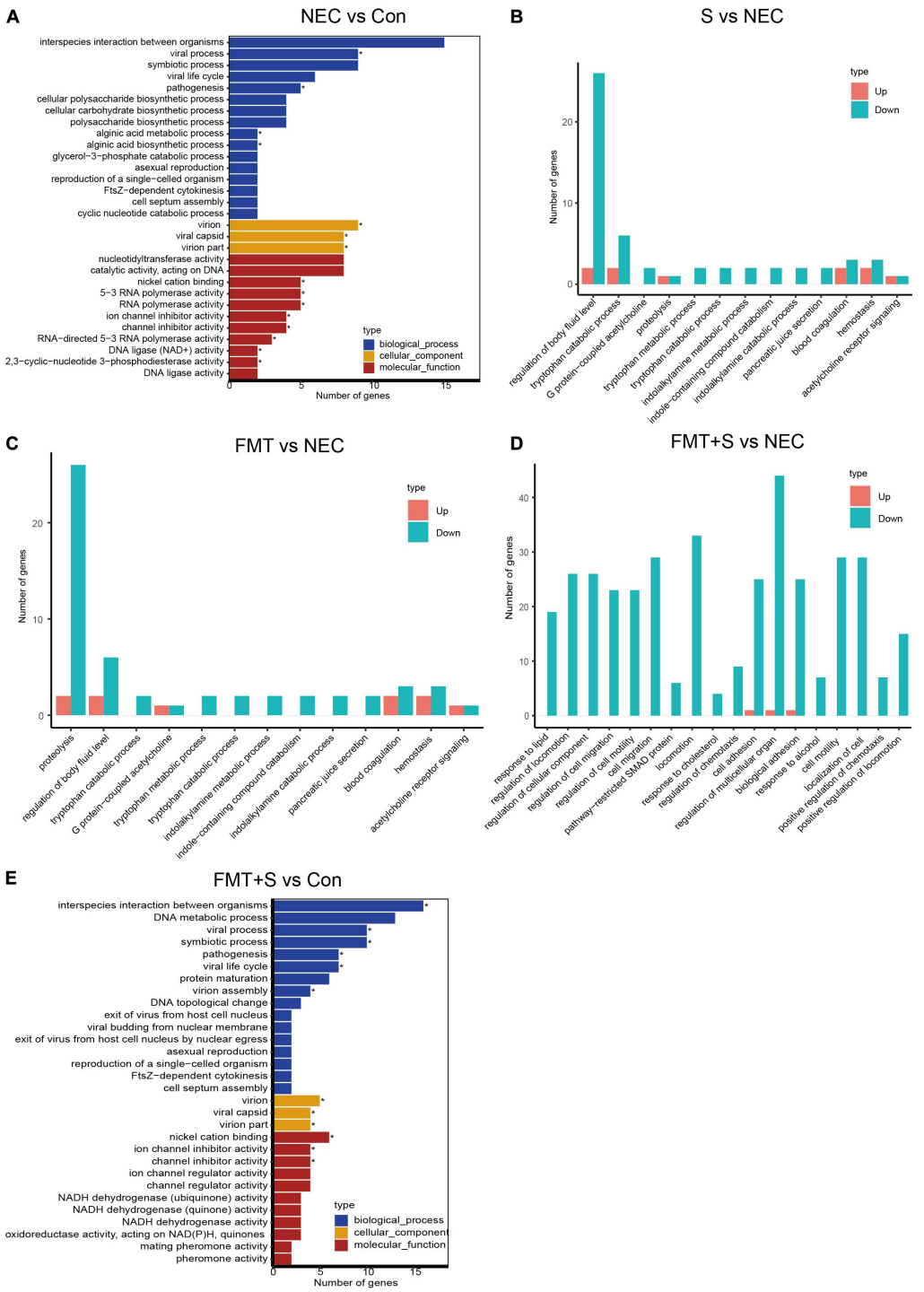

FIGURE 4 | The transcriptome shared a similarity to the healthy group after FMT and sulperazone combination treatment. **(A)** GO enrichment for NEC vs. control. **(B)** GO enrichment for sulperazone vs. NEC. **(C)** GO enrichment for fecal microbiota transplantation vs. NEC. **(D)** GO enrichment for sulperazone plus fecal microbiota transplantation vs. NEC. **(E)** GO enrichment for sulperazone plus fecal microbiota transplantation vs. control. Con, control; NEC, necrotizing enterocolitis; S, Sulperazone; FMT, fecal microbiota transplantation; GO, gene ontology. *Represents for the statistic difference (*, $p < 0.05$).

cholesterol metabolism. Furthermore, the gut microbe diversity is reversed in which *Enterococcus* is significantly elevated. As previously reported, *Enterococcus* faecalis showed benefits for NEC. Another is *Subdoligranulum* that can protect the gut by butyrate production. We think that *Enterococcus faecalis* and *Subdoligranulum* may have the potential to treat bacteria for

NEC, and further study is needed. However, our design also has some deficiencies. The data of the different levels should be further verified by molecular experiments.

DATA AVAILABILITY STATEMENT

The datasets presented in this study can be found in online repositories. The names of the repository/repositories and accession number(s) can be found below: https://www.ncbi.nlm.nih.gov/, PRJNA753453 and PRJNA753003.

ETHICS STATEMENT

The animal study was reviewed and approved by Ethics Committee of Southern Medical University (No.2019 R001-F05).

AUTHOR CONTRIBUTIONS

HL conceived, planned, wrote, and revised the manuscript. QG planned, wrote, and revised the manuscript. YR wrote and revised the manuscript. All authors have read and approved the final manuscript.

FUNDING

This work was done in the frame of a service agreement supported by the National Natural Science Foundation of China (Nos. 81770529 and 82070543), the General Project of Jiangxi Provincial Department of Science and Technology Key R&D Program (No. S2020ZPYFB0148), the Fujian Health Science Research Talent Training Project (No. 2019-1-23), and the Qihang Fund for Scientific Research, Fujian Medical University (No. 2018QH1145).

REFERENCES

Alganabi, M., Lee, C., Bindi, E., Li, B., and Pierro, A. (2019). Recent advances in understanding necrotizing enterocolitis. *F1000Research* 8:107. doi: 10.12688/f1000research.17228.1

Altintas, I., Andrews, V., and Larsen, M. V. (2020). First reported human bloodstream infection with Vagococcus lutrae. *New Microbes New Infect.* 7:100649. doi: 10.1016/j.nmni.2020.100649

Antushevich, H. (2020). Fecal microbiota transplantation in disease therapy. *Clin. Chim. Acta* 503, 90–98. doi: 10.1016/j.cca.2019.12.010

Bi, L. W., Yan, B. L., Yang, Q. Y., Li, M. M., and Cui, H. L. (2019). Probiotic strategies to prevent necrotizing enterocolitis in preterm infants: a meta-analysis. *Pediatr. Surg. Int.* 35, 1143–1162. doi: 10.1007/s00383-019-04547-5

Bozeman, A. P., Dassinger, M. S., Birusingh, R. J., Burford, J. M., and Smith, S. D. (2013). An animal model of necrotizing enterocolitis (NEC) in preterm rabbits. *Fetal Pediatr. Pathol.* 32, 113–122. doi: 10.3109/15513815.2012.681426

Chassard, C., de Wouters, T., and Lacroix, C. (2014). Probiotics tailored to the infant: a window of opportunity. *Curr. Opin. Biotechnol.* 26, 141–147. doi: 10.1016/j.copbio.2013.12.012

Choi, Y. H., Kim, I. O., Cheon, J. E., Kim, J. E., Kim, E. K., Kim, W. S., et al. (2010). Doppler sonographic findings in an experimental rabbit model of necrotizing enterocolitis. *J. Ultrasound Med.* 29, 379–386. doi: 10.7863/jum.2010.29.3.379

Cussotto, S., Delgado, I., Anesi, A., Dexpert, S., Aubert, A., Beau, C., et al. (2020). Tryptophan metabolic pathways are altered in obesity and are associated with systemic inflammation. *Front. Immunol.* 11:557. doi: 10.3389/fimmu.2020.00557

Delaplain, P. T., Bell, B. A., Wang, J., Isani, M., Zhang, E., Gayer, C. P., et al. (2019). Effects of artificially introduced *Enterococcus faecalis* strains in experimental necrotizing enterocolitis. *PLoS One* 14:e0216762. doi: 10.1371/journal.pone.0216762

Du, R., Jiao, S., Dai, Y., An, J., Lv, J., Yan, X., et al. (2018). Probiotic *Bacillus amyloliquefaciens* C-1 improves growth performance, stimulates GH/IGF-1, and regulates the gut microbiota of growth-retarded beef calves. *Front. Microbiol.* 9:2006. doi: 10.3389/fmicb.2018.02006

Esber, N., Mauras, A., Delannoy, J., Labellie, C., Mayeur, C., Caillaud, M. A., et al. (2020). Three candidate probiotic strains impact gut microbiota and induce anergy in mice with cow's milk allergy. *Appl. Environ. Microbiol.* 86, e1203–e1220. doi: 10.1128/AEM.01203-20

Gao, W., Howden, B. P., and Stinear, T. P. (2018). Evolution of virulence in *Enterococcus faecium*, a hospital-adapted opportunistic pathogen. *Curr. Opin. Microbiol.* 41, 76–82. doi: 10.1016/j.mib.2017.11.030

Goyal, A., Yeh, A., Bush, B. R., Firek, B. A., Siebold, L. M., Rogers, M. B., et al. (2018). Safety, clinical response, and microbiome findings following fecal microbiota transplant in children with inflammatory bowel disease. *Inflamm. Bowel. Dis.* 24, 410–421. doi: 10.1093/ibd/izx035

Guo, J., Ren, C., Han, X., Huang, W., You, Y., and Zhan, J. (2021). Role of IgA in the early-life establishment of the gut microbiota and immunity: Implications for constructing a healthy start. *Gut Microbes* 13, 1–21. doi: 10.1080/19490976.2021.1908101

Hiippala, K., Kainulainen, V., Suutarinen, M., Heini, T., Bowers, J. R., Jasso-Selles, D., et al. (2020). Isolation of anti-inflammatory and epithelium reinforcing *Bacteroides* and *Parabacteroides* Spp. from a healthy fecal donor. *Nutrients* 12:935. doi: 10.3390/nu12040935

LaVergne, S., Gaufin, T., and Richman, D. (2019). Myroides injenensis bacteremia and severe cellulitis. *Open Forum Infect. Dis.* 6:ofz282. doi: 10.1093/ofid/ofz282

Lee, P., Yacyshyn, B. R., and Yacyshyn, M. B. (2019). Gut microbiota and obesity: an opportunity to alter obesity through faecal microbiota transplant (FMT). *Diabetes Obes. Metab.* 21, 479–490. doi: 10.1111/dom.13561

Liu, J., Li, Y., Feng, Y., Pan, L., Xie, Z., Yan, Z., et al. (2019). Patterned progression of gut microbiota associated with necrotizing enterocolitis and late onset sepsis in preterm infants: a prospective study in a Chinese neonatal intensive care unit. *PeerJ* 7:e7310. doi: 10.7717/peerj.7310

Liu, J., Miyake, H., Zhu, H., Li, B., Alganabi, M., Lee, C., et al. (2020). Fecal microbiota transplantation by enema reduces intestinal injury in experimental necrotizing enterocolitis. *J. Pediatr. Surg.* 55, 1094–1098. doi: 10.1016/j.jpedsurg.2020.02.035

Lordan, C., Thapa, D., Ross, R. P., and Cotter, P. D. (2020). Potential for enriching next-generation health-promoting gut bacteria through prebiotics and other dietary components. *Gut Microbes* 11, 1–20. doi: 10.1080/19490976.2019.1613124

Matson, V., Fessler, J., Bao, R., Chongsuwat, T., Zha, Y., Alegre, M. L., et al. (2018). The commensal microbiome is associated with anti-PD-1 efficacy in metastatic melanoma patients. *Science* 359, 104–108. doi: 10.1126/science.aao3290

Oliveira, A., Oliveira, L. C., Aburjaile, F., Benevides, L., Tiwari, S., Jamal, S. B., et al. (2017). Insight of genus corynebacterium: ascertaining the role of pathogenic and non-pathogenic species. *Front. Microbiol.* 8:1937. doi: 10.3389/fmicb.2017.01937

Papillon, S. C., Short, S. S., and Ford, H. R. (2017). "Necrotizing enterocolitis," in *Newborn Surgery*, 4th Edn, Vol. 364, ed. P. Puri (New York, NY: CRC Press), 1–1237.

Pilla, R., and Suchodolski, J. S. (2020). The role of the canine gut microbiome and metabolome in health and gastrointestinal disease. *Front. Vet. Sci.* 6:498. doi: 10.3389/fvets.2019.00498

Plaza-Díaz, J., Fontana, L., and Gil, A. (2018). Human milk oligosaccharides and immune system development. *Nutrients* 10:1038. doi: 10.3390/nu10081038

Rasmussen, M. (2016). Aerococcus: an increasingly acknowledged human pathogen. *Clin. Microbiol. Infect.* 22, 22–27. doi: 10.1016/j.cmi.2015.09.026

Shahoei, S. H., and Nelson, E. R. (2019). Nuclear receptors, cholesterol homeostasis and the immune system. *J. Steroid Biochem. Mol. Biol.* 191:105364. doi: 10.1016/j.jsbmb.2019.04.013

Shao, Y., Forster, S. C., Tsaliki, E., Vervier, K., Strang, A., Simpson, N., et al. (2019). Stunted microbiota and opportunistic pathogen colonization in caesarean-section birth. *Nature* 574, 117–121. doi: 10.1038/s41586-019-1560-1

Stewart, C. J., Marrs, E. C. L., Magorrian, S., Nelson, A., Lanyon, C., Perry, J. D., et al. (2012). The preterm gut microbiota: changes associated with necrotizing enterocolitis and infection. *Acta Paediatr. Int. J. Paediatr.* 101, 1121–1127.

Yusufu, I., Ding, K., Smith, K., Wankhade, U. D., Sahay, B., Patterson, G. T., et al. (2021). Tryptophan-deficient diet induces gut microbiota dysbiosis and increases systemic inflammation in aged mice. *Int. J. Mol. Sci.* 22:5005. doi: 10.3390/ijms22095005

Zhou, Y., Shan, G., Sodergren, E., Weinstock, G., Walker, W. A., and Gregory, K. E. (2015). Longitudinal analysis of the premature infant intestinal microbiome prior to necrotizing enterocolitis: a case-control study. *PLoS One* 10:e0118632. doi: 10.1371/journal.pone.0118632

Conflict of Interest: The authors declare that the research was conducted in the absence of any commercial or financial relationships that could be construed as a potential conflict of interest.

Publisher's Note: All claims expressed in this article are solely those of the authors and do not necessarily represent those of their affiliated organizations, or those of the publisher, the editors and the reviewers. Any product that may be evaluated in this article, or claim that may be made by its manufacturer, is not guaranteed or endorsed by the publisher.

frontiers in Microbiology

ORIGINAL RESEARCH
published: 09 December 2021
doi: 10.3389/fmicb.2021.753688

Freeze-Thaw Pretreatment Can Improve Efficiency of Bacterial DNA Extraction From Meconium

Yuntian Xin[1†], Jingxian Xie[2†], Bingru Nan[1,3,4], Chen Tang[3], Yunshan Xiao[2], Quanfeng Wu[2], Yi Lin[3], Xueqin Zhang[2] and Heqing Shen[1,3*]*

[1]Key Laboratory of Urban Environment and Health, Institute of Urban Environment, Chinese Academy of Sciences, Xiamen, China, [2]Department of Obstetrics, Women and Children's Hospital, School of Medicine, Xiamen University, Xiamen, China, [3]State Key Laboratory of Molecular Vaccinology and Molecular Diagnostics, School of Public Health, Xiamen University, Xiamen, China, [4]University of Chinese Academy of Sciences, Beijing, China

OPEN ACCESS

Edited by:
Jialiang Yang,
Geneis (Beijing) Co. Ltd., China

Reviewed by:
Mehmet Demirci,
Kırklareli University, Turkey
Zhengxiao Zhang,
Jimei University, China

***Correspondence:**
Xueqin Zhang
wind459@126.com
Heqing Shen
hqshen@xmu.edu.cn

[†]These authors have contributed equally to this work and share first authorship

Specialty section:
This article was submitted to Systems Microbiology, a section of the journal Frontiers in Microbiology

Received: *05 August 2021*
Accepted: *18 November 2021*
Published: *09 December 2021*

Citation:
Xin Y, Xie J, Nan B, Tang C, Xiao Y, Wu Q, Lin Y, Zhang X and Shen H (2021) Freeze-Thaw Pretreatment Can Improve Efficiency of Bacterial DNA Extraction From Meconium. Front. Microbiol. 12:753688. doi: 10.3389/fmicb.2021.753688

Although the presence of live microbes *in utero* remains under debate, newborn gastrointestinal bacteria are undoubtedly important to infant health. Measuring bacteria in meconium is an ideal strategy to understand this issue; however, the low efficiency of bacterial DNA extraction from meconium has limited its utilization. This study aims to improve the efficiency of bacterial DNA extraction from meconium, which generally has low levels of microflora but high levels of PCR inhibitors in the viscous matrix. The research was approved by the ethical committee of the Xiamen Maternity and Child Health Care Hospital, Xiamen, China. All the mothers delivered naturally, and their newborns were healthy. Meconium samples passed by the newborns within 24 h were collected. Each sample was scraped off of a sterile diaper, transferred to a 5-ml sterile tube, and stored at −80°C. For the assay, a freeze-thawing sample preparation protocol was designed, in which a meconium-InhibitEX buffer mixture was intentionally frozen 1–3 times at −20°C, −80°C, and (or) in liquid nitrogen. Then, DNA was extracted using a commercial kit and sequenced by 16S rDNA to verify the enhanced bacterial DNA extraction efficiency. Ultimately, we observed the following: (1) About 30 mg lyophilized meconium was the optimal amount for DNA extraction. (2) Freezing treatment for 6 h improved DNA extraction at −20°C. (3) DNA extraction efficiency was significantly higher with the immediate thaw strategy than with gradient thawing at −20°C, −80°C, and in liquid nitrogen. (4) Among the conditions of −20°C, −80°C, and liquid nitrogen, −20°C was the best freezing condition for both improving DNA extraction efficiency and preserving microbial species diversity in meconium, while liquid nitrogen was the worst condition. (5) Three freeze-thaw cycles could markedly enhance DNA extraction efficiency and preserve the species diversity of meconium microflora. We developed a feasible freeze-thaw pretreatment protocol to improve the extraction of microbial DNA from meconium, which may be beneficial for newborn bacterial colonization studies.

Keywords: meconium, DNA extraction, 16S rDNA, gene sequencing, gut microbiome

INTRODUCTION

The human intestinal microflora is a highly diversified ecosystem composed of trillions of gastrointestinal bacteria with counts approximately 10 times the number of human cells (Bäckhed et al., 2005; Biagi et al., 2017). These microorganisms form the "human biome" by coexisting with the host (Sundman et al., 2017). Many of their signaling molecules and/or metabolites play important roles in innate and adaptive immune responses (O'Callaghan et al., 2016), maintenance of the host immune system (Deriu et al., 2016), protection of the host from pathogen invasion, and synthesis of essential vitamins and nutrients (Buffie et al., 2015). The intestinal microflora has the function of transforming nutrients into endocrine signals, which can not only affect metabolism inside the intestine (Eckburg et al., 2005) but also affect the gut nervous system (Hooper and Gordon, 2001). Alterations in the intestinal flora can cause obesity, colorectal cancer (CRC), diabetes, cardiovascular disease, liver disease, and other diseases (Loscalzo, 2013; Qian et al., 2015; Aron-Wisnewsky and Clément, 2016; Forsythe et al., 2016; Gensollen et al., 2016).

The presence of bacteria has been considered to lead to systemic inflammatory reactions and multiple organ damage, which pose a threat to the growth and development of the foetus and can even lead to abortion, premature birth, and stillbirth. During normal pregnancy, foetal growth and development *in utero* have been widely accepted to occur in a sterile environment. In 2008, *Enterococcus* and *Staphylococcus* were mainly identified in 21 healthy newborns by investigating their meconium (Jiménez et al., 2008); this work ignited an ongoing debate regarding whether the *in utero* environment is sterile. In 2010 (Mshvildadze et al., 2010), microbial DNA in meconium was detected, and meconium was confirmed to be rich in bacteria in 2014 (Guo, 2014), implying that infants may have started to establish their intestinal flora before birth. In 2015 (Hansen et al., 2015), evidence demonstrated a low number of bacteria in first-pass meconium from healthy, vaginally delivered, breastfeeding infants. Research on 151 vaginally born or Caesarean-section-born healthy babies in 2016 showed that several bacterial branches may already exist in the intestines of term infants (Nagpal et al., 2016). Bacterial 16S rRNA genes were characterized in first-pass meconium samples from 218 newborns in 2018 at the same hospital (Tapiainen et al., 2018), which revealed the general profiles of infants' fecal microorganisms to some extent. Studies in 2019 further showed that all meconium and most amniotic fluid samples contain bacterial DNA (Stinson et al., 2019; Willis et al., 2019). In summary, human meconium contains complex microbial communities, and these bacteria may have and may continue to affect the development of the foetal immune system and host-microbe interactions.

Meconium is a viscid, odorless, greenish-black material that is quite different from watery and light-yellow newborn stools (Bearer, 2003). Usually, meconium begins to form *in utero* at approximately the 13th week of gestation and accumulates in the foetus until birth. Meconium is passed naturally by full-term neonates within 48 h after birth (Lisowska-Myjak and Pachecka, 2006, 2007). Meconium is a multicomponent mixture that can include bile pigments, water-soluble substances, such as proteins, and chloroform-soluble substances containing unsaturated lipids, fatty acids, and cholesterol (Pallem et al., 2010). These components originate from the foetus swallowing amniotic fluid containing shed epithelial cells and intestinal secretions (Harries, 1978; Sun et al., 1993). To some extent, the components in meconium can reflect the developmental environment of the foetus in the womb, and increasing attention has been devoted to investigating the matrix, including bacteria. However, studying meconium is challenging. One of the main problems is that the existence of microbial communities in the uterine environment is still controversial. Such debate was mainly due to the following problems: (i) The prokaryotic DNA content is approximately 1 % in 1-year-old infant stool samples (Wampach et al., 2017), and only a small proportion of extracted DNA can amplify the prokaryote bands (Hansen et al., 2015). However, current researches used DNA-based approaches with an insufficient detection limit to study "low-biomass" microbial communities; (ii) molecular assessments lacked appropriate controls for contamination; and (iii) failed to provide evidence of bacterial viability. Additionally, previous study stated if microbes were detected, bacteria in the first stool of the newborn could also be contributed to the result of postnatal colonization (Perez-Muñoz et al., 2017).

Scientists have suggested that the reason for the low efficiency of DNA extraction in meconium derives from the presence of many PCR inhibitors in the matrix. These inhibitors can be bile acids and salts (Al-Soud et al., 2005), glycolipids (Karlsson and Larson, 1978), and urea (Schrader et al., 2012), which are difficult to remove during the DNA extraction process and can cause difficultly for subsequent experiments. In addition, the absolute content of microorganisms in meconium may also lead to a low DNA detection rate. Low levels of bacterial DNA are usually caused by high concentrations of PCR inhibitors in meconium (Villanueva et al., 2000; Hansen et al., 2015), and the amplification rate of extracted DNA in meconium samples is commonly very low (10–52.9%; Ardissone et al., 2014; Hansen et al., 2015). Establishing a meconium-specific sampling extraction protocol is important for investigating the microbiome in the newborn gut (Stinson et al., 2018).

In the present study, a commercial QIAamp® Fast DNA Stool Mini Kit (cat. no. 51604) was used to develop the extraction protocol for DNA in meconium. We found that freeze-thaw treatment of meconium in lysis buffer can increase the DNA yield. As a result, we established a freeze-thaw procedure and verified the factors affecting the efficiency of DNA extraction.

MATERIALS AND METHODS

Sample Collection

The research was approved by the ethics committee of the Xiamen Maternity and Child Health Care Hospital (XMCH), Xiamen, China. The newborns were delivered at the Women and Children's Hospital, School of Medicine, Xiamen University,

from June 1st, 2017, to August 15th, 2017. When written informed consent was provided, the participants were recruited according to the following criteria: (1) gestational age between 37 and 42 weeks; (2) fulfilment of regular prenatal visits and complete clinical data; and (3) full-term deliveries. Pregnant women with the following complications were excluded: (1) infectious diseases caused by bacteria, viruses, or parasites; (2) inflammatory diseases (e.g., ankylosing spondylitis); (3) metabolic diseases such as diabetes mellitus; (4) pregnancy-associated illnesses including preeclampsia and gestational hypertension; (5) reproductive system disorders (e.g., an ovarian cyst); (6) abnormal pregnancy state (e.g., preterm birth); (7) genetic diseases such as thalassemia; and (8) tumors including pituitary adenomas and uterine fibroids. All mothers delivered naturally, and their newborns were healthy. Meconium was passed by the newborns within 24 h, and samples were collected immediately from sterile baby diapers. Samples were scraped off from baby diapers with sterilized metal scalpel handles and transferred to 5.0-ml sterilized tubes for subsequent analysis. Each meconium sample was divided into two fractions: one part was numbered and directly stored at −80°C, the other part was lyophilized under vacuum conditions, and the freeze-dried samples were numbered and stored at −80°C.

DNA Extractions Methods

In this study, protocols for extracting DNA in meconium were explored using the basic protocol (blue blocks in **Supplementary Figure S1**) of the commercial QIAamp® Fast DNA Stool Mini Kit (cat. no. 51604). Because of the poor dispersion of meconium in the InhibitEX buffer, each sample was first mixed with 1 ml InhibitEX buffer and vortexed for 30 min. Then, a mixture of meconium and InhibitEX buffer was obtained and named the meconium lysis cocktail. Extra treatments (red block in **Supplementary Figure S1**) were applied to the cocktail before the following steps of DNA extraction (these remaining steps were consistent with the instructions offered by the kit manufacturer). The treatments were designed to improve DNA excretion from the meconium matrix, and factors that may affect excretion were assessed. All experimental details for these factors are listed as follows:

1. Status and amount of meconium: DNA was extracted from either fresh or freeze-dried meconium, and the extraction efficiency was assessed to test which conditions are better for fresh meconium (40, 80, 120, 160, and 200 mg) and freeze-dried meconium (10, 20, 30, 40, 50, and 60 mg). These conditions were tested with five duplicate samples for each test.
2. Freezing time for the meconium lysis cocktails: For DNA extraction, the cocktail samples were intentionally frozen for 0, 6, 12, 18, 24, 36, and 48 h at −20 or −80°C. The remaining steps were performed by following the basic steps in the protocol (**Supplementary Figure S1**). All samples were freeze-dried meconium, and each sample weighed approximately 30 mg.
3. DNA extraction efficiency with immediate and gradient thawing: After vortexing, the meconium lysis cocktails were immediately frozen at −20 or −80°C or in liquid nitrogen for 6 h. Then, different thawing methods were carried out, which involved either immediate thawing or gradient thawing. These tests were designed to assess both freezing temperatures and thawing methods, where the frozen meconium lysis cocktails were thawed immediately or were thawed according to gradient programs (**Supplementary Figure S2**): ① −20°C-frozen meconium lysis cocktails were transferred to 4°C for 6 h. ② −80°C-frozen meconium lysis cocktails were transferred to 4°C for 6 h. ③ Meconium lysis cocktails frozen at −80°C were transferred to −20°C for 6 h and then transferred to 4°C for 6 h. ④ Liquid nitrogen-frozen meconium lysis cocktails were transferred to 4°C and incubated for 6 h. ⑤ Liquid nitrogen-frozen meconium lysis cocktails were transferred to −80°C for 6 h, then transferred to −20°C for 6 h, and finally transferred to 4°C for 6 h. After the thawing steps, the remaining steps all followed the DNA extraction kit instructions. Each sample was a 30-mg freeze-dried meconium specimen.
4. DNA extraction efficiency with immediate and gradient freezing: The measures of immediate and gradient freezing for the meconium lysis cocktails were tested after vortexing (**Supplementary Figure S3**). For immediate freezing, the meconium lysis cocktails were frozen immediately for 6 h at −80°C or in liquid nitrogen. For gradient freezing treatments, the cocktails were frozen stepwise until the target temperatures were reached: ① the cocktails were frozen at −20°C for 6 h and then transferred to −80°C for 6 h; ② the cocktails were frozen at −20°C for 6 h and then transferred to liquid nitrogen for 6 h; and ③ the cocktails were frozen at −20°C for 6 h and then transferred to −80°C for 6 h and in liquid nitrogen for 6 h. After the freezing step, the samples were thawed immediately for the remaining steps of DNA extraction. Each sample was a 30-mg freeze-dried meconium specimen.
5. DNA extraction efficiency with freeze-thaw recycling: The meconium lysis cocktails were immediately frozen at −20 and −80°C and in liquid nitrogen for 6 h to verify the efficiency of DNA extraction for duplicate freeze-thaw cycles. For each cycle, the cocktails were immediately thawed at room temperature. The freeze-thaw operation was carried out for one, two, and three cycles (**Supplementary Figure S4**). Finally, the thawed meconium lysis cocktails were subjected to the remaining steps of DNA extraction. Each sample was a 30-mg freeze-dried meconium specimen.

Quantitative Real-Time PCR

All DNA samples were amplified by quantitative real-time PCR (qPCR) for the hypervariable V3-V4 region of the 16S rRNA gene to verify the DNA extraction efficiency. The PCR system contained 10 μl Roche LightCycler® 480 SYBR® Green I Master, 1 μl of 10 μM each of the forward (5′-CCTAYGGGRBGCASCAG-3′) and reverse (5′-GGACTACHVGGGTWTCTAAT-3′) primers (final concentration 0.5 μM), 5 μl of template or water (negative template control), and 3 μl of water. All samples, including the reference controls, were run in duplicate. The instrument used in this assay was a Roche LightCycler 480II.

The amplification procedure was as follows: predenaturation at 94°C for 10 min; 40 cycles of denaturation at 94°C for 30 s, annealing at 55°C for 30 s, and extension at 72°C for 30 s; melting curves of 94°C for 5 s and 65°C for 1 min; continuous collection of the fluorescent data until 97°C; and cooling. In practice, the DNA amplification efficiency is usually lower than the theoretical value of 100%. To acquire high-quality data, a group of standard curves was set, and the calculated amplification efficiency was approximately 80% in this assay.

16S rDNA Sequencing

To further evaluate the effect of freezing treatment on meconium bacterial diversity, in addition to testing the impact of freezing treatment on DNA extraction efficiency, six different meconium matrixes were treated by using seven different DNA extraction methods. The protocols were meconium lysis cocktails frozen at −20 or −80°C or in liquid nitrogen and treated with one-, two-, and three-freeze-thaw cycles. The samples were coded by the method name (frozen methods tandem freeze-thaw cycle number) plus meconium identification. The meconium identifications were coded as A, B, C, D, E, and F; the frozen methods were marked as 20, 80, and N for −20°C, −80°C, and liquid nitrogen, respectively, and the freeze-thaw cycle number was marked as I, II, and III, respectively. For example, A80II represented meconium A that had been frozen at −80°C and underwent two freeze-thaw recycling cycles. All extracted DNA was sequenced by 16S rDNA sequencing technology. 16S rDNA is the DNA sequence corresponding to the rRNA encoded in bacteria that exists in all bacterial genomes. The 16S rDNA in this assay was sequenced on an Illumina HiSeqTM 2500 by Gene Denovo Biotechnology Co., Ltd. (Guangzhou, China). And the raw data microbiome sequencing was uploaded into NCBI database under the accession number of PRJNA759695.

Data Analysis

All data were processed by SPSS19 and Excel. Student's *t*-test was used to verify the significance of differences in the intergroup data, and all *p*-values were applied to the two-sided tests unless otherwise specified. Bioinformatic analysis was performed using Omicsmart, which is a dynamic real-time interactive online platform for data analysis.[1]

RESULTS AND DISCUSSION

Meconium Status and Loading Amount Affect DNA Extraction Efficiency

The recommended sample for the kit was a 200-mg fresh sample. As shown in **Supplementary Table S1**, the water content of meconium was approximately 60–70% in this assay calculated by the following formulation:

$$H_2O(\%) = (WW - DW) / WW \times 100\%$$

Among them, WW and DW represented the wet and dry weight of meconium, respectively. Therefore, 200 mg fresh meconium and 60 mg freeze-dried meconium were initially applied in the protocol development.

The relationship between DNA extraction efficiency and sample weight presented an inverted U-shape for both fresh and freeze-dried samples (**Figure 1**; **Supplementary Table S2**). The DNA extraction efficiency reached the peak values when fresh meconium weighed 120 mg (**Figure 1A**) and freeze-dried meconium weighed 30 mg (**Figure 1C**). The DNA extraction efficiency of the frozen samples was generally higher than that of the fresh samples. In addition, both fresh samples (**Figure 1B**) and dry samples (**Figure 1D**) could clog the column filters when they were overloaded as liquid above the adsorption column could not enter the lower side. When comparing the DNA extraction efficiency between fresh and freeze-dried meconium, the overall efficiency for freeze-dried meconium was higher than that for fresh meconium.

The above results showed that the sample status and loading amount were two important factors in DNA extraction. Overloading can cause a lower DNA extraction efficiency than proper loading, possibly because of the following reasons: (1) Samples cannot be fully lysed to release DNA. (2) The fragments of samples blocked the filter column, which affected the subsequent operations. (3) More PCR inhibitors (Villanueva et al., 2000; Hansen et al., 2015) were loaded in the overloaded meconium. Interestingly, freeze-dried meconium showed a better DNA extraction efficiency than fresh meconium, possibly because freeze-dried meconium is homogeneous. Then, 30 mg freeze-dried meconium was chosen in the final protocol.

Freezing Pretreatment Affects Meconium DNA Extraction Efficiency

Accidentally, we observed that freezing meconium in lysis buffer can increase the DNA yield. Because some physical treatments (van Burik et al., 1998; Salonen et al., 2010) can improve the efficiency of DNA extraction more obviously than chemical treatments (Rohland and Hofreiter, 2007), the observational improvement encouraged the following experimental designs to test the effects of freezing time, freezing temperature, thawing conditions, and freeze-thaw cycles on the DNA extraction efficiency.

Freezing Time for Meconium

To determine the appropriate time for meconium freezing, two freezing temperatures of −20 and −80°C were assessed in both fresh and freeze-dried meconium at times ranging from 0 to 48 h. The results showed that the DNA extraction efficiency of the frozen samples was generally higher than that of the control, and the efficiency at −20°C was higher than that at −80°C. Similar time trends for the changed DNA extraction efficiencies were observed for the two freezing temperatures (**Supplementary Figure S5**). When the meconium lysis cocktails were frozen from 1 to 6 h, the efficiency was significantly improved, implying that the meconium lysis cocktails were fully lysed to release DNA and that the PCR inhibitors were inactive after freezing (Patton et al., 2007; Yadava et al., 2008).

[1]http://www.omicsmart.com

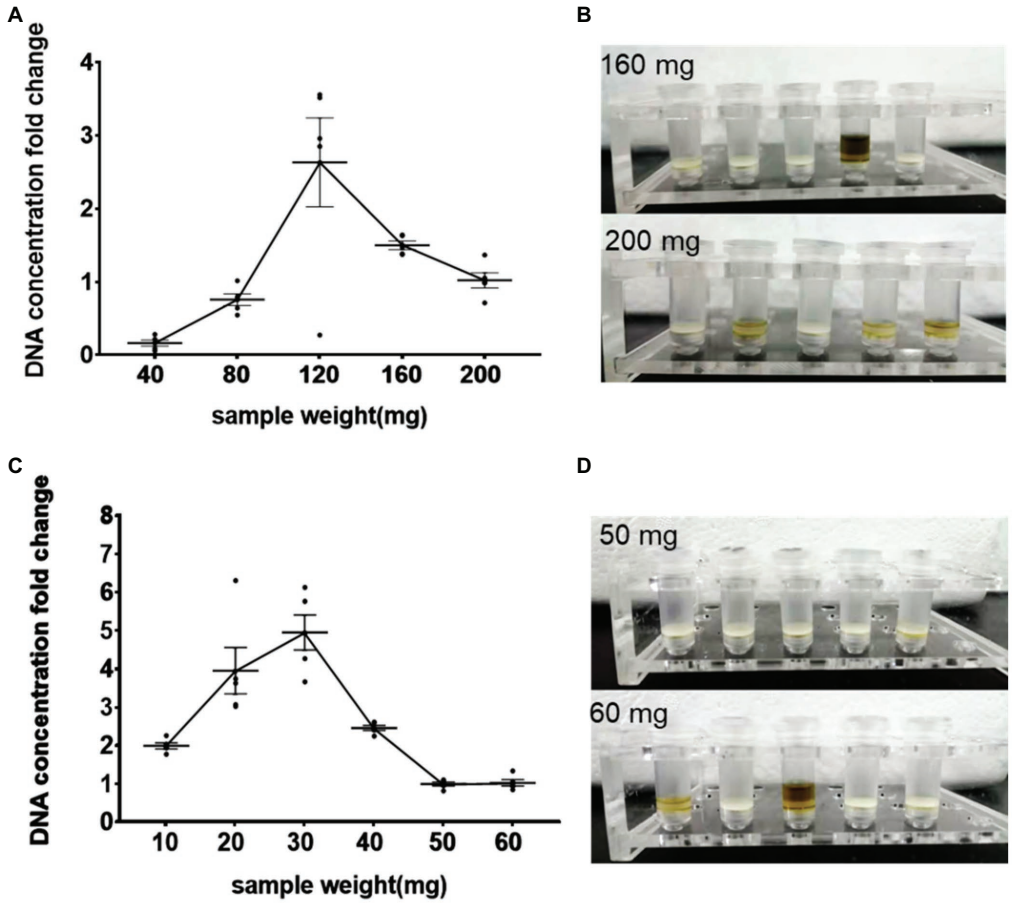

FIGURE 1 | Effects of meconium status and loading amount on DNA extraction efficiency. **(A)** DNA concentration (fold change) vs. fresh meconium loading amount (mg); **(B)** Columns could be blocked by overloaded fresh samples (loading with 160 and 200 mg after centrifugation); **(C)** DNA concentration (fold change) vs. freeze-dried meconium loading amount (mg); **(D)** Columns could be blocked by overloaded freeze-dried samples (loading with 50 mg and 60 mg after centrifugation). The results are presented as the average of five duplicates ± SEM. The corresponding data were shown in **Supplementary Table S2**.

From 6 to 24 h, the extraction efficiency tended to be stable, while the efficiency slightly decreased when the samples were frozen for longer than 24 h. These results further proved that freezing treatments could improve DNA extraction efficiency. Regarding the time cost, 6 h was selected for the freezing time in the final protocol.

Different Thawing Operations

Regarding thawing operations for the frozen meconium with the different protocols (immediate or gradient thawing) and for the different freezing patterns (freezing at −20°C or −80°C, or in liquid nitrogen), the DNA extraction efficiency changed significantly according to a comparison with the reference protocol (**Figure 2**; **Supplementary Table S3**). Among all immediately thawed meconium samples, the DNA extraction efficiencies for samples frozen at −20 and −80°C were much higher than those for samples frozen in liquid nitrogen; however, all freezing patterns can improve the efficiency compared to the reference (**Figure 2A**). These data suggested that freezing meconium at any investigated temperature with immediate thawing can enhance DNA extraction, and freezing at −20 and −80°C was more efficient than freezing in liquid nitrogen.

Combining the factor of immediate or gradient thawing, the DNA extraction efficiency of gradient thawing was significantly lower than that of immediate thawing for meconium frozen at −20°C (**Figure 2B**). Similarly, meconium frozen at −80°C had a similar trend to that frozen at −20°C, where the DNA yields with gradient thawing were obviously lower than those with immediate thawing (**Figure 2C**). However, for meconium frozen in liquid nitrogen, both immediate and gradient thawing had nearly the same efficiency for DNA extraction (**Figure 2D**).

The above results demonstrated that freezing pretreatments can improve DNA extraction efficiency. The immediate thaw operation has better extraction efficiency than gradient thawing. The liquid nitrogen freezing groups had significantly lower DNA extraction efficiencies than the other two freezing groups. We suspected that −20 and −80°C were the proper temperatures to facilitate DNA release and avoid DNA breaking in the meconium matrix. Therefore, the immediate thawing operation was selected for the final protocol.

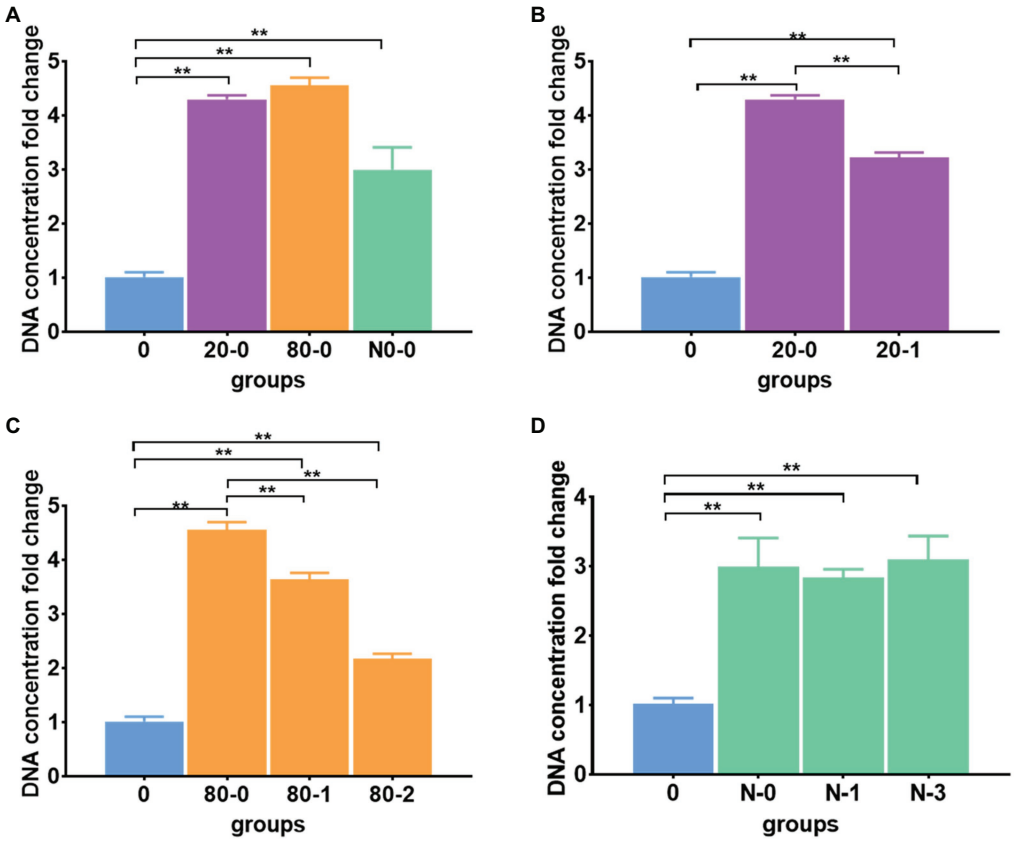

FIGURE 2 | Different thawing protocols affected DNA extraction efficiency. **(A)** The DNA extraction efficiencies for immediately thawed meconium frozen at −20 and −80°C and in liquid nitrogen; **(B)** The DNA extraction efficiencies for immediately thawed and gradient thawed meconium frozen at −20°C; **(C)** The DNA extraction efficiencies for immediately thawed and gradient thawed meconium frozen at −80°C; **(D)** The DNA extraction efficiencies for immediately thawed and gradient thawed meconium frozen in liquid nitrogen. The corresponding data were shown in **Supplementary Table S3**. $^{**}P < 0.01$.

Different Freezing Patterns

When comparing the different freezing temperatures (**Figure 2A**), both −20 and −80°C-frozen meconium samples showed significantly improved DNA yields after immediate thawing (**Supplementary Table S4**). In addition to the thawing operation, freezing by immediate and gradient cooling to −80°C and liquid nitrogen conditions were assessed (**Figure 3A**). The results showed that immediately cooling down to −80°C can result in a better improvement than gradient cooling (**Figure 3B**); however, immediate cooling in the liquid nitrogen condition showed no difference with gradient cooling in terms of the DNA extraction efficiency (**Figure 3C**), which implied that the temperature of freezing in liquid nitrogen was too low to damage the yield of DNA. Instead, the results suggested that freezing at −20 and −80°C was sufficient to improve DNA yields, and immediate cooling was better than gradient cooling.

Freeze-Thaw Duplication

The DNA extraction efficiencies of repeated freeze-thaw operations were investigated (**Supplementary Table S5**). For each freeze-thaw cycle, immediate cooling and thawing were carried out. For all freezing conditions of cooling to −20 and −80°C and freezing in liquid nitrogen, the DNA extraction efficiencies increased with freeze-thaw cycle number (**Figures 4A–C**). When comparing the freezing temperature-dependent efficiencies at each cycle (**Figures 4D–F**), the highest efficiency was achieved −20°C freeze-thaw operation after the 3rd cycle.

All data showed that freeze-thaw operation can improve the DNA extraction efficiency significantly, which may be due to the multiple freeze-thaw cycles that can result in the meconium lysis cocktails being completely lysed to release DNA. In addition to the total DNA extraction efficiency, bacterial DNA abundance in meconium and their stability during the investigated protocols are key to relating the final detection rate of PCR analysis (Patton et al., 2007; Yadava et al., 2008; Zhang et al., 2008; Chen et al., 2018).

Bacterial DNA Abundance and Freezing Temperature Related Sequencing

Six different meconium samples were sequenced for their 16S rDNA by reference DNA extraction (0) and six other protocols (20I: one freeze-thaw cycle at −20°C, 20III: three freeze-thaw cycles at −20°C, 80I: one freeze-thaw cycle at −80°C, 80III: three freeze-thaw cycles at −80°C, NI: one freeze-thaw cycle in liquid nitrogen, and NIII: three freeze-thaw cycles in liquid

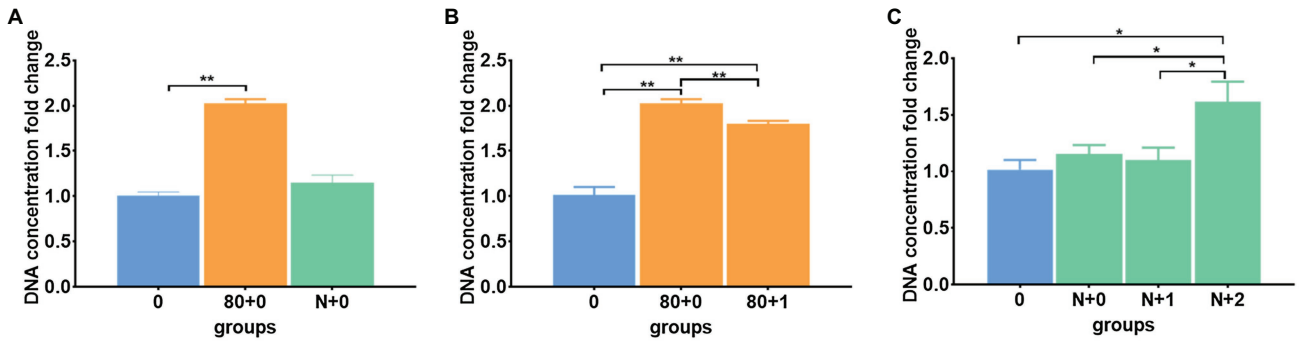

FIGURE 3 | Different freezing patterns affected DNA extraction efficiency. **(A)** The DNA extraction efficiencies in the immediate freezing groups; **(B)** The DNA extraction efficiencies in the immediate and gradient freezing groups when samples were frozen at −80°C; **(C)** The DNA extraction efficiencies in the immediate and gradient freezing groups when samples were frozen in liquid nitrogen. The corresponding data were shown in **Supplementary Table S4**. $^{*}P < 0.05$, $^{**}P < 0.01$.

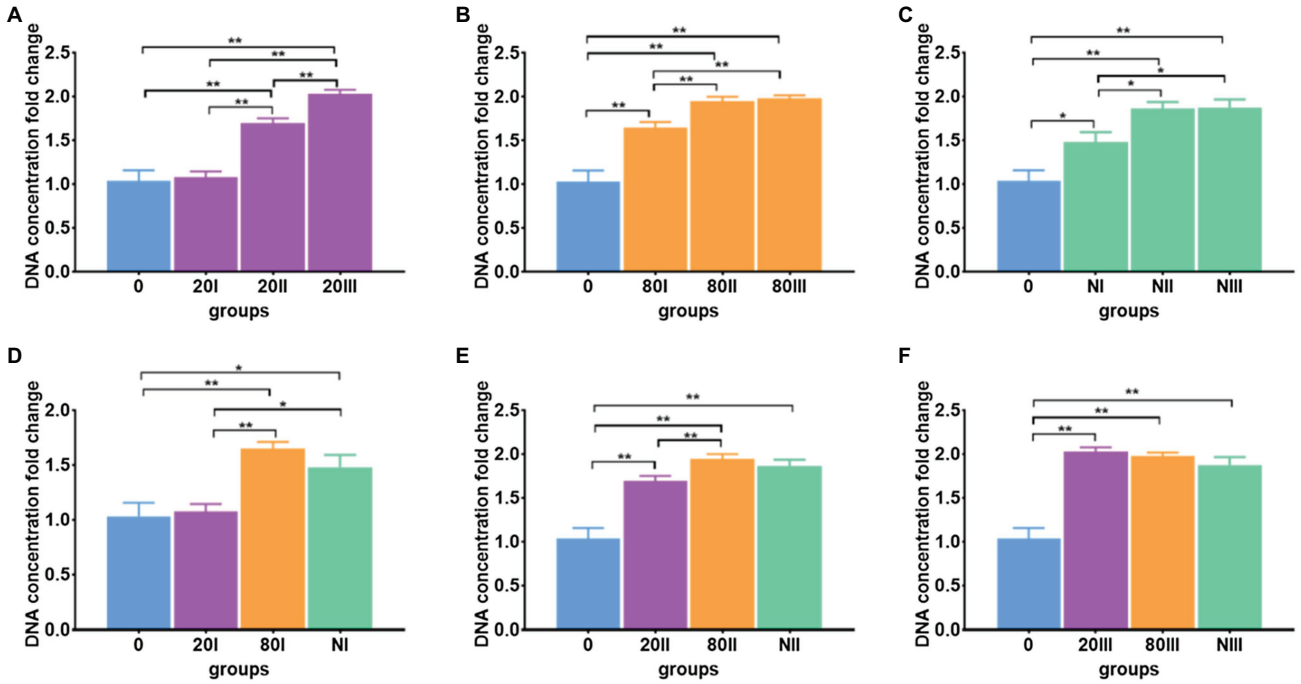

FIGURE 4 | Freeze-thaw cycle number-dependent DNA extraction efficiency. **(A)** The freeze-thaw cycle-dependent DNA extraction efficiency for meconium frozen at −20°C; **(B)** The freeze-thaw cycle-dependent DNA extraction efficiency for meconium frozen at −80°C; **(C)** Freeze-thaw cycle-dependent DNA extraction efficiency for meconium frozen in liquid nitrogen; **(D)** The DNA extraction efficiencies with one freeze-thaw cycle; **(E)** The DNA extraction efficiencies with two freeze-thaw cycles; **(F)** The DNA extraction efficiencies with three freeze-thaw cycles. The corresponding data were shown in **Supplementary Table S5**. $^{*}P < 0.05$, $^{**}P < 0.01$.

nitrogen) at different freezing temperatures, and freeze-thaw cycles were applied. The positive detection of meconium samples A, B, C, D, E, and F from high to low rates was 6 (B), 6 (E), 4 (F), 2 (D), 2 (A), and 1 (C). The PCR sequencing method has equal sensitivity to the different extraction protocol-treated samples. Meconium B and E can be sequenced positively by six protocols (**Figure 5**) except the NI protocol, which implied that B and E have the most abundant bacterial DNA and can meet 16S rDNA sequencing requirements for low or high DNA extraction efficiencies. However, meconium C can only be sequenced by protocol 20III (C20III), which has the highest DNA extraction efficiency (**Figures 4A,F**). Therefore, meconium C may have the lowest bacterial DNA abundance among the six samples. Meconium A can be sequenced by protocols 20I (A20I) and NIII, which may imply that bacterial DNA in A is slightly higher than that in C. Samples F and D may have bacterial DNA abundance levels lower than those in B and E because both D and F can be sequenced when treated by protocols 20I and 20III. In addition, meconium F can be sequenced by the protocol of 80I (F80I) and NIII (FNIII), which may imply that the level of bacterial DNA in F was slightly higher than that in D. In summary, the bacterial DNA levels from high to

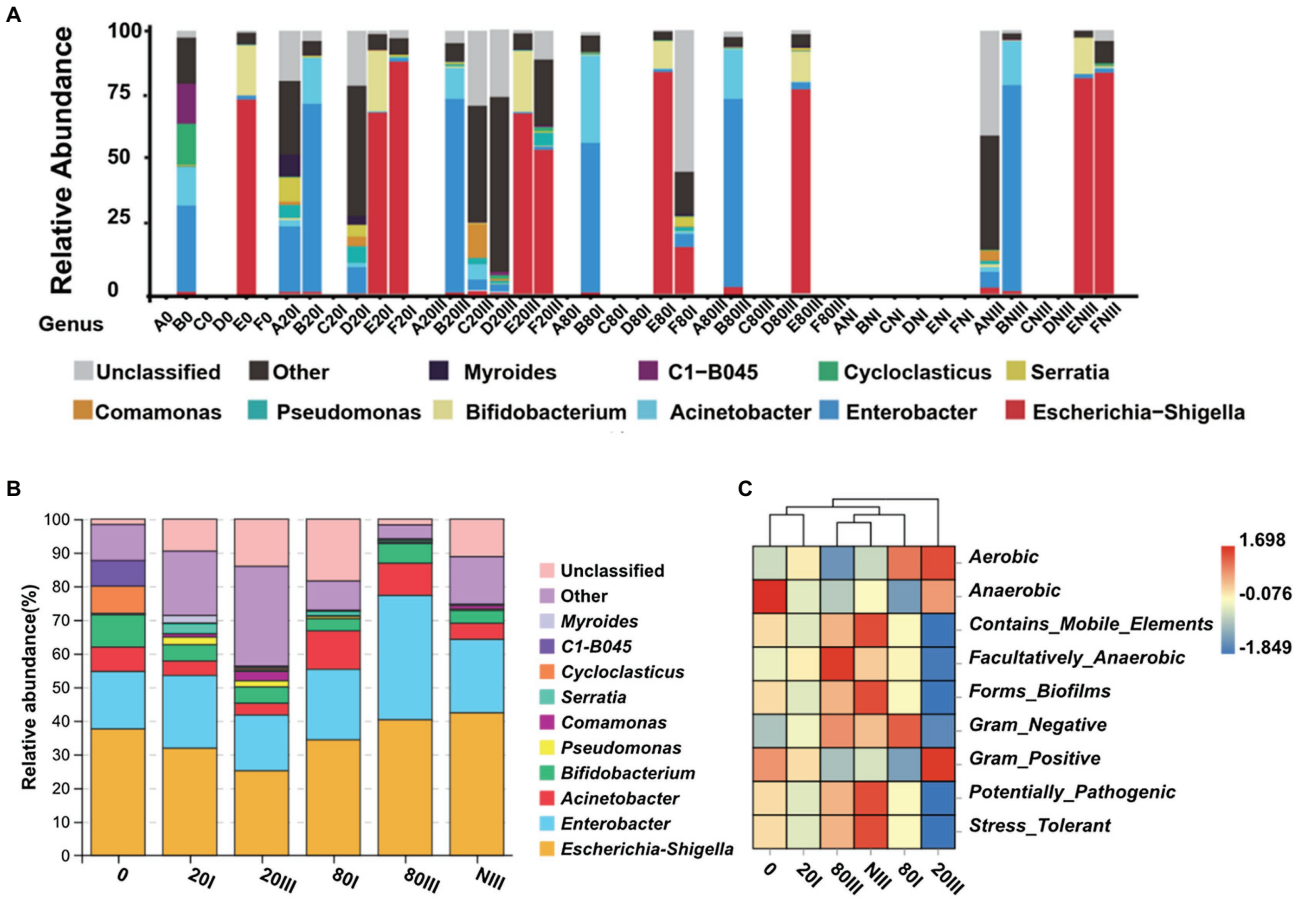

FIGURE 5 | Relative abundance and functional prediction of bacteria at the genus level. **(A)** The relative abundance of bacterial DNA at the genus level from the perspective of sample. A0–F0: Two (B and E) of six samples could be positively sequenced for bacterial DNA by the reference protocol; A20I–F20I: Five (A, B, D, E, and F) of six samples could be positively sequenced for bacterial DNA with a one-cycle −20°C freeze-thaw protocol; A20III–F20III: Five (B, C, D, E, and F) of six samples could be positively sequenced for bacterial DNA with a three-cycle −20°C freeze-thaw protocol; A80I–F80I: Three (B, E, and F) of six samples could be positively sequenced for bacterial DNA with a one-cycle −80°C freeze-thaw protocol; A80III–F80III: Two (B and E) of six samples could be positively sequenced for bacterial DNA with a three-cycle −80°C freeze-thaw protocol; ANI–FNI: No samples could be positively sequenced for bacterial DNA with a one-cycle liquid nitrogen freeze-thaw protocol; ANIII–FNIII: Four (A, B, E, and F) of six samples could be positively sequenced for bacterial DNA with a three-cycle liquid nitrogen freeze-thaw protocol; **(B)** The relative abundance of bacterial DNA at the genus level from the perspective of group; **(C)** Functional prediction of bacterial DNA among five pretreated groups.

low in these samples were B≈E>F≥D>A≈C. At the median levels of bacteria, a −20°C freeze-thaw cycle could improve the DNA extraction efficiency.

Meconium can be sequenced not only because of its bacterial DNA abundance but also because of its DNA extraction efficiency and stability during the protocol. The positive detection of all meconium samples for the 0, 20I, 20III, 80I, 80III, NI, and NIII protocols from the high to low rates was 5 (20I), 5 (20III), 4 (NIII), 3 (80I), 2 (80III), 2 (0), and 0 (NI), respectively (**Figure 5**). Among all one cycle freeze-thaw protocols, the DNA extraction efficiencies of 80I and NI were higher than those of 20I (**Figure 4D**). However, five of six samples could be sequenced positively by the 20I protocol, and no sample could be sequenced by the NI protocol. These results suggested that too low of a freezing temperature may damage the bacterial DNA for sequencing. The DNA extraction efficiencies of all three freeze-thaw cycles were almost equal. However, the samples sequenced from high to low were 20III>NIII>80III. These results further supported that too low of a freezing temperature may damage bacterial DNA sequencing. When comparing their DNA extraction efficiencies (**Figures 4A–D**), three freeze-thaw cycles were higher than one freeze-thaw cycle. However, five of six samples could be sequenced positively by both 20I and 20III protocols, which implied that 20I and 20III were the most effective protocols for sample sequencing. The meconium C with the lowest bacterial DNA abundance could only be sequenced by pretreatment with the 20III protocol, which implied that 20III was more effective than 20I. Regardless, illustrating that meconium A can be sequenced by 20I and NIII but not by 20III is difficult. In summary, the protocol with −20°C pretreatment showed the highest rates of bacterial DNA sequencing, and the reference and liquid nitrogen pretreatment protocols showed the lowest rates. Therefore, −20°C was the best pretreatment temperature.

The microbial species diversity at the genus level was different according to the different DNA extraction protocols. The number

TABLE 1 | The genus numbers measured in each group.

Sample/protocol	0	20I	20III	80I	80III	NI	NIII
A	/	196	/	/	/	/	117
B	131	145	188	122	95	/	93
C	/	/	237	/	/	/	/
D	/	139	172	/	/	/	/
E	80	195	188	128	131	/	98
F	/	188	201	156	/	/	125

*Meconium samples and the related DNA extraction protocols are marked by using the same codes as in **Figure 5**.*

of genera was calculated on the fully profiled bacterial DNA in meconium A, B, C, D, E, and F (**Figure 5A**), which is listed in **Table 1** and visualized in **Supplementary Figures S6A–D**. All results indicated that pretreatment at −20°C yielded the highest genera, which was additional evidence that −20°C was the best choice, possibly because −20°C has more influence on DNA integration than −80°C, and temperatures that are too low could break some bacterial DNA with high genera diversity (**Supplementary Figures S6A–E**); however, the destructiveness of organic tissue at −3 to −10°C (Khan and Vincent, 1996; Bortolin et al., 2017) may have been reduced. When comparing the genera numbers between the 20I and 20III pretreatment groups, the 20III was higher than 20I in samples B, D, and F but the 20I was higher than 20III in samples E. Generally, pretreatment of three freeze-thaw cycles at −20°C can retain the highest DNA genera diversity, and this may be the optimal protocol to extract meconium. Analyses of α diversity further confirmed the above conclusion, which showed 20I generated the highest DNA genera diversity, followed by 20III, while α diversity was almost equal between 80I and 80III (**Supplementary Figure S8**). Species analysis presented that 20III dominated by other genera (29.64%), *Escherichia-Shigella* (25.16%), and *Enterobacter* (16.53%), while control group was dominated by *Escherichia-Shigella* (37.56%), *Enterobacter* (17.07%), and other genera (10.76%) (**Figure 5B**). These results partially confirmed the conclusions conducted by Stinson et al. (2019), and the relatively high abundance of other genera in 20III group indicated freeze-thaw pretreatment would be beneficial to the release of low abundance bacterial DNA. And by utilizing this protocol, the relative abundances of genera of *Akkermansia* ($p=0.047$), *Ruminococcus* ($p=0.010$), *Acidipila* ($p=0.011$), and *Caulobacter* ($p<0.001$) were significantly higher comparing with the 20I group, while no genus was detected to be decreased in our study according to Wilcoxon analysis. In addition, the major effects of 20III pretreatment was shown to be associated with the increased diversity of aerobic, anaerobic, and Gram-positive bacteria, which was hypothesized that the freeze-thaw method mainly promoted the release of bacterial DNA with such characteristics (**Figure 5C**).

However, several limitations of this research are noted. One is that DNA-based assessments of low microbial biomass samples are extremely prone to confounding findings from contaminant DNA. Despite the rigorous sterile operations were adopted, bacterial DNA from reagents, consumables, and components of DNA extraction kits may not be avoided, which may affect the reliability of our results (Tanner et al., 1998; Grahn et al., 2003; Mühl et al., 2010). The other limitation is that our conclusions were largely based on the macroscopic descriptions. The specific mechanisms for enhancing the DNA extraction efficiency by freeze-thaw pretreatment were unexplored, as well as rare in the previous researches. Therefore, explaining these mechanisms was urgently demanded, and that could be one of the future research directions.

CONCLUSION

Microbial DNA in meconium was difficult to extract using general commercial stool DNA extract kits due to the extremely low microbial biomass. The amplification rate of extracted DNA from meconium is usually approximately 10–52.9% (Ardissone et al., 2014; Hansen et al., 2015). In this assay, we found that freeze-thaw recycling pretreatment can enhance the efficiency of bacterial DNA extraction from meconium, and an improved protocol was developed and verified using the commercial QIAamp® Fast DNA Stool Mini Kit (cat. no. 51604).

Finally, we concluded that (1) 30 mg lyophilized meconium was the optimal amount for DNA extraction. (2) Lysis cocktail freezing can improve DNA extraction efficiency, with 6 h being a suitable freezing time. (3) To improve DNA extraction efficiency, thawing the frozen lysis cocktail immediately is better than thawing gradually; similarly, freezing the lysis cocktail immediately is better than freezing gradually. (4) Regarding freezing temperatures, −20°C better maintains the stability of bacterial DNA than at −80°C and liquid nitrogen. (5) Finally, we suggested that three cycles of freeze-thaw treatment of the meconium lysis cocktail at −20°C can markedly increase the bacterial DNA extraction amount and genus diversity. In summary, this work offers a protocol to enhance meconium bacterial DNA extraction, which may be helpful to promote the study of foetal and/or newborn microbiome exposure.

DATA AVAILABILITY STATEMENT

The raw data of 16S rRNA sequence used in this study have been deposited at NCBI database under the accession number of PRJNA759695.

ETHICS STATEMENT

The studies involving human participants were reviewed and approved by the Ethics Committee of the Xiamen

Maternity and Child Health Care Hospital (XMCH), Xiamen, China. Written informed consent to participate in this study was provided by the participants' legal guardian/next of kin.

AUTHOR CONTRIBUTIONS

YXin, JX, BN, CT, QW, YXia, and YL designed and performed the experiments and analyzed the data. YXin wrote the original manuscript. HS and XZ designed the study and edited the manuscript. All authors contributed to the article and approved the submitted version.

FUNDING

This work was financially supported by the Xiamen Medical and Health Project (Instructional Project; No. 3502Z20189050), Xiamen Medical and Health Key Project (No. 3502Z20191102), and Xiamen Science and Technology Plan Project (No. 3502Z20199138).

SUPPLEMENTARY MATERIAL

The Supplementary Material for this article can be found online at: https://www.frontiersin.org/articles/10.3389/fmicb.2021.753688/full#supplementary-material

REFERENCES

Al-Soud, W. A., Ouis, I. S., Li, D. Q., Ljungh, S., and Wadström, T. (2005). Characterization of the PCR inhibitory effect of bile to optimize real-time PCR detection of helicobacter species. *FEMS Immunol. Med. Microbiol.* 44, 177–182. doi: 10.1016/j.femsim.2004.12.004

Ardissone, A. N., de la Cruz, D. M., Davis-Richardson, A. G., Rechcigl, K. T., Li, N., Drew, J. C., et al. (2014). Meconium microbiome analysis identifies bacteria correlated with premature birth. *PLoS One* 9:e90784. doi: 10.1371/journal.pone.0090784

Aron-Wisnewsky, J., and Clément, K. (2016). The gut microbiome, diet, and links to cardiometabolic and chronic disorders. *Nat. Rev. Nephrol.* 12, 169–181. doi: 10.1038/nrneph.2015.191

Bäckhed, F., Ley, R. E., Sonnenburg, J. L., Peterson, D. A., and Gordon, J. I. (2005). Host-bacterial mutualism in the human intestine. *Science* 307, 1915–1920. doi: 10.1126/science.1104816

Bearer, C. F. (2003). Meconium as a biological marker of prenatal exposure. *Ambul. Pediatr.* 3, 40–43. doi: 10.1367/1539-4409(2003)003<0040:MAABMO>2.0.CO;2

Biagi, E., Rampelli, S., Turroni, S., Quercia, S., Candela, M., and Brigidi, P. (2017). The gut microbiota of centenarians: signatures of longevity in the gut microbiota profile. *Mech. Ageing Dev.* 165, 180–184. doi: 10.1016/j.mad.2016.12.013

Bortolin, R. C., Gasparotto, J., Vargas, A. R., da Silva Morrone, M., Kunzler, A., Henkin, B. S., et al. (2017). Effects of freeze-thaw and storage on enzymatic activities, protein oxidative damage, and immunocontent of the blood, liver, and brain of rats. *Biopreserv. Biobank.* 15, 182–190. doi: 10.1089/bio.2016.0023

Buffie, C. G., Bucci, V., Stein, R. R., McKenney, P. T., Ling, L., Gobourne, A., et al. (2015). Precision microbiome reconstitution restores bile acid mediated resistance to Clostridium difficile. *Nature* 517, 205–208. doi: 10.1038/nature13828

Chen, Q., Xie, Y., Xi, J., Guo, Y., Qian, H., Cheng, Y., et al. (2018). Characterization of lipid oxidation process of beef during repeated freeze-thaw by electron spin resonance technology and Raman spectroscopy. *Food Chem.* 243, 58–64. doi: 10.1016/j.foodchem.2017.09.115

Deriu, E., Boxx, G. M., He, X., Pan, C., Benavidez, S. D., Cen, L., et al. (2016). Influenza virus affects intestinal microbiota and secondary salmonella infection in the gut through type I interferons. *PLoS Pathog.* 12:e1005572. doi: 10.1371/journal.ppat.1005572

Eckburg, P. B., Bik, E. M., Bernstein, C. N., Purdom, E., Dethlefsen, L., Sargent, M., et al. (2005). Diversity of the human intestinal microbial flora. *Science* 308, 1635–1638. doi: 10.1126/science.1110591

Forsythe, P., Kunze, W., and Bienenstock, J. (2016). Moody microbes or fecal phrenology: what do we know about the microbiota-gut-brain axis? *BMC Med.* 14:58. doi: 10.1186/s12916-016-0604-8

Gensollen, T., Iyer, S. S., Kasper, D. L., and Blumberg, R. S. (2016). How colonization by microbiota in early life shapes the immune system. *Science* 352, 539–544. doi: 10.1126/science.aad9378

Grahn, N., Olofsson, M., Ellnebo-Svedlund, K., Monstein, H. J., and Jonasson, J. (2003). Identification of mixed bacterial DNA contamination in broad-range PCR amplification of 16S rDNA V1 and V3 variable regions by pyrosequencing of cloned amplicons. *FEMS Microbiol. Lett.* 19, 87–91. doi: 10.1016/S0378-1097(02)01190-4

Guo, H. (2014). Comparative analysis of fecal microbiota of full-term infants born with different methods of delivery. dissertation/doctor's thesis. Beijing: Chinese PLA Medical School.

Hansen, R., Scott, K. P., Khan, S., Martin, J. C., Berry, S. H., Stevenson, M., et al. (2015). First-pass meconium samples from healthy term vaginally-delivered neonates: an analysis of the microbiota. *PLoS One* 10:e0133320. doi: 10.1371/journal.pone.0133320

Harries, J. T. (1978). Meconium in health and disease. *Br. Med. Bull.* 34, 75–78. doi: 10.1093/oxfordjournals.bmb.a071462

Hooper, L. V., and Gordon, J. I. (2001). Commensal host-bacterial relationships in the gut. *Science* 292, 1115–1118. doi: 10.1126/science.1058709

Jiménez, E., Marín, M. L., Martín, R., Odriozola, J. M., Olivares, M., Xaus, J., et al. (2008). Is meconium from healthy newborns actually sterile? *Res. Microbiol.* 159, 187–193. doi: 10.1016/j.resmic.2007.12.007

Karlsson, K. A., and Larson, G. (1978). Molecular characterization of cell-surface antigens of human fetal tissue: meconium, a rich source of epithelial blood-group glycolipids. *FEBS Lett.* 87, 283–287. doi: 10.1016/0014-5793(78)80352-4

Khan, A., and Vincent, J. F. V. (1996). Mechanical damage induced by controlled freezing in apple and potato. *J. Texture Stud.* 27, 143–157. doi: 10.1111/j.1745-4603.1996.tb00065.x

Lisowska-Myjak, B., and Pachecka, J. (2006). Trypsin and antitrypsin activities and protein concentration in serial meconium and feces of healthy newborns. *J. Matern. Fetal Neonatal Med.* 19, 477–482. doi: 10.1080/14767050600746720

Lisowska-Myjak, B., and Pachecka, J. (2007). Alpha-1-antitrypsin and IgA in serial meconium and faeces of healthy breast-fed newborns. *Fetal Diagn. Ther.* 22, 116–120. doi: 10.1159/000097108

Loscalzo, J. (2013). Gut microbiota, the genome, and diet in atherogenesis. *N. Engl. J. Med.* 368, 1647–1649. doi: 10.1056/NEJMe1302154

Mshvildadze, M., Neu, J., Shuster, J., Theriaque, D., Li, N., and Mai, V. (2010). Intestinal microbial ecology in premature infants assessed with non-culture-based techniques. *J. Pediatr.* 156, 20–25. doi: 10.1016/j.jpeds.2009.06.063

Mühl, H., Kochem, A. J., Disqué, C., and Sakka, S. G. (2010). Activity and DNA contamination of commercial polymerase chain reaction reagents for the universal 16S rDNA real-time polymerase chain reaction detection of bacterial pathogens in blood. *Diagn. Microbiol. Infect. Dis.* 66, 41–49. doi: 10.1016/j.diagmicrobio.2008.07.011

Nagpal, R., Tsuji, H., Takahashi, T., Kawashima, K., Nagata, S., Nomoto, K., et al. (2016). Sensitive quantitative analysis of the meconium bacterial microbiota in healthy term infants born vaginally or by cesarean section. *Front. Microbiol.* 7:1997. doi: 10.3389/fmicb.2016.01997

O'Callaghan, T. F., Ross, R. P., Stanton, C., and Clarke, G. (2016). The gut microbiome as a virtual endocrine organ with implications for farm and domestic animal endocrinology. *Domest. Anim. Endocrinol.* 56, S44–S55. doi: 10.1016/j.domaniend.2016.05.003

Pallem, V., Kaviratna, A. S., Chimote, G., and Banerjee, R. (2010). Effect of meconium on surface properties of surfactant monolayers and liposomes. *Colloid. Surface. A* 370, 6–14. doi: 10.1016/j.colsurfa.2010.08.002

Patton, A. J., Cunningham, S. M., Volenec, J. J., and Reicher, Z. J. (2007). Differences in freeze tolerance of zoysiagrasses: ii. Carbohydrate and proline accumulation. *Crop Sci.* 47, 2170–2181. doi: 10.2135/cropsci2006.12.0784

Perez-Muñoz, M. E., Arrieta, M. C., Ramer-Tait, A. E., and Walter, J. (2017). A critical assessment of the "sterile womb" and "in utero colonization" hypotheses: implications for research on the pioneer infant microbiome. *Microbiome* 5:48. doi: 10.1186/s40168-017-0268-4

Qian, L. L., Li, H. T., Zhang, L., Fang, Q. C., and Jia, W. P. (2015). Effect of the gut microbiota on obesity and its underlying mechanisms: an update. *Biomed. Environ. Sci.* 28, 839–847. doi: 10.1016/S0895-3988(15)30116-1

Rohland, N., and Hofreiter, M. (2007). Comparison and optimization of ancient DNA extraction. *Biotechniques* 42, 343–352. doi: 10.2144/000112383

Salonen, A., Nikkilä, J., Jalanka-Tuovinen, J., Immonen, O., Rajilić-Stojanović, M., Kekkonen, R. A., et al. (2010). Comparative analysis of fecal DNA extraction methods with phylogenetic microarray: effective recovery of bacterial and archaeal DNA using mechanical cell lysis. *J. Microbiol. Methods* 81, 127–134. doi: 10.1016/j.mimet.2010.02.007

Schrader, C., Schielke, A., Ellerbroek, L., and Johne, R. (2012). PCR inhibitors—occurrence, properties and removal. *J. Appl. Microbiol.* 113, 1014–1026. doi: 10.1111/j.1365-2672.2012.05384.x

Stinson, L. F., Boyce, M. C., Payne, M. S., and Keelan, J. A. (2019). The not-so-sterile womb: evidence that the human fetus is exposed to bacteria prior to birth. *Front. Microbiol.* 10:1124. doi: 10.3389/fmicb.2019.01124

Stinson, L. F., Keelan, J. A., and Payne, M. S. (2018). Comparison of meconium DNA extraction methods for use in microbiome studies. *Front. Microbiol.* 9:270. doi: 10.3389/fmicb.2018.00270

Sun, B., Curstedt, T., and Robertson, B. (1993). Surfactant inhibition in experimental meconium aspiration. *Acta Paediatr.* 82, 182–189. doi: 10.1111/j.1651-2227.1993.tb12635.x

Sundman, M. H., Chen, N. K., Subbian, V., and Chou, Y. H. (2017). The bidirectional gut-brain-microbiota axis as a potential nexus between traumatic brain injury, inflammation, and disease. *Brain Behav. Immun.* 66, 31–44. doi: 10.1016/j.bbi.2017.05.009

Tanner, M. A., Goebel, B. M., Dojka, M. A., and Pace, N. R. (1998). Specific ribosomal DNA sequences from diverse environmental settings correlate with experimental contaminants. *Appl. Environ. Microbiol.* 64, 3110–3113. doi: 10.1128/AEM.64.8.3110-3113.1998

Tapiainen, T., Paalanne, N., Tejesvi, M. V., Koivusaari, P., Korpela, K., Pokka, T., et al. (2018). Maternal influence on the fetal microbiome in a population-based study of the first-pass meconium. *Pediatr. Res.* 84, 371–379. doi: 10.1038/pr.2018.29

van Burik, J. A., Schreckhise, R. W., White, T. C., Bowden, R. A., and Myerson, D. (1998). Comparison of six extraction techniques for isolation of DNA from filamentous fungi. *Med. Mycol.* 36, 299–303. doi: 10.1046/j.1365-280X.1998.00161.x

Villanueva, M. E., Svinarich, D. M., Gonik, B., and Ostrea, E. M. (2000). Detection of cytomegalovirus in the meconium of infected newborns by polymerase chain reaction. *Infect. Dis. Obstet. Gynecol.* 8, 166–171. doi: 10.1002/1098-0997(2000)8:3/4<166::AID-IDOG12>3.0.CO;2-X

Wampach, L., Heintz-Buschart, A., Hogan, A., Muller, E. E. L., Narayanasamy, S., Laczny, C. C., et al. (2017). Colonization and succession within the human gut microbiome by archaea, bacteria, and microeukaryotes during the first year of life. *Front. Microbiol.* 8:738. doi: 10.3389/fmicb.2017.00738

Willis, K. A., Purvis, J. H., Myers, E. D., Aziz, M. M., Karabayir, I., Gomes, C. K., et al. (2019). Fungi form interkingdom microbial communities in the primordial human gut that develop with gestational age. *FASEB J.* 33, 12825–12837. doi: 10.1096/fj.201901436RR

Yadava, P., Gibbs, M., Castro, C., and Hughes, J. A. (2008). Effect of lyophilization and freeze-thawing on the stability of siRNA-liposome complexes. *AAPS PharmSciTech* 9, 335–341. doi: 10.1208/s12249-007-9000-1

Zhang, L., Li, P., Li, D., Guo, S., and Wang, E. (2008). Effect of freeze-thawing on lipid bilayer-protected gold nanoparticles. *Langmuir* 24, 3407–3411. doi: 10.1021/la703737q

Conflict of Interest: The authors declare that the research was conducted in the absence of any commercial or financial relationships that could be construed as a potential conflict of interest.

Publisher's Note: All claims expressed in this article are solely those of the authors and do not necessarily represent those of their affiliated organizations, or those of the publisher, the editors and the reviewers. Any product that may be evaluated in this article, or claim that may be made by its manufacturer, is not guaranteed or endorsed by the publisher.

frontiers | Frontiers in Microbiology

ORIGINAL RESEARCH
published: 19 April 2022
doi: 10.3389/fmicb.2022.826487

Ginsenoside Rb1 Improves Metabolic Disorder in High-Fat Diet-Induced Obese Mice Associated With Modulation of Gut Microbiota

Hong Zou[1,2], Man Zhang[3], Xiaoting Zhu[4], Liyan Zhu[4], Shuo Chen[5], Mingjing Luo[5], Qinglian Xie[2], Yue Chen[3], Kangxi Zhang[3], Qingyun Bu[3], Yuchen Wei[6], Tao Ye[4], Qiang Li[7], Xing Yan[8], Zhihua Zhou[8], Chen Yang[8], Yu Li[2], Haokui Zhou[5], Chenhong Zhang[9]*, Xiaoyan You[3,10]*, Guangyong Zheng[11]* and Guoping Zhao[1,3,5,6,7,8,11]**

[1] State Key Laboratory of Genetic Engineering, Department of Microbiology and Immunology, School of Life Sciences, Fudan University, Shanghai, China, [2] Engineering Laboratory for Nutrition, Shanghai Institute of Nutrition and Health, Chinese Academy of Sciences, Shanghai, China, [3] Master Lab for Innovative Application of Nature Products, National Center of Technology Innovation for Synthetic Biology, Tianjin Institute of Industrial Biotechnology, Chinese Academy of Sciences, Tianjin, China, [4] Zhejiang Hongguan Bio-Pharma Co., Ltd., Jiaxing, China, [5] CAS Key Laboratory of Quantitative Engineering Biology, Shenzhen Institute of Synthetic Biology, Shenzhen Institute of Advanced Technology, Chinese Academy of Sciences, Shenzhen, China, [6] Department of Microbiology, The Chinese University of Hong Kong, Hong Kong, China, [7] Suzhou BiomeMatch Therapeutics Co., Ltd., Shanghai, China, [8] CAS-Key Laboratory of Synthetic Biology, CAS Center for Excellence in Molecular Plant Sciences, Shanghai Institute of Plant Physiology and Ecology, Chinese Academy of Sciences, Shanghai, China, [9] State Key Laboratory of Microbial Metabolism, School of Life Sciences and Biotechnology, Shanghai Jiao Tong University, Shanghai, China, [10] College of Food and Bioengineering, Henan University of Science and Technology, Luoyang, China, [11] Bio-Med Big Data Center, Shanghai Institute of Nutrition and Health, Chinese Academy of Sciences, Shanghai, China

Gut microbiota plays an important role in metabolic homeostasis. Previous studies demonstrated that ginsenoside Rb1 might improve obesity-induced metabolic disorders through regulating glucose and lipid metabolism in the liver and adipose tissues. Due to low bioavailability and enrichment in the intestinal tract of Rb1, we hypothesized that modulation of the gut microbiota might account for its pharmacological effects as well. Here, we show that oral administration of Rb1 significantly decreased serum LDL-c, TG, insulin, and insulin resistance index (HOMA-IR) in mice with a high-fat diet (HFD). Dynamic profiling of the gut microbiota showed that this metabolic improvement was accompanied by restoring of relative abundance of some key bacterial genera. In addition, the free fatty acids profiles in feces were significantly different between the HFD-fed mice with or without Rb1. The content of eight long-chain fatty acids (LCFAs) was significantly increased in mice with Rb1, which was positively correlated with the increase of *Akkermansia* and *Parasuttereller,* and negatively correlated with the decrease of *Oscillibacter* and *Intestinimonas*. Among these eight increased LCFAs, eicosapentaenoic acid (EPA), octadecenoic acids, and myristic acid were positively correlated with metabolic improvement. Furthermore, the colonic expression of the *free fatty acid receptors 4* (*Ffar4*) gene was significantly upregulated after Rb1 treatment, in response to a notable increase of LCFA in feces. These findings suggested that Rb1 likely modulated the gut microbiota and intestinal free fatty acids profiles, which

OPEN ACCESS

Edited by:
Jialiang Yang,
Geneis (Beijing) Co., Ltd., China

Reviewed by:
Xue-Song Zhang,
Rutgers, The State University of New Jersey - Busch Campus, United States
Mingxiong He,
Biogas Institute of Ministry of Agriculture (CAAS), China

***Correspondence:**
Haokui Zhou
hk.zhou@siat.ac.cn
Chenhong Zhang
zhangchenhong@sjtu.edu.cn
Xiaoyan You
youxy@tib.cas.cn
Guangyong Zheng
zhenggy@sibs.ac.cn
Guoping Zhao
gpzhao@sibs.ac.cn

Specialty section:
This article was submitted to Systems Microbiology, a section of the journal Frontiers in Microbiology

Received: *30 November 2021*
Accepted: *07 March 2022*
Published: *19 April 2022*

Citation:
Zou H, Zhang M, Zhu X, Zhu L, Chen S, Luo M, Xie Q, Chen Y, Zhang K, Bu Q, Wei Y, Ye T, Li Q, Yan X, Zhou Z, Yang C, Li Y, Zhou H, Zhang C, You X, Zheng G and Zhao G (2022) Ginsenoside Rb1 Improves Metabolic Disorder in High-Fat Diet-Induced Obese Mice Associated With Modulation of Gut Microbiota. Front. Microbiol. 13:826487. doi: 10.3389/fmicb.2022.826487

should be beneficial for the improvement of metabolic disorders in HFD-fed mice. This study provides a novel mechanism of Rb1 for the treatment of metabolic disorders induced by obesity, which may provide a therapeutic avenue for the development of new nutraceutical-based remedies for treating metabolic diseases, such as hyperlipidemia, insulin resistance, and type 2 diabetes.

Keywords: ginsenoside Rb1, metabolic disorder, gut microbiota, long-chain fatty acids, free fatty acid receptor, lipidomics, fecal metabolome

INTRODUCTION

The prevalence of obesity and related comorbidities continues to rise worldwide. The prevention and treatment of obesity and its metabolic complications remain a major public health concern.

Gut microbiota plays an important role in the development of obesity with related hyperlipidemia and diabetic symptoms (Festi et al., 2014). Intestinal microbes affect nutrient acquisition and energy regulation of the host (Kimura et al., 2013). Gut microbiota dysbiosis damages the intestinal epithelial barrier and intestinal mucosal immunity, which leads to insulin resistance and inflammation (Paone and Cani, 2020). Thus, modulating the gut microbiota may be an effective strategy for the treatment of obesity and related metabolic disorders.

Metabolomic analysis can deepen the understanding of host-microbe interactions (Heinken and Thiele, 2015). The fecal metabolome investigates the outcomes of the metabolic interactions among diet, gut microbiota and host through analyzing the remaining unabsorbed metabolites (Matysik et al., 2016). Lipidomics study may be useful in understanding the contribution of fatty acids and lipids profile toward maintaining or disturbing the metabolic homeostasis, particularly indicated by the readouts of insulin resistance (IR) and obesity (Shetty and Kumari, 2021).

Panax ginseng and *Panax notoginseng* are widely used for 1000 of years in Asia due to their effectiveness in strengthening health and recovering from deficiency of "vital energy (*QI*)." Ginsenosides are the main bioactive components. Ginsenoside Rb1 (Rb1) is the most abundant and thought to be an important active factor in protopanaxadiol ginsenosides. Previous studies have shown that ginsenoside Rb1 exerts significant anti-obesity and anti-diabetic effects (Zhou et al., 2019). Rb1 can decrease body weight, increase insulin sensitivity, suppress liver fat accumulation, regulate adipocyte function and improve glucose tolerance in obese mice and rats (Xiong et al., 2010; Shen et al., 2013, 2015; Lin et al., 2014; Yu et al., 2015; Song et al., 2017; Lim et al., 2019). Rb1 exerts multi-target effects and its molecular mechanism mainly involves in activating AMP-activated protein kinase (Shen et al., 2013; Zhao et al., 2019) and regulating PPARγ signaling (Mu et al., 2015; Song et al., 2020). However, these pharmacological effects were observed in the treatment *via* intraperitoneal injection of Rb1, and the molecular targets analyzed were mainly in the liver, skeletal muscle and adipose tissues. It is well known that most herbal medicine, including ginsenosides, are orally administrated. However, the oral bioavailability of Rb1 is relatively low, around 0.1–4.35%(Odani et al., 1983; Xu et al., 2003; Liu et al., 2015). After being orally administrated, the levels of Rb1 in the blood and target tissues are far below the effective concentrations used in intraperitoneal administration studies. So, the AMPK and PPARγ pathways may not actually be followed *in vivo* by Rb1 via oral administration. Therefore, the current mechanistic hypotheses of Rb1 are insufficient to explain the results of *in vivo* animal studies which are orally given with Rb1.

Since poor bioavailability, Rb1 concentration is low in the plasma but is very high in the gut (especially in the large intestine), which provides the possibility of interaction between Rb1 and the gut microbes. In addition, it has been reported that after Rb1 was orally administrated, intestinal microbes were involved in the transformation of Rb1. β- D-glucosidase produced by gut microbes converts Rb1 into other saponins (Akao et al., 1998a). Germ-free rats (Akao et al., 1998b) and factors affecting gut microbes such as antibiotics (Xu et al., 2014), stress (Kang et al., 2016) etc., affect Rb1 degradation into other saponins and also Rb1 pharmacokinetics. Therefore, we hypothesize that the gut microbiota might be an alternative therapeutic target for Rb1.

Recent studies have reported that some saponins treated by oral administration could regulate gut microbiota and metabolites profiles to improve physiological indices. For instance, *Panax notoginseng* saponins modulate the gut microbiota accompanied by increasing fecal fatty acids, which promotes adipose thermogenesis in diet-induced obese mice (Xu et al., 2020). Ginseng extract can increase *Enterococcus faecalis* that can produce myristoleic acid, which leads to reducing adiposity (Quan et al., 2020). However, there is limited data about the influences of pure Rb1 on gut microbiota and metabolites. In this study, in the process of evaluating the anti-obesity effects of Rb1 in HFD-fed mice, we studied the alteration of gut microbiota and profiles of fecal metabolites in response to Rb1 treatment. Through correlation analysis, we explored the multiscale mechanisms that might account for the therapeutic effect of Rb1 against obesity.

MATERIALS AND METHODS

Chemicals

Ginsenoside Rb1 was purchased from the FEIYUBIO (Nantong, China). Rb1 was dissolved in saline and gavaged to mice or rats.

Animals and Experimental Design

C57BL/6J mice (Shanghai Laboratory Animal Co.) and SD rats (Beijing Vital River Laboratory Animal Technology Co.) were

raised under a 12:12 h light/dark cycle in a temperature and humidity-controlled room.

High-Fat Diet-Induced Obese Mouse Model

Mice were divided into three groups: (1) ND: normal diet treated with saline (n = 5), (2) HFD: high-fat diet treated with saline (n = 5), (3) Rb1: high-fat diet treated with Rb1 at a dose of 120 mg/kg (n = 7). Male mice of 7 weeks of age were provided with a normal chow diet or high-fat diet (D12492: 60% fat, 20% carbohydRate, 20% protein, Research Diets, Inc., NY, United States) for 12 weeks. Then mice in the ND group and the HFD group were gavaged with saline and mice in the Rb1 group were gavaged with Rb1 for 28 days. Blood samples were collected after Rb1 treatment for 24 days after mice fasting overnight. Fecal samples of mice were collected before Rb1 treatment (day 0) and after Rb1 treatment for 9, 20, 24, and 27 days (day 9, day 20, day 24, and day 27). At the end of the trial, mice fasted overnight and proximal colon, liver and epididymal fat tissues were collected. Samples of serum, feces, and tissues were stored at –80°C.

Diet-Induced Hyperlipemia Rat Model

Male SD rats were divided into three groups (8 rats per group): (1) a normal diet treated with saline (ND), (2) a high-fat diet treated with saline (HFD), (3) a high-fat diet treated with Rb1 (Rb1, 60 mg/kg). Firstly, rats were fed with the normal diets or normal diets added with 20.0% sucrose, 15% lard, 1.2% cholesterol, and 0.2% sodium cholate for 2 weeks. Blood was collected and group division based on the level of serum total cholesterol (TC). Then rats were gavaged with Rb1. After four weeks of treatment, blood was obtained and stored at –80°C. The liver and epididymal fat were collected for histopathology analysis.

Measurement of Blood Chemistry and Hepatic Lipid Contents

Serum triglycerides (TG), total cholesterol (TC), low-density lipoprotein cholesterol (LDL-c), and glucose were measured using commercial detection kits (NJJCBIO Co., Ltd., Nanjing, China). Glycosylated hemoglobin (GHb) was tested using a commercial kit (Jianglai Biotechnology Co., Ltd., Shanghai). Insulin was determined using a commercial ELISA kit (Mercodia). Insulin resistance was assessed using the index of HOMA-IR: fasting blood glucose (mmol/L) × fasting blood insulin (mU/L)/22.5. Hepatic lipids from the mice liver homogenate were extracted and hepatic TG and TC were determined using assay kits (NJJCBIO Co., Ltd., Nanjing, China).

Intraperitoneal Glucose Tolerance Test

Intraperitoneal glucose tolerance test was performed after Rb1 treatment for 16 days. After fasting for 6h, mice were given glucose (2 g/kg body weight) intraperitoneally. Tail blood was used to inspect glucose levels at 0, 15, 30, 60, and 120 min after glucose injection.

Analysis of Histopathology

The liver and epididymis fat tissues of rats were fixed with formalin and embedded in paraffin. 4 μm sections were stained with hematoxylin and eosin (H&E). For hepatic fat accumulation analysis, livers were embedded in frozen sections and 10 μm sections were stained with oil red O (ORO).

RNA Isolation and Real-Time Quantitative PCR Analysis

Total RNA was extracted from the colon tissues with RNeasy Plus Universal Mini Kit (QIAGEN). Then cDNA was prepared with PrimeScript RT reagent Kit (TAKARA). Quantitative real-time PCR (qRT-PCR) was performed with SYBR Premix Ex TaqTM (TAKARA) on the Step-One-Plus Real-Time PCR Systems (Applied Biosystem) by using Gapdh as the internal control. Primers that were used in qRT-PCR were shown in **Supplementary Table 1**.

Gut Microbiota Detection and Microbial Function Prediction

Fecal samples of mice collected at days 0, 9, 20, and 27 were used for gut microbiota profiling. Genomic DNA was extracted from feces with a QIAamp DNA stool mini kit (QIAGEN, Germany). Subsequently, the V3–V4 region of the 16S rRNA gene was amplified by PCR and then amplicons were purified and sequenced on a MiSeq system.

Sequencing reads were analyzed using the QIIME II software (Bolyen et al., 2019). In practice, chimeric sequences and low-quality sequencing reads were filtered by the DADA2 method included in the qiime2 software, which was an ASV-based community comparison method for 16S amplicon data analysis (Callahan et al., 2016). After that, high-quality reads were kept to build a feature table, which contained counts (frequencies) of each unique sequence in each sample. Then taxonomic annotation analysis based on the feature table was carried out to explore the microbial profile of samples. Subsequently, alpha and beta diversity analyses were conducted. In detail, the alpha diversity of each group was calculated by the Shannon index and Pielou evenness index; while the beta diversity was calculated with the principal coordinate analysis (PCoA) method based on the unweighted UniFrac distance matrices. Adonis (permutational multivariate analysis of variance using distance matrices) was used to compare the significant difference between groups. To identify microbial markers between groups, the approach of linear discriminant analysis effect size (LEfSe) was applied and the threshold of linear discriminant analysis (LDA) score was set to 3.0. Finally, based on the feature table, the tax4fun software (Aßhauer et al., 2015) was adopted to infer involved signal pathways of microbes so as to predict the functional profiles of the microbial communities.

Fecal Metabolite Analysis

Fecal samples of mice collected on day 24 after Rb1 treatment were used for metabolite analysis.

Metabolite Extractions

To extract metabolites from fecal samples, 800 μL of cold methanol/acetonitrile/water (2:2:1, vol/vol/vol) extraction solvent was added to 30–80 mg feces, and vortexed adequately. Stock solutions of stable-isotope internal standards were added

to the extraction solvent simultaneously. Then samples were under vigorous shaking (2 min) and followed by incubation (20 min, 4°C). After centrifugation (14,000 g, 20 min, 4°C), the supernatant flowed through a 96-well protein precipitation plate, the elution was vacuum-dried at 4°C. Then the samples were re-dissolved in 100 μL acetonitrile/water (1:1:1, vol/vol/vol) solvent and transferred to LC vials.

LC-MS/MS Analysis

Analyses were performed using a UHPLC (1290 Infinity LC, Agilent Technologies) coupled to a 6500 QTRAP MS (AB Sciex). The analytes were separated on UPLC BEH C18 columns (2.1 × 100 mm, 1.7 μm; Waters). The column temperature was set at 40°C, and the injection volume was 2 μL. The mobile phase A was 50 mM ammonium formate and 0.4% formic acid in the water, and B was methanol. A gradient (5% B at 0 min, 60% B at 5 min, 100% B at 11–13 min, 5% B at 13.1–16 min) was then initiated at a flow rate of 400 μL/min. The sample was placed at 4°C during the whole analysis process. 6500 QTRAP was performed in positive and negative switch mode. The ESI positive source conditions were set as follows: source temperature: 550°C; ion Source Gas1: 55; Ion Source Gas2: 55; Curtain gas: 40; ion Sapary Voltage Floating: + 4500. The ESI negative source conditions were set as follows: source temperature: 550°C; ion Source Gas1: 55; Ion Source Gas2: 55; Curtain gas: 40; ion Sapary Voltage Floating: –4500 V. MRM method was used for mass spectrometry quantitative data acquisition. A pooled sample was set in the sample queue as quality control (QC) to evaluate the stability and repeatability of the system.

Data Processing

The Analyst software was used for quantitative data processing. The QCs were processed together with the biological samples. Peak values of each metabolite were normalized by the weight of the feces and peaks of internal standards.

Statistical Analysis

The student's *t*-test was performed to compare data between two groups and a one-way analysis of variance followed by Tukey's *post hoc* test was applied to compare data among more than two groups. To compare values among three groups of different time points, a two-way analysis of variance followed by Tukey's multiple comparison test was performed. To evaluate the correlation between physiology phenotypes, gut microbes, or fecal metabolites, *Spearman*'s correlation analysis was used. A *P*-value < 0.05 was considered statistically significant. Data were expressed as means ± SEM (standard errors of the means).

RESULTS

Orally Administrated Ginsenoside Rb1 Improves Insulin Resistance and Lipid Metabolism in High-Fat Diet-Fed Rodents

A high-fat diet-fed obese model was established by feeding C57BL/6J male mice with a high-fat diet for 12 weeks. Therapeutics via daily oral administration of Rb1 was performed in the following 4 weeks (**Figure 1A**). Compared to the HFD group, Rb1 treatment significantly lowered the serum LDL-c ($P < 0.05$, **Figure 1B**) and TG ($P < 0.05$, **Figure 1C**), with no effect on the serum TC, body weight, and food intake (**Figures 1D,L,M**). On the other hand, Rb1 unaffected either fasting blood glucose (**Figure 1E**) or glucose tolerance (**Figure 1H**), but significantly lowered the fasting blood insulin ($P < 0.01$, **Figure 1F**) and the HOMA-IR index ($P < 0.01$, **Figure 1G**). In addition, compared to the HFD group, Rb1 lowed liver TG and epididymal fat mass for a trend but had no effect on liver TC (**Figures 1I,J,K**).

These results were reproduced in the diet-induced hyperlipemia rat model (**Figure 2A**). As shown in **Figure 2**, compared to the HFD group, Rb1 could significantly decrease the levels of LDL-c ($P < 0.001$, **Figure 2B**), TG ($P < 0.01$, **Figure 2C**) and TC ($P < 0.05$, **Figure 2D**), and did not affect HDL-c, body weight and food intake (**Figures 2E,H,I**). Meanwhile, the GHb ($P < 0.01$, **Figure 2F**) detected in the Rb1 group was much lower compared to that of the HFD group although blood glucose showed only a trend of decline (**Figure 2G**). Rb1 also reduced the accumulation of lipid droplets in the liver tissues of rats observed by oil red O staining and H&E staining (**Figure 2J**). The results of H&E staining of epididymal fat tissues showed that the adipocytes in the Rb1 group were significantly smaller than those in the HFD group (**Figure 2K**).

Taken together, Rb1 treatment has consistent results in mice and rats and thus strongly suggests that Rb1 treatment improves the lipid metabolism and insulin resistance in HFD-fed rodents. For further exploration of the possible mechanisms of Rb1 function, only mice samples were used for evaluation.

Rb1 Treatment Partly Recovers the Gut Microbiota Destructed by High-Fat Diet in Mice

To explore whether gut microbiota plays a significant role in Rb1 treatment in HFD-fed rodents, mouse fecal samples collected at day 0, day 9, day 20, and day 27 were used to analyze the dynamic change of gut microbiota. The bacterial 16S rRNA (V3-V4 region) gene was sequenced for these fecal samples. After removing low-quality sequencing reads (Methods), a total of 55M raw reads, and an average of 0.8M reads per sample were obtained. Subsequently, feature table construction and taxonomic annotation were conducted to generate the microbial profiles for evaluating the alteration of gut microbiota for different groups of mice.

The alpha diversity was estimated by the Shannon index and Pielou evenness index. As shown in **Figures 3A,B**, both Shannon index and Pielou evenness index of the Rb1 group began to decrease from day 9 and were significantly lower than those of the HFD group on day 27 ($P < 0.05$), showing an obvious temporal effect with Rb1 treatment. And this result indicated that Rb1 might reduce the diversity of the gut microbes of HFD-fed mice. The beta diversity was estimated by PCoA based on the unweighted UniFrac distance matrices.

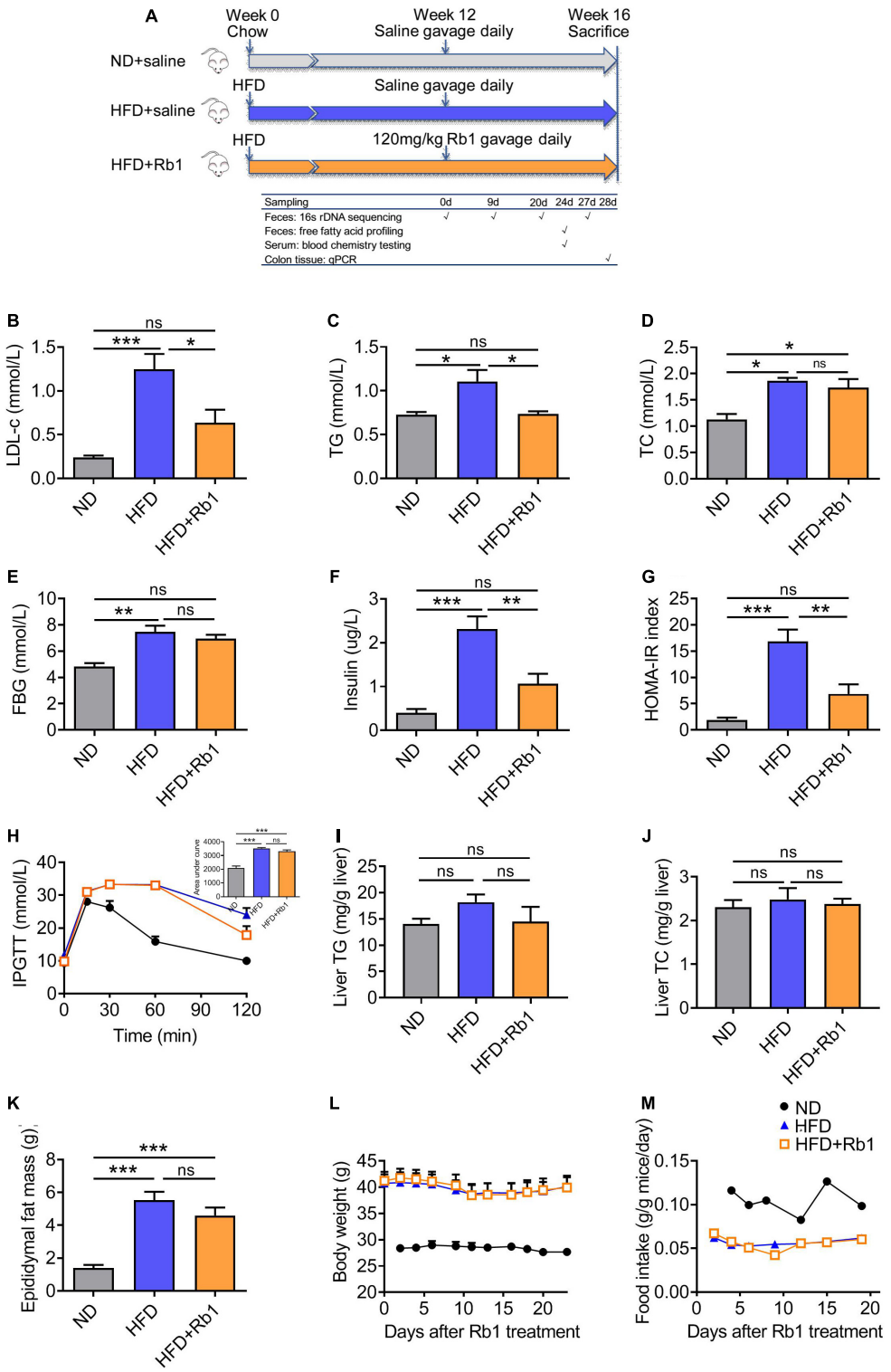

FIGURE 1 | Rb1 treatment improved lipid metabolism and insulin resistance in high-fat diet (HFD)-fed mice. **(A)** Mice were fed with a high-fat diet for 12 weeks and then subjected to Rb1 treatment (120 mg/kg) by gavage for 4 weeks. Blood samples of day 24 were used to test serum metabolic parameters. Tissues were collected on day 28. **(B)** Low-density lipoprotein cholesterol (LDL-c), **(C)** triglyceride (TG), **(D)** total cholesterol (TC), **(E)** fasting blood glucose (FBG), **(F)** fasting insulin was tested in serum and **(G)** homeostasis model assessment of insulin resistance (HOMA-IR) index was assessed. **(H)** An Intraperitoneal glucose tolerance test was performed on day 16. **(I)** Liver TG, **(J)** liver TC, and **(K)** epididymal fat were assessed. **(L)** Body weight and **(M)** food intake data were recorded twice a week. All data were presented as the mean ± SEM (n = 5–7). A one-way analysis of variance followed by Tukey's *post hoc* test was applied to compare data among groups. $^{*}P < 0.05$; $^{**}P < 0.01$; $^{***}P < 0.001$. ns, not significant.

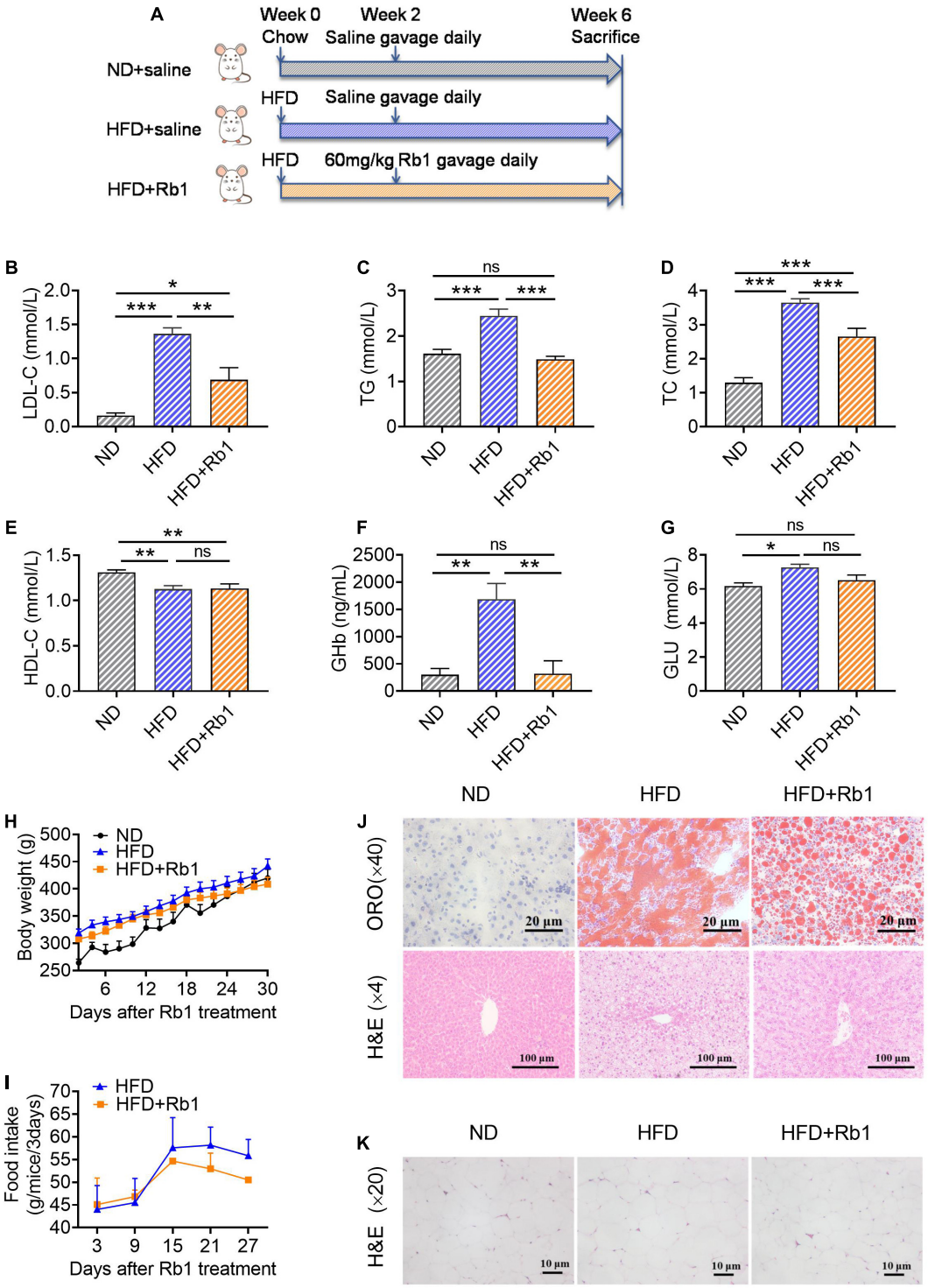

FIGURE 2 | Rb1 treatment improved lipid metabolism in HFD-fed rats. **(A)** Rats were provided with a high-fat diet for 2 weeks and then subjected to treatment with Rb1 (60 mg/kg) by gavage for 4 weeks. Blood samples of day 28 were used to test serum metabolic parameters, including **(B)** low-density lipoprotein cholesterol (LDL-c), **(C)** triglyceride (TG), **(D)** total cholesterol (TC), **(E)** high-density lipoprotein cholesterol (HDL-c), **(F)** glycosylated hemoglobin (GHb), and **(G)** blood glucose (Glu). **(H)** Body weight and **(I)** food intake were also recorded. **(J)** Oil red O (ORO) staining and hematoxylin and eosin (H&E) staining of liver tissues. **(K)** H&E staining of epididymal fat tissues. All data were expressed as the mean ± SEM (n = 8). Significant difference among groups were evaluated using one-way analysis of variance followed by Duncan's *post hoc* test. $^{*}P < 0.05$; $^{**}P < 0.01$; $^{***}P < 0.001$. ns, not significant.

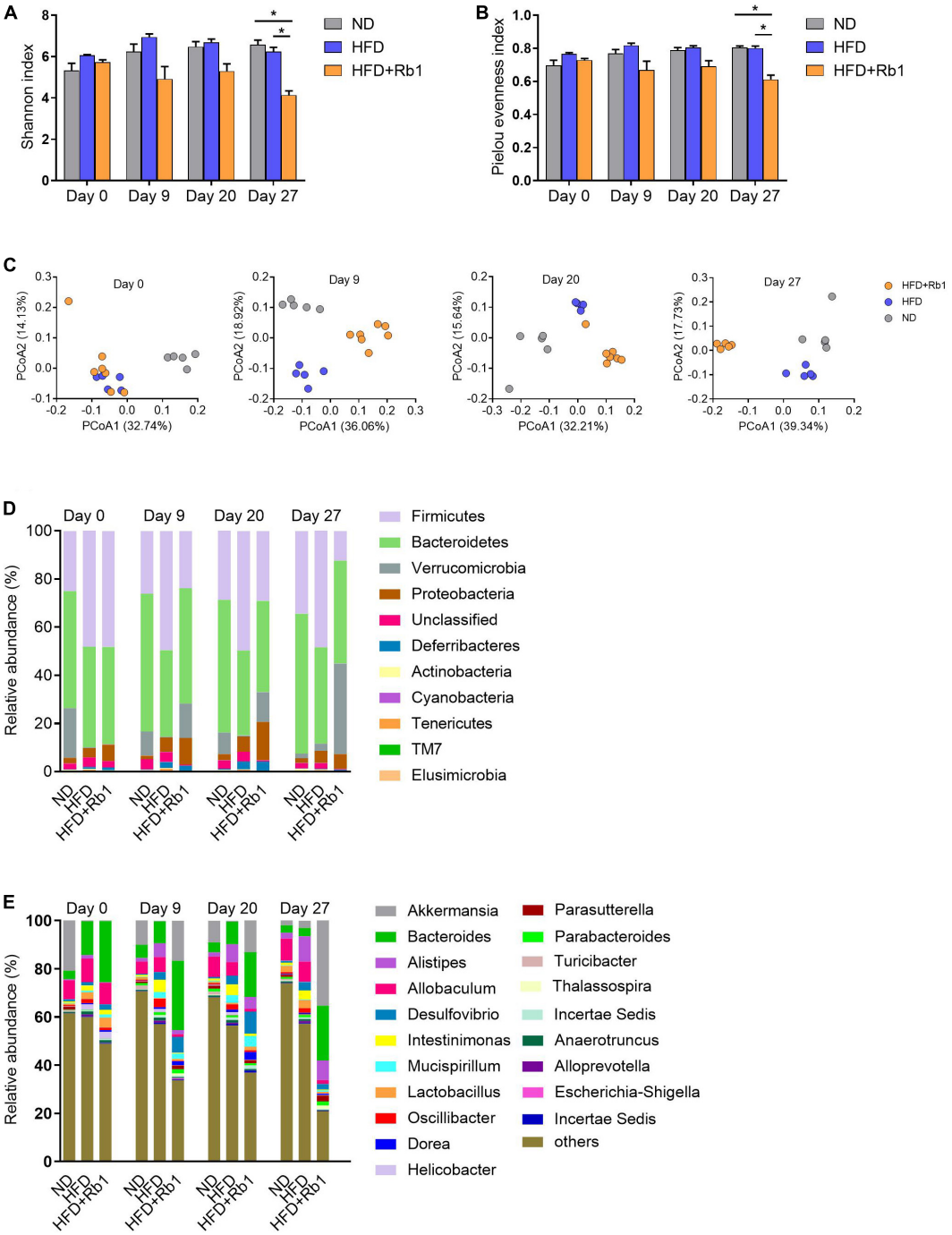

FIGURE 3 | Rb1 treatment altered the composition of gut microbiota in HFD-fed mice. Fecal samples of mice were collected before Rb1 treatment (day 0) and after Rb1 treatment (day 9, day 20, and day 27). Bacterial 16S rRNA (V3-V4 region) sequencing was conducted for these fecal samples. The alpha diversity was estimated by the **(A)** Shannon Index and **(B)** Pielou evenness index. The beta diversity was assessed by **(C)** principal coordinates analysis (PCoA). Relative abundance of taxa **(D)** at the phylum level and **(E)** at the genus level is shown. All data were expressed as the mean ± SEM (n = 5–7). Significant difference among groups were evaluated using two-way analysis of variance followed by Tukey's multiple comparison test. *$P < 0.05$; ** $P < 0.01$; ***$P < 0.001$.

For mice in the Rb1 group, they were classified into an independent cluster compared to those of the HFD group on day 9 (Adonis, $P < 0.01$), day 20 (Adonis, $P < 0.01$), and day 27 (Adonis, $P < 0.05$), whereas mice from two HFD-fed groups were classified into the same cluster on day 0 (Adonis, $P > 0.05$) (**Figure 3C**). The results indicated that Rb1

treatment might alter the gut microbial composition of HFD-fed mice.

Additionally, the gut microbial composition was classified and exhibited at the phylum level (**Figure 3D**) and the genus level (**Figure 3E**). As shown in **Supplementary Figures 1A-D**, the relative abundance of Firmicutes was significantly increased by HFD and decreased by Rb1 treatment, meanwhile, HFD increased the ratio of Firmicutes to Bacteroidetes, whereas Rb1 reversed. Notably, compared with the HFD group, Rb1 treatment significantly increased the relative abundance of *Akkermansia* which belongs to Verrucomicrobia (**Figures 3D, E**).

To identify the specific intestinal bacterial markers responding to Rb1 treatment, linear discriminate analysis effect size (LEfSe) analysis was conducted (**Supplementary Figure 2**). As shown in **Figure 4A**, compared to the HFD group, a total of 18 genera were significantly altered in abundance by Rb1 treatment, with seven genera increased and eleven genera decreased, at each time point respectively. Among them, eight genera were significantly altered at two or three-time points, indicating the solid and persistent response of these genera to Rb1 treatment. Three of them were enriched, including *Bacteroides*, *Parasutterella,* and *Akkermansia* (highlighted with red diamonds in **Figure 4A**) and the remaining five of them were reduced, including *Allobaculum*, *Intestinimonas*, *Oscillibacter*, *Alistipes, and Helicobacter* (highlighted with blue triangles in **Figure 4A**). Notably, 6 genera were recovered by Rb1 treatment which were previously altered by the high-fat diet, including *Parasutterella*, *Akkermansia*, *Allobaculum*, *Intestinimonas*, *Oscillibacter,* and *Alistipes* (highlighted in red text in **Figure 4A**).

Furthermore, microbial functions were predicted using tax4fun software to find out differential functional pathways among the three groups. **Figure 4B** shows the main significantly differential pathways in response to Rb1 treatment in different time points. Compared with the HFD group, a higher abundance of gut microbiota in the Rb1 groups was associated with pathways involved in lipids metabolism, including fatty acid biosynthesis (day 20), biosynthesis of unsaturated fatty acids (day 27), primary bile acid biosynthesis (day 9) and secondary bile acid biosynthesis (day 9 and 20). On the contrary, compared with the ND group, a lower abundance of gut microbiota in the HFD group was associated with these pathways.

These results indicate that oral administration of Rb1 modulates the gut microbiota, and partially reverses the gut dysbiosis in HFD-Fed mice. Microbial functional pathway prediction indicates pathways associated with lipids metabolism.

Rb1 Treatment Increases Long-Chain Fatty Acids in the Feces of High-Fat Diet-Fed Mice

Considering that gut microbiota of the Rb1 group was predicted to play a role in lipid metabolism, especially in fatty acid metabolism, we further measured the content of free fatty acids in fecal samples which were collected after Rb1 treatment for 24 days. As shown in **Figure 5A**, a total of 42 free fatty acids was detected, including six short-chain fatty acids, two medium-chain fatty acids, nine long-chain saturated fatty acids, and 25 long-chain unsaturated fatty acids.

As shown in **Figure 5B**, compared to the HFD group, a total of nine free fatty acids were significantly changed in the Rb1 group (**Figure 5B**), with eight increased and one decreased. Among eight increased fatty acids, six were long-chain unsaturated fatty acids. Compared to the HFD group, eicosapentaenoic acid (EPA, C20:5n3, $P < 0.05$) was significantly increased by 3.5 times in the Rb1 group. Three octadecenoic acids, including linoleic acid (C18:2n6, all-cis, $P < 0.05$), linoelaidic acid (C18:2n6, all-trans, $P < 0.05$), and conjugated linoleic acids (CLA, C18:2, $P < 0.05$), were significantly increased by 2.8, 3.0 and 2.9 times respectively in the Rb1 group. Additionally, 10Z-heptadecenoic acid (C17:1n-7, cis, $P < 0.01$) and 10E-heptadecenoic acid (C17:1n-7, trans, $P < 0.05$) were increased by 4.2 and 3.9 times respectively, while heptadecanoic acid (C17:0, $P < 0.01$) was decreased (not detected in the Rb1 group). Furthermore, two long-chain saturated fatty acids, including 12-hydroxystearic acid (12-HAS, C18:0, $P < 0.05$) and myristic acid (C14:0, $P < 0.05$) were significantly increased by 3.3 and 2.2 times respectively.

These results suggest that Rb1 treatment increases the content of a group of free fatty acids in feces, especially long-chain unsaturated fatty acids including EPA and octadecenoic acids.

Rb1 Treatment Adjusts Expression of Free Fatty Acid Receptor-Related Genes in the Colon of High-Fat Diet-Fed Mice

Increasing evidence indicated that free fatty acids are natural ligands for a group of free fatty acid receptors (FFARs). To date, four FFARs have been identified (Kimura et al., 2020). *Ffar2* and *Ffar3* are activated by SCFAs (Brown et al., 2003), *Ffar1* is activated by MCFAs (Briscoe et al., 2003), while *Ffar4* is activated by LCFAs (especially unsaturated LCFAs) (Hirasawa et al., 2005). In this study, we tested FFARs gene expression in the colon to find out whether their expression was associated with the increase of free fatty acids induced by Rb1 treatment. Our results showed that the expression of *Ffar4* was significantly increased in the Rb1 group ($P < 0.01$), while it was decreased in the HFD group (**Figure 6A**). And other fatty acid receptors including *Ffar1* (**Figure 6B**), *Ffar2* (**Figure 6C**), and *Ffar3* (**Figure 6D**) were unaffected with Rb1 treatment.

Additionally, *Pparg* which can be activated by unsaturated LCFAs and abundant in the colon (Su et al., 2007) was also significantly upregulated by Rb1 ($P < 0.05$, **Figure 6E**).

Previous reports show that diets and gut microbes may affect intestinal barrier function (Moreira et al., 2012; Rohr et al., 2020). Tight junction protein and antimicrobial peptides in the intestine are contributing to the gut barrier function (Everard et al., 2014; Zihni et al., 2016). A high-fat diet can induce oxidative stress in the intestine which triggers gut barrier injury and endotoxemia (Moreira et al., 2012; Rohr et al., 2020). Here, we further assessed the gene expression of several marker genes associated with intestinal barrier function in the colon. Claudin consists of the main chain of the tight junction complex (Venugopal et al., 2019). We found that the expression of *Cldn4* (encoding claudin 4) and *Cldn2* (encoding claudin 2) were higher in mice treated with Rb1

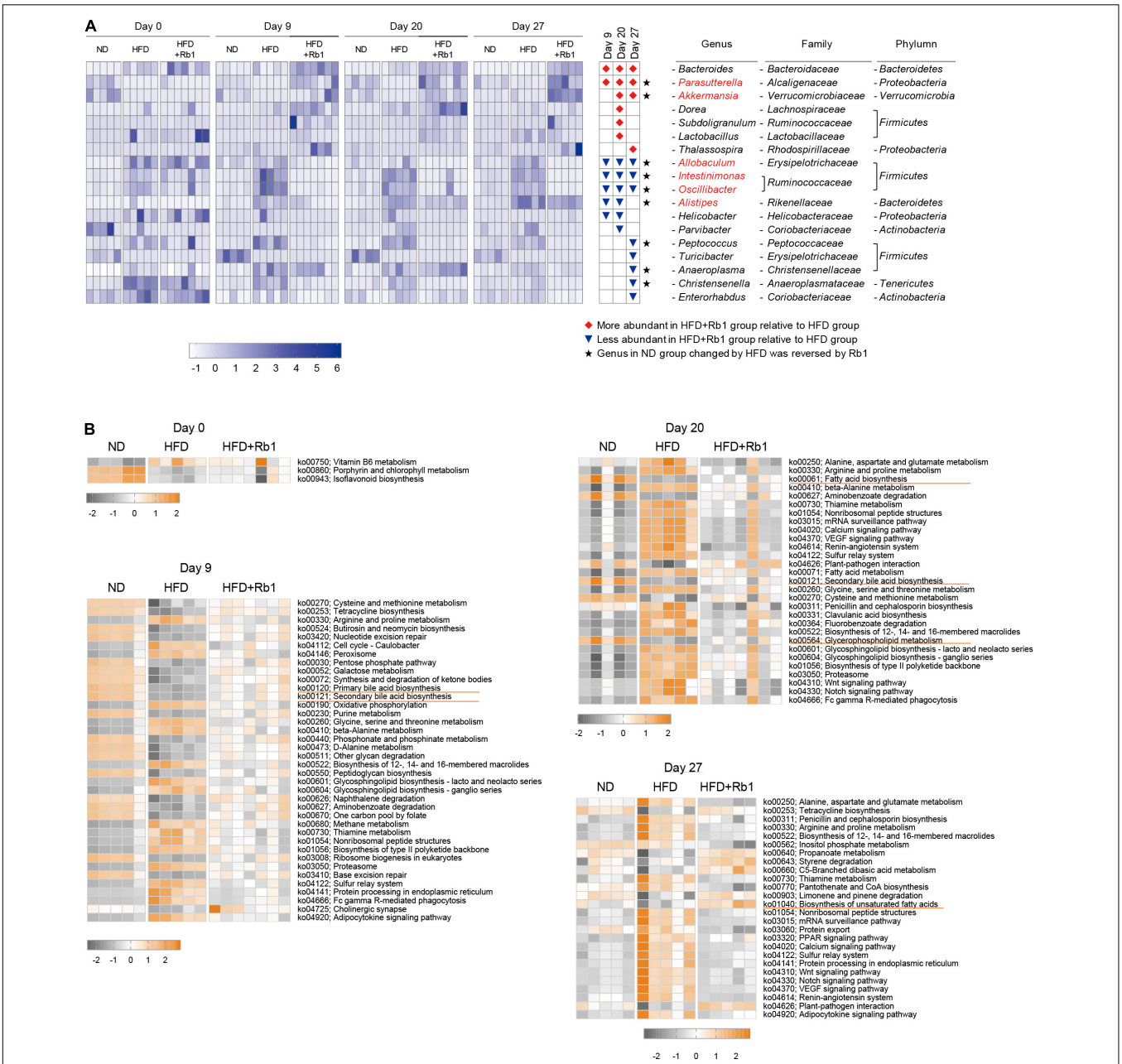

FIGURE 4 | Key bacterial alterations in response to Rb1 treatment in HFD-fed mice and functional pathway prediction. Key genera significantly altered by Rb1 treatment were selected by Linear discriminate analysis effect size (LEfSe) analysis. Functional pathway prediction was performed by the tax4fun software. **(A)** Heatmap presents the relative abundance of key genera significantly altered by Rb1 treatment (LDA scores > 3)**. (B)** Heatmap presents the abundance of differential pathways in day 0, day 9, day 20, and day 27. Pathways with significant differences between Rb1 and HFD are shown in the top 20 (pathways with the same *P*-value are shown all). The abundance of pathways was normalized by Z-score method. Kruskal-Wallis rank-sum test was used to calculate the significant difference between groups ($P < 0.05$).

when compared to untreated HFD-fed mice (*Cldn4*, $P < 0.05$, **Figures 6F,G**), while *Muc2* gene expression was unaffected (**Figure 6H**). Additionally, higher expression of antimicrobial peptides gene *Reg3g* was observed in the Rb1 group than that in the HFD group for a trend (**Figure 6I**). Our results showed that Rb1 significantly increased the expression of oxidative-stress-related genes in the colon, including *Sod1*($P < 0.01$, **Figure 6J**), *Cat* ($P < 0.05$, **Figure 6K**) and *Nfe2l2* ($P = 0.052$, **Figure 6L**), compared to the HFD-fed mice.

Taken together, these results suggest that Rb1 adjusts colonic gene expression associated with free fatty acid receptors, intestinal barrier function, and oxidative stress in HFD-fed mice, which may partly explain the mechanism of beneficial effects of Rb1.

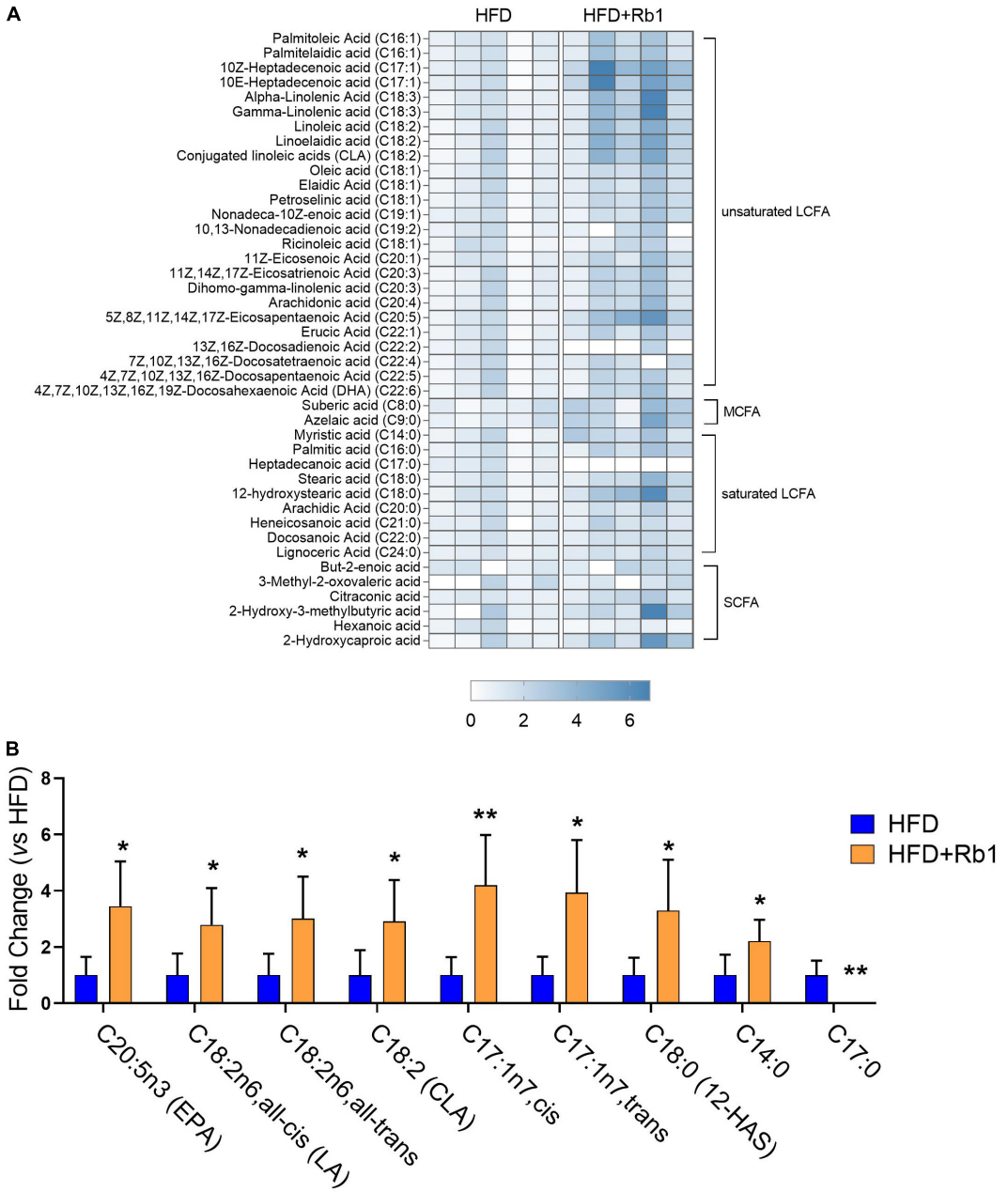

FIGURE 5 | Rb1 modified fecal free fatty acids profiles in HFD-fed mice. The content of free fatty acids in fecal samples collected after Rb1 treatment for 24 days was determined by LC-MS/MS. **(A)** Heatmap of fecal free fatty acids in mice of the HFD and Rb1 group is shown. **(B)** Fold change of differential fecal free fatty acids of the Rb1 group compared to the HFD group is displayed. All data were expressed as the mean ± SEM ($n = 5$). *P*-values were evaluated using a *t*-test analysis. $^{*}P < 0.05$; $^{**}P < 0.01$. LCFA, long-chain fatty acid, MCFA: medium-chain fatty acid; SCFA, short-chain fatty acid.

Rb1-Induced Changes of Gut Microbiota, Fecal Lipid Profiles, and Colonic Gene Expression Associate With Improvement of Metabolic Phenotypes in High-Fat Diet-Fed Mice

Rb1 treatment ameliorated metabolic disorders in HFD-fed mice, accompanied by altered gut microbiota, fecal lipid profiles, and colonic gene expression. To find out whether there are correlations between physiological phenotypes and gut microbes or fecal metabolites, *Spearman* correlation analysis is used to calculate the relationship between any two of them. As shown in **Figures 7A,B**, Rb1 treatment decreased insulin, IR, and TG, which was positively correlated with the decreased abundance of *Alistipe* in feces, and was negatively correlated with the increased content of three octadecenoic acids (linoleic acid,

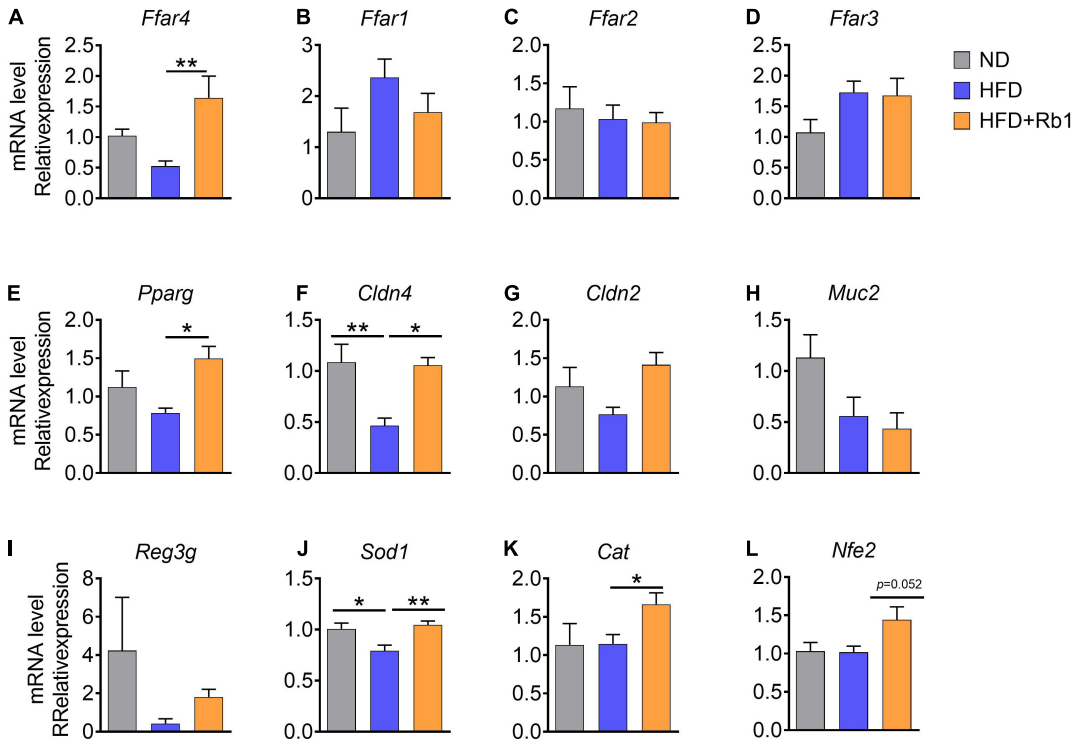

FIGURE 6 | Rb1 treatment adjusted colonic gene expression associated with free fatty acids receptors and the intestinal barrier function in HFD-fed mice. Relative mRNA expression in colon was determined by real-time PCR. **(A–E)** Free fatty acids receptor-related genes, **(F–I)** intestinal barrier function-related genes, **(J–L)** oxidate stress-related genes are shown. Relative expression levels were normalized to those of GAPDH. All data were expressed as the mean ± SEM (n = 5–7). P-values were determined using a t-test analysis. *$P < 0.05$; **$P < 0.01$.

linoelaidic acid, and conjugated linoleic acids) in feces, and was also negatively correlated with upregulated *Ffar4* gene expression in the colon. Additionally, eight LCFAs were increased in feces in response to Rb1 treatment, which had a positive correlation with the increased abundance of *Akkermansia* (day 20 and 27) and *Parasutterella* (day 27), but had a negative correlation with the decreased abundance of *Intestinimonas* (day 27), *Oscillibacter* (day 20 and 27) and *Allobaculum* (day 20 and 27). Moreover, the expression of fatty acid receptors genes (*Ffar4 and Pparg*) was upregulated in the colon, which was positively correlated with the increased abundance of *Akkermansia* (day 20) and *Parasutterella* (day 20 and 27), but was negatively correlated with the decreased abundance of *Intestinimonas* (day 20 and 27), *Oscillibacter* (day 20 and 27) and *Allobaculum* (day 27). Similarly, increased expression of intestinal-barrier-related genes (*Cldn2, Cldn4, and Reg3g*) also had the same association with the trend of these microbes. Notably, the increased *Ffar4* gene expression had a significantly positive correlation with the content of eight LCFAs that were enriched by Rb1 in feces.

These results suggest that the metabolic improvement by Rb1 treatment might have a strong correlation with alteration in gut microbiota, fatty acids profiles, and colonic gene expression. In detail, Rb1 administration modulates the gut microbiota by increasing the relative abundance of *Akkermansia* and *Parasuttereller* and decreasing the relative abundance of *Intestinimonas* and *Oscillibacter*. Moreover, Rb1 administration also increases free fatty acids content in feces (mainly EPA and octadecenoic acids) and upregulates the gene expression of fatty acid receptors (*Ffar4 and Pparg*), intestinal barrier function (*Cldn4*), and oxidative stress (*Sod1* and *Cat*) in the colon, which makes beneficial effects on metabolic improvement in HFD-fed mice (**Figure 7C**).

DISCUSSION

Previous studies have demonstrated that ginsenoside Rb1 may improve metabolic disorders induced by obesity through regulating glucose and lipid metabolism in the liver and adipose tissues (Zhou et al., 2019). In this study, we found that Rb1 treatment *via* oral administration reduced serum TG, LDL-c, and insulin in HFD-induced obese mice, and the lipid-lowering effect was further verified in a hyperlipidemia rat model, which indicated that Rb1 may improve hyperlipidemia, hyperinsulinemia, and insulin resistance in metabolic disorders.

Rb1 Treatment Modulates Gut Microbiota

Considering that ginseng-related products are mostly taken orally, the role of intestinal microbes is especially important. Due to the low bioavailability, Rb1 is enriched in the distal intestine, in which Rb1 may interact directly and thoroughly

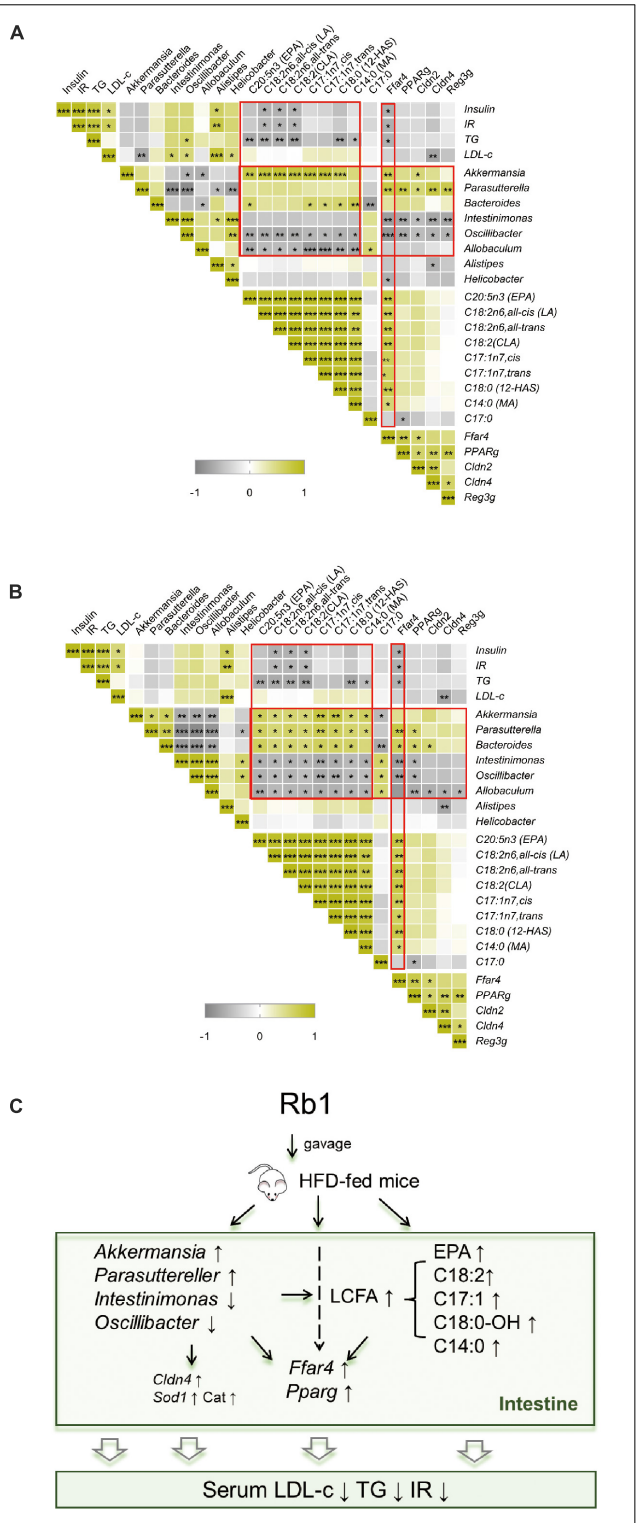

FIGURE 7 | Correlation analysis and potential mechanism of improvement of metabolic disorder *via* Rb1 treatment. *Spearman* rank correlation between gut microbiota against the corresponding host metabolic parameters, fecal free fatty acids profiles or colonic gene expression for samples of day 20 **(A)** or day 27 **(B)** were individually calculated. The correlation analysis inferred potential mechanism of Rb1-treatment improved metabolic disorder is shown in panel **(C)**. $^{*}P < 0.05$, $^{**}P < 0.01$, $^{***}P < 0.001$.

with intestinal microbes and epithelial cells, resulting in some pharmacological effects. Therefore we explored the dynamic pattern of gut microbiota in response to Rb1 treatment *via* oral administration through analyzing microbial components of fecal samples. In this study, we found Rb1 has a beneficial effect on the improvement of metabolic disorders both in mice and rats. Considering that species differences make the composition of gut bacteria significantly different, and different diets were used to set up models in mice and rats, only mice were further discussed to explore whether gut microbiota was involved in the Rb1 pharmacological effect.

The beta diversity shows that gut microbes are significantly changed within only 9 days after Rb1 treatment in HFD-fed mice. Moreover, alpha diversity was also found decreased from 9 days after Rb1 treatment, which reveals that Rb1 treatment might reduce the diversity of gut microbes. The decline in alpha diversities may be due to Rb1 induced increases in unsaturated LCFAs in the gut. Many unsaturated LCFAs have been found to have antibacterial effects and are considered to be novel antibacterial agents (Casillas-Vargas et al., 2021). The decrease in alpha diversities may also be due to upregulation of the antimicrobial-peptide-related gene *Reg3g* expression in the colon by Rb1. This finding is consistent with previous research on *Panax notoginseng* saponins (PNS) which showed that PNS decreased the diversity of the gut microbes in HFD-fed mice (Xu et al., 2020).

At the genus level, we found high-fat diet decreased the relative abundance of *Parasutterella* and *Akkermansia*, increased the relative abundance of *Intestinimonas* and *Oscillibacter*. However, the relative abundance of these genera was significantly reversed by Rb1 treatment in HFD-fed mice. ***Akkermansia***, belonging to *Verrucomicrobia*, has been shown to represent a human gut commensal that supports host health (Cani and de Vos, 2017; Zhang et al., 2019). *Akkermansia* supplementation can reverse metabolic disorders such as hyperlipidemia and insulin resistance in diet-induced obese mice (Everard et al., 2013) and humans (Depommier et al., 2019). *Akkermansia* can improve gut barrier function (Everard et al., 2013; Li et al., 2016). A recent study found that *Akkermansia* was increased by *Panax notoginseng* saponins (PNS) in HFD-fed mice (Xu et al., 2020). Consistent with these reports, we found that *Akkermansia* was significantly increased by Rb1 treatment and was negatively associated with serum TG, insulin, and IR index. ***Parasutterella*** is defined as a core component of the human and mouse intestinal microbes (Ju et al., 2019). Clinical studies showed that *Parasutterella* was reduced in patients with NAFLD (Yun et al., 2019), gestational diabetes (Ma et al., 2020), colorectal cancer (Wang et al., 2012), and pancreatic cancer (Ren et al., 2017). However, *Parasutterella* was shown an increase in inflammatory diseases, such as irritable bowel syndrome (Chen et al., 2018). *Parasutterella* has a potential role in metabolisms of bile acid and cholesterol (Ju et al., 2019). Previous studies showed that increasing levels of *Parasutterella* correlated with improving LDL-c levels after taking resistant starch of potato in healthy adults (Bush and Alfa, 2020). Studies found that long-term treatment of *Panax ginseng* extracts can increase *Parasutterella* in rats (Sun et al., 2018). Our study

found *Parasutterella* was increased in 9 days after Rb1 treatment and was negatively correlated with serum LDL-c. ***Oscillibacter*** is a potential opportunistic pathogen. It is reported to be increased in HFD-induced obese mice and was associated with increased gut permeability (Lam et al., 2012; Duca et al., 2014). *Oscillibacter* is detected to be enriched in mice with AOM/DSS-induced colorectal cancer (Wang et al., 2018). ***Intestinimonas*** has a capacity of butyrate-producing and is considered to be a beneficial genus (Kläring et al., 2013; Yang et al., 2019); however, enrichment of *Intestinimonas* is also observed in HFD-fed rats (Lin et al., 2019).

Taken together, these results demonstrate that oral administration of Rb1 modulates gut microbes, which is beneficial to improve HFD-induced metabolic disorder.

Rb1 Treatment Increases Free Fatty Acids in Feces

As metabolites are the end products of a range of biochemical reactions, metabolic alteration may more accurately reflect the response against perturbations in organisms (Zierer et al., 2018). In this study, we studied the fecal free fatty acids profiles and found that the content of a group of LCFAs was increased in response to Rb1 treatment. EPA which is a long-chain n-3 polyunsaturated fatty acid is reported to prevent hypertriglyceridemia and maintains insulin/glucose homeostasis (Soni et al., 2019; Zhuang et al., 2020; Pal et al., 2021). LA and CLA (a type of linoleic acid isomer) have health benefits (Shen and McIntosh, 2016; Hamilton and Klett, 2021) and are associated with a lower risk of T2DM (Mousavi et al., 2021). Additionally, myristic acid (C14:0) is reported to increase desaturase activity in rat hepatocytes (Jan et al., 2004) and increase the tissue content of C20:5 n-3 and C20:3 n-6 in the rat (Rioux et al., 2005).

It was reported that a higher level of fatty acids (such as oleic acid, phosphonic acid, and lactic acid) was found in the feces of PNS-treated HFD-fed mice in the process of the improvement of metabolic disorders (Xu et al., 2020). Ginseng extract can increase *Enterococcus faecalis* which has the ability of producing myristoleic acid (C14:1) and can decrease body weight gain and the fat mass in db/db mice (Quan et al., 2020). Consistent with these results, we observed that Rb1 treatment increased EPA and octadecenoic acids in feces, which was negatively correlated with decreased insulin, IR, and serum TG in HFD-induced obese mice.

Rb1 Treatment Upregulates Free Fatty Acid Receptor 4 Gene Expression in the Colon

Free fatty acids play important roles not only as energy sources (Hue and Taegtmeyer, 2009) but also as signaling molecules by activating specific receptors important in regulating many physiological processes (Boden, 2011; Shetty and Kumari, 2021). FFARs, activated by different chain lengths of free fatty acids, are G protein-coupled receptors (GPCRs) and are involved in the energy metabolism and immune response (Kimura et al., 2020). FFARs have been considered as targets for the treatment of metabolic disorders (Secor et al., 2021; Son et al., 2021). *Ffar4* is highly expressed in intestinal L cells in the colon (Oh et al., 2010). Activation of FFAR4 can enhance GLP-1 secretion and improve insulin resistance and chronic inflammation in obese mice (Xiong et al., 2010; Oh et al., 2014), and improve colonic permeability in inflammatory bowel diseases mice (Salaga et al., 2021). A growing number of studies report that supplementary fish oil and LCFAs, including omega-3, omega-6, can activate FFAR4 in mice and rats and bring benefits to health (Kimura et al., 2020). Studies also reported that ginsenoside Rb2, which exhibited regulatory activities in glucose and lipid metabolism, upregulated *Ffar4* expression in macrophages (Huang et al., 2017), endothelial cells, and monocytes (Sun et al., 2020). Accordingly, in this study, we found colonic gene expression of *Ffar4* was significantly upregulated by Rb1 in HFD-fed mice, which was positively correlated with fecal content of eight Rb1-increased-LCFAs, and was negatively correlated with decreased insulin, IR, and serum TG. These results suggest that LCFA increased by Rb1 might activate *Ffar4* in the intestine, which further improves insulin resistance. However, how *Ffar4* mediates insulin-sensing effects needs more experiments to explore the mechanism.

Correlation Analysis Indicates That Gut Microbes Might Involve in Modulating Intestinal Fatty Acids Composition

Gut microbes modify host fatty acid composition by transformation, absorption, metabolism, and excretion (Lamichhane et al., 2021). In this study, we found fecal content of eight Rb1-increased-LCFAs was positively correlated with the increased abundance of *Akkermansia*, *Parasutterella,* and *Bacteroides*, and was negatively correlated with the decreased abundance of *Intestinimonas, Oscillibacter,* and *Allobaculum*, which indicates that gut microbes might involve in modulating fatty acids composition. LCFAs in the intestine mainly come from diet. Studies showed that *Oscillibacter* and *Alistipes* were positively associated with obese and diabetic phenotypes (Lam et al., 2012; Qin et al., 2012). They are enriched by a high-fat diet, indicating that they can fully utilize lipids (Lam et al., 2012; Wan et al., 2019). Therefore, the decrease of *Oscillibacter* and *Alistipes* during Rb1 treatment in HFD-fed mice may lead to reduced utilization of LCFAs. Additionally, in this study, functional pathway prediction of gut microbes shows that Rb1 treatment increases pathways including fatty acid biosynthesis and biosynthesis of unsaturated fatty acids, whereas HFD decreases these pathways, which indicates that microbes might increase fatty acids biosynthesis. Collectively, these results imply that gut microbes might participate in the regulation of intestinal fatty acids composition in HFD-fed mice.

Limitation

The interaction between gut microbiota and the host is extremely complex. In this study, we only report the association between gut microbiota and the beneficial effect of Rb1. It needs more experiments to verify how microbes in the gut involve in the pharmacological effects of Rb1.

CONCLUSION

Overall, we find Rb1 treatment by oral administration improves hyperlipidemia, hyperinsulinemia, and insulin resistance in HFD-fed mice. This metabolic improvement may benefit from the modulation of gut microbes and intestinal fatty acids profiles by Rb1 treatment. We find the relative abundance of some key bacterial genera, including *Akkermansia, Parasuttereller*, *Intestinimonas,* and *Oscillibacter* are recovered following Rb1 treatment in HFD-fed mice. Especially, the content of a group of LCFAs is significantly increased in feces in response to Rb1 treatment, and this change is notably correlated with the relative abundance of key bacterial genera in the intestine. Furthermore, this alteration of LCFAs is sensed by free fatty acid receptors in the colon, which may further lead to the improvement of energy metabolism in HFD-fed mice. This study provides an alternative mechanism for Rb1 to treat metabolic disorders induced by obesity and that may contribute to the development of new nutraceutical-based remedies accordingly.

DATA AVAILABILITY STATEMENT

The raw 16S rRNA sequencing data and metabolite abundance of each sample can be obtained through the National Omics Data Encyclopedia with the accession number OEP002877 (https://www.biosino.org/node/project/detail/OEP002877).

ETHICS STATEMENT

Mouse experimental protocols were approved by the institutional animal care and use committee of Shanghai Institute of Nutrition and health, Chinese Academy of Sciences (Shanghai, China); Rat experimental protocols were approved by the institutional animal care and use committee of Nankai University (Tianjin, China).

AUTHOR CONTRIBUTIONS

GPZ gave a general research direction and manuscript revision. HZ contributed to the experimental design, data analysis, and manuscript writing. HZ, XZ, QX, LZ, and TY experimented on mice. MZ, YC, KZ, and QB experimented on rats. GYZ, HKZ, ML, SC, and YW performed bioinformatics analysis. CY gave the constructional suggestions on lipidomics analysis. QL, XY, and ZZ contributed to the research discussion. YL contributed the constructional suggestions for revision. GYZ, HKZ, CZ, and XYY contributed to manuscript revision. All authors made the final approval of the version to be submitted.

FUNDING

This work was supported by grants from the Tianjin Synthetic Biotechnology Innovation Capacity Improvement Project (TSBICIP-KJGG-002 and TSBICIP-CXRC-008) and the Key Research Program of the Chinese Academy of Sciences (grant KFZD-SW-219).

SUPPLEMENTARY MATERIAL

The Supplementary Material for this article can be found online at: https://www.frontiersin.org/articles/10.3389/fmicb.2022.826487/full#supplementary-material

REFERENCES

Akao, T., Kanaoka, M., and Kobashi, K. (1998a). Appearance of compound K, a major metabolite of ginsenoside Rb1 by intestinal bacteria, in rat plasma after oral administration–measurement of compound K by enzyme immunoassay. *Biol. Pharm. Bull.* 21, 245–249. doi: 10.1248/bpb.21.245

Akao, T., Kida, H., Kanaoka, M., Hattori, M., and Kobashi, K. (1998b). Intestinal bacterial hydrolysis is required for the appearance of compound K in rat plasma after oral administration of ginsenoside Rb1 from Panax ginseng. *J. Pharm. Pharmacol.* 50, 1155–1160. doi: 10.1111/j.2042-7158.1998.tb03327.x

Aßhauer, K. P., Wemheuer, B., Daniel, R., and Meinicke, P. (2015). Tax4Fun: predicting functional profiles from metagenomic 16S rRNA data. *Bioinformatics* 31, 2882–2884. doi: 10.1093/bioinformatics/btv287

Boden, G. (2011). Obesity, insulin resistance and free fatty acids. *Curr. Opin. Endocrinol. Diabetes Obes.* 18, 139–143. doi: 10.1097/MED.0b013e3283444b09

Bolyen, E., Rideout, J. R., Dillon, M. R., Bokulich, N. A., Abnet, C. C., Al-Ghalith, G. A., et al. (2019). Reproducible, interactive, scalable and extensible microbiome data science using QIIME 2. *Nat. Biotechnol.* 37, 852–857. doi: 10.1038/s41587-019-0209-9

Briscoe, C. P., Tadayyon, M., Andrews, J. L., Benson, W. G., Chambers, J. K., Eilert, M. M., et al. (2003). The Orphan G Protein-coupled Receptor GPR40 Is Activated by Medium and Long Chain Fatty Acids*. *J. Biol. Chem.* 278, 11303–11311. doi: 10.1074/jbc.M211495200

Brown, A. J., Goldsworthy, S. M., Barnes, A. A., Eilert, M. M., Tcheang, L., Daniels, D., et al. (2003). The Orphan G Protein-coupled Receptors GPR41 and GPR43 Are Activated by Propionate and Other Short Chain Carboxylic Acids*. *J. Biol. Chem.* 278, 11312–11319. doi: 10.1074/jbc.M211609200

Bush, J. R., and Alfa, M. J. (2020). Increasing levels of Parasutterella in the gut microbiome correlate with improving low-density lipoprotein levels in healthy adults consuming resistant potato starch during a randomised trial. *BMC Nutr.* 6:72. doi: 10.1186/s40795-020-00398-9

Callahan, B. J., McMurdie, P. J., Rosen, M. J., Han, A. W., Johnson, A. J., and Holmes, S. P. (2016). DADA2: High-resolution sample inference from Illumina amplicon data. *Nat. Methods.* 13, 581–583. doi: 10.1038/nmeth.3869

Cani, P. D., and de Vos, W. M. (2017). Next-Generation Beneficial Microbes: The Case of Akkermansia muciniphila. *Front. Microbiol.* 8:1765. doi: 10.3389/fmicb.2017.01765

Casillas-Vargas, G., Ocasio-Malavé, C., Medina, S., Morales-Guzmán, C., Del Valle, R. G., Carballeira, N. M., et al. (2021). Antibacterial fatty acids: An update of possible mechanisms of action and implications in the development of the next-generation of antibacterial agents. *Prog. Lipid. Res.* 82:101093. doi: 10.1016/j.plipres.2021.101093

Chen, Y. J., Wu, H., Wu, S. D., Lu, N., Wang, Y. T., Liu, H. N., et al. (2018). Parasutterella, in association with irritable bowel syndrome and intestinal chronic inflammation. *J. Gastroenterol. Hepatol.* 33, 1844–1852. doi: 10.1111/jgh.14281

Depommier, C., Everard, A., Druart, C., Plovier, H., Van Hul, M., Vieira-Silva, S., et al. (2019). Supplementation with Akkermansia muciniphila in overweight and obese human volunteers: a proof-of-concept exploratory study. *Nat. Med.* 25, 1096–1103. doi: 10.1038/s41591-019-0495-2

Duca, F. A., Sakar, Y., Lepage, P., Devime, F., Langelier, B., Doré, J., et al. (2014). Replication of obesity and associated signaling pathways through transfer of microbiota from obese-prone rats. *Diabetes* 63, 1624–1636. doi: 10.2337/db13-1526

Everard, A., Belzer, C., Geurts, L., Ouwerkerk, J. P., Druart, C., Bindels, L. B., et al. (2013). Cross-talk between Akkermansia muciniphila and intestinal epithelium controls diet-induced obesity. *Proc. Natl. Acad. Sci.U.S.A.* 110, 9066–9071. doi: 10.1073/pnas.1219451110

Everard, A., Lazarevic, V., Gaïa, N., Johansson, M., Ståhlman, M., Backhed, F., et al. (2014). Microbiome of prebiotic-treated mice reveals novel targets involved in host response during obesity. *ISME J.* 8, 2116–2130. doi: 10.1038/ismej.2014.45

Festi, D., Schiumerini, R., Eusebi, L. H., Marasco, G., Taddia, M., and Colecchia, A. (2014). Gut microbiota and metabolic syndrome. *World J. Gastroenterol.* 20, 16079–16094. doi: 10.3748/wjg.v20.i43.16079

Hamilton, J. S., and Klett, E. L. (2021). Linoleic acid and the regulation of glucose homeostasis: A review of the evidence. *Prostaglandins Leukot. Essent. Fatty Acids.* 175:102366. doi: 10.1016/j.plefa.2021.102366

Heinken, A., and Thiele, I. (2015). Systems biology of host-microbe metabolomics. Wiley interdisciplinary reviews. *Syst. Biol. Med.* 7, 195–219. doi: 10.1002/wsbm.1301

Hirasawa, A., Tsumaya, K., Awaji, T., Katsuma, S., Adachi, T., Yamada, M., et al. (2005). Free fatty acids regulate gut incretin glucagon-like peptide-1 secretion through GPR120. *Nat. Med.* 11, 90–94. doi: 10.1038/nm1168

Huang, Q., Wang, T., and Wang, H. Y. (2017). Ginsenoside Rb2 enhances the anti-inflammatory effect of ω-3 fatty acid in LPS-stimulated RAW264.7 macrophages by upregulating GPR120 expression. *Acta Pharmacol. Sinica.* 38, 192–200. doi: 10.1038/aps.2016.135

Hue, L., and Taegtmeyer, H. (2009). The Randle cycle revisited: a new head for an old hat. *Am. J. Physiol. Endocrinol. Metab.* 297, E578–E591. doi: 10.1152/ajpendo.00093.2009

Jan, S., Guillou, H., D'Andrea, S., Daval, S., Bouriel, M., Rioux, V., et al. (2004). Myristic acid increases delta6-desaturase activity in cultured rat hepatocytes. *Reprod. Nutr. Dev.* 44, 131–140. doi: 10.1051/rnd:2004020

Ju, T., Kong, J. Y., Stothard, P., and Willing, B. P. (2019). Defining the role of Parasutterella, a previously uncharacterized member of the core gut microbiota. *ISME J.* 13, 1520–1534. doi: 10.1038/s41396-019-0364-5

Kang, A., Zhang, S., Zhu, D., Dong, Y., Shan, J., Xie, T., et al. (2016). Gut microbiota in the pharmacokinetics and colonic deglycosylation metabolism of ginsenoside Rb1 in rats: Contrary effects of antimicrobials treatment and restraint stress. *Chem. Biol. Interact.* 258, 187–196. doi: 10.1016/j.cbi.2016.09.005

Kimura, I., Ichimura, A., Ohue-Kitano, R., and Igarashi, M. (2020). Free Fatty Acid Receptors in Health and Disease. *Physiol. Rev.* 100, 171–210. doi: 10.1152/physrev.00041.2018

Kimura, I., Ozawa, K., Inoue, D., Imamura, T., Kimura, K., Maeda, T., et al. (2013). The gut microbiota suppresses insulin-mediated fat accumulation via the short-chain fatty acid receptor GPR43. *Nat. Commun.* 4:1829. doi: 10.1038/ncomms2852

Kläring, K., Hanske, L., Bui, N., Charrier, C., Blaut, M., Haller, D., et al. (2013). Intestinimonas butyriciproducens gen. nov., sp. nov., a butyrate-producing bacterium from the mouse intestine. *Int. J. Syst. Evol. Microbiol.* 63, 4606–4612. doi: 10.1099/ijs.0.051441-0

Lam, Y. Y., Ha, C. W., Campbell, C. R., Mitchell, A. J., Dinudom, A., Oscarsson, J., et al. (2012). Increased gut permeability and microbiota change associate with mesenteric fat inflammation and metabolic dysfunction in diet-induced obese mice. *PLoS One.* 7:e34233. doi: 10.1371/journal.pone.0034233

Lamichhane, S., Sen, P., Alves, M. A., Ribeiro, H. C., Raunioniemi, P., Hyötyläinen, T., et al. (2021). Linking Gut Microbiome and Lipid Metabolism: Moving beyond Associations. *Metabolites* 11, 1. doi: 10.3390/metabo11010055

Li, J., Lin, S., Vanhoutte, P. M., Woo, C. W., and Xu, A. (2016). Akkermansia Muciniphila Protects Against Atherosclerosis by Preventing Metabolic Endotoxemia-Induced Inflammation in Apoe-/- Mice. *Circulation* 133, 2434–2446. doi: 10.1161/circulationaha.115.019645

Lim, S., Park, J., and Um, J. Y. (2019). Ginsenoside Rb1 Induces Beta 3 Adrenergic Receptor-Dependent Lipolysis and Thermogenesis in 3T3-L1 Adipocytes and db/db Mice. *Front. Pharmacol.* 10:1154. doi: 10.3389/fphar.2019.01154

Lin, H., An, Y., Tang, H., and Wang, Y. (2019). Alterations of Bile Acids and Gut Microbiota in Obesity Induced by High Fat Diet in Rat Model. *J. Agric. Food Chem.* 67, 3624–3632. doi: 10.1021/acs.jafc.9b00249

Lin, N., Cai, D. L., Jin, D., Chen, Y., and Shi, J. J. (2014). Ginseng panaxoside Rb1 reduces body weight in diet-induced obese mice. *Cell Biochem. Biophys.* 68, 189–194. doi: 10.1007/s12013-013-9688-3

Liu, C., Hu, M., Guo, H., Zhang, M., Zhang, J., Li, F., et al. (2015). Combined Contribution of Increased Intestinal Permeability and Inhibited Deglycosylation of Ginsenoside Rb1 in the Intestinal Tract to the Enhancement of Ginsenoside Rb1 Exposure in Diabetic Rats after Oral Administration. *Drug Metab. Dispos.* 43, 1702–1710. doi: 10.1124/dmd.115.064881

Ma, S., You, Y., Huang, L., Long, S., Zhang, J., Guo, C., et al. (2020). Alterations in Gut Microbiota of Gestational Diabetes Patients During the First Trimester of Pregnancy. *Front. Cell. Infect. Microbiol.* 10:58. doi: 10.3389/fcimb.2020.00058

Matysik, S., Le Roy, C. I., Liebisch, G., and Claus, S. P. (2016). Metabolomics of fecal samples: A practical consideration. *Trends Food Sci. Technol.* 57, 244–255. doi: 10.1016/j.tifs.2016.05.011

Moreira, A. P., Texeira, T. F., Ferreira, A. B., Peluzio Mdo, C., and Alfenas Rde, C. (2012). Influence of a high-fat diet on gut microbiota, intestinal permeability and metabolic endotoxaemia. *Br. J. Nutr.* 108, 801–809. doi: 10.1017/s0007114512001213

Mousavi, S. M., Jalilpiran, Y., Karimi, E., Aune, D., Larijani, B., Mozaffarian, D., et al. (2021). Dietary Intake of Linoleic Acid, Its Concentrations, and the Risk of Type 2 Diabetes: A Systematic Review and Dose-Response Meta-analysis of Prospective Cohort Studies. *Diabetes Care* 44, 2173–2181. doi: 10.2337/dc21-0438

Mu, Q., Fang, X., Li, X., Zhao, D., Mo, F., Jiang, G., et al. (2015). Ginsenoside Rb1 promotes browning through regulation of PPARγ in 3T3-L1 adipocytes. *Biochem. Biophys. Res. Commun.* 466, 530–535. doi: 10.1016/j.bbrc.2015.09.064

Odani, T., Tanizawa, H., and Takino, Y. (1983). Studies on the absorption, distribution, excretion and metabolism of ginseng saponins. III. The absorption, distribution and excretion of ginsenoside Rb1 in the rat. *Chem. Pharm. Bull.* 31, 1059–1066. doi: 10.1248/cpb.31.1059

Oh, D. Y., Talukdar, S., Bae, E. J., Imamura, T., Morinaga, H., Fan, W., et al. (2010). GPR120 is an omega-3 fatty acid receptor mediating potent anti-inflammatory and insulin-sensitizing effects. *Cell* 142, 687–698. doi: 10.1016/j.cell.2010.07.041

Oh, D. Y., Walenta, E., Akiyama, T. E., Lagakos, W. S., Lackey, D., Pessentheiner, A. R., et al. (2014). A Gpr120-selective agonist improves insulin resistance and chronic inflammation in obese mice. *Nat. Med.* 20, 942–947. doi: 10.1038/nm.3614

Pal, A., Sun, S., Armstrong, M., Manke, J., Reisdorph, N., Adams, V. R., et al. (2021). Beneficial effects of eicosapentaenoic acid on the metabolic profile of obese female mice entails upregulation of HEPEs and increased abundance of enteric Akkermansia muciniphila. Biochimica et biophysica acta. *Mol. Cell Biol. Lipids.* 1867:159059. doi: 10.1016/j.bbalip.2021.159059

Paone, P., and Cani, P. D. (2020). Mucus barrier, mucins and gut microbiota: the expected slimy partners? *Gut* 69, 2232–2243. doi: 10.1136/gutjnl-2020-322260

Qin, J., Li, Y., Cai, Z., Li, S., Zhu, J., Zhang, F., et al. (2012). A metagenome-wide association study of gut microbiota in type 2 diabetes. *Nature* 490, 55–60. doi: 10.1038/nature11450

Quan, L. H., Zhang, C., Dong, M., Jiang, J., Xu, H., Yan, C., et al. (2020). Myristoleic acid produced by enterococci reduces obesity through brown adipose tissue activation. *Gut* 69, 1239–1247. doi: 10.1136/gutjnl-2019-319114

Ren, Z., Jiang, J., Xie, H., Li, A., Lu, H., Xu, S., et al. (2017). Gut microbial profile analysis by MiSeq sequencing of pancreatic carcinoma patients in China. *Oncotarget* 8, 95176–95191. doi: 10.18632/oncotarget.18820

Rioux, V., Catheline, D., Bouriel, M., and Legrand, P. (2005). Dietary myristic acid at physiologically relevant levels increases the tissue content of C20:5 n-3 and C20:3 n-6 in the rat. *Reprod. Nutr. Dev.* 45, 599–612. doi: 10.1051/rnd:2005048

Rohr, M. W., Narasimhulu, C. A., Rudeski-Rohr, T. A., and Parthasarathy, S. (2020). Negative Effects of a High-Fat Diet on Intestinal Permeability: A Review. *Adv. Nutr.* 11, 77–91. doi: 10.1093/advances/nmz061

Salaga, M., Bartoszek, A., Binienda, A., Krajewska, J. B., Fabisiak, A., Mosińska, P., et al. (2021). Activation of Free Fatty Acid Receptor 4 Affects Intestinal Inflammation and Improves Colon Permeability in Mice. *Nutrients* 13:8. doi: 10.3390/nu13082716

Secor, J. D., Fligor, S. C., Tsikis, S. T., Yu, L. J., and Puder, M. (2021). Free Fatty Acid Receptors as Mediators and Therapeutic Targets in Liver Disease. *Front. Physiol.* 12:656441. doi: 10.3389/fphys.2021.656441

Shen, L., Haas, M., Wang, D. Q., May, A., Lo, C. C., Obici, S., et al. (2015). Ginsenoside Rb1 increases insulin sensitivity by activating AMP-activated protein kinase in male rats. *Physiol. Rep.* 3:9. doi: 10.14814/phy2.12543

Shen, L., Xiong, Y., Wang, D. Q., Howles, P., Basford, J. E., Wang, J., et al. (2013). Ginsenoside Rb1 reduces fatty liver by activating AMP-activated protein kinase in obese rats. *J. Lipid Res.* 54, 1430–1438. doi: 10.1194/jlr.M035907

Shen, W., and McIntosh, M. K. (2016). Nutrient Regulation: Conjugated Linoleic Acid's Inflammatory and Browning Properties in Adipose Tissue. *Ann. Rev. Nutr.* 36, 183–210. doi: 10.1146/annurev-nutr-071715-050924

Shetty, S. S., and Kumari, S. (2021). Fatty acids and their role in type-2 diabetes (Review). *Exper. Therap. Med.* 22:706. doi: 10.3892/etm.2021.10138

Son, S. E., Kim, N. J., and Im, D. S. (2021). Development of Free Fatty Acid Receptor 4 (FFA4/GPR120) Agonists in Health Science. *Biomol. Ther.* 29, 22–30. doi: 10.4062/biomolther.2020.213

Song, B., Ding, L., Zhang, H., Chu, Y., Chang, Z., Yu, Y., et al. (2017). Ginsenoside Rb1 increases insulin sensitivity through suppressing 11β-hydroxysteroid dehydrogenase type I. *Am. J. Trans. Res.* 9, 1049–1057.

Song, B., Sun, Y., Chu, Y., Wang, J., Zheng, H., Liu, L., et al. (2020). Ginsenoside Rb1 Alleviated High-Fat-Diet-Induced Hepatocytic Apoptosis via Peroxisome Proliferator-Activated Receptor γ. *BioMed Res. Int.* 2020:2315230. doi: 10.1155/2020/2315230

Soni, N., Ross, A. B., Scheers, N., Nookaew, I., Gabrielsson, B. G., and Sandberg, A. S. (2019). The Omega-3 Fatty Acids EPA and DHA, as a Part of a Murine High-Fat Diet, Reduced Lipid Accumulation in Brown and White Adipose Tissues. *Int. J. Mol. Sci.* 20:23. doi: 10.3390/ijms20235895

Su, W., Bush, C. R., Necela, B. M., Calcagno, S. R., Murray, N. R., Fields, A. P., et al. (2007). Differential expression, distribution, and function of PPAR-gamma in the proximal and distal colon. *Physiol. Genom.* 30, 342–353. doi: 10.1152/physiolgenomics.00042.2007

Sun, J. L., Abd El-Aty, A. M., Jeong, J. H., and Jung, T. W. (2020). Ginsenoside Rb2 Ameliorates LPS-Induced Inflammation and ER Stress in HUVECs and THP-1 Cells via the AMPK-Mediated Pathway. *Am. J. Chin. Med.* 48, 967–985. doi: 10.1142/s0192415x20500469

Sun, Y., Chen, S., Wei, R., Xie, X., Wang, C., Fan, S., et al. (2018). Metabolome and gut microbiota variation with long-term intake of Panax ginseng extracts on rats. *Food Funct.* 9, 3547–3556. doi: 10.1039/c8fo00025e

Venugopal, S., Anwer, S., and Szászi, K. (2019). Claudin-2: Roles beyond Permeability Functions. *Int. J. Mol. Sci.* 20:22. doi: 10.3390/ijms20225655

Wan, Y., Wang, F., Yuan, J., Li, J., Jiang, D., Zhang, J., et al. (2019). Effects of dietary fat on gut microbiota and faecal metabolites, and their relationship with cardiometabolic risk factors: a 6-month randomised controlled-feeding trial. *Gut* 68, 1417–1429. doi: 10.1136/gutjnl-2018-317609

Wang, C. S., Li, W. B., Wang, H. Y., Ma, Y. M., Zhao, X. H., Yang, H., et al. (2018). VSL#3 can prevent ulcerative colitis-associated carcinogenesis in mice. *World J. Gastroenterol.* 24, 4254–4262. doi: 10.3748/wjg.v24.i37.4254

Wang, T., Cai, G., Qiu, Y., Fei, N., Zhang, M., Pang, X., et al. (2012). Structural segregation of gut microbiota between colorectal cancer patients and healthy volunteers. *ISME J.* 6, 320–329. doi: 10.1038/ismej.2011.109

Xiong, Y., Shen, L., Liu, K. J., Tso, P., Xiong, Y., Wang, G., et al. (2010). Antiobesity and antihyperglycemic effects of ginsenoside Rb1 in rats. *Diabetes* 59, 2505–2512. doi: 10.2337/db10-0315

Xu, Q. F., Fang, X. L., and Chen, D. F. (2003). Pharmacokinetics and bioavailability of ginsenoside Rb1 and Rg1 from Panax notoginseng in rats. *J. Ethnopharmacol.* 84, 187–192. doi: 10.1016/s0378-8741(02)00317-3

Xu, R., Peng, Y., Wang, M., Fan, L., and Li, X. (2014). Effects of broad-spectrum antibiotics on the metabolism and pharmacokinetics of ginsenoside Rb1: a study on rats× gut microflora influenced by lincomycin. *J. Ethnopharmacol.* 158, 338–344. doi: 10.1016/j.jep.2014.10.054

Xu, Y., Wang, N., Tan, H. Y., Li, S., Zhang, C., Zhang, Z., et al. (2020). Panax notoginseng saponins modulate the gut microbiota to promote thermogenesis and beige adipocyte reconstruction via leptin-mediated AMPKα/STAT3 signaling in diet-induced obesity. *Theranostics* 10, 11302–11323. doi: 10.7150/thno.47746

Yang, F., Li, J., Pang, G., Ren, F., and Fang, B. (2019). Effects of Diethyl Phosphate, a Non-Specific Metabolite of Organophosphorus Pesticides, on Serum Lipid, Hormones, Inflammation, and Gut Microbiota. *Molecules.* 24:10. doi: 10.3390/molecules24102003

Yu, X., Ye, L., Zhang, H., Zhao, J., Wang, G., Guo, C., et al. (2015). Ginsenoside Rb1 ameliorates liver fat accumulation by upregulating perilipin expression in adipose tissue of db/db obese mice. *J. Ginseng Res.* 39, 199–205. doi: 10.1016/j.jgr.2014.11.004

Yun, Y., Kim, H. N., Lee, E. J., Ryu, S., Chang, Y., Shin, H., et al. (2019). Fecal and blood microbiota profiles and presence of nonalcoholic fatty liver disease in obese versus lean subjects. *PLoS One.* 14:e0213692. doi: 10.1371/journal.pone.0213692

Zhang, T., Li, Q., Cheng, L., Buch, H., and Zhang, F. (2019). Akkermansia muciniphila is a promising probiotic. *Microb. Biotechnol.* 12, 1109–1125. doi: 10.1111/1751-7915.13410

Zhao, D. D., Bai, Y., Wu, R., Mo, F. F., Liu, C. Y., Zhu, R. Y., et al. (2019). Effects of Ginsenoside Rb1 on Skeletal Muscle Insulin Resistance and Adenosine Monophosphate-activated Protein Kinase Signaling Pathway in Obese Mice. *World J. Trad. Chinese Med.* 5:42

Zhou, P., Xie, W., He, S., Sun, Y., Meng, X., Sun, G., et al. (2019). Ginsenoside Rb1 as an Anti-Diabetic Agent and Its Underlying Mechanism Analysis. *Cells* 8:3. doi: 10.3390/cells8030204

Zhuang, P., Zhang, Y., Shou, Q., Li, H., Zhu, Y., He, L., et al. (2020). Eicosapentaenoic and Docosahexaenoic Acids Differentially Alter Gut Microbiome and Reverse High-Fat Diet-Induced Insulin Resistance. *Mol. Nutr. Food Res.* 64:e1900946. doi: 10.1002/mnfr.201900946

Zierer, J., Jackson, M. A., Kastenmüller, G., Mangino, M., Long, T., Telenti, A., et al. (2018). The fecal metabolome as a functional readout of the gut microbiome. *Nat. Gen.* 50, 790–795. doi: 10.1038/s41588-018-0135-7

Zihni, C., Mills, C., Matter, K., and Balda, M. S. (2016). Tight junctions: from simple barriers to multifunctional molecular gates. Nature reviews. *Mol. Cell Biol.* 17, 564–580. doi: 10.1038/nrm.2016.80

Conflict of Interest: XZ and LZ were employed by the Zhejiang Hongguan Biopharma Co., Ltd., Jiaxing, China. QL was employed by the Suzhou BiomeMatch Therapeutics Co., Ltd., Shanghai, China. HZ, GPZ, and YL are inventors of patent application (202210320411.3), related to this work.

The remaining authors declare that the research was conducted in the absence of any commercial or financial relationships that could be construed as a potential conflict of interest.

Advantages of publishing in Frontiers

OPEN ACCESS
Articles are free to read for greatest visibility and readership

FAST PUBLICATION
Around 90 days from submission to decision

HIGH QUALITY PEER-REVIEW
Rigorous, collaborative, and constructive peer-review

TRANSPARENT PEER-REVIEW
Editors and reviewers acknowledged by name on published articles

Frontiers
Avenue du Tribunal-Fédéral 34
1005 Lausanne | Switzerland

Visit us: www.frontiersin.org
Contact us: frontiersin.org/about/contact

REPRODUCIBILITY OF RESEARCH
Support open data and methods to enhance research reproducibility

DIGITAL PUBLISHING
Articles designed for optimal readership across devices

FOLLOW US
@frontiersin

IMPACT METRICS
Advanced article metrics track visibility across digital media

EXTENSIVE PROMOTION
Marketing and promotion of impactful research

LOOP RESEARCH NETWORK
Our network increases your article's readership